The University Of Sheffield.

Effect of urban morphology on the distribution of traffic noise

By:

Bo Wang

A thesis submitted in partial fulfilment of the requirements for the degree of Doctor of Philosophy

The University of Sheffield
Faculty of Social Science
School of Architecture

October 2016

ABSTRACT

The thesis explores the effects of the urban morphological characteristics on the general level and the spatial distribution of urban traffic noise with employing the state-of-the-art noise mapping method and a series of quantitative research approaches. A series of systematic tests on the applicability of state-of-the-art EU noise-mapping calculation method were conducted in a series of urban scenarios with typical morphological features selected in Wuhan, China. It was found that with appropriate configurations, the applicability is acceptable in most of the complicated urban space scenarios selected in Wuhan, China; while for some complicated urban environment features, optimisation of the calculation configuration, modelling method, or calculation algorithm is required to ensure acceptable accuracy. A comparison study was then conducted between a series of urban areas with similar functions and distinct urban morphological features in two typical urbanised areas selected in the UK and China. The result reveals strong influences of urban morphological features on the noise distribution patterns. For instance, the maximum noise level in the latter was found to be averagely 2.8 dBA higher, while the spatial median noise level is averagely 6.5 dBA lower than the former due to the typical street canyons with wide major road and high-rise flanking buildings. The effect of the social-economic factors on the spatial distribution of traffic noise was also explored. In Wuhan, China it was found that comparing with a typical high-income area, a typical low-income area has lower average and median noise level and higher minimum and background noise level. A parametric study based on a series of idealised cases was conducted to further explore the effects of urban morphological features on the traffic noise. A number of urban morphological indices were found to have significant effects on the general level and distribution of traffic noise, especially the urban-density-related indices and the indices related to building and street canyon geometric features. A series of prediction models were also developed based on multilinear regression analyses, and it was found that the variation of up to 73.1% of the ground noise level and 70.7% of the indoor noise level can be predicted by 2-3 urban morphological indices. Based on the findings, a series of practical suggestions were then given for the potential of predicting and mitigating the traffic noise impact through urban planning and urban design measures.

ACKNOWLEDGEMENTS

First of all, I would like to thank my supervisor Prof. Jian Kang for his dedication and an enormous amount of support and patience all these years, his strong support gave me the confidence to conquer a series of unimaginable obstacles throughout the entire research process.

This research is partially related to a Project led by Prof. Jie Zhou from Wuhan University: The Study of Environmental Conditions for Urban Low-income Residential Areas Using Digital Techniques, funded by the Chinese Natural Science Foundation (2007-2010). Only with the kind help of Prof. Jie Zhou and researchers, students like Dr. Bo Xie and more from Wuhan University who have involved in this project, the in-situ measurement, questionnaire survey and digital data acquisition could have been made possible.

I would also like to express my most sincere gratitude also go to my Acoustics Group colleagues, Neil Johnson, Hongseok Young, Michael Barclay for the most valuable discussions and selfless knowledge sharing, Hui Xie for the enduring friendship and his inspirations, Yuliya Smyrnova, Reinhard O. Neubauer, Yiying Hao, Chia-Jen Yu, Shen Chen, Lei Yu for all their priceless support all the time; my SSoA colleagues and friends Xuemei Li, Bing Chen, Bing Jiang, Jiangtao Du, Xi Wang and more for the kindest help you have given. Sincere appreciations also go to my best mates and friends Yisheng Wang, Xiongwei Song, Yi Fu, Xi Lin, Si Cao, Rui Liu, Yuchan Zhang, Ying Hu, Qiang Shao and Zhoumeijun Jing for their encouragement, love and companion during the tough times. Thanks also go to Dr. Dan Jiang and Mr. Hang Li for the family-like hospitality and support; Yonathan Timar, Yili Yu and Dr. Liqin Zhao for their care and accommodation provided. Last but most importaantly, I have owed too much to my family, Li Shenghua, Wang Hui, Wang Weiyi, Wang Xiyuan and Wang Xijun, thank you for your priceless love, financial support and enduring patience over the years.

This thesis is dedicated to my father Dewen Wang, may he rest in peace.

CONTENTS

LIST OF ABBREVIATIONS

AGMA	Association of Greater Manchester Authorities (UK)
BBAI	Building block area index
BFASAI	Building frontal area to street area index
BFLI	Building frontal length index
BFR	Building façade ratio
BPRLI	Building perimeter to road length index
BSAPAR	Building surface area index
CAR	Complete aspect ratio
CNOSSOS	Common Noise Assessment Methods in Europe
CNY	Chinese Yuan (Currency unit)
CRTN	Calculation of Road Traffic Noise (UK)
dB	Decibel (unweighted)
dBA	Decibel (A-Weighted)
Defra	Department for Environment, Food & Rural Affairs (UK)
DfT	Department of Transportation (UK)
DSTD	Daily spatial traffic density
DTM	Digital Terrain Map
EC	European Commission
EEA	European Environment Agency (Ireland)
END	The Environnemental Noise Directive (EU)
FMoT	Federal Ministry of Transportation (Germany)
FSI	Floor space index
GFL	Ground façade (spatial noise) level

GIS	Geographic information system
GL	Ground (spatial noise) level
GSI	Ground space index
HWR	Height-to-width Ratio
Hz	Hertz
ISO	International Standard Organization
ISUF	International Seminar on Urban Form
kHz	Kilohertz
MEP	The Ministry of Environmental Protection (China)
N	Road network density
OSR	Open space ratio
RI	Rugosity index
RSR	Road coverage ratio
RWI	Road width index
SEL	Sound exposure level: The equivalent noise level normalised to 1 second.
SEPA	China State Environmental Protection Administration
SPL	Sound pressure level
TFL	Total façade (spatial noise) level
Veh/h	Vehicles per hour
WCTPDI	Wuhan Institute of Integrated Transportation Planning and Design
WG-AEN	European Working Group – Assessment of Exposure to Noise

LIST OF FIGURES

LIST OF TABLES

Chapter 1 Introduction

1.1 Research background

Traffic noise as a major source of negative impact on the well-being of urban residents especially those live in the highly urbanised areas (B. Berglund; T. Lindvall, 1995) has brought the attention of both researchers and policy. The Green Paper on Future Noise Policy (EC, 1996) stated that there are 80 million EU citizens are severely affected by the day time noise. A series of existing and newly developed noise-mapping methods are employed for the assessment and prediction of noise in EU cities, e.g. UK method CRTN (UK DfT, 1988) published in 1988, and international standard ISO 9613 (ISO, 1996) published in 1996 for general environment noise calculation, etc. The state-of-the-art strategic noise mapping methods illustrate the noise distribution from macroscale perspective based on the urban environment features of typical EU cities.

In the last decade, there are prompt and broad developments in computer-aided environmental noise simulation in terms of research and practice in Europe, following the publication of END 2002/49/EC (EC, 2002). A series of significant progress has been made in the field of environmental noise prediction, in terms of both the assessment methods and the noise indicators, and the strategic noise maps as one of the major forms of publishing noise exposure information. Correspondingly, a number of noise mapping packages have been developed and applied in practice. A series of studies on the accuracy of the urban noise calculation methods have also been published in the EU (WG-AEN, 2005; Licitra & Memoli, 2008; Garg & Maji, 2014). According to the international standard ISO 9613-2, the noise calculation accuracy in ideal conditions could be within ±3 dB (ISO, 1996). Higher inaccuracy level is also reported in real urban situations by using different combinations of methods or packages. Nonetheless, in general, the performance of mainstream EU noise mapping methods and packages are acceptable especially for the need of strategic noise mapping (Murphy & King, 2010).

Due to the unprecedented urbanisation process and increasing number of vehicles in China, urban traffic noise is becoming one of the major environmental issues (MEP China,

2011), China has started its plan of adopting and developing state-of-art noise-mapping method regional noise-mapping practice is also initiated (MEP China, 2015). Due to the intensive urban construction activities and massive population increase in Chinese cities, the typical Chinese urban noise environment in terms of urban morphology and traffic noise sources exhibit significant disparities comparing with EU cities (Wang, Kang, & Zhou, 2008).

As discussed in a number of research on the urban environmental issues, e.g. urban daylight availability (Cheng et al., 2006), urban energy consumption (Rodríguez-Álvarez, 2016), ventilation and air quality (Edussuriya, Chan, & Ye, 2011), etc., it can be see that here is a permanent contradiction between the rapid increase of urban density and the severe urban environmental concerns. For the environment issue caused by traffic noise, it is interesting to know that, is it necessary that the increasing of urban density must sacrifice the tranquillity of urban outdoor and indoor environment; and do more roads consequently mean more severe noise impact; if the answer is no, then is there an efficient way to predict and mitigate the imp

act of the traffic noise in the early phase of urban planning process? This study attempted to explore these questions with the help of EU noise mapping techniques in a logically consequent manner.

With the help of the researchers involved in this project in Wuhan, China who were working on a Chinese National Scientific Funding Project on the environment sensitivity of the low-income residential areas, the in-situ measurement and digital data acquisition were carried out; some socio-economic data such as personal income level of the residents are also collected via in- situ questionnaires survey. In the comparison study part, the potential correlation between income level and traffic noise impact is explored briefly.

1.2 Research questions and objectives

1.2.1 Research questions

Several research questions following the main topic are raised and explored correspondingly in each chapter:

- **Chapter 4**: whether the calculation algorithm and the recommended calculation configurations are applicable and optimisable in typical Chinese urban environment, and what are the pattern and reason;
- **Chapter 5**: how is the performance of typical EU strategic noise mapping software in typical urban environment with heavily constructed road infrastructures and dense buildings in major cities of China, and what are the feasible measures to optimise the applicability;
- **Chapter 6**: whether the general noise level and distribution in high-density Chinese urban environment distinct from that of similar EU cities; what urban morphological features have caused the difference in the traffic noise level and distribution pattern;
- **Chapter 7**: how do a certain urban morphological feature and relevant morphological index affect the noise distribution pattern; is it predictable and how.

1.2.2 Research aim and objective

The thesis is trying to explore the questions in a progressive manner, the following research objectives are set and to be achieved:

- Validate and optimise the default configuration of EU noise calculation method in typical Chinese urban environment;
- Examine the applicability of EU noise mapping method in typical Chinese urban environment;
- Compare the general noise level and distribution in representative EU and Chinse urban forms with similar urban functions and distinct morphology characteristics;
- Explore the potential correlation between socio-economic indices in terms of income and noise level;
- Compare the urban noise level and attenuation pattern in different urban forms with distinct building and road network density;
- Quantitatively analyse the potential correlations between urban morphological indices and spatial noise indices through parametric study;
- Analyse key urban morphological indices that have significant correlations with traffic noise distribution;

- Discuss the implication of the effects found in the significant correlations, using the measures of urban planning and design;
- Propose models for the prediction of traffic noise distribution.

1.3 Research framework

The research objectives are expanded and explored progressively according to the following chapter structures:

- ***Chapter 2: Literature review***

The literature reviews in Chapter 2 explores the background and existing literature related to the research topics of this study. The chapter starts with the brief introduction of the two research fields involved, the urban noise and the urban morphology. The major difference between the west and the east in terms of urban sound environment and urban morphology are then analysed through comparison, especially the sound environment features of typical Chinse cities. The state of the art development of the noise mapping methods and packages are then reviewed, the literature and practices regarding the potential accuracy issues are emphasised. Relevant issues and literature regarding the parametric study approach are discussed.

- ***Chapter 3: Methodology***

This chapter is divided into three major parts, according to the main framework of the study: the applicability test on current EU noise mapping calculation techniques in typical Chinese urban environment; comparison of sound environment between typical low and high density urban areas in EU and China; the parametric study approach and selection of urban morphological and spatial noise indices. Relevant research methods adopted in some previous research are discussed too. The framework and boundary scope of the research is defined, and the research methodology of each part is introduced in detail.

- ***Chapter 4: A pilot study on the optimisation of EU noise calculation method in typical Chinese urban environment***

A systematic test on the recommended noise calculation configurations and the effect of typical Chinese urban form features on the noise calculation is conducted. The environmental noise simulation package Cadna/A is chosen for the calculation of noise distribution in this study, the CRTN and ISO 9613-2 are selected to represent typical EU noise calculation methods.

A pilot test on the applicability of the EU calculation method in typical Chinese urban sound environment features is also conducted. A case is chosen in the city of Wuhan, China which relatively simple traffic pattern and building form. The sound propagation path between the source and receiver is also relatively simple. At a series of locations with height and slant distance from the road, the A-weighted SPL or full spectrum SPL are measured and compared with the calculation results. Visible calculation errors are then analysed, relevant modelling and configuration optimisation measure are tested and discussed.

- ***Chapter 5: Applicability examination of EU traffic noise calculation method in typical urban environment of China***

Following the pilot test in Chapter 4, four cases study areas are selected in Wuhan, China, the selected cases possess relatively more complicated urban-form features that are typical to China, including high-density low-rise urban village, high-rise street canyon with double-layer main road in relatively open street canyon, and barrier-sealed elevated road in narrow street canyon, respectively. 10-20 Receiver points with general noise level or full spectrum noise level in each area are measured at a variety of sensitive locations with different height and distance from the road are selected and tested. Both calculation configurations and modelling methods are tested for the sake of systematically revealing the applicability of the selected calculation method.

- ***Chapter 6: Effects of urban morphology on traffic noise distribution: a comparative study between the UK and China***

In Chapter 6, a comparative study is conducted between a series of sampled urban area in Greater Manchester of the UK and Wuhan of China, for the sake of finding the effect of urban morphology on the traffic noise distribution. The selected case study areas of the

same category in the two cities have the identical scales, similar land-use and functions and distinct urban morphological features. A brief comparison between two representative residential areas in the Chinese city with distinct income level is conducted, too.

The difference of noise distributions in similar sample areas in the two cities are quantitatively analysed using a series of spatial noise indices derived from the noise maps using a user-developed graphic processing program. Three basic urban morphological indices are also derived. Potential causes of the difference in the spatial distribution of traffic noise both in the open ground and on the building façades are discussed. A brief correlation analysis is initiated to find potential connections between different types of indices. The major parts of Chapter 6 are based on a journal paper in the Applied Acoustics, Vol. 72, page 556–568 (Wang & Kang, 2011).

- ***Chapter 7: A parametric study on the effect of urban morphological characteristics on traffic noise distribution***

In Chapter 7, a further study on the effect of urban morphological features on the general impact and distribution of traffic noise is conducted. The noise maps of 36 idealised cases study areas with hierarchical building and road network density are calculated, three types of spatial noise indices describing the general noise level and noise attenuation on all exposing façades are calculated. The chapter consists of three major parts:

Firstly, through systematic comparison of the spatial noise indices in cases groups categorised based on three pre-defined density indices, the effect of urban density on the traffic noise distribution is discussed. The implications of the finding in urban noise planning are discussed. Then a multilinear correlation analysis between the urban morphological features described by 16 different indices and the noise impact and distribution to the open space and to the indoor environment is conducted. The practical denotations of the correlations found are discussed. Last but not the least, a series of quantitative models for the prediction of key spatial noise indices are proposed based on a series of hierarchical multiple regression, for the sake of providing a viable tool of quantitative noise assessment and mitigation, for urban planner and policy makers.

- ***Chapter 8 Conclusions and future works***

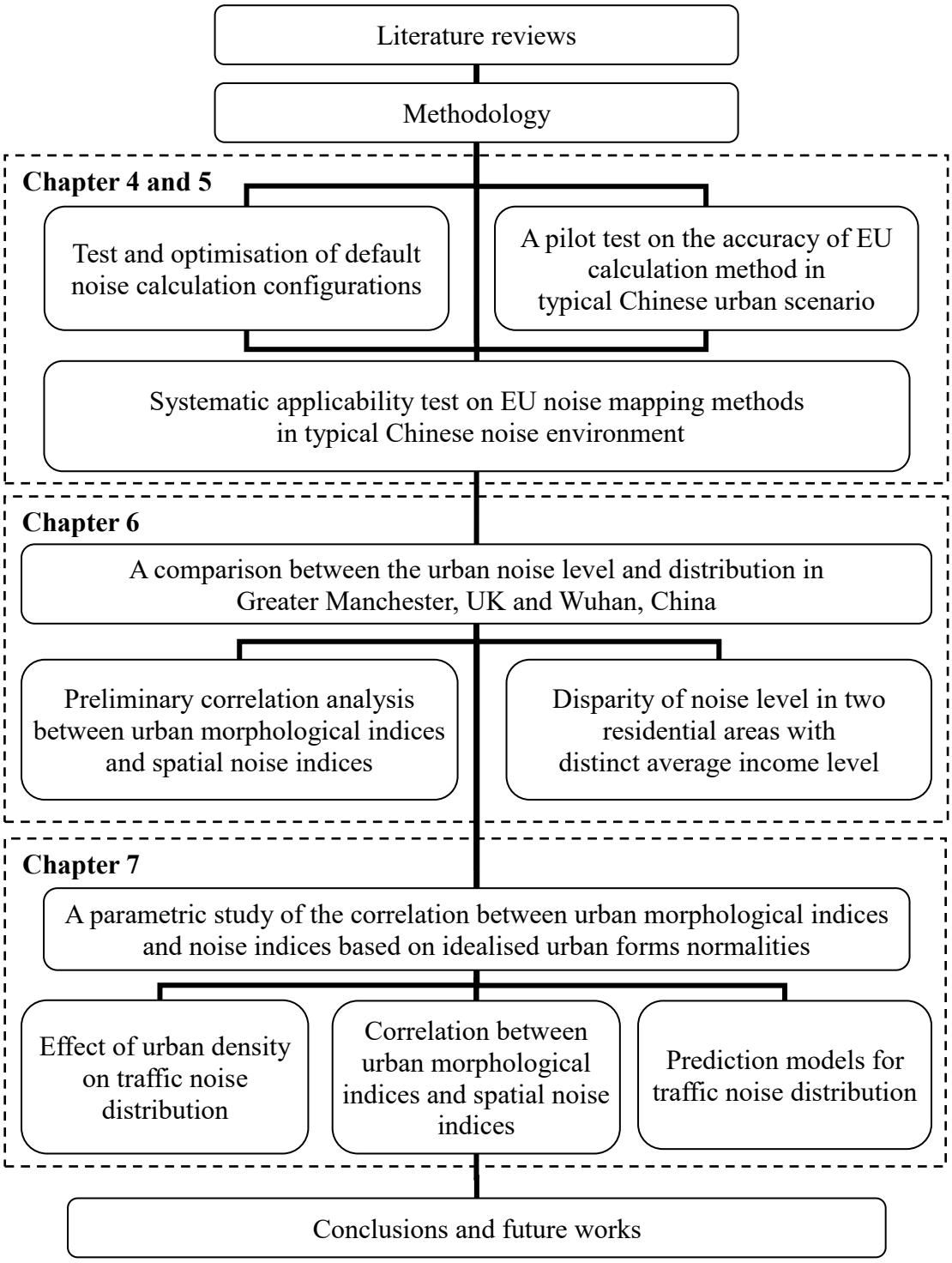

Figure 1.1 Research framework and structure of the thesis

The chapter 8 firstly listed the major findings and contributions of each part of this thesis. Then the limitation due to the scope and research scale of the research, and corresponding potential works in the future are also discussed.

In summary, the chapter is developed in a consequent manner in three major parts. The first part consists of two chapters, the Chapter 4 and 5 discussed the potential accuracy issues and provides a feasible tool for future research; with the optimised calculation and modelling method. In the second part, Chapter 6 compares the major difference of urban noise distribution in low and high-density urban environment with varying morphological features. In part 3, the correlations between urban morphology and traffic noise distribution found in Chapter 6 are further explored the parametric study in Chapter 7. A brief illustration of the thesis framework and structure is showing in Figure 1.1.

Chapter 2 Literature review

2.1 Introduction

In this chapter, a systematic literature review is given on the state of the art of the research fields that are related to the thesis: the research advances in the field of urban morphology as well as the difference of urban morphology between the EU and China in Section 2.2; the urban general issues to be studied that are related with sound environment and traffic noise issues in the EU and China in Section 2.3; the state of the art noise mapping calculation methods, packages and relevant directives and practices in Section 2.4; the existing research literatures regarding the inaccuracy and uncertainty in the traffic noise simulation process in Section 2.5; lastly, a horizontal review of relevant researches on the correlation analyses and parametric study methods between urban morphology and urban traffic in Section 2.6. The pros and cons of different theories, methods, and practices are systematically compared. For the sake of providing references to the research approaches used in present and future researches, the measures of data obtaining, processing, comparison, and statistical analysis are also introduced.

2.2 Urban morphology

2.2.1 Introduction

Modern urban morphology research is originated from the central Europe tradition of morphogenetic research, especially the work of Schlüter in the late 19th century (Gu, 2001). M.R.G. Conzen (1960) further promoted the research of urban morphology since the 1960s. The current studies in this field are mainly initiated by two of the renowned morphologists: M.R.G. Conzen from the UK and Saverio Muratoric from Italy. According to Moudon (1997), there are three major research schools of urban morphological research according to differences in approaches and emphasises when building their theories:

- The Birmingham school focuses on the study of urban form from the perspective of both descriptive and explanatory, aiming at the theory of city building.
- The Italian school pays more attentions on the study of urban form the perspective of prescriptive purposes, aiming at the theory of city design.
- The French school researches the urban form via the assessment of the impact caused by design theories on the city building.

A group of urban morphologists from countries including major western countries, Japan and the USA founded the International Seminar on Urban Form (ISUF), which has since created an interdisciplinary research domain that covers a number of disciplines including geography, archaeology, architecture, planning and history, etc. (Moudon, 1997). The advances of urban morphology research hasve helped to concentrate the focuses on the real-world city building phenomena (Konvitz, 1985).

2.2.2 Content and framework of urban morphology research

2.2.2.1 The concept of urban morphology

As defined by Moudon (1997), urban morphology as known as urban form or urban landscape is “the study of the city as human habitat”. The ISUF is the most important and influential research organisation on urban morphology which acknowledges that the extension of urban morphology covers much more than its original definition and boundary in geography, and its importance as an emerging interdisciplinary field (ISUF, 2009).

According to American Planning Association (2006), the urban morphology researchers consider the physical world as a result of dynamic social and economic forces. The physical characteristics of urban morphology are inseparable from the urban development and renewing processes.

2.2.2.2 The components of a city

From the elemental level, the urban morphology is to be analysed from three main aspects: form, resolution, and time constitute. Among which the urban form is defined by three of the most fundamental elements: buildings and the neighbouring open spaces; the land lots of plots; and the street space. Based on the three fundamental elements, the urban resolution can thus be defined into four levels: the buildings or the lots, the roads or block, the city, and the region. In the meantime, the aspect of time constitutes indicates the historical perspective of understanding the continuous transformation and the replacement of the urbanised area. (Haupt, Pont, & Moudon, 2005; Moudon, 1997)

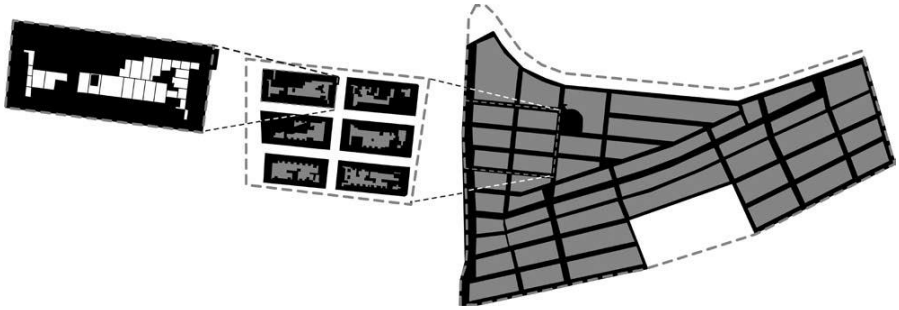

Figure 2.1 Three aggregation levels of a typical European city: island, fabric, and district. Derived from Pont & Haupt (2005)

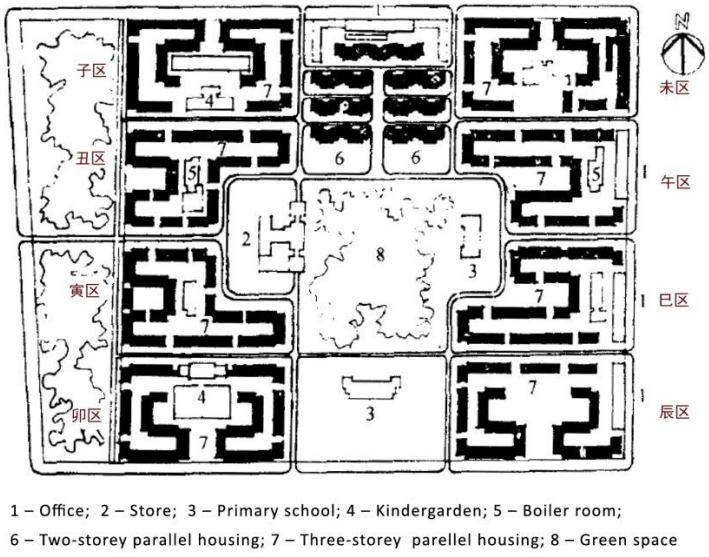

Figure 2.2 Plan of a typical low-density *Danwei* built in the 1950's in Beijing – the Baiwanzhuang residential community. Source: Principles of urban planning (3rd ed.) (Li, 2001)

According to Cozen (1960), the smallest cell that a city is composed of the so-called the plan units, which is the combination of individual pieces of land, building and the adjancent open spaces. The time constitute and the social-economic situation are relfected in the the current condition of the most basic urban cells. Moudon (1997) further indicated that as groups of buildings, open spaces, lots, and potentially some streets for local transportation, the plan units can be regarded as a whole that is cohesively united together, due to either the context of the site or because of the common transformation process occurred to them. This definition is analogous to the contemporary urban unit named *Danwei* emerged in China in late 20th century, literally means 'work unit'—the basic urban morphologic and sociologic cell as a workplace organisation, although the latter has a relatively larger scale in general (Kai, 2001). Nevertheless, the structure of a city substantially manifests as a more complex intertwined system, e.g. in typical Chinese *Danwei*, there are planned local roads but rarely transportation activities and traffic occurring on them (Bray, 2005).

According to Pont & Haupt (2005), the urban space can be seen as a hierarchy system consists of five different layers: building, lot, island, fabric and district, the smallest of which is the island that is surrounded by local roads, as shown in Figure 2.1. A typical *Danwei* as shown in Figure 2.2 by this standard could be seen neither as an island because it contains transport infrastructures i.e. local roads; nor a fabric, as the roads inside the *Danwei* has relatively limited access to the transportation system connecting to other parts of the city. It indicates that it is necessary to analysis the typical Chinese urban morphology from a different perspective (Gaubatz, 2014; Bray, 2005).

2.2.2.3 Urban morphology analysis approach

The increasingly diverse and complex urban morphology research provides a broad range of methodologies for the analysis and explanation of the complicated urban pattern in different contexts (Moudon, 1997). One of the principal challenges for the urban morphologic researchers is to define the change of the cities and built environment in different contexts (A.J. Lane, 1993).

2.2.3 Major differences of urban morphology between EU and China

Cities in China and the western countries, especially that of the traditional EU countries have huge differences with regard to the historical background and development status. Consequently, the urban morphology also has distinctive features. The diversity underlying the appearance of urban forms can be revealed through in-depth comparisons. According to a comparative study of urban planning by Friedmann (1967), three major variables are to be introduced: the level of economic development, the form of political organisation and the historical traditions of a country's planning system. McCallum (1976) believes that the planning practice and the urban morphology is substantially shaped by the political culture.

2.2.3.1 The evolution of urban morphology of major Chinese cities

Kai (2001) indicated that the typical traditional form of a major ancient Chinese city is a walled enclosure with north-to-south orientation, symmetrical layout with axiality, and the closed courtyards. Which was originally recorded in the last section of one of the most ancient Encyclopaedia of technology in the world: the *Zhouli (Rites of Zhou)* written in *the* Western Zhou Dynasty (1046-771BC), the *Kaogongji* (Jun, 2013), an illustration of which is shown in Figure 2.3. Jin (1993) believe the unique urban form of Chinese cities reflects the highly centralised government political system, as well as with the Confucian philosophical and cultural traditions, and these tradition does not vanish after years of war and revolution.

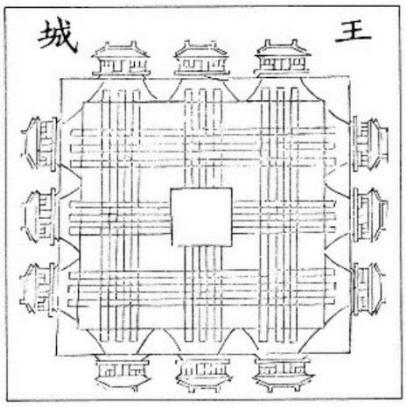

Figure 2.3 An illustration of the ideal imperial city form described in *Zhouli Kaogongji* (Schoenauer, 1981)

World Bank (1996) indicates that the planning system in China is profoundly conditioned by its attempts to establish a classless communist society based on Marxism since 1949. Before 1978, China's urban planning system is primarily shaped by the centralised planned economy in which all means of production were publicly owned. The close juxtaposition of workplace and residence are caused by the land-use policies in the 1950s, and that accelerates the use of low-cost transportations.

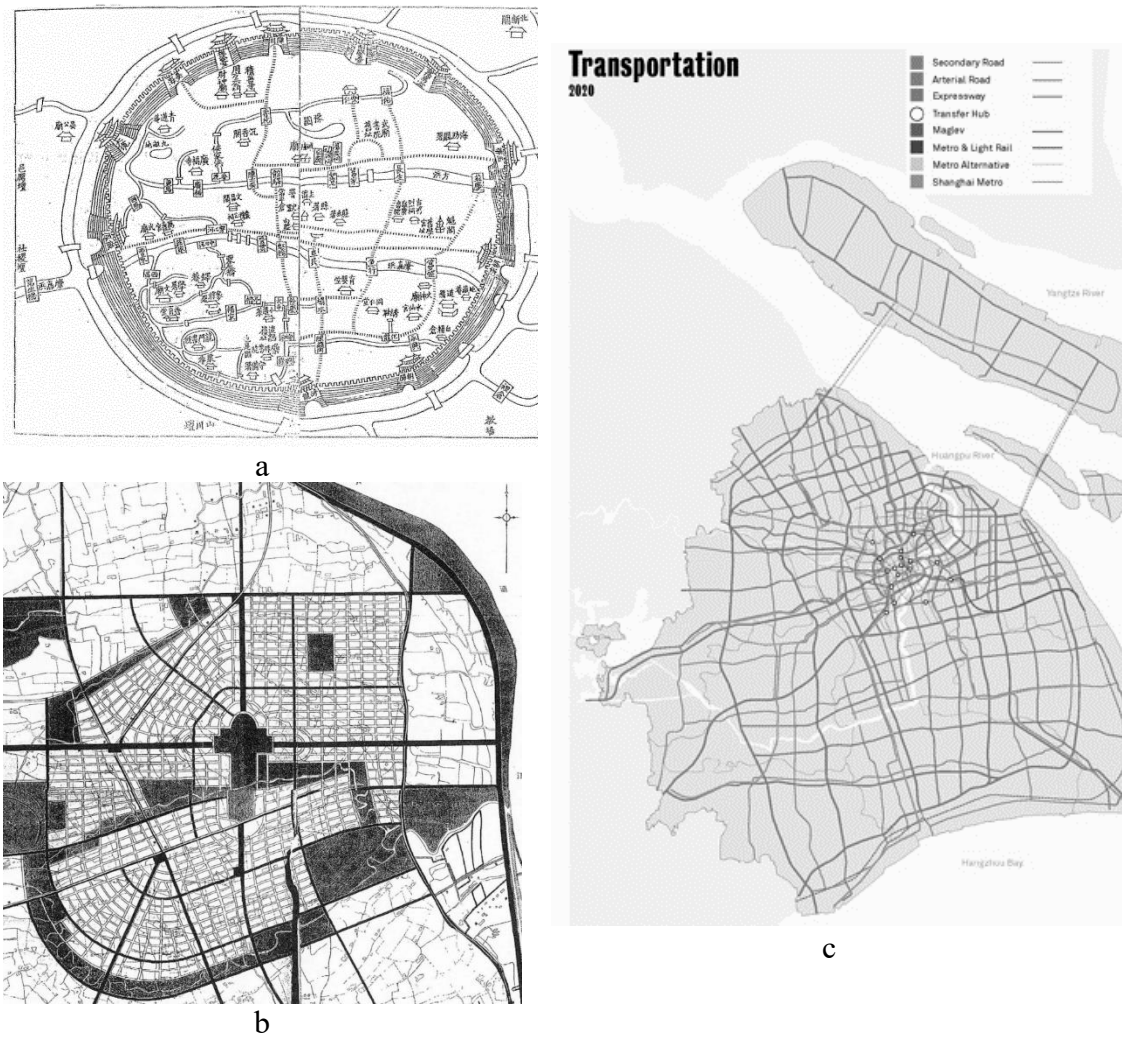

Figure 2.4 Historical development of the road network patterns of Shanghai. (a) The city of Shanghai County during late Qing, derived from Shanghai Xian Zhi (Gazette of Shanghai County) 1872 ed.; (b) Map of road system in the downtown of Shanghai municipality, derived from Business Report of the Construction Committee of the Downtown of Shanghai Municipality, August 1929 to June 1930; (c) Shanghai transportation planning derived from the Comprehensive Plan of Shanghai 1999-2020, the roads shown are all the main arteries and connection lines that are available to public access. Source: Ge (2002)

As can be seen in the historical map of Shanghai in Figure 2.4a that, Shanghai as the largest city of China today, originally was a small local county centre before the colonial era and has distinctive city boundary defined by the wall. The roads are connected with a series of gates built according to ancient planning scheme with a loosely orthogonal structure. When China steps into 20th century, the western influence shows distinctively in this unfulfilled road planning system as can be seen in Figure 2.4b. And Figure 2.4c shows how the rapid economic booming and increase of vehicle transportation has shaped the planning prospects of the city in the 21st century with large scale motor way and main road grids, dividing the urban area into a series of super blocks with different scales (Ge, 2002).

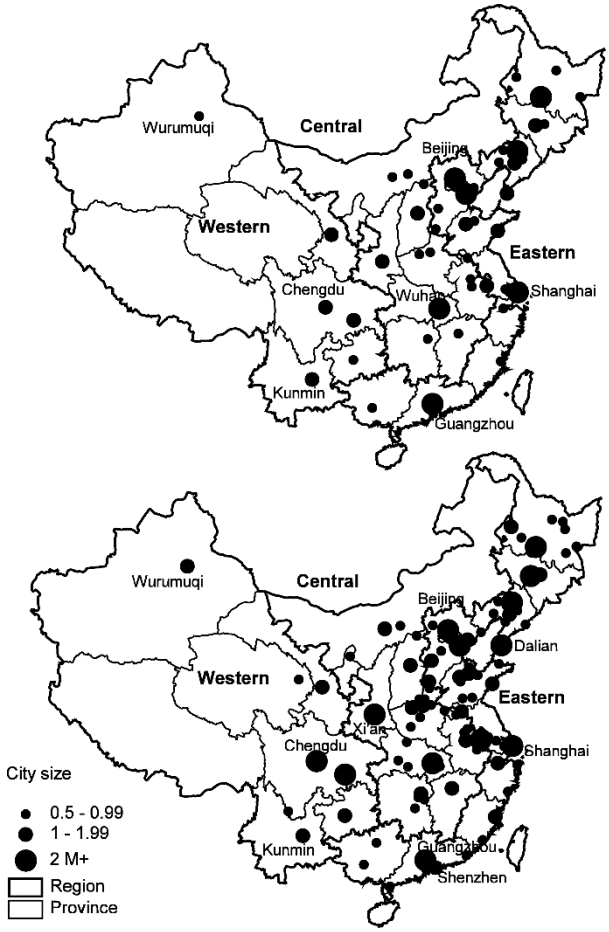

Figure 2.5 Cities with Non-agricultural Populations greater than 500,000 in 1982 and 2000. Source: Urban statistical yearbook of China 2001 (NBS China, 2001) Derived from Urban development in contemporary China (Huang, 2006).

Andrusz et al. (1996) believe that the 'socialist city' in China has transformed into a post-socialism era since 1978. World Bank (1996) indicated that the liberalisation of labour

and land market in the 1980-1990s created a longer journey from home to workplace, that leads to an increased dependence on motorised vehicles and reduced the use of bicycles. The cities expand accordingly, both the urban area and the urbanisation level in China increases considerably (Zhou, 2005; ADB, 2006), especially in eastern China, as can be seeing in Figure 2.5.

According to the United Nations (2010), the urbanised population in China was only 19.6% of the total population in 1980, in less than 30 years it had risen rapidly to 42.2% in 2007. The speed of increasing is unstoppable: in just three years till 2010 the total urban population has increased to 50.7%. The urbanisation population in China will reach 70% by 2050 according to a prediction by United Nations (2013).

Gu (2001) summed that corresponding to the historical development and changes of planning and city building, the landscape of most of the China cities can be divided into the following three categories:

- The old city core is mainly pedestrian area and concentrated low-level buildings that were formed before 1949;
- According to the socialist planning system that learnt from the Soviet Union, the old city core is surrounded by uniform *Danweis* with mixed land-use patterns. They were mainly built from1949 to 1978 and early 1980s.
- The newly developed zones since the economic reform started from December 1978 that consists of the commercial zone in the city centres, the economic development districts which are mainly industrial parks in the suburb area, the real-estate developments in the newly developed areas, and the urban renew in the old town centres (Gu, 2001).

As shown above, the urban morphology of major Chinese cities is largely a fusion of traditional Chinese urban forms with little motorised vehicle access and implanted modern urban developments that are forged on the foundation of large scale road infrastructures and high-density buildings. This process occurred in a relatively short period in last decades as can be seen in Figure 2.6 (Fang & Yu, 2016). The most distinct feature of the newly planned zones since 1949 is the group clusters or linear clusters that are formed and divided by the major road

network, with highly-concentrated traffic flow and wide interval space in between (Gu, 2001; Khakee, 1996).

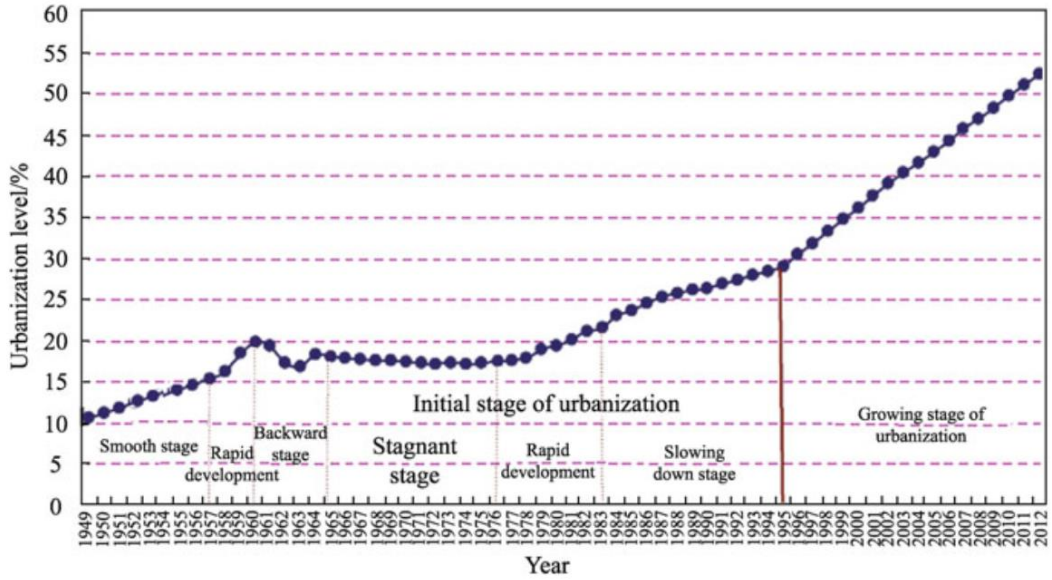

Figure 2.6 Urbanisation stages in China from 1949 to 2012 Source: Fang & Yu (2016)

In the other hand, the EU cities generally manifest rather dissimilar urban morphology features comparing with that of China, in terms of urban density, road network pattern and urban spatial features, due to the relatively more modest and consistent urbanisation process, generally lower population density, as well as distinctive different historical urban structure and forms in the EU comparing with that of China.

2.2.3.2 Difference in urban density and transportation needs

Statistic data shows that the major cities in China generally have much higher population density than that of the major western cities. It can be seen in the statistical result of 1990 shown in Figure 2.7 that generally the population density in China and some other Asian cities are evidently higher than that of the EU countries, and this difference may still be enlarging due to the difference in the urbanisation phase in China and the EU. Taking Wuhan of China and Greater Manchester of the UK as examples, the population density in the urban area of Wuhan is 10371 persons per km^2 in 2005 and it keeps increasing to 11502 persons per km^2 in 2010, (Wuhan Statistics Bureau, 2006, 2011), which is much higher than that of the Greater Manchester, which is 4024 persons per km^2 in 2001 according to Pointer (2005), and it had already dropped 6.1% since 1991. It can be seen

that the urban density in terms of population in Wuhan is more than two times higher than that of Greater Manchester, and the gap is enlarging due to the rapid urbanisation in China and shrinking urban population in the UK.

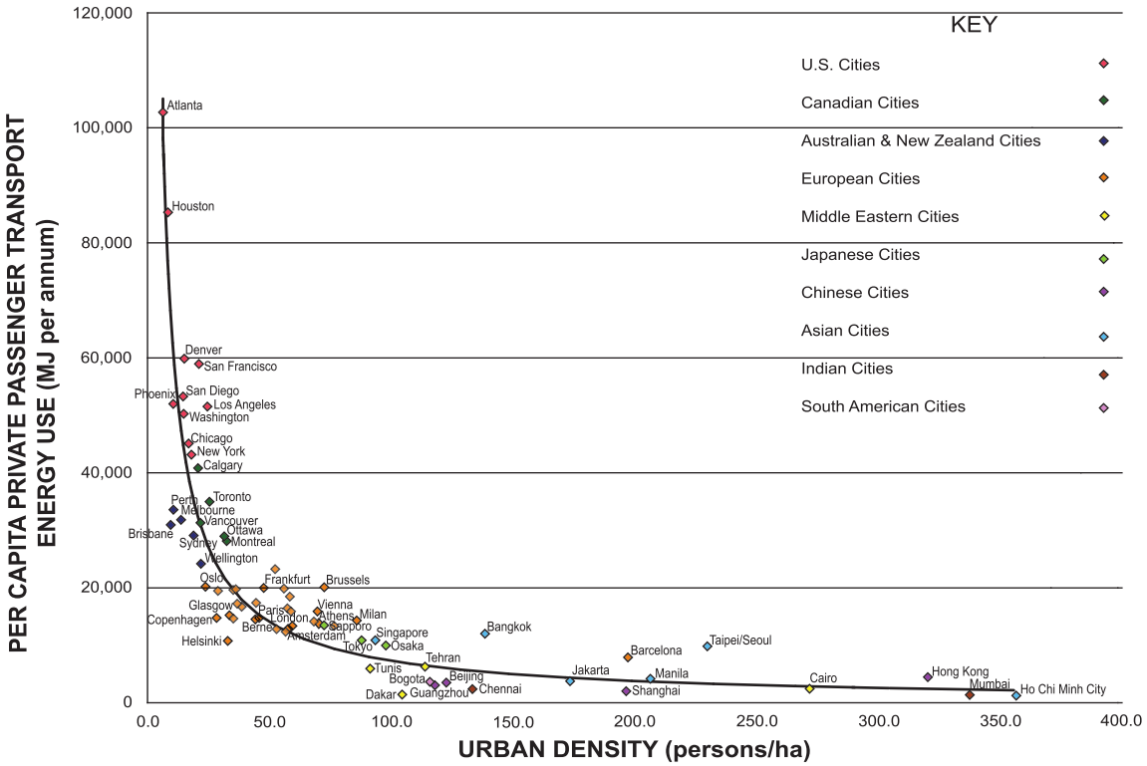

Figure 2.7 Population density and transport energy use per capita for selected cities (2015). Derived from Accessibility in Cities: Transport and Urban Form (Rode et al., 2014)

In the meantime, it is also notable that the vehicle usage in terms of transport energy consumption per capita in the former is generally lower than that of the latter (Petersen, 2004). It can be seen from Figure 2.7 that, cities with higher density generally have lower personal usage of vehicles, and less energy consumption. This implies that the significant difference in urban morphology between cities with different density especially differences in terms of road pattern, building forms and urban spatial features may also bring different levels and patterns of environmental impact caused by road traffic. Studies by Burton, Jenks, & Williams (2004) reveals that the western style low-density urban sprawl may have a series of potentially negative spread effect of the environmental impact compared with that of the high-density urban areas.

The huge disparities in the eastern and western cities in terms of city planning system, and urban development tradition and history may contribute to the differences in urban forms, consequently (Shelton, 1999). Some key characters of the urban form in typical high-density major cities in China are different comparing to that of the typical EU cities. For instance, the urban density of typical urban areas in terms of building coverage in Wuhan, China is found to be higher than that of Manchester, UK, which creates huge areas with low vehicle-access and high-rise street canyons in the former; In the meantime, the road coverage in the former is much lower than the later, by 1.7% to 11.3% (Wang & Kang, 2011).

2.2.3.3 Road network planning

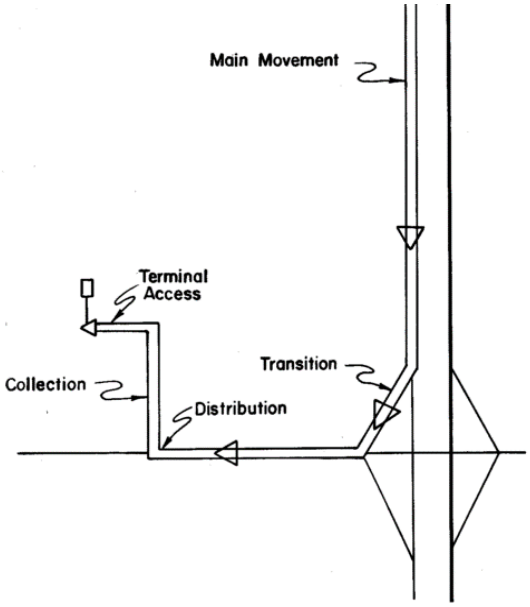

Figure 2.8 Hierarchy of movement. Derived from: AASHTO (2001)

Historically, the road classification system and the arrangement of the road network in human inhabitants have experienced a long process of evolvement and have a variety of forms all over the world (Kostof & Tobias, 2004; Svensson, 2004). In the process of connecting and distributing human and goods from one the origin to the destination, the essential process is universal.

As also can be seen in Figure 2.8 (AASHTO, 2001) that the movement of the vehicles is naturally divided into 5 different segments, while among which the Main Movement

refers to the national highway system that has very limited access to the city; for the sake of efficient traffic management, the basic structure of the major arteries are therefore also similar, for major metropolises the number and length of major motorways are limited, as can be seen in Table 2.1, the relative disparity in-between the cities listed main mainly due to the population and overall transportation needs (Xu & Huang, 2007).

Table 2.1 Number and length of major motorways. Source: Xu & Huang (2007)

Cities	London	Berlin	Paris	Washington	Moscow	Beijing	Shanghai
Numbers of major arteries	10	17	18	11	14	9	9
Major arteries length (km)	9-14	14-16	11-18	13-18	10-17	17-20	10-17

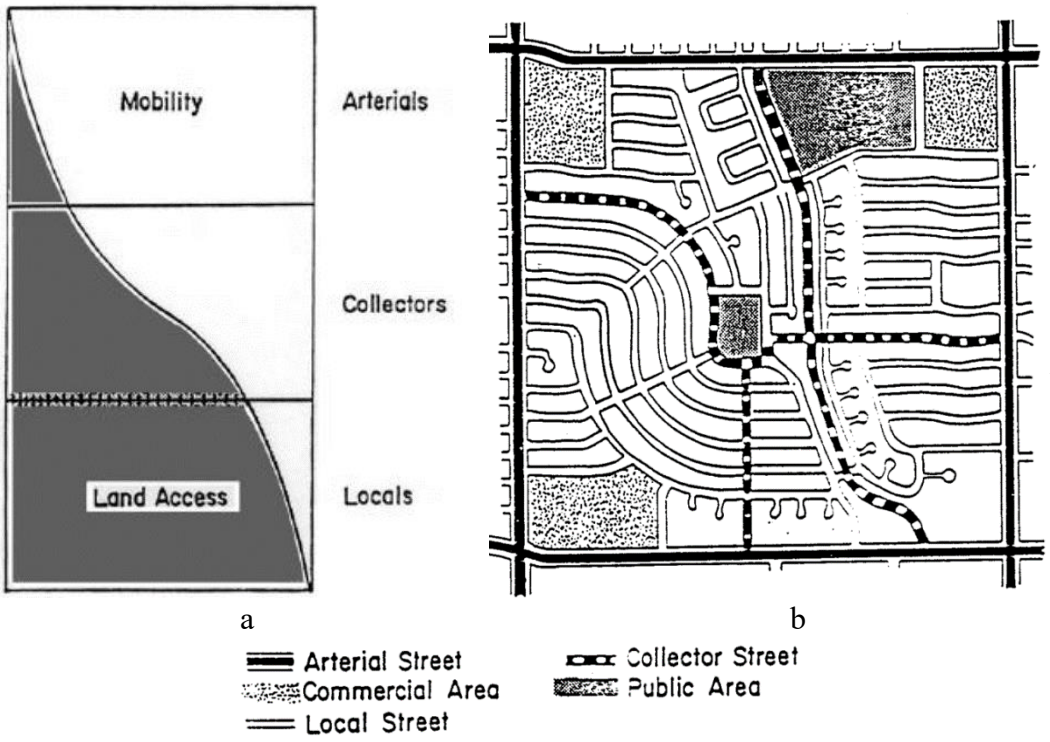

Figure 2.9 (a) Relationship of functionally classified system in serving traffic mobility and land access, (b) Schematic illustration of a portion of a suburban street network. Source: AASHTO (2001).

An urban road network transacts the functions of transition, distribution, collection and terminal access. As can be seen in Figure 2.9 that the proportion of urban roads as defined by the AASHTO (2001) need to be balanced by the demands of mobility and land access, the smaller the roads, it tend to has less mobility freedom and serves more to the function of land access. And in the typical western style suburb residential area, it can be seen that

the vehicle-accessible roads are extremely evenly distributed to full fill the high demand of personal transportation needs.

2.2.3.4 Difference in grid system and urban texture

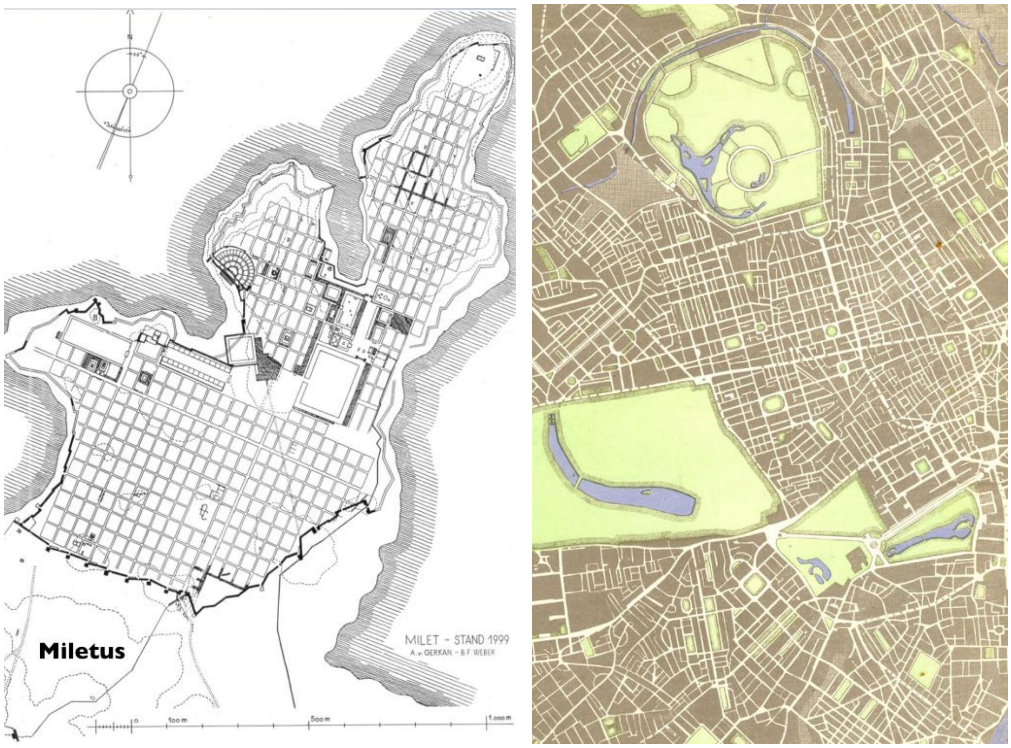

a b

Figure 2.10 The plan of ancient Greek city Miletus (around 479 BC), source: Schoenauer (1981) (a); and the street structure of part of 20th century London, source: County of London Plan 1943 (Forshaw & Abercrombie, 1943) (b).

The origin or most of the planned modern EU cities can be traced back to ancient Greek cites, as can be seen in Figure 2.10 that, the ancient Greek city Miletus has already manifests three key characteristics that were inherited by many of the modern EU cities (Schoenauer, 1981), e.g. London, including largescale monumental buildings for religious or political purposes, open space for public activities, and gridiron road patterns, which are planned perpendicular roads that divides the city into relatively medium or small size blocks.

The high-density road grid system across districts is well preserved in most of the major cities in EU, even when the major arteries designed for high-speed transportation were implanted into existing townscape; the small local roads pattern is remained to function for the inter-district connections. As can be seen in Figure 2.11 that, when a new motor

way in London was planned to replace an original commercial street, a series of path ways through the existing residential area are designed explicitly with different structure but similar inter-road gap and grid size (Marshall, 2005).

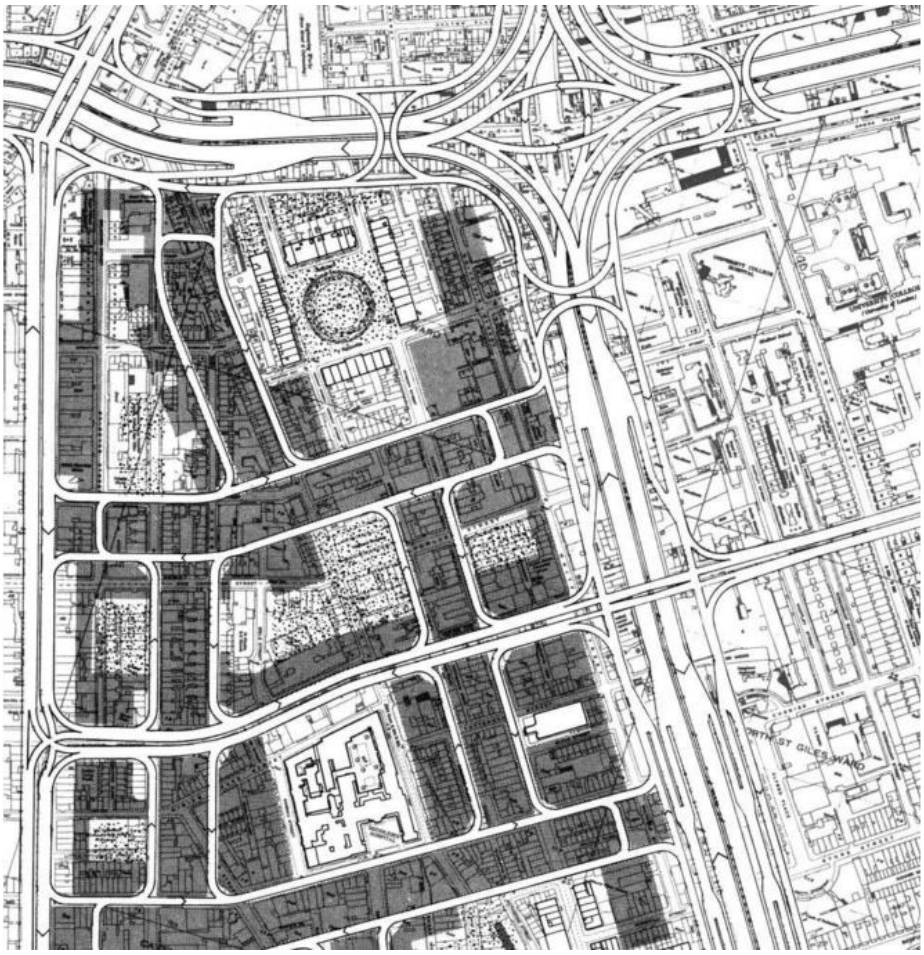

Figure 2.11 A urban transformation plan in Inner London, in which the Tottenham Court Road from north to south is replaced by a multi-lane motorway. Source: Marshall (2005)

In contrast, the typical Chinese road grid system and street patterns has a significant difference and is undergoing dramatic changes. The key difference lies in the neglect of small roads in super blocks surrounded by main roads and arteries. As can be seen in Figure 2.12 that, the ancient imperial capitals of China are also well-planned with perpendicular road grids, but the gap between the main roads are much higher, and the large scale blocks surrounded by the thoroughfares was called the *Lifang*. It is also notable that both cities have inhabited more than one million people at their time, which are much higher than most of the EU cities in the same period (Schoenauer, 1981). The formation of the *Lifang* is closely related with typical centralised political and social scheme of

China (Tang, 2010). The late 20th century urbanisation reinforced this tradition by replacing the super traditional supper block, the *Lifang* (Li, 2013) with modern supper block, the *Danwei* and real-estate communities as discussed earlier.

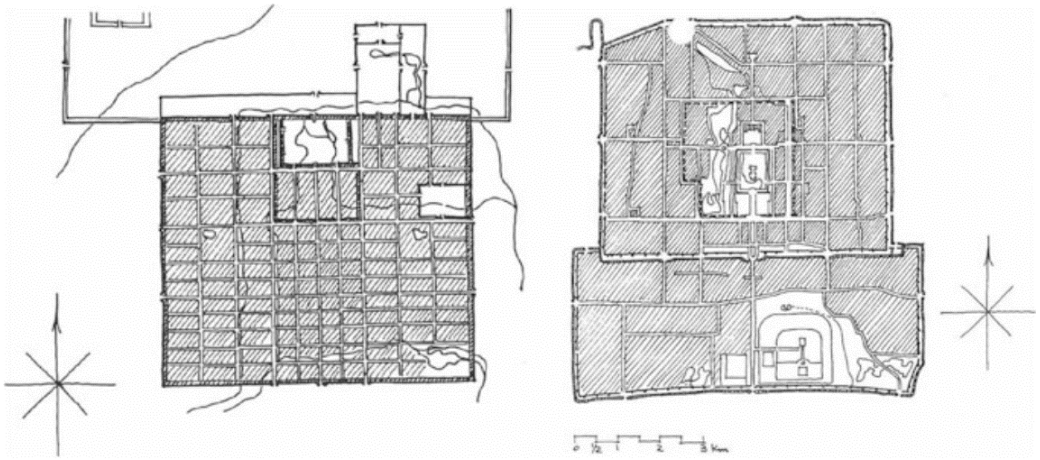

a b

Figure 2.12 Plans of Chinese ancient capitals: (a) Plan of ancient Chang'An in the Tang Dynasty (618–907 AD); (b) Plan of Beijing from the seventeenth through the nineteenth centuries (Steinhardt, 1990)

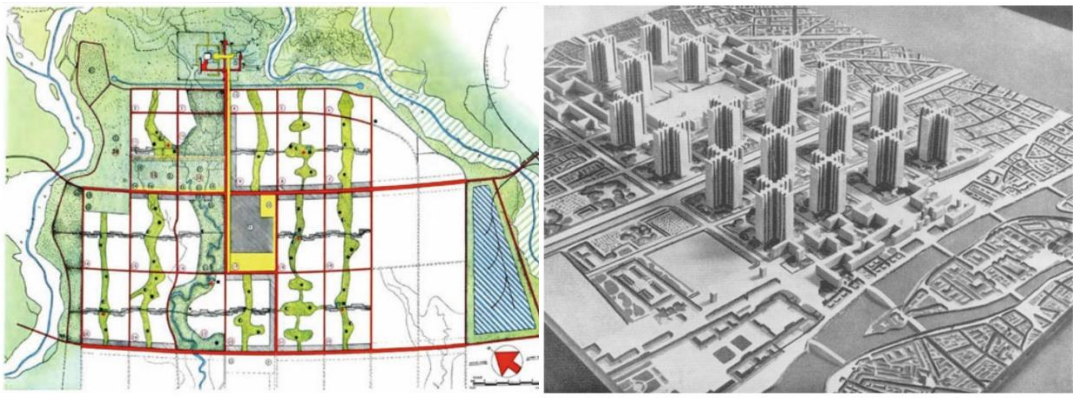

Figure 2.13 French Architect Le Corbusier's plan for Chandigarh, India. Source: V. Oliveira, (2016) and Pont & Haupt (2009).

It is also notable that, although the super block system with high density buildings are more popular in China and some other emerging economies, it is significantly influenced by the European planning trends in the mid-twentieth century, while as can be seen in Figure 2.13 that the socialism style sky-scrapers apartments with large open space and land blocks, planned by Le Corbusier for the developing country was not as welcomed

nor realistic for the relatively low-density EU cities, and hence has very limited influence on the urban morphology in the modern EU cities (Oliveira, 2016; Schoenauer, 1981).

Figure 2.14 Illustrations of typical building massing within a Superblock System and an Urban Network: (a) and (b), Super block plan; (c) and (d), small block plan. Source: Calthorpe Associates (2012).

Zhao (2002) deemed that, in contrast with typical European cities where the road network consists of evenly-distributed roads, and vehicles are accessible to a wide range of roads, in typical Chinese urban area, the main road network with large width distributes across the urban area with typical spacing of 350–500 m (Li, 2001), and only a few low-traffic local roads running through or connecting with the main roads in the interval space among the main roads (Tang, 2000). As shown in Figure 2.14, on the left a typical Chinese urban area with high urban density is planned with the traditional urban from of super blocks, with concentrated building blocks and limited traffic access; on the right an example is given to demonstrate a design with the same amount of buildings and roads, at the same time typical western-style smaller blocks (Calthorpe Associates, 2012). It can be seen that

the urban forms of the two scenarios have dramatic disparities in terms of building form, building arrangement, and transportation patterns, etc.

2.3 Urban sound environment

2.3.1 Urban noise as an environmental issue

Noise is one of the most important urban environmental health concerns, which is majorly caused by the traffic, industrial and domestic activities. Among which the traffic noise is the most disturbing impact to the urban residents. Research shows that when at the SPL of 65 dBA, sleep can be evidently disturbed (Berglund and Lindvall, 1995).

The traffic noise has also become one of the unneglectable social and public health issues in China. In the early 1990s when China's economy and urbanisation boom has just started, the China environmental authorities received over 130,000 complaints per year from 1991 to 1993, amongst which noise pollution accounted for over 20.7% of all the complaints (Dasgupta and Wheeler, 1996), and it was just ranked number three after the water and air pollutions. The situation is getting worse along with unprecedentedly rapid urban development. According to the Ministry of Environmental Protection of China (2015), noise has become the biggest source of urban environmental complaint with whopping 4,570,000 complaints in 2014, which accounts for 56.4% in all complaints on environmental issues, and is even 16.6% higher comparing with that of 2013. In a research on traffic noise annoyance by Li et al. (2008), it is found that the daily noise impact to the indoor environment of the tested dwellings in Beijing can be as higher as 79.2 dBA, and at least 39% of the 1293 people tested are highly annoyed by the traffic noise impact.

In the EU, the *Green Paper on Future Noise Policy* published by EC (1996) indicated that at least 20% of people in the Europe were suffering from the impact of urban traffic noise. According to the latest EU noise survey by EEA (2014) on 33 member countries till 2012, 24% percent of the total EU population are likely to be exposed to road traffic noise in terms of L_{den} of over 55 dBA. It is to note that this number is reported based on the average value of both urban areas and rural areas, it was also reported that in the urban area the percentage of population that are impacted by road traffic noise are much higher than the

rural area, in some highly urbanised countries in Belgium, Bulgaria and Luxembourg, this over all figure can be as high as 75%, while it is also reported that in some due to the development of technology, policy, and law factors, the overall affected population by the road traffic noise from 2007 to 2012 in some well-developed EU countries had dropped obviously, e.g. in the UK, for over 2 percent (EEA, 2014).

The noise impact on the public especially the urban inhabitants in China is also severe. Due to the constant economic booming, the urban population density and traffic noise are also growing dramatically. The government mainly monitors the noise pollution via in-situ measurements. It is found that the noise pollution is also becoming one of the most influential environmental issues in major Chinese cities (China SEPA, 2004). In the meantime, the regional noise survey conducted by the MEP China (2015) in 327 major cities in China in 2014 indicates that in general 28.4% of the monitored urban areas are affected by traffic noise of over 55 dBA, ranked as China's national standard of above lever 3. The situation is getting worse, in 2015, the total region measured with daytime noise level of over 55 dBA had risen to 31.5% (MEP China, 2016).

Although as mentioned above, the traffic noise is a major environment issue in both EU and China, it is also important to note that, the road traffic noise impact in the urban area may have different overall level and distribution pattern, and the rapid urbanisation process in China may enhance the pace of change (MEP China, 2016; EEA, 2014)

2.3.2 Differences in urban sound environment between urban areas with different morphology

As shown earlier, although the overall traffic noise impact in the EU and China are similar, the overall road traffic noise impact in the EU is similar to that of the surveyed urban traffic noise level, it is to note that, if only toi compare the traffic noise impact to the urban agglomerations, the general impact of traffic noise in the EU may be higher than that of China. It was reported that, in the EU, the percentage of population affected by traffic noise in the urban area in the EU can be three times higher than that in the non-urban area (EEA, 2014). In the meantime, as reported in the regional noise survey of 31 provincial capital cities in China in 2014 with population mostly over 5 million as can be seen in Figure 2.15. In most of the cities, the average urban noise impact is within

acceptable range, with day time L_{eq} below 55 dBA; while it is to note that, the only several cities with higher average noise level are not the ones that are best developed that has more motorised vehicles and high-rise buildings; two of the most develop cities in China, Beijing and Shanghai, are both within acceptable range (MEP China, 2016).

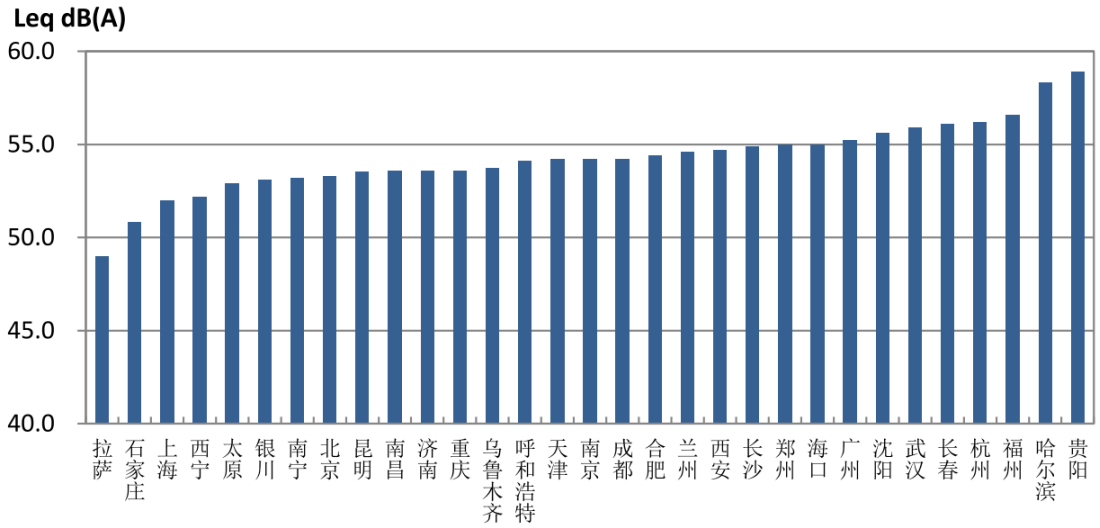

Figure 2.15 The average day time L_{eq} surveyed in 31 China's provincial capital cities. Derived from China Environmental Noise Prevention and Control Annual Report 2016 (MEP China, 2016)

A series of researches has been conducted in last decade to explore the connections between noise distribution and urban morphological features, and it is found that, the traffic noise distribution appears to have a different pattern in cities or urban areas with different morphological features. Kihlman and Berillon (1999), compared different cities with various structures and automobile dependencies, the noise from the traffic flow and the screening of noise due to the buildings are considered. It is found that in general, compact cities are not more problematic than more sprawled ones. Margaritis and Jian (2016) found that the increasing of internal road connectivity could have contributed to the increase of traffic noise in general, and more intriguingly, urban areas with the same level of building coverage could have distinguishing general noise level.

It is also to note that the uneven distribution pattern of traffic flow in Chinese cities is a common phenomenon. By comparing traffic statistics data from AGMA (2006) and Wuhan Statistics Bureau (2006) it can be found that the traffic flow on the highly concentrated main roads in Wuhan are two to three times higher than that of Greater

Manchester, and the vehicles ownership in Wuhan increased 4.7% than the former year. The number of vehicles in most of the Chinese major cities are increasing rapidly (NBS China, 2006), this may bring even further impact on the urban sound environment and the general public, especially along the overcrowded main roads in major cities.

A survey by Tao and Dawson (2002) indicates that the traffic flow along the main roads in Beijing in 2001 can already be considered as saturated, and the flow level is much higher than the designed capacity. Consequently, the hourly equivalent noise level L_{Aeq} along the main roads in the centre of Beijing are unevenly spread and averagely 5.2 dBA higher than the National Standard (GB 3096-93, 1993), while the maximum L_{Aeq} exceeded for 9.2 dBA. Similar results are also found in a research by Zhou (2007), in which the SPL of the traffic noise from the major artery of Guangzhou, a mega city in south China, and it is found that the daytime roadside noise SPL is 6.6 – 9.9 dBA higher than the national standard of 70 dBA. According to Wang and Kang (2011; 2008), The two typical major cities, Greater Manchester in the UK and Wuhan in China, manifest significant disparities in the traffic noise distribution in compared urban areas:

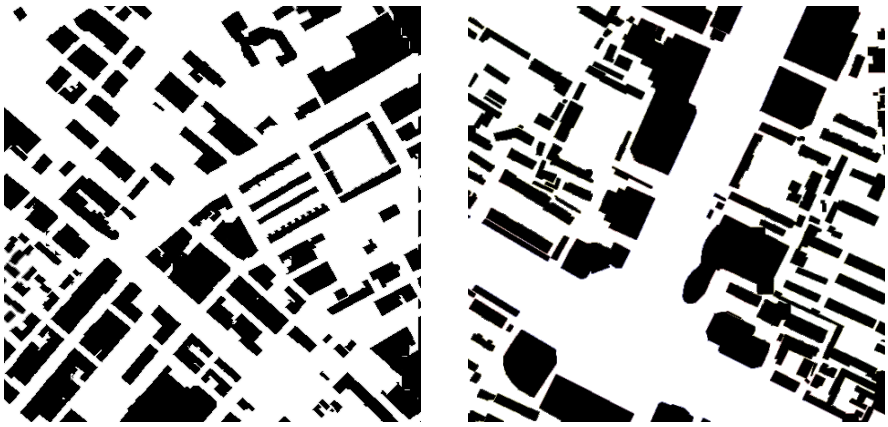

Figure 2.16 Typical urban morphology of mixed use areas in city centres of Greater Manchester, UK (left) and Wuhan, China (right)

- The maximum ground noise level in Wuhan is higher than those in Greater Manchester, due to the urban morphological differences mentioned earlier, especially the highly concentrated main roads and lack of minor roads in typical Chinese urban areas as shown in Figure 2.16.

- Both average and minimum noise level in the shadowed zone in Wuhan is much lower than that in Greater Manchester, due to the screening effect or the high-rise flanking buildings alongside the main roads.
- Regarding building noise impact to the indoor space, the differences in the average and spatial minimum noise indices between these two cities are even higher (Wang and Kang, 2008).

2.3.3 *Major difference between the urban noise sources in typical major cities in EU and China*

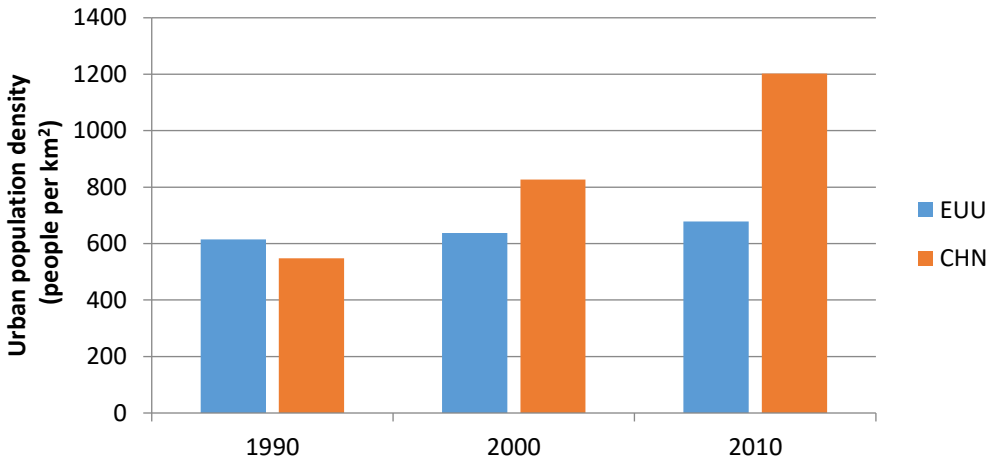

Figure 2.17 Urban Population density of EU and China. The chart is calculated and drawn by the author based on the World Development Indicators derived from the Data Bank service of the World Bank (World Bank, 2017); the urban land area data is derived from the Urban-Rural Population and Land Area Estimates Version 2 by the Centre for International Earth Science Information Network (CIESIN), Columbia University (2013); the urban population is estimated by the World Bank staff based on the United Nations Population Division's World Urbanization Prospects (UN, 2015).

The main concern in this study is the traffic noise, which mainly refers to the direct emissions from the running cars, motorcycles, and heavy vehicles. It is notable that the major cities in China with relatively similar size normally have higher population density comparing with that of the typical European cities, as can be seen in Figure 2.17 (World Bank, 2017), while at the same time the vehicle ownership rate is much lower than that of the latter.

Major cities in China have generally higher population density and lower amount of vehicles compared with that of typical EU cities, say, cities in the UK. According to the

National Bureau of Statistics of China (NBS China, 2001) and the Office for National Statistics UK (ONS UK, 2001). Taking Wuhan of China and Greater Manchester of the UK as examples, the population density in the urban area of Wuhan is 10371 per km^2 (Wuhan Statistics Bureau, 2006), which is much higher than that of the Greater Manchester which is 4024 per km^2 (Pointer, 2005). In the meantime, the vehicle ownership in 2005 is 464.8 per thousand people in Greater Manchester (AGMA, 2006), whereas in the same year in Wuhan, the number is 125.0 per thousand people (WCTPDI, 2006), which is much lower than that of Greater Manchester. The evident differences found in between the two cities in terms of urban density and vehicle ownership imply potential differences in both urban morphology and the traffic distribution patterns.

- ***Difference in the road traffic noise sources***

Wang et al. (2011) indicated that soaring vehicle amount in China especially in major cities demands more roads to be built amid existing high-density urban area. In typical European cities, the road distribution is relatively even, and the vehicles are accessible to a wide range of roads, whereas in typical Chinese cities, the traffic mostly concentrated on the main roads with 6–8 carriageways which are distributed (Zhao, 2002). Tang (2000) and Khakee (1996) found that inside the grids divided by the network of main roads, commonly there are only a few low-traffic roads running through or connecting with the main roads. This road distribution pattern is also part of the master planning system of China since the early 1950's.

In the meantime, with the unevenly distributed road network in typical Chinese cities are designed to meet the increasing transportation demands, the physical forms of the roads also have to be transformed. Zhang and Wang (2014) indicated that due to the rapidly increasing transportation demand, the current main road networks in Chinese major cities, like Wuhan, soon become much more crowded, and in some extreme cases, huge investment is made to build viaducts, a second deck to accommodate the extra traffic flows and break the overheated traffic jam in some road intersections. The total vehicle amount in Wuhan in 2005 had risen 15.3% from the year before (WCTPDI, 2006), which indicates that requirement to new roads is increasing dramatically, and may be caused by the expansion of urban area, as well as the ascending purchasing power of the new citizens, considering that the GDP of Wuhan also increases sharply according to Wuhan Statistics

Bureau (2006, 2014). Calderón and Servén (2004) indicates that the trend of building double-decker roads is further enhanced by the tremendous infrastructure investment during the last decade or so, which are typical to China compare with that of the typical British cities, and the sound environment may thus be further affected and creates dramatically distinctions.

- ***Difference in other transportation noise sources***

In a typical high-density urban district, tram and light rail, together with interregional railway may also introduce regular rail noise to the urban environment. Edmonds (1994) pointed out that in China, the trams and light rails are often built upon the main roads, which cut through the built up areas, running close to the residential and commercial buildings. Similar situation also occurs when the elevated roads are constructed to enhance the transportation capability of the original road on the ground, the situation in the EU is relatively rare (Calderón & Servén, 2004), thus it is essential to avoid or consider the impact of these structures and sources when conducting traffic noise simulation study in major Chinese cities.

Due to the expansion of the urban area around the airports, built-up urban areas may also be partially covered by the fly-over aircrafts. Xie et al. (2014) indicated that Chinese residents are more prone to be affected by the aircrafts noise, and due to the rapid crawling of urban built-up areas and construction of airports, the aviation noise may have impact on the traffic noise simulation results in some cases, and it is essential to take it into consideration when choosing study cases for traffic noise simulation, and to evaluate the traffic noise simulation accuracy in urban areas that are in the vicinity of airports. Neverthless, it is to note that, in both China and the EU, the population exposed to road traffic noise are still well beyond that affected by rail, air and industry nosie source (King, Murphy, & Rice, 2011)

- ***Miscellaneous noise sources***

Table 2.2 In-situ measurement results of typical non-traffic noise in public space in Wuhan, collected by the author in 2008 and 2011 [a]

Noise source type	Location	Distance to source (m)	Measured SPL (dBA)
Food stalls, domestic activities [b] and trace of non-motor vehicle noise	Local roads with little amount of motor vehicles	5–50	67.9–71.5
Noise from the speakers in stores along the commercial street	In the centre of commercial pedestrian street	5–30	70.9–76.0
Noise from pedestrian talking and walking	In the centre of a busy pedestrian square	1–10	66.1–68.5
Noise from exhaust fan	Air conditioner attached on the external wall	2	76.9
Loudspeaker (voice)	Temporary stage for advertisement activity	1	90.0–104.5
Music from loud Speaker	Music CD stores and street stalls	1–4	80.2–86.0
Instrument and loud speaker for Guangchangwu [c]	At the centre of a public open square	3	83.0–93.3
Domestic activities	Amid urban village with no motor vehicle access [d]	5–20	57.3–57.7
Domestic activities and trace of traffic noise	Small roads amid a multi-storey residential area with limited vehicle access [d]	10–50	59.5–59.9
Announcement from the buses' speakers	Platform of major bus station	2	67.7–78.6

[a] Calculation with only considering the attenuation of geometric divergence defined in ISO 9613-2: $A_{div}=[20lg(d/d_0)+11]$ dB (ISO, 1996)

[b] Observed domestic noise includes audible sound from household cooking, talking, instruments playing, TV and music playing and sound from animals etc.

[c] Guangchangwu (Square Dance), a typical type of outdoor exercise activity performed by middle-aged and senior people, normally occurs in the open public space in Chinese cities. The music played for the square dance from the loudspeakers and instruments is one of the major complaints of noise (Beijing Review, 2013). The SPL measured here is from a typical square in the evening near a major commercial building in Wuhan.

[d] There are no motor vehicles during the measurement period, but due to the location of the urban villages, the measurement may be affected by the background traffic noise from remote main roads and planes flying over.

Although the selected measuring points are close to the main roads in the studied sites, the mentioned and non-mentioned miscellaneous noise sources below may still be taken into consideration while estimating the accuracy and efficiency of the current noise mapping performance in typical Chinese urban sound environment.

Except for the noise from the vehicles, there is a variety of event noise sources in some of the researched sites that may affect the measurement result, which is mostly recorded and eliminated from the study area. Nonetheless, it is still important to take the miscellaneous community noise into consideration in some urban scenarios, especially the pedestrian dominated areas. In the regional noise survey conducted by the Wuhan Environmental Protection Bureau (2011), it is reported that 75.7% of the noise related complaints are from miscellaneous civic noise sources. The complained noise sources include air conditioner fans, interior decoration and building refurbishment, loudspeakers in the public space and shops, and various community events. A survey and measurement of some commonly perceived community noise sources were conducted during the in-situ measurement in 2008 and 2011, as listed in Table 2.2. Beyond the noise from the civic activities, the noise from the construction sites of buildings and civil infrastructures may also be a source of background noise. It was reported by Barboza (2011) that there were around 5700 sites were under construction simultaneously in the entire city.

2.4 State of the art of noise mapping techniques

2.4.1 The State of the art of noise mapping in the EU

Environmental noise as a major source of annoyance and complaints in the modern urban areas (MEP China, 2011; WHO, 2009; EC, 1996) is sometimes hard to define for researchers due to its largely subjective nature, but can nonetheless be broadly described as the “unwanted sound” that may do harm to human or animal life, which can cause senses of interference, distraction and irritation (Murphy & King, 2014; Hendy, 2013).

Following the publishing of Green Paper on Future Noise Policy (EC, 1996), the Noise Mapping techniques began to develop rapidly in EU countries based on a series of calculation methods specified in a variety of international (ISO, 1993) and national

standards, for various noise sources including aircraft (ECAC 1997), road (H.G. Jonasson; S. Storeheier, 2001; UK DfT, 1988)railway (UK DfT, 1995) and industry (DAL, 1987). In different criteria, the procedures and indices of noise calculation often vary (J. Kang, 2006).

The *IMAGINE–State of the Art* (AEAT NL, 2004) indicates that, noise mapping is not an entirely new activity in the 21st century, since the 1970s the concept and relevant technology it has been used to produce noise maps in some EU countries, especially when the computer aided noise mapping techniques are rapidly developed and put into practice for the simulation of urban noise in recent decades.

2.4.1.1 EU policies and directives

The *Environmental Noise Directive* (END) *2002/49/EC* was published by the European Commission (2002) as a new framework for noise policy, which aims at using strategic noise mapping to determining the noise exposure by applying noise indicators and assessment methods common to member states. It was reviewed by EC in 2009 and is the guideline of noise assessment practices of the EU Member States. The END 2002/49/EC marks the beginning of the large-scale computer-aided noise assessment activities across the EU. It draws a blueprint for the noise calculation methods and strategic noise mapping practices for the EU states with or without existing national calculation methods, and is mainly based on the following three fundamental principles:

- *"The harmonisation of noise indicators, noise evaluation, calculation methods, measurement methods, monitoring, strategy, and legislation;*
- *"Collecting of information on noise in the form of noise maps;*
- *"Informing the public of the current noise situation and on strategy and financing of nois*e reduction *(EC, 2002)."*

The traditional methods of noise mapping based on measurement results are not feasible in fulfilling the requirement of END 2002/49/EC. It is to note that, although according to the END, the yearly average noise level at all locations for assessment purpose is required, while in practice this is not practical. The amount of noise measurements and accessibility of the monitored locations are out of controllable range in the urban area. Therefore the

END 2002/49/EC designated in Annex II (EC, 2002) that, only the computer aided calculation methods are applicable in the practices of predicting noise levels (WG-AEN, 2007).

2.4.1.2 Concept and principle of noise mapping

According to END 2002/49/EC (EC, 2002) for the purpose of assessing the impact of noise on a certain urban area, the noise mapping data on an existing or predicted noise situation shall be presented in terms of noise indicators. The END 2002/49/EC recommends the energy-based noise indicator L_{den} and L_{night} as the indicator for day-evening-night and night noise assessment across a year. As being defined by the Ireland Ministry for the Environment (2006) in the Ireland *Environmental Noise Regulation* according to the END 2002/49/EC (EC, 2002):

> *"'Noise mapping' shall mean the presentation of data on an existing or predicted noise situation in terms of a noise indicator, indicating breaches of any relevant limit value in force, the number of people affected in a certain area, or the number of dwellings exposed to certain values of a noise indicator in a certain area."*

In another word, the noise mapping is majorly a strategic tool for the assessment of noise environment and the policy and strategic making in relevant fields.

The strategic noise mapping was defined by EC (European Commission) (2002) as an assessment or prediction tool for the exposure of noise of different noise sources in a certain area, which includes most of the attempt to indicate the location dependent noise situation on the background of the topography of the site (ARPAT, 2007). According to the WG-AEN (2007), there are three types of beneficiaries of the strategic noise mapping in the EU: the EC as the policy maker who could utilise it as an assessment tool in prospective policy making; the general public of the EU; the local decision and action plan makers who can access the noise exposure information expediently.

2.4.1.3 Definition of the noise indicators

There are a series of environmental noise indicators adopted in the noise mapping practices in the EU as listed in Table 2.3, for most of the EU calculation methods, the

temporal noise indicators are actually different forms of the L_{Aeq} of a certain period according to the calculation requirement as shown in Equation 2.2 (Murphy & King, 2010). On the other hand, in the UK national standard CRTN (UK DfT, 1988), a statistical noise indicator L_{A10} is adopted to present the total A-weighted noise level of 18 hours (6:00-24:00) of a day as shown in Equation 2.3 (Abbott & Nelson, 2002).

Table 2.3 Explanation of several commonly used convention noise indices

Index	Description
L_{den}	The day/evening/night long-term average sound pressure level.
L_{day}	The daytime (07:00–19:00) A-weighted long-term average sound pressure level.
$L_{evening}$	The evening time (19:00–23:00) A-weighted long-term average sound pressure level.
L_{night}	The night time (23:00–07:00) A-weighted long-term average sound pressure level.
L_{Aeq}	The equivalent continuous A-weighted sound pressure level.
L_{10}	The level of noise exceeded 10% of the time during the test period.
L_{90}	The level of noise exceeded 90% of the time during the test period.
L_{max}	The maximum noise level recorded over the test period.
SEL	Sound Exposure Level: the equivalent noise level normalised to 1 second.

Source: Strategic environmental noise mapping: methodological issues concerning the implementation of the EU Environmental Noise Directive and their policy implications (Murphy & King, 2010)

$$L_{den} = 10 \times log_{10}\left(\frac{1}{24}\right)\left(12 \times 10^{L_{day}/10} + 4 \times 10^{(5+L_{evening})/10} + 8 \times 10^{(10+L_{night})/10}\right) dBA \quad 2.1$$

$$L_{Aeq,T} = 10 \times log_{10}\left(\frac{1}{T}\right)\int 10^{L_{(t)}/10}\, dt \;\; dBA \quad 2.2$$

$$L_{A10,18h} = \frac{1}{18}\sum_{t=6}^{t=23} L_{A10,t} \quad dBA \quad 2.3$$

The difference in the calculation methods of the indicators may cause a slight gap between the actual results calculated (Abbott & Nelson, 2002). The recommended correction from has been adopted by mainstream calculation packages as an optional choice when selecting the noise indicators when using the CRTN method (DataKustik, 2012a).

2.4.2 *Data acquisition for strategic noise mapping*

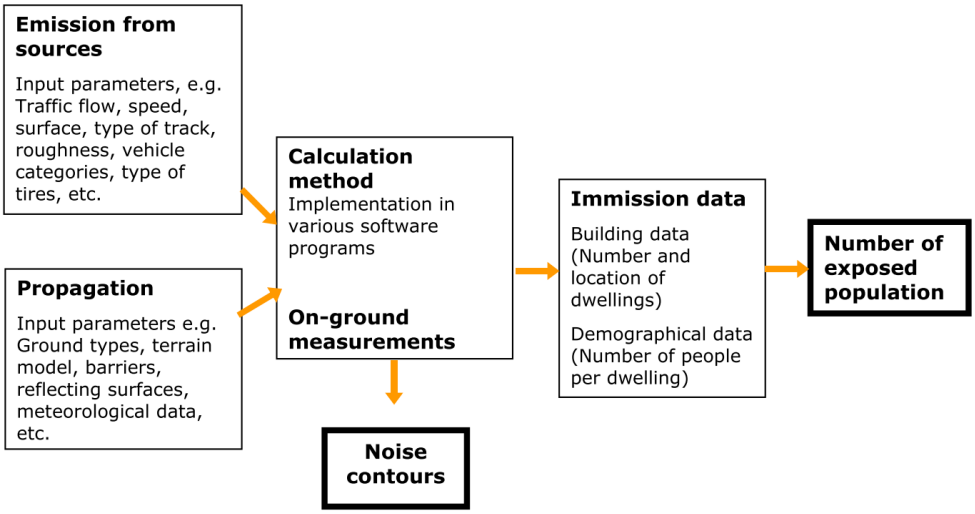

Figure 2.18 A conceptual diagram of the noise mapping process. Derived from EEA – *State of the art of noise mapping in Europe* (ETC/TE EEA, 2005)

As mentioned in the *Good practice guide on noise mapping* produced by the WG-AEN (2007) that, data acquisition is one of the major tasks for the EU member states in the strategic noise mapping practice. As there are different ways of making the noise maps, if noise modelling were chosen as the method, then in the process of noise-mapping a wide range of input data needs to be acquired.

According to the EEA *State of the art report on noise mapping* (ETC/TE EEA, 2005), the data acquisition should focus on three aspects: the emission from source, the data about the propagation path, and the noise emission or nuisance data for the purpose of noise impact evaluation as can be seen in Figure 2.18.

In the European countries, the digital databases of topography, land-use, buildings or traffic flow are usually obtainable from local or national authorities and some commercial data suppliers — in some cases, the data have to be bought from the data provider (EEA/ETC-LUSI, 2005). Some tools based on GIS system to support the transformation and storage of data and to speed up the process of noise mapping are developed or under

developing (CSTB, 2007). There are some other ways of acquiring the geographical data if the digital database is not available or complete, e.g. in-situ observation, aerial photographs, measurement or monitoring of unknown noise sources and buildings (ARPAT, 2007).

It can be seen that, for accurate noise modelling, the amount of data needed is huge. There are also complaints about the noise mapping practice for being considered expensive because of its low output compared to the high inputs in terms of data collection (ARPAT, 2007).

2.4.3 Noise mapping practices and action plans

2.4.3.1 Noise mapping practices in the EU

Following the publication of the END 2002/49/DC (EC, 2002) and the development of a series of computer aided noise mapping methods and packages, there has a movement of noise mapping in the entire EU. The EU member states are requested to fulfill the obligation under the END 2002/49/DC to map the traffic noise emission of major roads every five years. Before and after the first five years (2002-2007) of noise mapping actions in the EU countries (EC, 2002), there has been a series of reports published following some important noise mapping research projects and related plans:

- *Noise climate assessment: A review of national and European practices*

The report is based on a project carried out by the UK Department for Environment, Food and Rural Affairs (Defra), which covers the initiative noise mapping development and practices at the national and regional level. The noise related legislation in several European countries is also introduced (UK Defra, 1999).

- *IMAGINE–State of the Art*

It is a report produced in 2004 for the Improved Methods for the Assessment of the Generic Impact of Noise in the Environment (IMAGINE) project, which is coherently connected with the Harmonoise that designed for the development of the Harmonoise noise simulation method (Salomons et al., 2011). This report gives an overview of the

state-of-the-art calculation methods, regulations, and theories used in the practice of noise map production in different European countries (AEAT NL, 2004).

- *State of the art of noise mapping in Europe*

It is proposed by the European Environment Agency (EEA) to outline the data collection and noise mapping methods adopted in EU countries. The European Topic Centre on Terrestrial Environment (ETC/TE) is the main contributor to the noise topic of this report (ETC/TE EEA, 2005).

- *Good practice guide for strategic noise mapping and the production of associated data on noise exposure*

It is the version 2 of a position paper produced by the *Working Group of European Commission* that based on the Assessment of Exposure to Noise project (WG-AEN). WG-AEN (2007) believes that in the second phase of the EU noise mapping action plan, more detailed modelling and assessment measures may be required especially at the local government level. This report introduces major aspects of the noise mapping methodologies regarding the END 2002/49/EC (EC, 2002).

A series of traffic noise calculation methods are developed or adopted in the EU noise mapping practices following the END 2002/49/EC (EC, 2002) and are widely available in current noise calculation packages in the EU (Garg & Maji, 2014).

2.4.3.2 Noise mapping practice in China

Due to the economic booming in China in the last decades, the urban population density and traffic noise are also growing rapidly. The noise impact caused by certain noise sources may affect more people than in EU due to the relatively higher building density and height (Ma and Chen, 2002); while due to the lack of tools and method, noise mapping practice in China is still in a relatively preliminary stage in comparison with that of the Europe.

Figure 2.19 The first official noise map of China, a 12.7 Km^2 pilot noise-mapping project combining multiple methods, including in-situ measurement, EU noise mapping technique and GSI. Source: Beijing Daily (Cai, 2009)

Urban noise control has gained increasing attentions in China's national five-year plans as part of the efforts of mitigation of the impact of environmental pollutions. Although the *National Environmental Protection Plan in the Eleventh Five-Years (2006-2010)* (State Council of China, 2006) was aimed to intensify noise pollution control via a series of measures, noise mapping was yet a national strategy. Some of the relatively more developed cities though, e.g. Guangzhou and Beijing has initiated small-scale noise-mapping practices since 2006, and a series of issues is found in the application of mainstream noise mapping techniques (Cai, 2009; Zhou, 2007). A sample noise map of a urban area in central Beijing is demonstrated in Figure 2.19.

Regarding the noise calculation method and packages, the research and policy making of traffic noise calculation is also initiated. the Ministry of Environment Protection published the national standard *HJ 2.4-2009 Technical Guidelines for Noise Impact Assessment* in 2009 (MEP China, 2009), in which a brief method of noise assessment, measurement, and calculation methods are proposed.

In the *National Environmental Protection Plan in the Twelfth Five-Years (2011-2015)* (State Council of China, 2011), the topic of noise mapping is mentioned only in the working report of the research framework as one of the measures of creating quiet community and quiet cities in experimental zones and cities, especially major cities (J. Wang, 2010). Although deemed as necessary by the strategy and policy makers, there are still difficulties in the application of EU noise mapping technique in major urban areas of China, the development of an applicable national noise-mapping calculation method is necessary and of great significance.

2.4.4 Comprehensive reviews on state of the art of noise mapping technology

A series of comprehensive reviews are published by researchers and institutions upon years of noise mapping practices, the pros and cons of the methods are compared (Garg & Maji, 2014; Licitra, 2013; Probst, 2010a; Kephalopoulos, Paviotti, & Gergely, 2008; Nijland & Van Wee, 2005; Steele, 2001). From the reviews, it can be seen that generally since the publication of the Green Paper 1996 (EC, 1996), especially since the publication of END 2002/49/DC, there has been a huge leap in the theory and practice of the noise mapping in the EU and some other developed countries.

It can be seen that as far as the efficiency and accuracy of noise calculation methods are concerned, in-situ environment conditions are not always sufficiently considered in the calculation process, e.g. traffic composition and temporal composition, road conditions and transportation facilities, the conditions of the propagation path and receiver side, i.e. the urban environment where the methods and packages are utilised. For instance, for the calculation of the ground effect, the ISO 9613-2 (ISO, 1996) and most of the EU traffic noise calculation methods process the ground surface as fully or partially absorptive surface, and only considers the calculation of ground effect at limited distance close to the source and the receiver; the actual reflective waves from the ground surface are largely ignored, except in the Harmonoise model (Salomons et al., 2011) and the Japanese method (Yamamoto, 2010).

Moreover, besides the limitations in the calculation configurations of the current EU calculation methods, the energy based ray tracing algorithm for noise transmission applied in most of the current methods also have limitations in dealing with complicated

reflection and refraction scenarios (Probst, 2014), and alternative methods are proposed to enhance or reduplicate the current algorithm (Kang & Huang, 2005) in special urban conditions or to fulfil different strategic proposes (Bennett et al., 2010; King & Rice, 2009).

A series of reviews on the accuracy of current noise mapping techniques are published in recent years on the inaccuracy occurs in different phase of the noise-mapping practice from different perspectives (Arana et al., 2011; Murphy & King, 2010; Probst, 2010b), which will be discussed in latter part of this chapter.

2.4.5 State-of-the-art Noise calculation methods and packages

Since 1952, the road noise prediction models are developed (Bolt et al., 1952) and continued to be refined for road noise simulation based on the traffic flow data (ETC/TE EEA, 2005). There has since been a series of calculation models developed in some developed countries, especially since the late 1990s due to the increasing car ownership and public interests in environmental matter (Steele, 2001).

The calculation methods adopted according to the END (EC, 2002) in the EU noise mapping activities vary across the member states, UK (UK DfT, 1988), Germany (Germany FMoT, 1990), Switzerland (Heutschi, 2004), Scandinavian countries including Norway, Denmark, Sweden and Finland (Kragh et al., 2006), France (Sétra, 2009), some commercial company like 01 dB(CSTB, 2000), and the Harmonoise method (Salomons et al., 2011). US (FHWA, 2004) and Japan (Yamamoto, 2010) have also developed their own traffic noise calculation models. The latest of some state-of-the-art traffic noise calculation method published in recent years is the CNOSSOS-EU 2012 (Kephalopoulos, Paviotti, & Anfosso-Lédée, 2012). Amongst 20 member states that had provided the noise assessment methods they had used, 5 states used their own national methods, 7 states used interim methods according to Annex II of END (EC, 2002), and 8 states selected the methods based on the noise source (Paviotti and Kephalopoulos, 2008).

The basic algorithms of most of the current noise calculation methods are similar, as can be seen in Table 2.4. The differences that lead to the disparities of calculation results mainly lie in the calculation method of the road source level and a series of corrections

occurred in the path of propagation (Garg & Maji, 2014). A series of noise simulation packages were developed by deploying various types of digital input data types and national or international calculation methods. For instance, Cadna/A (DataKustik, 2012a) as one of the widely used environmental noise packages, in the UK it adopts the the British national method for road noise calculation CRTN (UK DfT, 1988).

Table 2.4 Major noise mapping methods adopted in the EU, US and Japan. Source: Steele (2001)

State/Company	Name Abbreviation	Descriptor	Weight
UK	CRTN	L_{10} (1h/18h)	dBA
Germany	RLS 90	L_{eq}	dBA
EU States	Harmonoise	L_{eq}	dBA
Switzerland	EMPA97	L_{eq}	1/3 octave dBA
Scandinavian[5]	Nord2000	L_{eq}	dBA
France	NMPB2008	L_{eq}	dBA
EU States	CNOSSOS-EU 2012	L_{eq}	dBA
01 dB (France and Belgium)	MITHRA	L_{eq} (8-20h)	Octave dBA
US	FHWA	L_{eq} / quasi L_{10} (18h)	1/3 octave dBA
Japan	ASJ-1993	L_{eq} / quasi-L_{50}	dBA

2.5 Uncertainty in the noise simulation process

2.5.1 Typical noise simulation process

The major concern of the noise calculation can be divided into three major aspects, the source, propagation path and receiver side as can be seen in Figure 2.18, whereas in this research, the non-standard scenarios of the traffic noise source are not considered, in which the corrections of speed, the road surface, and the gradient are to be considered according to the site conditions. In this research the focus is the applicability of the mainstreams noise calculation methods and packages when in typical Chinese urban

environment. Thus, the major concern is the potential inaccuracy that may occur in the calculation of attenuation in the propagation path.

To acquire acceptable accuracy level for traffic noise calculation, there are a series of procedures to be followed, though the sensitivity of the results may also be affected by the uncertainty in each step. In CRTN, the correction for noise attenuation shall be calculated according to the following Equation 2.4 and 2.5 (UK DfT, 1988):

$$L_{receiver} = L_{source} + \Delta_d + \Delta_{scr} + \Delta_G + \Delta_{ref} + \Delta_{\,view\ angle} \quad 2.4$$

$$\Delta_{\text{total}} = \Delta_d + \Delta_{scr} + \Delta_G + \Delta_{ref} + \Delta_{\,view\ angle} \quad 2.5$$

Where the Δ_d shows the atmosphere attenuation caused by geometric divergence; the Δ_{scr} shows the attenuation due to screening effect of any obstacles; Δ_G indicates the attenuation caused by the ground effect, the Δ_{ref} indicates the correction due to the reflections, the $\Delta_{\,view\ angle}$ adjusts the total corrections with considering the view angel from the road source to the receiver.

Similarly, according to ISO 9613 (ISO, 1996), the total attenuation can be calculated as shown in Equation 2.6:

$$A = A_{div} + A_{atm} + A_{gr} + A_{bar} + \Delta_{ref} + A_{misc} \quad 2.6$$

where the attenuation caused by five major the physical effects are considered including the geometrical divergence A_{div}; the atmospheric absorption A_{atm}; the screening by obstaclesA_{bar}; and the ground effect A_{gr}; the reflection from reflective surfaces Δ_{ref} and the miscellaneous attenuations A_{misc}caused by housing, industrial sites or foliage, etc. It is to note that, the calculation of both methods are very similar except that the CRTN (UK DfT, 1988) did not take the meteorological conditions and miscellaneous sources of corrections into consideration, while this is solved in state-of-the-art noise simulation packages by combining the calculation method and a series of specific configurations of handling the real-site conditions. For instance, in Cadna/A, a modelling option of the transparency ratio of the buildings is especially helpful when the partially screening

structures are involved, such as industrial plants, or urban village or temporary buildings with thin walls or wide openings.

It can also be seen that there are a series of conditions that may cause inaccuracy need to be considered in the calculation considering the limitation of the calculation methods. The accuracy level according to ISO 9613-2 (ISO, 1996) when all screening and reflection effects are not considered, is within ±3 dBA when the mean height of the source and receiver h is lower than 5 m, and as low as ±1 dBA when the receiver is less than 100 m from the source when 5 m < h < 30 m. A series of studies shows varied accuracy level and found a series of different causes of the inaccuracy.

2.5.2 Previous research on noise simulation accuracy

It is believed that in a typical simulation system, there are four aspects where the uncertainties may occur: uncertainty in input, propagation uncertainty due to uncertainty in input, uncertainty due to different models and uncertainty in predictions due to uncertainties in evaluation data. All uncertain aspects are interrelated, for instance, while validating the simulated noise level, uncertainty may also lie in the results of the environment noise measurement (Isukapalli & Georgopoulos, 2001).

WG-AEN (2005) listed 3 major factors that may affect the accuracy of results of strategic noise mapping: technical, economic impact and public perception. Amongst which it is estimated that the ideal technical accuracy shall be within 2 dBA, while empirical researches show rather diverse results as can be seen below.

2.5.2.1 Same package, different calculation methods

Wolde (2002) analysed a series of empirical research and found that while using different calculation methods, and reported that the disparity at certain receiver point could be as large as 5 Dba. The accuracy of the results differs significantly. Berg and Gerretsen (1996) also found 6–10 dBA difference while applying Austrian, German, French or Dutch methods on road traffic noise calculation in a series of different traffic situations. The greatest calculation error can be as high as 15 dBA according to Nijland and Wee (2005).

2.5.2.2 *Same calculation method, different packages*

When conducting noise mapping calculation using different packages with the same method, the specific configurations may also increase the variations among the calculation results. Hepworth (2006) compared the calculation results of several commercial packages using the British method CRTN by conducting calculation in an area of one square kilometre, and the result shows that the difference ranging averagely from 2 dBA to 11 dBA on individual points. Nijland and Wee (2005) reviewed a variety of studies on the calculation accuracy and reported that by adopting different commercial noise mapping packages, the inaccuracy level could be as high as 6 dBA (Mank, 2000) and may mainly be caused by the specific interpretations in the packages adopted.

Garg and Maji (2014) deemed that the geographical divergence and the atmosphere absorption are the two main factors that generating noise attenuation. The latter is only considered in some calculation methods but not separately listed in CRTN. The method of calculating the geometric divergence correction or the distance correction is determined mainly based on the slant distance *d'* according to Chart 7 of CRTN (UK DfT, 1988) as shown in Equation 2.7 :

$$\Delta_d = -10Log_{10}\left(\frac{\mathrm{d}'}{13.5}\right) \text{ dBA} \qquad 2.7$$ [1]

Jian and Huang (2005) found that the accuracy level of two methods are similar within near field, but along with the distance increasing between source and receiver, the underestimation of the SPL is up to 4 dBA in the square and 3 dBA on the street.

According to ISO 9613-2 (1996), generally for the calculation of attenuation caused by the ground effect, the path of the propagation line is divided into three parts, among which the ground surface close to the source line and the receiver mainly affects the propagation curving downward, thus the ground effect is mainly applicable to the relatively flat

[1] The distance of 4 m is adapted instead of the real slant distance of the receiver locates less than 4 m from the effective source line.

ground, horizontal or constantly inclining. Therefore, the inaccuracy may not be clear when noise transmission is calculated above the curvy ground with employing the ISO 9613-2 and similar methods. A fundamental difference between the Harmonoise model, NMPB-2008 and ISO 9613-2 was found regarding the calculation of the ground effect (Defrance, 2009), the Harmonoise model is considered as a "coherent" model, as it records the coherent summation of the direct wave and the ground reflected wave, and it predicts a +6 dB increases of noise level for a receiver near to the source by using the sound power output under free-field radiation (Kephalopoulos et al., 2014). Jian and Huang (2005) also indicated that the simplification way of the calculating the ground effect in noise mapping software may bring systematic errors.

2.5.3 Specific accuracy issues

2.5.3.1 Calculation of higher order reflections from parallel surfaces

For large-scale noise mapping practices, the high-orders of reflection tend to be simplified or neglected in many calculation methods, in END (EC, 2002), it was also noted that: "Some existing methods will also have to be adapted as regards the exclusion of the façade reflection." In some calculation method, e.g. CRTN (UK DfT, 1988) and RLS-90 (Germany FMoT, 1990), the calculations of reflection order higher than one are conducted using correction value.

To save the calculation time in the large scale noise mapping practice, the default reflection order is even set to 0 by default in some noise calculation packages, e.g. Cadna/A, but it is recommended to change it according to the calculation needs (DataKustik, 2012a).

According to the specification of some of industrial calculation methods, e.g. ISO 9613-2 (ISO, 1996), façade reflections can be calculated using the mirror image method. The image source method is based on the assumption that the reflecting surface is a mirror-like flat "acoustically", and it can be replaced by an additional source in a mirrored position, is recommended to be applied in the calculation of multiple orders of reflections (Probst, 2014). Licitra (2013) deemed that due to the nature of the ray-tracing calculation method adopted in major noise-mapping methods, theoretically increasing the reflection

order is helpful to increase the accuracy level especially when the reflection from the building façades and barriers is countable.

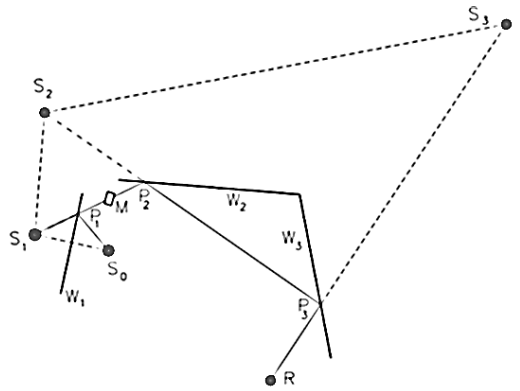

Figure 2.20 A typical 3rd order reflection using mirror source method. Source: (Probst, 1998)

The higher reflection orders are worth mentioning for the reason of accuracy, however, the consumption of time also increases because of more surrounding façades to be taken into consideration. The paths of ray can also be displayed throughout calculation of reflections of high orders in calculation packages such as Cadna/A (DataKustik, 2012a), Figure 2.20 illustrates three mirror image sources calculated for a typical 3rd order reflection in Cadna/A. In the same time, in a research by Kang and Huang (2005), it is tested that the maximum reflection order of three is sufficient and most time efficient for the regular calculations in the typical EU urban acoustic environment. As can be seen in Figure 2.21. Probst (2010) also suggested that a higher reflection order is not always necessary.

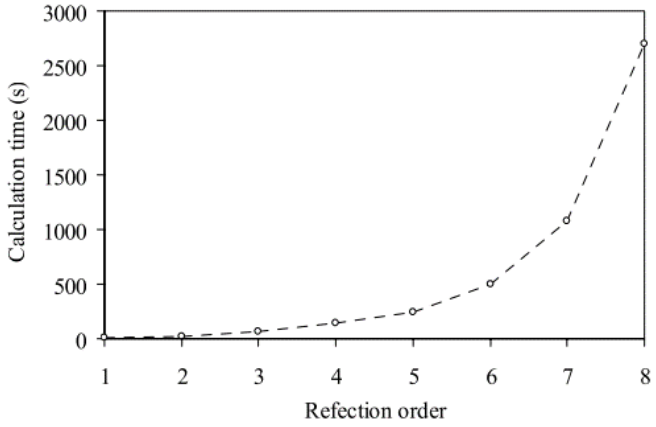

Figure 2.21 Case study on calculation time consuming with increasing reflection order Source: Kang & Huang (2005)

2.5.3.2 *Attenuation correction of the ground effect*

The ground effect is caused by the interference of the reflected noise level and the directly transmitted noise from the source (ARPAT, 2007). Kephalopoulos et al. (2014) indicates that most of the current noise-mapping methods do not coherently combine the ground effect to the direct wave and the reflected wave, and it is found that for a receiver close to the noise source the increase of SPL due to the neglected ground reflection could be as large as +6.0 dBA especially at low frequencies (Garg & Maji, 2014). The actual reflection from the ground surface is largely ignored by the mainstream methods (Garg & Maji, 2014).

A ground absorption coefficient *G* is introduced in most of the EU calculation methods and packages to calculation the correction caused by the ground effect. Practically when there are absorptive surface areas between the noise source and the receiver, majorly only the absorption effect is considered. The calculation of ground absorption is dealt by two means in the Cadna/A, the ground absorption coefficient which defines the global ground absorption setting of surveyed terrain, and the ground absorption map which can be set up by patches of ground absorption areas or ground absorption map (DataKustik, 2007).

The Harmonoise (Salomons et al., 2011) and the Japanese ASJ RTN-Model 2008 (Yamamoto, 2010) also considers the reflected sound rays in the calculation by considering extra coefficient describing the physical condition of the ground into the calculation.

2.5.3.3 *Reflection in the street spaces*

It is a well-proven method to calculate the sound levels on the roads with complicated and closed façades for only up to the first or second order of reflections, then a correction value of multi-reflections are added to the road emissions, especially for large projects for the sake of decreasing the time consumption of calculation. For instance, a correction of 1.5 dBA is recommended in Cadna/A for the calculation of higher orders of specular reflections (DataKustik, 2012a), which is also a widely used in major calculation packages (Probst, 2014).

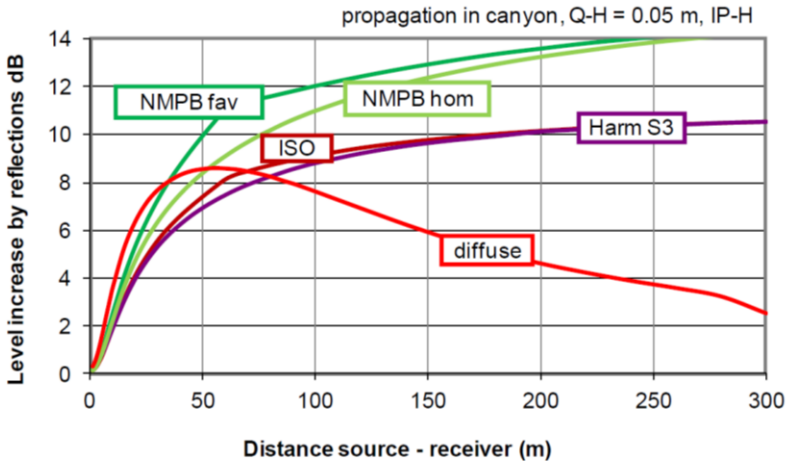

Figure 2.22 The increase of calculated SPL with different standardised methods (Harmonoise, NMPB and ISO 9613-2) applying mirror image method and with a radiosity model for diffuse reflections. Derived from Probst (2014).

In the other hand, in a typical street canyon scenario due to the multiple reflections in-between the flanking façades, the calculation inaccuracy along with the increasing of source-receiver distance may not easily be mitigated by increasing the reflection order using the mirror image method. Kang (2000) applied the radiosity method in the calculation of sound propagation in the street canyon and found that when the diffusing boundaries of the street canyon are replaced with geometrical ones, the sound attenuation along the street canyon tends to be decreasing significantly. Probst (2014) also compared the results of using a series of standardised calculation methods that uses the mirror source method, and the result of a calculation using the radiosity method for diffusing reflection. As can be seen in Figure 2.22, the increase of SPL along with distance reaches the maximum at a close distance and becomes less when the flanking façades are diffusing.

2.6 Correlation analysis and a parametric study approach

2.6.1 Researches on urban environment and urban morphology

A framework to integrate the urban structure in terms of land use, transport, urban form and the urban environment pollutions (Burton, Jenks, & Williams, 2004). Studies are conducted to explore the relationship between the urban form and the urban environment, especially the air polution is not new (Marquez & Smith, 1999; Newton, 1997). There has

since been a series of studies on the correlation between the urban morphology and the urban environmental issues including solar energy (Sarralde et al., 2014; Hachem et al., 2011), energy consumption, air quality in the urban area (Edussuriya et al., 2011; Yuan et al., 2014) or along the urban roads (Bowker et al., 2007), day lighting (Leder et al., 2006), ventilation (Letzel et al., 2008; Barclay et al., 2012), and urban noise (Silva, Oliveira, & Silva, 2014).

As a multidisciplinary research field, a variety of novel research methods are proposed and adopted in relevant researches. For instance, The Artificial Neural Networks (ANN) method is employed to study the influence of urban indices on the sound ambience of the streets (Souza & Giunta, 2011). Tang and Wang (2007) researched both the noise and the air pollution in the pre-colonial historical Chinese city of Macao using GIS method, it is found that the narrow roads across the historical areas tend to have lower noise impact while the street canyon effect increases the concentration of CO pollution. Ariza-Villaverde et al. (2014) studied the correlation between total noise level and a series of urban morphological parameters using the joint multifractal analysis method.

It is to note that, due to the lack of mature environmental noise simulation tools, there was only few researches that have explored the potential influence of urban form on the distribution of traffic noise before 2007 (Tang & Wang, 2007; Kang & Huang, 2005). With the development of strategic noise mapping methods and packages in the first decades of the 21st century, researchers have made a series of successful attempts to study the correlation between the environmental noise impact and urban morphological and typological features. Marry and Baulac (2010) associates the factors of urban typology and building type with the subjective perception of noise qualitative in a series of urban public spaces. Ariza-Villaverde et al. (2014) found that the SW/H ratio and the total noise pollution has a certain level of correlation. Margaritis & Kang (2016) found that the green space ratio and the general structure of the city are partially related with the traffic noise levels.

2.6.2 Urban form typology and categorisation

2.6.2.1 Difference forms of road grid and urban texture

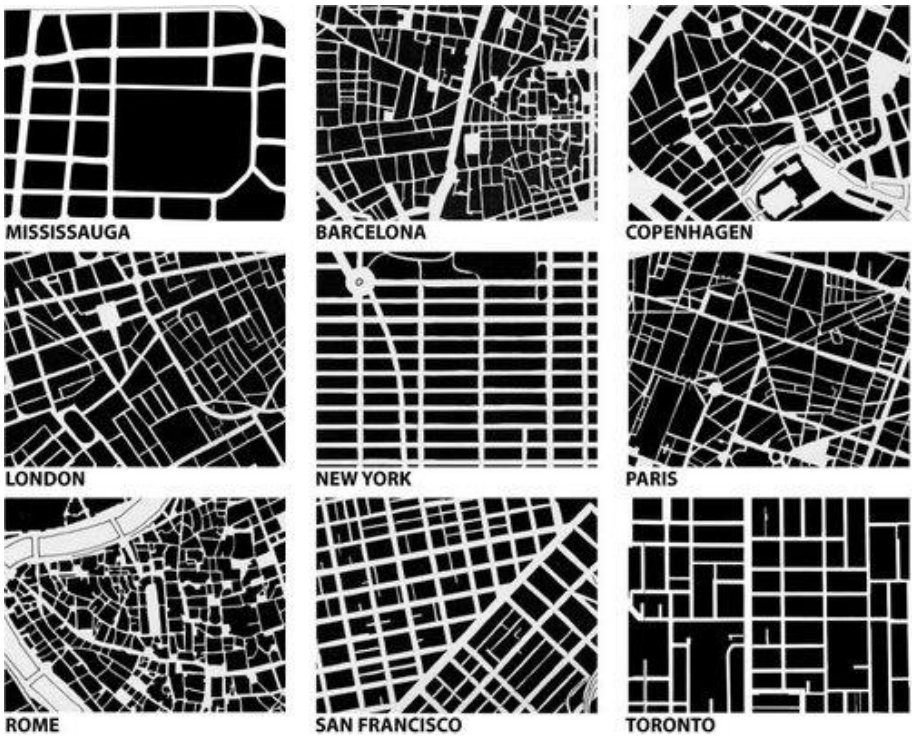

Figure 2.23 Some representative urban forms of major historical and modern calcites Source: (Jenkins, 2012)

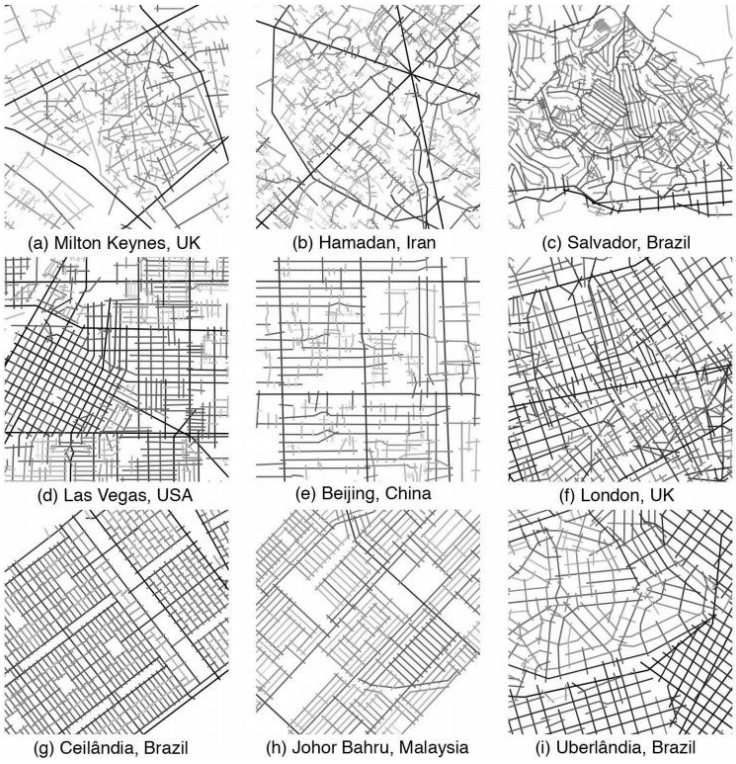

Figure 2.24 The urban network grid of the world cities. Derived from Tobergte & Curtis (2013), the darkness of the grey lines marks the grade of the road in the hierarchy system, and the darkest ones are the main roads.

It can be seen that, from east to the west, from ancient to modern cities, the urban morphology in terms of road pattern and building form has distinct features (Jenkins, 2012). Figure 2.23 shows the distinctly varied urban forms in terms of road network topology and accordingly the urban texture patterns are distinctive in different cities.

The hierarchy and structure of the road system also vary and hence may also determine the traffic noise distribution pattern and the building forms. Figure 2.24 shows the road network grid of nine cities worldwide, from left to right, the degree of aggregation or the irregularity increases; from top to bottom, the structure tends to change from tree-style to grid. (Tobergte & Curtis, 2013)

2.6.2.2 Urban form categorisation

It could be seen that there are huge differences in existing urban morphology in terms of road grid system, road hierarchy, and the urban fabric scale, etc. It is, therefore, essential to find the definitive parameters that categorise the huge differences among different urban form typologies.

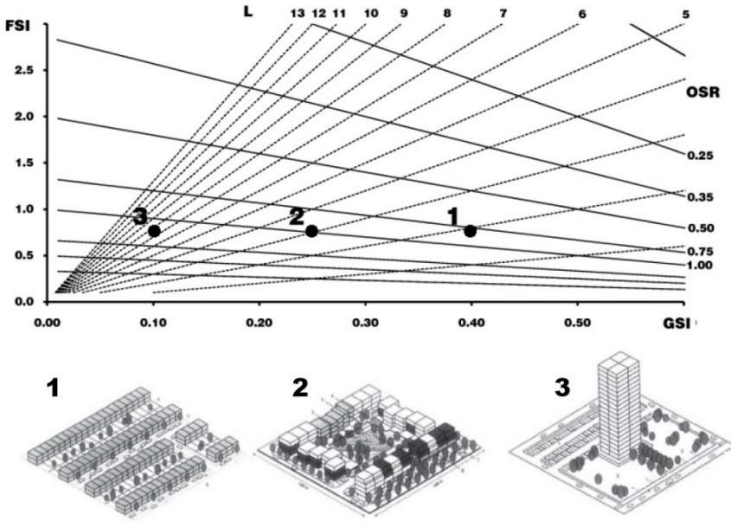

Figure 2.25 The Spacemate is used to illustrate three types of distinct building forms with the same FSI (Pont & Haupt, 2009; Mozas & Per, 2006)

A series of attempts has been made to categorise and simplify the typology of existing urban forms. Cheng et al. (2006) study the solar potential of 18 idealiiised urban forms with different density and building forms, the horizontal arrangement, and height of the buildings are tested in uniform modality and randomly scattered modality, while the urban

fabric size are fixed and the road grid size and arrangement are not tested. In a research by Ariza-Villaverde et al. (2014), the tool of Space Syntax are introduced to simplify the spatial configuration of the urban from by drawing the axis map, the correlation between urban noise and urban morphological indices are then analysed using the joint multi-fractal spectrum method.

Pont & Haupt (2005; 2009) simplifies the urban form into a framework of urban district, urban fabric, and island, and the urban density urban forms are quantified by a series of urban morphological parameters. The system is called the Spacemate, in which two basic diagrams are illustrated to present the four fundamental parameters of urban form and two three parameters presenting the road network modalities. The method provides an intuitive and straightforward tool for urban morphology related research, and it can be used in a wide variety of urban environmental related research, e.g. day lighting (Pont & Haupt, 2009) and noise (Salomons & Pont, 2012).

As shown in Figure 2.25 that according to Pont & Haupt (2009), the floor space index (FSI) which is most commonly used in urban planning practice and related studies, is not sufficient for defining the characteristics of a certain type of urban form. It is, therefore, necessary to introduce a series of other metrics including the ground space index (GSI), open space ratio (OSR) and the L which is the average floor number of the buildings.

2.6.3 A parametric research approach

2.6.3.1 Introduction

The urban morphology in terms of building forms and road network patterns and their characteristics, e.g. scale, form, number and arrangement that can all determines the roughness of the urban area (Edussuriya, Chan, & Ye, 2011), and further affect the transmission of light, air and sound, it is significant to find the most relevant parameters to quantitatively measure the morphological characteristics. For instance, Adolphe (2000) defined a parameter named rugosity, which is defined specifically to reflect the measure the prominent obstacles that may affect the ventilation in the urban scale (Edussuriya, Chan, & Ye, 2011).

By simplifying the representative urban forms into given categories in which the typical typology of morphological parameters can be represented and studied. A parametric study approach can be then applied based on the parameters to further explore the relationship patterns between the morphological parameters and the environmental parameters, e.g. the urban noise impact. To determine how the change of noise distribution are affected by specific change in urban morphological characteristics, a series of urban morphological indicators that may have close correlation with the indices that represents the noise propagation are thus necessary to be selected and tested in this research.

2.6.3.2 Available urban morphological indices

Table 2.5 Seven geographical metrics adopted in a research by Huang, et al. (2007)

Abbreviations	Indicators	Definitions / Implications
AWMPFD	Area weighted mean patch fractal dimension	The shape irregularity of the patches
AWMSI	Area weighted mean shape index	The shape irregularity of the patches.
Centrality	Centrality	The degree to which the urban development is close to the central business district (CBD).
CI	Compactness Index	It means not only the individual patch shape but also the fragmentation of the overall urban land- scape.
CILP	Compactness index of the largest patch	It mainly represents the overall shape of the urban centre.
ROS	The porosity or the ratio of open space	The porosity measures the total area of these “holes” in relation to the calculated entire urbanized area, also designated the “ratio of open space” (ROS).

A number of urban morphological indices from different perspectives have been proposed to describe and identify certain characteristics of urban morphology. The range and definition of the indices are relatively broad and the choice of parameters often depends on the specific research topic, e.g. geography, land use, urban planning, and urban design, etc. Schwarz (2010) explored the features of 231 European cities through a series of abstracted parameters related to urban form characteristics, which are derived from 27

major landscape metrics listed from a systematic review of previous literature that is believed to be sufficient to cover all available landscape metrics.

Table 2.6 Six urban morphological parameters adopted by Hao and Kang (2014)

Abbreviations	Indicators	Definitions / Implications
BPAF	Building Plan Area Fraction	The ratio of the plan area of buildings to the total surface area of the study region.
CAR	Complete Aspect Ratio	The summed area of roughness elements and exposed ground divided by the total surface area of the study region.
BSAPAR	Building Surface Area to Plan Area Ratio	The sum of building surface area divided by the total surface area of the study region.
BFAI	Building Frontal Area Index	The total area of the façade areas parallel with the flight direction divided by the total surface area of the study region.
HWR	Height-to-Width Ratio	The average of the building heights is divided by the average of the horizontal distances between two adjacent buildings on the direction vertical to the flight direction.
HDFBFP	Horizontal Distance of First-row Building to Flight Path	The mean of the horizontal distances from the frontal façades of the first-row buildings to the flight path.

In a widely cited research by Huang, et al. (2007), six spatial metrics are adopted to analyse the urban morphology of 77 major metropolitan areas all over the world based on the analysis of the satellite maps, as can be seen in Table 2.5, the research emphases more on the analysis of macroscopic geographic features of the urban built-up areas.

When the research is related to environmental topics, e.g. noise in the urban area, only the urban morphological parameters that are most relevant to urban form would be considered. In a recent research by Hao and Kang (2014), six urban morphological parameters relevant to the transmission of aircraft noise are adopted for the sake of analysing the effect of urban morphology on the propagation of fly-by aircraft noise, as can be seen in A number of urban morphological indices from different perspectives have been proposed to describe and identify certain characteristics of urban morphology. The range and definition of the indices are relatively broad and the choice of parameters often depends on the specific research topic, e.g. geography, land use, urban planning, and urban design, etc. Schwarz (2010) explored the features of 231 European cities through a

series of abstracted parameters related to urban form characteristics, which are derived from 27 major landscape metrics listed from a systematic review of previous literature that is believed to be sufficient to cover all available landscape metrics.

Table 2.6. Hao et al. (2015) applied the similar approach and studied the birdsong loudness and a series of urban morphological indices that are related to the green space visibility in the urban area, including the Building Plan Area Fraction (BPAF), Green Area Perimeter (GAP), Green Area Dispersion Index (GADI) etc.

2.6.3.3 Selection of the urban morphological indices

Regarding the selection of urban morphological indicators, depending on the exact research topics, there are a number of different standards as well as different calculation methods on similar metrics.

In the research on the correlation of urban morphology and residential building forms by Silva et al. (2014), only three major parameters are considered, which are the spatial metrics of Compactness Index (CI) that measures the shape and the fragmentation of the urban patch and the landscape (Li and Yeh, 2004; Huang et al., 2007); the Index of Porosity or Ratio of Open Space (ROS) and the Complexity of the Perimeter Index or the Fractal that indicates the complexity of the perimeter of an urbanised area (Silva, Oliveira, & Silva, 2014).

All three factors can also be found in the research by Huang et al. (2007) with the same formula, but are provided with slightly difference definitions. For some indices, there are some evolved versions that are developed for specific purposes, e.g. the CILP is developed based on CI and shows the compactness index of the largest patch on the map for the sake of further estimating the compactness of the main built-up areas of the city centres. In A number of urban morphological indices from different perspectives have been proposed to describe and identify certain characteristics of urban morphology. The range and definition of the indices are relatively broad and the choice of parameters often depends on the specific research topic, e.g. geography, land use, urban planning, and urban design, etc. Schwarz (2010) explored the features of 231 European cities through a series of abstracted parameters related to urban form characteristics, which are derived

from 27 major landscape metrics listed from a systematic review of previous literature that is believed to be sufficient to cover all available landscape metrics.

Table 2.6 the parameter of CAR, BSAPAR and HDFBFP are also chosen as they are all related to the propagation of aircraft noise. It can be seen that the main concern is to meet the specific research needs and aims of the relevant studies.

2.7 Conclusions

In this chapter a comprehensive review surrounding the main research topics are presented, the concepts, historical literatures, and empirical studies are combed through in detail. The review of urban morphological research in section 2.2 provides a framework for the characterisation of the urban morphological features, based on a holistic literature review that analyses the significant differences between the urban morphology in typical urban areas in the EU and China. Through section 2.3, the theory and practice frameworks describing the urban sound environment, and some important temporal indicators that describes the SPL of the urban noise are reviewed, there are few researches explored the methods of indices that reflect the spatial distribution of SPL. A review of the difference between UK and China in which also found that the differences in urban morphology characteristics can create distinct urban sound environment. Further comparison between typical urban sound environment is necessary. A comparative review in section 2.4 is conducted on the state-of-the-art noise mapping techniques in the EU; together with the noise mapping accuracy related issues described in section 2.5, it can be seen that although the noise mapping methods and packages are widely applied, especially in the EU, there are still a number of issues and discussions on the inaccuracy of the calculation methods and configurations of typical EU when applied in special circumstances, it is worth exploring the applicability of which in typical Chinese urban sound environment. There is already a variety of studies related to urban morphology and environmental issues including noise, an approach of parametric study based on appropriate selection of key morphological indices is reviewed in section 2.6, and it is found to be efficient and significant for quantitatively studying and revealing the potential effect of urban morphology on the traffic noise distribution. The literature review constructed a whole

picture of the research background and existing literature and studies on related topics and hence justifies the scope of the research questions and aims of this study.

Chapter 3 Methodology

3.1 Introduction

This chapter introduces a framework of research methodology as well as the relevant notions and concepts. It consists of three major parts in accordance with the main research framework:

Section 3.2 introduces the methodology and process of the applicability test on representative EU traffic noise simulation methods and packages, which are conducted in Chapter 4 and Chapter 5. The main focus of which is to select the most typical Chinese urban environment cases. This part involves the selection of case study areas, the process of in-situ data acquisition and measurement, and the methods of the noise calculation and configurations, etc.

In Section 3.3, a comparative study method is introduced. It involves the case selection criteria and method in both China and EU. The method of a preliminary study based on the compared cases are also introduced in detail, including the method of the noise mapping calculation, the method for noise map data processing for the sake of acquiring a series of basic statistical spatial noise indices that representing the spatial noise distribution and urban morphological indices, etc.

Section 3.4 constructs a framework for a novel parametric study approach that focuses on the correlation between urban morphological indices and spatial noise indices. The concept and denotation of a series of existing and newly introduced urban morphological indices and spatial noise indices are presented. Then the analysis process of the correlation study is introduced step by step.

It is to note that the concepts and configurations introduced in the methodology part may also be briefly introduced in the specific sections in Chapter 4–7. The designated methods may be utilised in different chapters while only introduced once in certain parts in this chapter, e.g. the noise calculation configurations, the Matlab based grid map processing programme, and the in-situ investigation methods, etc.

3.2 Applicability test on current EU noise mapping calculation techniques in typical Chinese urban environment

3.2.1 Background

As mentioned in the literature review in Chapter 2, there is series of studies on the calculation accuracy published (Hepworth et al., 2006; Murphy, E. King, 2010; Manvell & Hartog van Banda, 2011), and the accuracy and efficiency are generally acceptable. It needs to mention that the applicability test was also conducted by the author in a series of sites in Greater Manchester, although the results are not listed as in most of the scenarios the accuracy level is also proved to be generally acceptable given sufficient data input and appropriate calculation configuration.

This section briefly introduces the research method framework of a systematically conducted test on the optimisation and applicability of representative EU noise mapping techniques in typical Chinese urban environment where potential calculation inaccuracies may occur. The contents of these sections cover the research method adopted in Chapter 4 and Chapter 5, in which five representative cases are selected in the city of Wuhan. The first one with relatively simple urban morphological and traffic noise environment features are selected for the pilot test of applicability and the optimisation of the recommended noise calculation configurations in Chapter 4. Four relatively more complicated cases are selected in Chapter 5 for the specific scenario tests on the applicability of state-of-the-art EU noise mapping methods typical in typical Chinese urban environment. The method of the cases selection, the in-situ data collection and measurement and the configuration and method of noise mapping calculation are introduced in detail.

3.2.2 Selection of cases

In the cases selection process, attention is especially paid to typical acoustic and urban morphological features that may have impact on the applicability of the typical EU noise mapping method. The cases chosen cases possess some of the most typical urban morphological features and road types including the pilot study case selected in Chapter 4. The complexity of Chinese urban environment made it impossible to find a case with

only one typical feature, the overlapping of certain features is inevitable. As shown in Table 3.1, there may be several features appear in one sampling area, though in each case focus will be put on the most representative sections.

Table 3.1 Cases with scenarios of typical urban and acoustic features

Typical Urban Sound Environment		Youyi Avenue	Luoshi Road	Renghe Road	Donghu Road	Xudong Road
Street space	Elevated road within wide and open street canyon					×
	Elevated road within narrow and confined street canyon		×			
	Street canyon	×			×	×
	Pedestrian alleys		×	×		
Building	With affiliated podium	×			×	×
	High-rise (> 12 storeys)	×			×	×
	Low-rise (< 6 storeys)			×	×	
	Stand-alone tower				×	
	Terrace flats	×	×			×
Barriers	Confined barrier		×			
	Open barrier					
Ground absorption	Plant covered patches	×				
	Large open space				×	
Noise sources	Extra heavy vehicles [a]			×		
	Community noise source [b]	×		×		

[a] It indicates that there are constantly heavy vehicles passing through the road mentioned.
[b] It indicates that the event noise from the residential communities are loud enough to affect the measurement result.

The typical forms of the street canyon that are formed due to the centralised urban planning system of China are paid special attention to in this research, in which most of the traffic is concentrated on the main roads with a span of 350–500 metres (Wu & Li, 2011). The studied sites are mostly divided by or bordered with one major main road. The propagation of the traffic noise from the main roads is measured using a series of receivers on various spots. The receiver points are selected in conjunction with the area selections. Receivers are spread in the research areas, both close to and far from the main roads. In some cases, to verify the noise transmission in 3D, some receivers are measured at different heights close to the building façade which faces the main road noise source.

3.2.3 Noise measurement

3.2.3.1 Measurement strategy

There are five studied areas and 15–20 points are selected to be measured in each area. The locations of these points are also considered regarding the representativeness of typical Chinese urban sound environment. To ensure the effectiveness as well as the coverage of the measurement, there are three types of points in each case: One reference point, 15–20 points with single A-weighted noise level measured using across the measured area, around five of which are measured with the SPL spectrum results and around the key areas close to the reference point and the main road source, i.e. on different heights close to the major building's façades.

UK DfT (1988) describes a measurement approach that shortened the measurement procedure in the CRTN, which estimates the 18-hour value by only using three representative measurements of an hourly value. NRA (2004) reported a method to estimate the 18-hour noise level by using three 15-minutes measurement results. King and Rice (2009) also found that the error of 15-minutes measurement results is generally within 3 dB comparing with the measurement of 12-hour L_{day} and he believe the method can be applied for determining the value for L_{A10} (18-hour), a statistical noise indicator defined in CRTN (DataKustik, 2007) of noise level based on the temporal noise index of L_{Aeq}. Therefore, in this study a series of short-term measurements lasting for 10-20 minutes are conducted at a variety of locations approximately simultaneous within the rush hour in the day time (7:00 to 19:00)

In the process of this research, efforts are made to ensure the urban areas with obvious impact of the community noise and construction noise source are excluded; and when there are unavoidable community noise or construction noise during the measuring hours, the measured receiver points are selected at locations that are mainly affected by the main traffic noise sources. For some cases, the reference value of the community event noise are recorded and modelled as point or line sources in the noise simulation process.

3.2.3.2 Reference points

King and Rice (2009) measured the continuous noise levels at a fixed location in Dublin city centre for one week. This measurement was used to determine the variation of noise throughout the day period, and these short-term measurement results would enable an accurate estimation of $L_{day.}$

In this research, one single reference point adjacent to the main road is also selected and measured for an hour which is enough to cover the rest of the measurement sessions during the rush hours of the day (WCTPDI, 2011) The full spectrum noise level of the measured period at the reference points were used to verify the noise simulation results of the main roads, and to correct the noise levels measured in each receiver point.

- ***Measurement locations***

One receiver point is introduced as a reference point close to the main road in each site. The reference point is selected approximately 4 metres from the outer motor-vehicle carriageway of the main road and 1.5 metres above the ground. The specific location of the reference receiver points varies, though it is normally at least 50 metres away from the closest road intersection, and not close to any walls, foliage or barriers on the roadside.

- ***Measurement settings***

The measurement of each reference point is processed for one hour using a full spectrum sound level metre, which covers all the other short-term measurements processed across the researched area. The microphone of the sound level metres is protected with windshield and point towards the road perpendicularly at the height of 1.5 m as can be seen in Figure 3.1. The sound level meter records a series of noise indicators, including the L_{Aeq} of each of the 1/3 octave bands per second for the whole measurement period.

Figure 3.1 Positioning of a sound level metre in the measurement process

- ***Objective of the measurement***

Except for the reference points, the measurement result from other receiver points may also be affected by the fluctuation of the traffic flow, therefore, it is important to correct potential errors. For each of the short-term receiver points across the studied area, the variance from the measurement result of the reference point during the same time slot could then be calculated and applied to correct the errors.

The measured results at the reference point are also used to validate the traffic flow counts. The wave shape of the fluctuation of the hourly result reflects how the changing traffic flow that influences the SPL during the measurement period. The source SPL calculated using the mean results of the reference points can essentially be used to correct the traffic flow counts of the main roads.

The reference receiver point measurement results are also used to simulate the road noise sources as line sources for the calculation of the SPL on specific frequencies. An assumption needs to be verified that, due to the complexity composition of the urban environment, the accuracy level of the calculation of SPL on specific frequency level may vary. Therefore, the SPL of the reference point measured on 1/3 octave bands can then be applied to simulate the distribution of the traffic noise level spectrum.

This method of the line source calculation follows the algorithms and configuration specified in ISO 9613-2 (ISO, 1996) and Cadna/A manual (DataKustik, 2012a). For the

validation of the measurement results from the full spectrum receiver points around the core region of the studied sites, the calculation results are then applied (DataKustik, 2014).

3.2.3.3 Single value points

In each site, there are approximately 10–15 receiver points across the area with only the SPL in dBA measured, spreading within a limited region in which the traffic noise from other sources rather than the main road is limited.

- ***Location of the measured receiver points***

These receiver points are measured at 1.5 metres above the ground, and the locations can be divided into three types: The façade points, which locate at 1 metre from the façades of the buildings, the buildings spread across the area from near side to far from the main road, which is selected based on the locations of other receiver points, in order to obtain corresponding measurement results. The selected open space points locate amid the area, inside the pedestrian pavement, the small square or green space close to the road or amid the buildings blocks; and some locate close to the smaller roads within the area, where the traffic flow are relatively small and negligible, although may still have impact on the measurement results.

- ***Measurement settings***

The measurements last for 10–20 minutes according to specific environment conditions. The configuration of these sound level metres is also set corresponding with that of the reference points. The noise indicator measured here is the A-weighted equivalent noise level L_{Aeq}, and the measurement range is set to high and the speed option of the measurement is set to fast to ensure reliable measurement of the dynamic traffic noise and incident noise from local community activities.

- ***Objectives***

The main purpose of testing these single value points across the studied sites is to check the validity of the grid map calculation function of typical European noise mapping methods, say, in this research the grid noise map calculation are performed, in which the

calculation method of road traffic noise is calculated based on the traffic flow counts, and the results are output into the format of grid noise maps that demonstrates the spatial noise distribution (DataKustik, 2007).

- ***Referential correction of the measurement results***

Take the case of Donghu Road area as an example, Table 3.2 lists out the measurement results collected at each receiver point as well as the correction made to each point based on the results during the selected time period measured at the reference point.

Table 3.2 Correction of measurement results in overall noise level

Point Name	Measured SPL (dBA)	Correction (dBA)	Corrected SPL (dBA)
A01	63.5	+0.6	64.1
A02	61.0	+0.5	61.5
A03	59.9	-0.3	59.6
A04	59.5	+1.0	60.5
B01	55.8	+0.6	56.4
B02	45.0	+0.5	45.5
B03	56.7	0.0	56.7
B04	47.0	0.0	47.0
C01	56.5	+3.7	60.2
C02	55.9	+0.6	56.5
C03	55.9	+0.5	56.4
C04	56.0	-0.6	55.4
E01	57.2	-0.2	57.4
E02	54.1	+1.0	55.1
E03	58.3	+0.1	58.4
E04	60.1	-0.4	59.7
E05	56.3	+0.4	56.7
E06	57.6	+1.0	58.6
E07	57.1	-0.5	56.6

The fluctuation of noise levels is mainly caused by the fluctuation of the traffic flow during the measured period. Based on the 1-hour constant measurement results of the reference point on a 1-second basis, the specific noise level measured at the reference point during the relatively shorter period of measurement conducted at each of the receiver points can then be calculated. The original SPL measured at each receiver points are then corrected based on the disparities between the shorter period value SPL and the

1-hour SPL at the reference point. It can be seen that firstly this is an approximated measure of correction as the geometric divergence is not considered; nonetheless, it can also be seen that the correction at each receiver points is relatively small, except that of the point C01.

3.2.3.4 Full spectrum points

5–10 full receiver points are selected around the core region of each area where the most typical Chinese urban morphological features can be observed, and the 1/3 octave bands SPL from at which are measured. These receiver points are chosen to verify the validity of the calculation results produced in these typical environment, in central frequencies of major octave bands, from 31.5–8000Hz. The calculation is executed based on the result converted from the 1/3 octave bands SPL measured at the reference points.

- ***Location of the measured receiver points***

The location of the full spectrum receiver points is selected with caution based on analysis of the digital map and in-situ observations, in order to ensure that they represent the most typical urban sound features of Chinese cities. Basically, there are three types of selected points—the open ground points, the façade points, and the points on different altitude.

- ***Measurement settings***

The equipment used to measure the full spectrum receiver points is the 01dB Solo, the configuration is set in accordance with that of the SVAN 801 Sound level meter used to measure the reference points. The measurement lasts for 10–20 minutes on each point, according to the nature of the noise — when the noise is more stable, the measurement tends to take less time, which is to ensure enough points are measured during the entire session. From the measurement of each point, a series of SPL parameters could be extracted.

- ***Conversion of the SPL spectrum measurement results***

The SPL spectrum of the full spectrum receiver points was originally collected at central frequencies of the main 1/3 octave bands, to ensure the accuracy, the 1/3 octave bands

SPL was thereafter converted to the SPL at the central frequencies of eight 1:1 major octave bands to represent the variation of the full SPL spectrum. A time-based correction is given to each receiver points based on the equivalent SPL measured in the same time period at the reference point. It is to note that the CRTN is not capable of calculating the SPL spectrum thus the corresponding calculation method adopted here is the ISO9613-2. (ISO, 1996)

- ***Objectives***

The purpose of measuring the full spectrum receiver points in accordance with the reference points is mainly to validate the validity of calculated the SPL of full spectrum, say, on central frequencies of eight main octave bands from 31.5–8000 Hz. The noise emission in the typical urban space in Chinese cities may be distinct from that of the typical European urban environment (Zhang et al., 2012; Wang et al., 2007). It is thus worth examining if the propagation of traffic noise especially on certain frequencies is affected by the certain urban morphological features in typical Chinese urban environment, as well as the form of the roads and the space, e.g. the elevated road, especially that of the high-rise building close to the main roads, the large open square close to main roads, and the extremely narrow alleys amid the urban village, etc.

3.2.4 Data collection

Table 3.3 Method for data collection for the noise calculation

Data type	Data to be collected	Source
Topographic conditions	DTM (contours with elevation)	Digital map from local authority
	Outlines of major land objects	
Building data	Outlines of the buildings	
	Façade roughness and material type	In-situ observation
Road data	Surface material type and roughness	
	Road width and carriageway amount	Satellite map and in-situ observation
Traffic conditions	Hourly traffic distribution of a day	Statistic data from local authority
	Peak time traffic counts	In-situ counts
	Heavy vehicles ratio	

To meet the requirement of the measurement and noise calculation, following types of data need to be collected through a variety of ways: Geographic data including DTM, building outline and height, façade type and material; Road data including road width, number of carriageways, surface type, traffic conditions including the real-time traffic counts during the rush hour and hourly traffic distribution of a day. The data collection method is listed in Table 3.3.

3.2.4.1 Topographic conditions

Digital map obtained from local authority is the major source of topographic data and physical data of the ground objects. In noise mapping packages, the modelling of digital terrain is of great significance, as the contour lines are calculated in the selected package by default as vertical barriers with absolute heights equivalent to the elevations values, and the ground unevenness also affects the gradient of the roads, etc. (DataKustik, 2007). In this research, the digital terrain map (DTM) is obtained from the local authority in DXF format, and the elevation points are transferred into contour lines and exported to the appropriate format. Relevant digital terrain data also includes the landscape objects and peculiar topologic forms which may influence the calculation results, e.g. the water surface, green belts, lawns, and foliage etc.

3.2.4.2 Building data

For the sake of accurate simulation of the typical outdoor sound environment in typical Chinese city like Wuhan, some peculiar façade and roof features of the buildings adjacent to main noise sources need to be specifically collected for detail modelling or redefinition of acoustic coefficients. The methods of modelling the buildings in the noise-mapping packages are constrained by the requirement of large-scale modelling —in some cases, the noise mapping software is employed to plot noise maps of tens or hundreds of square kilometres area, which requires rapid processing method for the building modelling. The outlines of the buildings are imported as closed polygon lines with elevation and converted into erected buildings blocks with predefined height. An attribute in the property options of the building objects is given to defining the height as absolute, relative or rooftop, and which simplifies the building model from the real building. Therefore,

some of the building details, e.g. balconies, sun shields, and roof pitches, etc. are modelled specifically.

Attention in the building data collection is mainly focused on the buildings adjacent to the main roads. The building outlines are abstracted from the digital map from the local authority, and the building location and morphological details are confirmed and amended with the help of several different sources. Firstly, in-situ observation and photos taken on the sites could help to confirm more details of the building shape and façades details; Secondly, with the help of 3D city map and street view map provided by 2 major online map websites of China: The Baidu Map (Badiu Inc., 2011) and the Tencent Map (Tencent Inc., 2011), which provides more reliable and up-to-date details of the building conditions and the street environment than the processed DTM. Here it should be noted that the Google Maps of China only has satellite images due to the limitation of its service. The third way is to validate the DTM using the satellite images obtained from Google Maps service (Google Inc.) and Baidu Map service (Badiu Inc., 2011).

3.2.4.3 General traffic flow counting

Table 3.4 The conversion method of traffic flow. Source: Good practice guide for strategic noise mapping and the production of associated data on noise exposure – version 2 (WG-AEN, 2007)

Road Traffic Flows	Metropolitan/Main Roads	Inter-District Roads
Day flow - 12 hours, day	$= Q_{\text{peak}} \times 12$	$= Q_{\text{peak}} \times 0.7 \times 12$
Evening flow - 4 hours, evening	$= Q_{\text{peak}} \times 0.7 \times 4$	$= Q_{\text{peak}} \times 0.5 \times 4$
Night flow - 8 hours, night	$= Q_{\text{peak}} \times 0.2 \times 8$	$= Q_{\text{peak}} \times 0.1 \times 8$

According to EC WG-AEN (2007), it is recommended that the measurement of the count, composition and speed of a long-term traffic flow could be obtain as the real traffic data for noise calculation, while in the meantime, the measured traffic flow count in a specific peak hour (Q_{peak}) could also be applied to and converted to the long- traffic data of a while day or a certain period based on the temporal distribution of traffic as shown in Table 3.4, in which an example method for obtaining the day, evening and night traffic flow from a measured peak hour flow (Q_{peak}) of different road types is provided.

Since the key methodology of computer-aided road noise mapping is converting the road segments into line sources, the collection of traffic data is essential for getting relatively more accurate calculation result to represent the real condition (DataKustik, 2012b). According to the British noise calculation method CRTN (UK DfT, 1988), the road source level L_{A10} is calculated based on the 18-hour daily traffic count from 6:00–24:00, or the Q, the 18-hour total traffic amount; while in this study the 1-hour measurement period is picked during the peak hours of the day, and the counted vehicle amount of this hour is used directly as the q or hourly vehicle amount, and then magnified in proportion to get the Q and then input into the software as the road source SPL for the calculation of the of the road traffic noise in accordance with the measurement results (DataKustik, 2012b).

Hourly noise level:

$$L_{10,1\mathrm{h}} = 42.2 + 10\,log_{10}\,q \quad dBA \tag{3.1}$$

The Daily noise level (18 hours):

$$L_{10,18h} = 29.1 + 10\log_{10} Q \quad dBA \tag{3.2}$$

Therefore, it can be deduced as:

$$q \;=\; 10^{-\frac{13.1}{10}} \times Q \tag{3.3}$$

The daily traffic count can be approximately summarised as:

$$Q \;=\; q \times\; 20.417 \tag{3.4}$$

To meet the requirement of the calculation method used in the noise-mapping package, the traffic flow counts are measured on an hourly basis during the rush hour. It is to note that, as mentioned above, the methodology applied in this study ensures that the while day average noise level $L_{10,18h}$ is equivalent to that of the measured hour, which can be obtained through by the constant measurement result thus the whole day traffic flow

counts is not necessary, which can be calculated directly based on the one-hour traffic count based on Equation 3.7, as the main purpose of the study is not to assess the general noise emission level of the tested area but to validate the calculation method. The majority of the receiver points were measured during the hour based on the traffic counts of the same hour. Thus, the priority is to make sure the traffic flow as well as noise level of the measured hour is enough stable. Therefore, the measurement house is chosen as close to the rush hour as possible, which is further explained below:

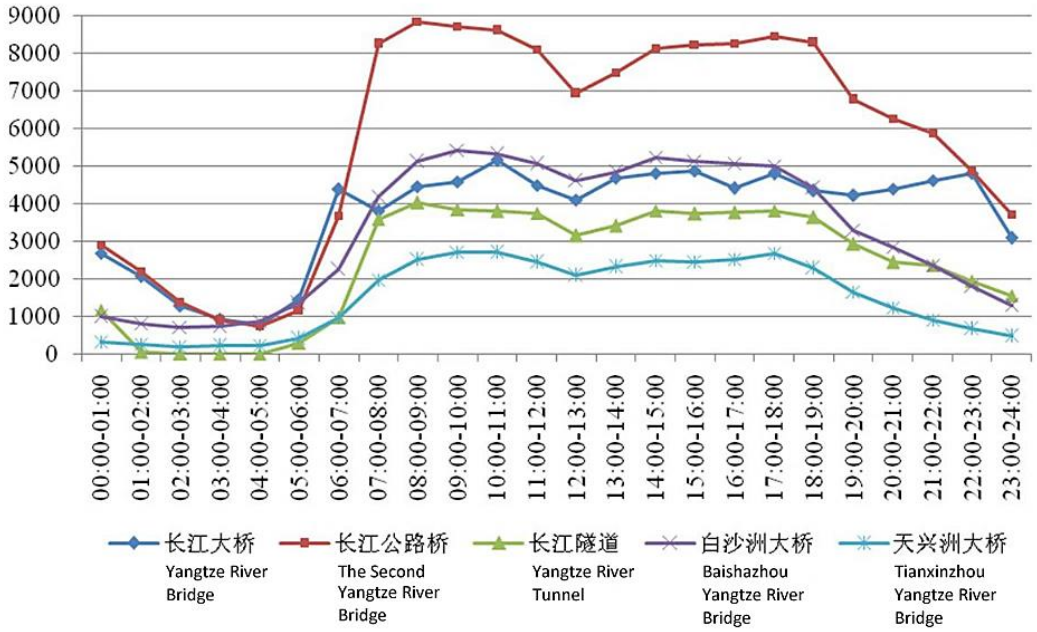

Figure 3.2 Diurnal traffic distribution of major traffic arteries of Wuhan. Source: Wuhan small-sample traffic investigation 2011 (WCTPDI, 2011)

Firstly, the measurement period is selected during the busy hours of a day, as can be seen in Figure 3.2 that the typical diurnal traffic distributions of Wuhan are used to determine the measurement time. It can be seen that the typical day traffic of the main arteries of Wuhan is relatively more evenly distributed between 8:00–18:00, especially during the hours close to the rush hours, say, 8:00–11:00 and 15:00–19:00. The measurement hours in this research are collected during these periods to ensure relatively stable traffic counts per unit time.

Secondly, as stated earlier, the fluctuation of the traffic in the measurement hours could be adjusted by using the reference result of reference point. The consecutive noise

measurement results of the reference point during the measured hour is temporally corresponding to the real-time traffic counts, therefore, the main SPL of the road during the hour is closely correlated with the traffic amount of the hour.

Lastly, the validation focuses on the validity of the effectiveness of the noise simulation package, rather than calculating the actual daily noise level of the selected sites. The q or the hourly traffic count is collected in situ and is treated as the average hourly traffic count, and is directly input into the noise-mapping software directly for the calculation of the 18-hour noise level according to CRTN as shown in 3.4, for the sake of obtaining the equivalent daily traffic noise level $L_{10,18h}$. Due to the nature of the applicability test, there is no fluctuation in the simulated noise environment, thus the calculated $L_{10,18h}$ in the noise maps is equivalent to the A-weighted SPL L_{Aeq} per se, which hence can also be directly used to compare with the temporally corrected in-situ noise measurement results of each receiver points, which was acquired during the same measurement period.

3.2.4.4 The method of acquiring the traffic speed

The traffic speed is measured in situ using a simplified method as illustrated in Figure 3.3. A segment of 50 metres with the relatively free flow are chosen to determine the real-time traffic speed. The observation is made at the end of the segment for a period of time, during which the mobility of the flow is relatively high. The time span t and numbers n of the vehicles passing through this segment are recorded. The approximate average speed of the traffic V could thereby be calculated according to the Equation 3.4, in which D is the distance the vehicles have travelled, i.e. 50 m in this study.

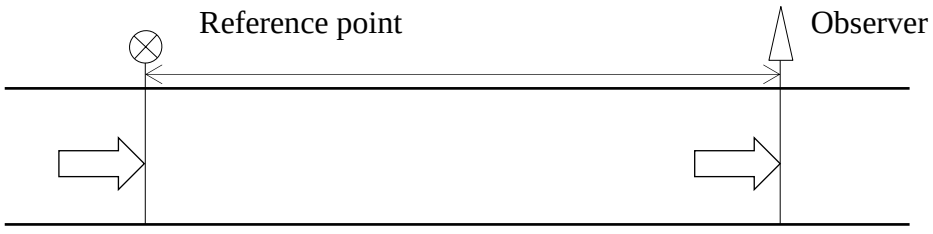

Figure 3.3 A simplified method for in-situ traffic speed test

$$V = D \div \frac{1}{n}\sum_{i=1}^{n} t_i$$

3.5

It is worth mentioning that, according to CRTN the traffic noise level in Equation 3.5 is calculated based on an assumption that the average traffic speed V=75 km/h and the heavy vehicle percentage p=0. Considering the real traffic condition is most likely to be different from the assumption, it is necessary to apply corrections to the calculation result based on the actual V and p of the traffic flow as shown in Equation 3.5 according to CRTN Chart 4–6 (UK DfT, 1988).

$$\Delta_{pV} = 33log_{10}\left(V + 40 + \frac{V}{500}\right) + 10log_{10}\left(1 + \frac{5p}{V}\right) - 68.8$$

3.6

In which the p and V could be obtained through utilising the method mentioned earlier.

3.2.5 Noise Calculations

The calculation method and package that were applied and validated in this study comply with the END 2002/49/EC (EC, 2002). The discussed calculation method is mainly the CRTN and ISO 9613-2; the noise-mapping package Cadna/A and corresponding calculation configurations were adopted (Datakustick, 2007).

3.2.5.1 Calculation methods recommended by END 2002/49/EC

The European Environmental Noise Directive (END) 2002/49/EC (EC, 2002) as the guideline of noise assessment practices of the EU Member States, marks the beginning of large-scale computer-aided noise assessment activities across the EU. END 2002/49/EC draws the blueprint of noise calculation methods and strategic noise-mapping methods for EU states either with or without existing national calculation methods (EC, 2002).

END 2002/49/EC requested the member states of EU to provide strategic noise maps for cities and towns with population of above 250,000 before June 2007, in which all the

major roads with traffic flow of over 3 million vehicles a year need to be simulated; In the second phase, agglomerations of over 100,000 need to be mapped by June 2012. To achieve the goals, the END 2002/49/EC recommends the member states to use existing national calculation methodology of their own; and for those countries that have no available national method, the French method NMPB is recommended (EC, 2002).

According to END 2002/49/EC for the purpose of assessing the impact of noise on a certain urban area, the noise-mapping data on the assessment or prediction of the noise situation shall be presented in terms of noise indicators. The recommended noise indicators in END 2002/49/EC are the energy based noise indicator L_{den} and L_{night} as the indicator for day-evening-night and night noise assessment across a year (EC, 2002).

The methodology adopted in the first phase in the EU varies across the member states. Amongst 20 member states that had provided the noise assessment methods they had used, five states used their own national methods, seven states used interim methods according to Annex II of END 2002/49/EC, and eight states select methods based on the noise source type. (Paviotti and Kephalopoulos, 2008)

3.2.5.2 Road noise calculation

The British national method CRTN is selected as the calculation method for road noise, the $L_{10,18h}$ is the main noise indicator to present the noise level of a day calculated using the 18-hour traffic data, which is the arithmetic mean of the 18 hours (6:00–24:00) of $L_{10,1h}$ (UK DfT, 1988). It is to not that in the multiple traffic noise calculations conducted in this research the reported disparity (O'Malley et al., 2009) between the time-based noise index L_{10} adopted by CRTN and L_{Aeq} which are adopted by most of the EU calculation methods can be ignored, and the traffic noise in different chapters of this research are based on the assumption that the traffic flow of the day is consistent; as the focus of this research is mainly the spatial distribution of the traffic noise rather than temporal. The data collected in the measured hour can, therefore, represent the whole day data, and the difference between L_{day}, L_{night} and L_{den} are ignored.

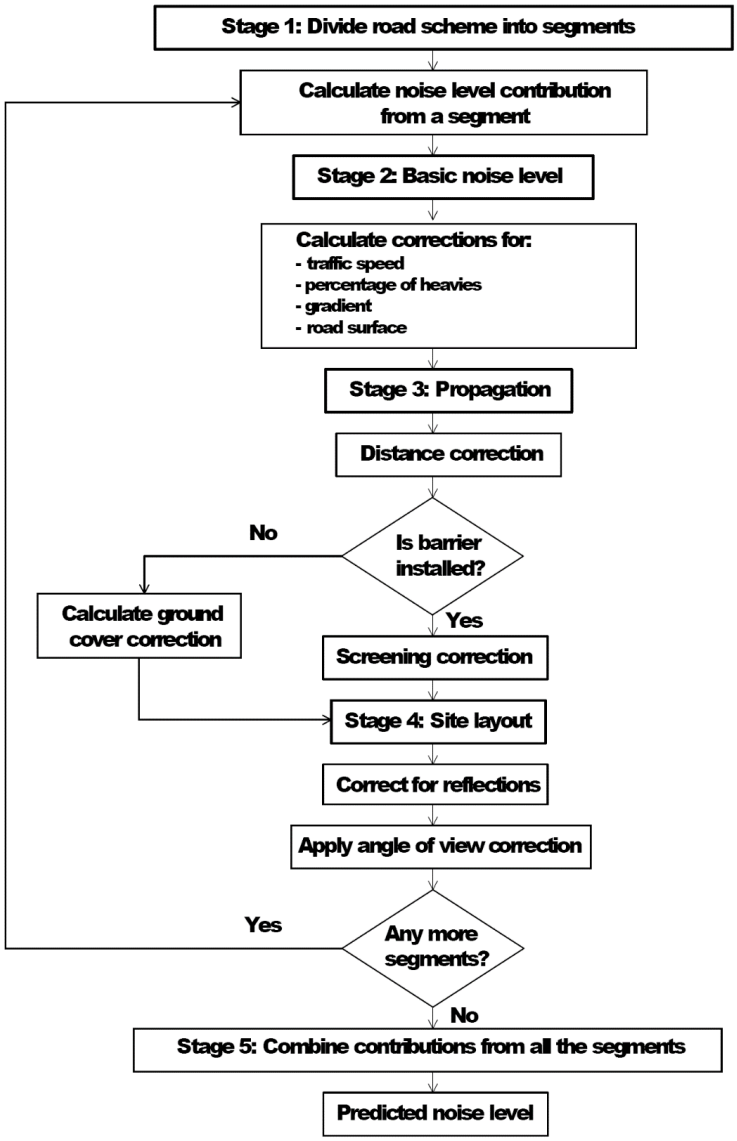

Figure 3.4 Flow chart for predicting noise from road schemes Source: CRTN Chart 1 (UK DfT, 1988)

In a typical EU noise calculation method, as shown in the flowchart derived from the UK national calculation method CRTN (UK DfT, 1988) in Figure 3.4 that, to acquire desirable accuracy for road noise calculation, there are a series of procedures to follow, the sensitivity of the results is also prone to be affected by the data collection and processing uncertainty occurred in each step. For instance, the daily traffic amount data.

In this research, the risk of errors caused by the inaccurate traffic data is eliminated by simply converting the one-hour traffic flow counts into daily traffic counts. As the main purpose of the calculation is to get the equivalent noise level of the measured time period

based on the coordinated traffic count data of the same period. The hourly traffic flow fluctuation is not a major concern and may cause extra inaccuracies if not counted accurately. The one-hour traffic amount is then directly transferred into 18h daily traffic by multiplied with a parameter of 20.147 (DataKustik, 2007) and calculated according to CRTN (UK DfT, 1988).

3.2.5.3 Calculation configurations

To ensure consistent accuracy level and comparability of the calculation results in the latter part of the research, a set of optimised general configurations is adopted based on the testing results on default configurations, as can be see Table 3.5.

Table 3.5 Selected calculation configurations using Canda/A (DataKustik, 2012a)

Tab	Options	Settings
General	Maximum Error (dB)	0.0
	Maximum search radius (m)	2000
	Minimum distance source to emission point (m)	0.0
	Grid interpolation	No
	Extrapolate grid ‘under’ buildings	Yes
	Fast screening	No
Partition	Grid/Raster factor	0.5
	Maximum length of section (m)	1000
	Minimum length of section (m)	1.0
	Projection as terrain model	No
	Maximum distance source–emission point (m)	2000
	Search radius source (m)	100
	Search radius emission point (m)	100
DTM	Model of terrain	Triangulation
	Explicit edges only	No
	Lift “source underground” to Ground-Niveau	No
Reflection	Maximum order of reflection [a]	3
	Maximum searching radius source to receiver (m)	100
	1.5 dB Mirror source reflection [b]	No
Ground Abs.	Default Ground Absorption [c]	Set accordingly
	Buildings are reflecting (G==0)	No

[a] Max. order of reflection is set to 3, based testing and previous studies, to ensure accuracy and efficiency of calculation.
[b] The mirror source reflection option is set to Yes by default assuring relatively quick calculation speed, especially in the grid calculation; while when calculating the noise level on individual receivers, it tends to be set to No to ensure accuracy.

[c] Ground absorption coefficient is set as 1.00 by default. It is set according to the real ground condition of the cases. (DataKustik, 2012a)

3.2.5.4 Line source calculation

A series of line source are used to simulate the road noise source according to the line source calculation method in ISO 9613-2 (ISO, 1996). The line sources are set at 0.5 m above the road surface and 3.5 m from to the nearside road kerbs. The line source calculation is to verify the noise in different central frequencies of the octave bands, using the SPL spectrum data measured at the reference point as well as a series of points in the sensitive region of the studied areas.

To be specific, two line sources are placed at corresponding locations following the calculation method of CRTN. When the road centre lines of the outer lanes are larger than 5 m, two roads should be introduced, and for these two road sources, there are four line sources in total to be introduced. In the calculation, it needs to be noted that only the line sources on the same side of the receivers are counted in the calculation.

The SPL of each central frequency of eight major octave bands was thereafter inputted into the line sources in the models. The SPL of the road source line is inverse-calculated based on the full-spectrum SPL measured at the reference receiver point, with considering the attenuation due to geometric divergence; similar method is implemented to determine the SPL of the point or line noise sources representing potentially influential event noise sources, e.g. exhaust fan, pedestrian pathway, etc.

3.2.6 Method for the applicability tests

The default configurations and calculation method of the selected typical EU noise-mapping method and package may have accuracy issues in certain specific urban environment, and it is necessary to test and find the most applicable combinations of configurations for the noise calculations in this research.

3.2.6.1 Validation methodology

The applicability test is conducted by systematically changing the default calculation configurations, the object properties and the modelling method, etc. The process is briefly

displayed in the flow chart in Figure 3.5. The calculation results and key statistical terms are demonstrated in dot charts and tables. The overall accuracy level is assessed via evaluating the key statistical variables, i.e. The mean error, the standard deviation, and the mean absolute error. The specific level and the potential causes of the evident errors (normally for errors greater than 3 dBA) are compared and discussed, further applicability tests are then conducted by alternating the calculation configurations, the coefficient settings of the objects in the noise maps, and lastly, the object modelling methods.

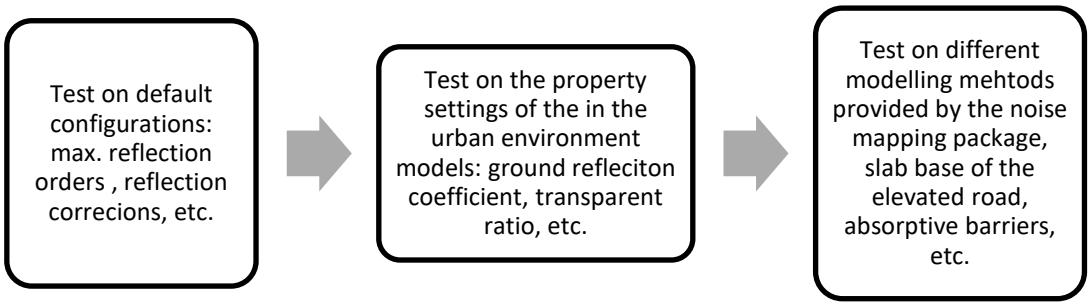

Figure 3.5 A flow chart demonstrating the process of the applicability test

The applicability test is conducted in two parts. Firstly, a thorough test on all the default calculation configurations designated in the calculation method and the noise mapping package are systematically tested. A set of optimised calculation method is then raised. Secondly, by using the optimised calculation method, four more typical urban scenarios with representative noise environmental characteristics and urban spatial features are tested.

As shown in Table 3.5, most of the configurations are set according to the default value, for the Ground absorption coefficient, it is set according to the site conditions. In the modelling process, the parameters of the objects are modelled as close to the real condition as possible.

3.2.6.2 Statistical comparison method and key statistical terms

Statistical comparisons are made between the calculated results and the measured noise levels at various receiver points in the tested areas, to examine the general accuracy of the calculation method of state-of-the-art noise calculation method and packages.

Three statistical indices, the Mean error, SD and MAE, are calculated and extracted from groups of calculation errors obtained through the calculations using certain calculation configurations or modelling method. The Mean error indicates the arithmetic average of all errors calculated (Field, 2005) as can be seen in Equation 3.1; the Standard Deviation (SD) quantifies the variation or dispersion of the tested group of errors (Field, 2005) as can be seen in Equation 3.2; the Mean Absolute Error (MAE) measures the absolute difference between two groups of results (Willmott & Matsuura, 2006) as shown in Equation 3.3.

$$Mean\ error = \frac{\sum_{i=1}^{n}(y_i - x_i)}{n} = \frac{\sum_{i=1}^{n} E_i}{n} \tag{3.1}$$

$$SD = \sqrt{\frac{\sum_{i=1}^{n}(E_i - \bar{E})^2}{n-1}} \tag{3.2}$$

$$MAE = \frac{\sum_{i=1}^{n}|y_i - x_i|}{n} = \frac{\sum_{i=1}^{n}|E_i|}{n} \tag{3.3}$$

Where y_i and x_i denote the calculated and measured SPL at a receiver point, respectively. E_i represents the calculation error.

3.3 Comparison of sound environment between typical low and high-density urban areas in EU and China

In Chapter 6, a comprehensive study on the noise distribution in typical EU and Chinese urban environment are conducted. The key approach of this is to compare the typical UK and Chinese urban environment with quantitative urban morphology indices and noise level indices and to find how and which urban indices have the most significant influence on the noise distribution.

The most significant procedure above all is to find comparable samples in typical UK and Chinese cities, then to compare the typical urban noise levels in each type of land-use in each city with a proper scientific method, and to find the correlation between urban morphologic elements and urban acoustic characteristics. In the meantime, validate the

efficiency of the state-of-the-art EU noise-mapping technique. More comparisons on samples from the broader range can be made based on this research.

3.3.1 Sampling of urban areas with typical urban morphological and noise source features

For the sake of using present urban noise simulation and urban morphology analyse methods to find how the noise distribution varies in urban spaces with distinct urban morphological features, through comparisons, the in-situ investigation and measurement is planned and are carried out in a series of case study areas in two representative cities in the UK and China. Some social indices are also considered.

The choice of the comparable cities is based on the similarity of urban characteristic and population. In this research, Greater Manchester in the UK and Wuhan in China is chosen as sample cities. The cities are both representative in each country with a similar class in the hierarchy ranking with regard to scale (NBS China, 2001; ONS UK, 2001).

A preliminary stratified sampling method is introduced to select the case study areas. The entire urban area of each city was briefly classified into six main categories with considering the land-sue, spatial features, building geometric features, road type, traffic flow scale etc. The sampling areas are then chosen in each category in both cities in a semi-random manner, the cases selected are effectively measurable, representative, and comparable. The accessibility of original topography, building and traffic data is also an important concern.

The residential areas are paid special attention to for its sensitivity to traffic noise and representative in building form and planning scheme. Two cases with low and high-density residential areas are selected in each city. Socio-economic indices, e.g. the income level of the residents in typical residential areas is also considered, two cases with distinct income level are chosen only in Wuhan.

Considering the accuracy and time limit, 500×500 m^2 is set to the size limit of sampling urban areas, with considering the feasibility of a large amount of simultaneous noise measurement and reasonable noise calculation time consuming.

3.3.2 Data collection

For the purpose of comparison, in-situ measurement and survey are necessary to obtain the 3D building and traffic flow data. Generic noise maps of the sample areas are then calculated based on the national and international standards. Most parameters are set to an empirical value to obtain comparable maps. Presently only traffic noise sources including roads, trams railway are calculated.

3.3.2.1 Digital data acquisition

For the purpose of simulating the 3D urban environment and noise calculation, it is important to get the data of the traffic flow and the acoustics-related urban morphological data, including the topographical data, the 3D data of the buildings, the condition of building façades and roads, etc.

The detailed 2D digital maps of sampled areas could be obtained from the online database of EDINA ordnance survey maps (2008) in the UK and the local authorities in China. The traffic statistic data of the typical major roads in the chosen samples can also be obtained from local authorities. With the help of newest Google digital map (Google Inc.), the data of buildings in some inaccessible areas could be estimated.

3.3.2.2 In-situ measurement – content and methods

Considering the morphology of the cities is rapidly changing, the digital map given by the authority could be imprecise or even totally changed. The traffic flow data is more variable and important, which means in-situ investigation is highly necessary.

3.3.2.3 Traffic flow

Efforts have been taken to find effective and scientific methods of in-situ traffic flow statistics. The traffic summit happens in different hours in UK and China, the driving behaviour and road types are also distinct, due to social reason and different urban textures. Relative traffic models are used together with the in-situ traffic flow measurement.

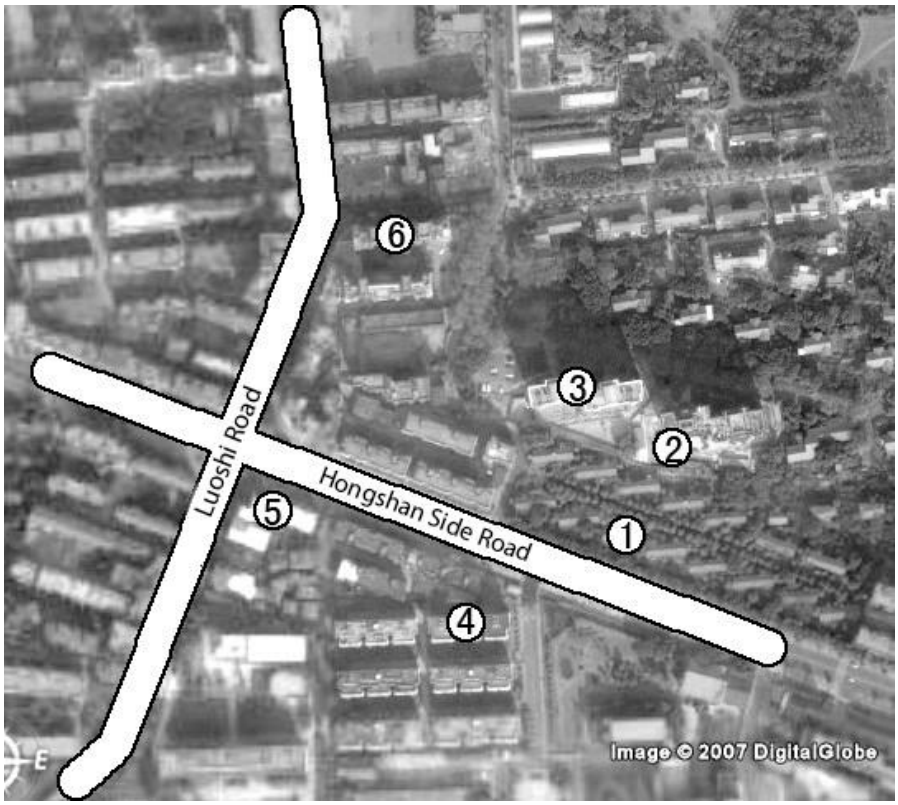

Figure 3.6 An illustrative map of the typical residential case sample – Hongshan Side Road area, Wuhan

Firstly, the most typical roads are measured in each sample area. In the urban transportation planning system in China, the urban road network could be classified into four classes: expressway and overhead road, trunk road, main road, branch roads. The traffic noise is majorly concentrated in the trunk road and main road. Therefore, only a certain amount of representative roads in each sample will be chosen to measure as shown in Figure 3.6. According to the road category classification in China, in each city, at least 20 representative samples amongst the 50 are chosen for in-situ measurement to simplify the typical traffic flow of each category of roads, especially the smaller roads. But in typical residential areas, the small roads need to be measured by in-situ measurement. For some special roads without traffic speed data, in-situ measurement is also necessary.

3.3.2.4 Building geometric information

On the digital map of a Chinese city, the position, the outline and the amount of building storey are marked, so if take 2.85 m as the average height of each storey of a building, the height of each building could be estimated according to the digital map and in-situ

survey. Considering the mass destruction and rebuilding happened every day in the process of Chinese urban development, in-situ investigation is also helpful to estimate the position, height, and condition of the buildings.

3.3.2.5 Building façade conditions

In-situ investigation need to be done to the representative buildings and special buildings made in the map as can be seen in the case example in Figure 3.6. Regarding the absorption coefficient, the buildings could be classified into three types: high, medium and low absorption according to the condition of the building and façade material used. The windows ratio of typical buildings need to be obtained to confirm the absorption coefficients, via classify buildings according to window ratio by high, medium and low based on photo analysis.

3.3.2.6 Socio-economic data

In previous studies, it was found that some socio-economic factors may have correlations with the urban noise (Xie & Kang, 2009, 2010). In this research, the work on finding the potential impact of socio-economically related factors to the general level and distribution of traffic noise in China, especially in the relatively more diversified urban area.

In some emerging economies, e.g. China, due to rapid economic booming and urbanisation process, the real-estate market is booming with soaring construction high-rise apartments, whilst the expansion of urban sprawl also creates a large amount of urban villages or slums (Crow, 2009). The social and economic disparity is getting more severe (R. W. Wang, 2010). The rapidly increasing vehicles and road infrastructure (Kenworthy & Hu, 2002) may bring adverse noise impact for both types of residents.

In the current study, two case study areas with distinct housing price are selected, the first one is a real-estate development with high-rise towers, the other is a mixed residential area with both multi-story working class apartments and a large area of the low-rise residential buildings which consists a typical urban village. The personal income data for over 30 examples are collected randomly in the studied sites, together with some basic social status and personal preference data.

For the sake of examining the income difference; an independent *t*-test for equality of means of the income data is then conducted to test the eligibility of the two compared cases. The comparison between the spatial noise indices in these two areas is conducted, as an initiative attempt for the sensitivity of sound environment for an urban area with different socio-economic properties. In future research, more socio-economic indices, such as population, age, gender, will be considered. The subjective perception and well-being of the residents can also be collected by further in-situ survey with questionnaires survey.

3.3.3 Noise mapping calculation

With the selected noise-mapping package, the calculation configuration is set by using the default international and national standard (ISO, 1996; UK DfT, 1988). The calculation of the noise level spectrum is conducted by converting the road sources into line sources then individually input the measured noise level of central frequencies of eight major octave bands into the line sources representing the traffic noise sources.

3.3.4 Abstraction of spatial noise indices by Matlab programming

A Matlab (The MathWorks, 2009) programme is developed by the author for the purpose of transforming the RGB grid noise maps into an array of A-weighted noise SPL values, based on which a series of spatial noise indices are then be derived, characterising both the general noise distribution and the traffic noise impact to the building façades.

Efforts have been taken to find effective and scientific methods of in-situ traffic flow statistics. The traffic summit happens in different hours in UK and China, the driving behaviour and road types are also distinct, due to social reason and different urban textures. Relative traffic models are used together with the in-situ traffic flow measurement.

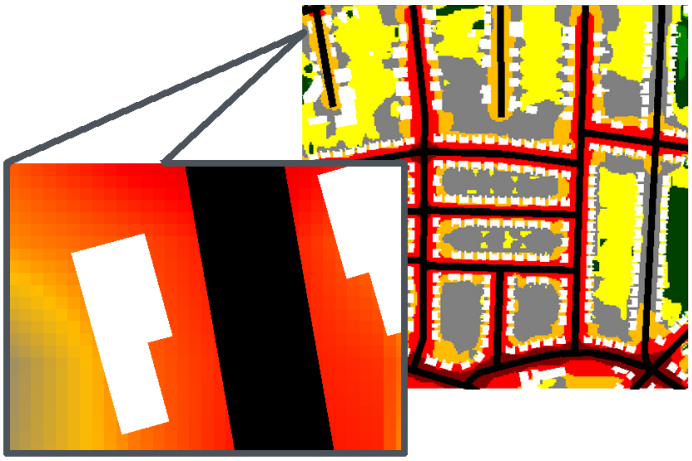

a

57	57	59	59	59	59	59	59	59	59	59	61	61	61	61	61	61	100	100	100	100	100	100	100	100	100	100	61	61	0	0	0
57	57	57	57	59	59	59	59	59	59	59	59	59	59	59	59	61	100	100	100	100	100	100	100	100	100	100	100	59	59	0	0
57	57	57	57	59	59	59	59	59	59	59	59	59	59	59	59	61	100	100	100	100	100	100	100	100	100	100	100	59	59	0	0
57	57	57	57	57	57	57	57	57	59	59	59	59	59	59	59	59	59	100	100	100	100	100	100	100	100	100	100	59	59	0	0
57	57	57	57	57	57	57	57	57	59	59	59	59	59	59	59	59	59	100	100	100	100	100	100	100	100	100	100	59	59	59	0
57	57	57	57	57	57	57	57	57	59	59	59	59	59	59	59	59	59	100	100	100	100	100	100	100	100	100	100	59	59	59	0
57	57	57	57	57	57	57	57	57	57	57	57	57	57	59	59	59	59	100	100	100	100	100	100	100	100	100	100	59	59	59	0
57	57	57	57	57	57	57	57	57	0	0	0	0	0	59	59	59	59	100	100	100	100	100	100	100	100	100	100	100	59	59	0
55	55	55	55	57	0	0	0	0	0	0	0	0	0	59	59	59	59	100	100	100	100	100	100	100	100	100	100	100	59	59	59
55	55	55	55	57	57	0	0	0	0	0	0	0	0	59	59	59	59	59	100	100	100	100	100	100	100	100	100	100	59	59	59
55	55	55	55	57	57	0	0	0	0	0	0	0	0	59	59	59	59	59	100	100	100	100	100	100	100	100	100	100	59	59	59
55	55	55	55	55	55	0	0	0	0	0	0	0	0	59	59	59	59	59	100	100	100	100	100	100	100	100	100	100	59	59	59
55	55	55	55	55	55	55	0	0	0	0	0	0	0	0	59	59	59	59	100	100	100	100	100	100	100	100	100	100	59	59	59
53	53	55	55	55	55	55	0	0	0	0	0	0	0	0	57	59	59	59	100	100	100	100	100	100	100	100	100	100	100	59	59
53	53	55	55	55	55	55	0	0	0	0	0	0	0	0	57	59	59	59	100	100	100	100	100	100	100	100	100	100	100	59	59
53	53	53	53	55	55	55	0	0	0	0	0	0	0	0	57	59	59	59	59	100	100	100	100	100	100	100	100	100	100	59	59
53	53	53	53	55	55	55	55	0	0	0	0	0	0	0	57	59	59	59	59	100	100	100	100	100	100	100	100	100	100	59	59
53	53	53	53	55	55	55	55	0	0	0	0	0	57	57	57	59	59	59	59	100	100	100	100	100	100	100	100	100	100	59	59
51	51	53	53	53	53	53	55	0	0	0	0	0	0	57	57	59	59	59	59	100	100	100	100	100	100	100	100	100	100	59	59
51	51	53	53	53	53	53	55	55	0	0	0	0	0	57	57	59	59	59	59	100	100	100	100	100	100	100	100	100	100	100	59
51	51	53	53	53	53	53	55	55	0	0	0	0	0	57	57	59	59	59	59	100	100	100	100	100	100	100	100	100	100	100	59
51	51	53	53	53	53	53	55	55	0	0	0	0	0	57	57	59	59	59	59	59	100	100	100	100	100	100	100	100	100	100	59
51	51	53	53	53	53	53	55	55	0	0	0	0	0	0	57	59	59	59	59	59	100	100	100	100	100	100	100	100	100	100	59
51	51	53	53	53	53	53	55	55	55	0	0	0	0	0	57	59	59	59	59	59	100	100	100	100	100	100	100	100	100	100	59
51	51	53	53	53	53	53	55	55	55	0	0	0	0	0	57	59	59	59	59	59	100	100	100	100	100	100	100	100	100	100	100
51	51	53	53	53	53	53	55	55	55	0	0	0	0	0	57	59	59	59	59	59	100	100	100	100	100	100	100	100	100	100	100
51	51	53	53	53	53	53	55	55	55	55	57	57	57	57	57	59	59	59	59	59	59	100	100	100	100	100	100	100	100	100	100
51	51	53	53	53	53	53	55	55	55	55	57	57	57	57	57	59	59	59	59	59	59	100	100	100	100	100	100	100	100	100	100
51	51	53	53	53	53	53	55	55	55	55	57	57	57	57	57	59	59	59	59	59	59	100	100	100	100	100	100	100	100	100	100
51	51	53	53	53	53	53	55	55	55	55	57	57	57	57	57	59	59	59	59	59	59	100	100	100	100	100	100	100	100	100	100

b

0	0	0	0	0	0	0	0	0	0	0	0	0	0	0	0	0	0	0	0	0	0	0	0	0	0	0	0	61	0	0	0
0	0	0	0	0	0	0	0	0	0	0	0	0	0	0	0	0	0	0	0	0	0	0	0	0	0	0	0	59	59	0	0
0	0	0	0	0	0	0	0	0	0	0	0	0	0	0	0	0	0	0	0	0	0	0	0	0	0	0	0	0	59	0	0
0	0	0	0	0	0	0	0	0	0	0	0	0	0	0	0	0	0	0	0	0	0	0	0	0	0	0	0	0	59	0	0
0	0	0	0	0	0	0	0	0	0	0	0	0	0	0	0	0	0	0	0	0	0	0	0	0	0	0	0	0	59	59	0
0	0	0	0	0	0	0	0	0	0	0	0	0	0	0	0	0	0	0	0	0	0	0	0	0	0	0	0	0	0	59	0
0	0	0	0	0	0	0	0	57	57	57	57	57	57	59	0	0	0	0	0	0	0	0	0	0	0	0	0	0	0	59	0
0	0	0	0	57	57	57	57	57	0	0	0	0	0	59	0	0	0	0	0	0	0	0	0	0	0	0	0	0	0	59	0
0	0	0	0	57	0	0	0	0	0	0	0	0	0	59	0	0	0	0	0	0	0	0	0	0	0	0	0	0	0	59	59
0	0	0	0	57	57	0	0	0	0	0	0	0	0	59	0	0	0	0	0	0	0	0	0	0	0	0	0	0	0	0	59
0	0	0	0	0	57	0	0	0	0	0	0	0	0	59	0	0	0	0	0	0	0	0	0	0	0	0	0	0	0	0	59
0	0	0	0	0	55	0	0	0	0	0	0	0	0	59	59	0	0	0	0	0	0	0	0	0	0	0	0	0	0	0	59
0	0	0	0	0	55	55	0	0	0	0	0	0	0	0	59	0	0	0	0	0	0	0	0	0	0	0	0	0	0	0	0
0	0	0	0	0	0	55	0	0	0	0	0	0	0	0	57	0	0	0	0	0	0	0	0	0	0	0	0	0	0	0	0
0	0	0	0	0	0	55	0	0	0	0	0	0	0	0	57	0	0	0	0	0	0	0	0	0	0	0	0	0	0	0	0
0	0	0	0	0	0	55	0	0	0	0	0	0	0	0	57	0	0	0	0	0	0	0	0	0	0	0	0	0	0	0	0
0	0	0	0	0	0	55	55	0	0	0	0	0	0	0	57	0	0	0	0	0	0	0	0	0	0	0	0	0	0	0	0
0	0	0	0	0	0	0	55	0	0	0	0	0	57	57	57	0	0	0	0	0	0	0	0	0	0	0	0	0	0	0	0
0	0	0	0	0	0	0	55	0	0	0	0	0	0	57	0	0	0	0	0	0	0	0	0	0	0	0	0	0	0	0	0
0	0	0	0	0	0	0	55	55	0	0	0	0	0	57	0	0	0	0	0	0	0	0	0	0	0	0	0	0	0	0	0
0	0	0	0	0	0	0	0	55	0	0	0	0	0	57	0	0	0	0	0	0	0	0	0	0	0	0	0	0	0	0	0
0	0	0	0	0	0	0	0	55	0	0	0	0	0	57	57	0	0	0	0	0	0	0	0	0	0	0	0	0	0	0	0
0	0	0	0	0	0	0	0	55	0	0	0	0	0	0	57	0	0	0	0	0	0	0	0	0	0	0	0	0	0	0	0
0	0	0	0	0	0	0	0	55	55	0	0	0	0	0	57	0	0	0	0	0	0	0	0	0	0	0	0	0	0	0	0
0	0	0	0	0	0	0	0	0	55	0	0	0	0	0	57	0	0	0	0	0	0	0	0	0	0	0	0	0	0	0	0
0	0	0	0	0	0	0	0	0	55	0	0	0	0	0	57	0	0	0	0	0	0	0	0	0	0	0	0	0	0	0	0
0	0	0	0	0	0	0	0	0	55	55	57	57	57	57	57	0	0	0	0	0	0	0	0	0	0	0	0	0	0	0	0
0	0	0	0	0	0	0	0	0	0	0	0	0	0	0	0	0	0	0	0	0	0	0	0	0	0	0	0	0	0	0	0
0	0	0	0	0	0	0	0	0	0	0	0	0	0	0	0	0	0	0	0	0	0	0	0	0	0	0	0	0	0	0	0
0	0	0	0	0	0	0	0	0	0	0	0	0	0	0	0	0	0	0	0	0	0	0	0	0	0	0	0	0	0	0	0
0	0	0	0	0	0	0	0	0	0	0	0	0	0	0	0	0	0	0	0	0	0	0	0	0	0	0	0	0	0	0	0

c

Figure 3.7 An example of the Matlab data processing of the grid noise map. (a) A section derived from the noise map of the Wilbraham Road residential area in Greater Manchester; (b) The initial arrays obtained by the Matlab data processing programme, including points representing noised levels, building and roads; (c) Arrays of the façade noise level obtained by a further data process.

Figure 3.7 demonstrates the whole data processing method with the Matlab programme developed. A sample area extracted from an urban area in Manchester is chosen, the RGB raster map of the pixels are substituted with noise values ranging from 30 dBA to 90 dBA as an array as shown in the 2D grid in Figure 3.7b, beside the noise levels, the pixels of the buildings in white colour are substituted with the value of 0, and the black pixels of the road surface are substituted with the value of 100, both are for the convenience of distinguishing with the noise map.

By utilising the Matlab programme based on the comprehensive array of shown in Figure 3.7b, a series of statistical spatial noise indices can be derived from the noise maps, including the L_{avg}, L_{min}, and L_{max}, that represents the spatial average noise level, the spatial minimum noise level, and the spatial maximum noise level respectively; the L_{50}, L_{90}, and L_{10} that represents the spatial median noise level, the spatial background noise level and the spatial intrusive noise level respectively.

To assess the general noise impact to the indoor space, a similar set of six façade spatial noise indices are specifically derived with similar method from a refined array shown in Figure 3.7c. The Matlab programme sweeps off all open space spatial noise indices that are not adjacent to the building edges, thus the outline of the buildings are illustrated by the only the noise values that are within approximately 1 m from the buildings, according to the resolution of the maps.

Furthermore, with the help of the Matlab programme, the proportion of the buildings, the road surface area, as well as the open space area can also be derived from the maps. In further studies, when the heights of the buildings are introduced, more urban morphological indices are also acquirable without the help of the programme. In this study, the method designed is also to test the feasibility of using this Matlab programme to obtain as much as possible information from the 2D grid noise maps which are the main form of strategic noise map presentation in the EU (WG-AEN, 2006), and in prospective noise-mapping practices in China.

3.4 The parametric study approach and selection of urban morphological and spatial noise indices

A parametric study approach is applied in this research. The urban areas are divided into several different groups, the value of a series of urban indices are fixed or classified to define a variety of representative urban morphological modalities with typical density and urban fabric and traffic pattern. Meanwhile, in each group, a series of urban morphological features are altered systematically based on typical urban environment features in relatively low, medium and high-density urban areas. The effect of urban morphological indices on noise distribution is tested by analysing the correlation between the morphological indices and spatial noise indices.

3.4.1 Selection of morphological indices

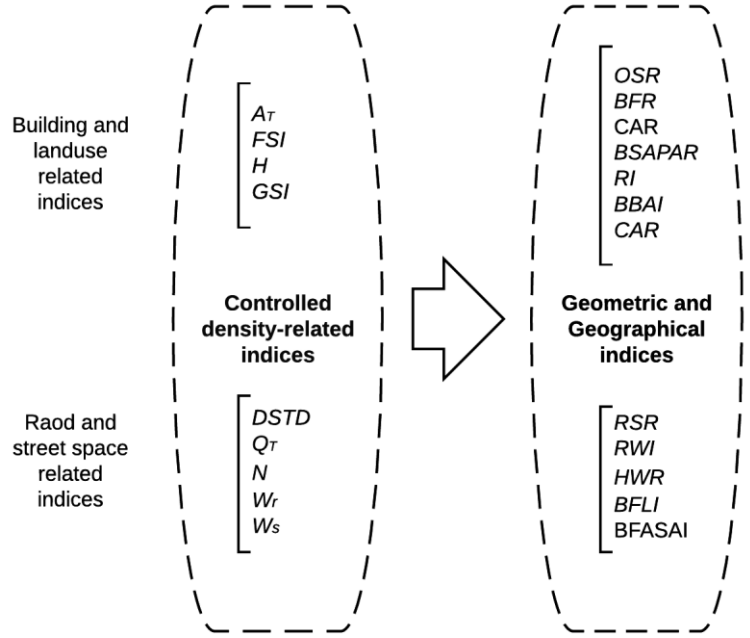

Figure 3.8 Urban morphological selection and calculation process

There are three types of parameters introduced in this research. The main research approach in this research is to study the impact of the changes of one or more parameters on other indices. By fixing or controlling part of the morphological factors, there are a series of other urban factors could be determined thereafter. As can be seen in Figure 3.8 that the entire process of indices calculation consists of three phases, both urban form, road, and traffic indices are controlled and calculated.

3.4.1.1 Basic urban form indices FSI, GSI, and OSI

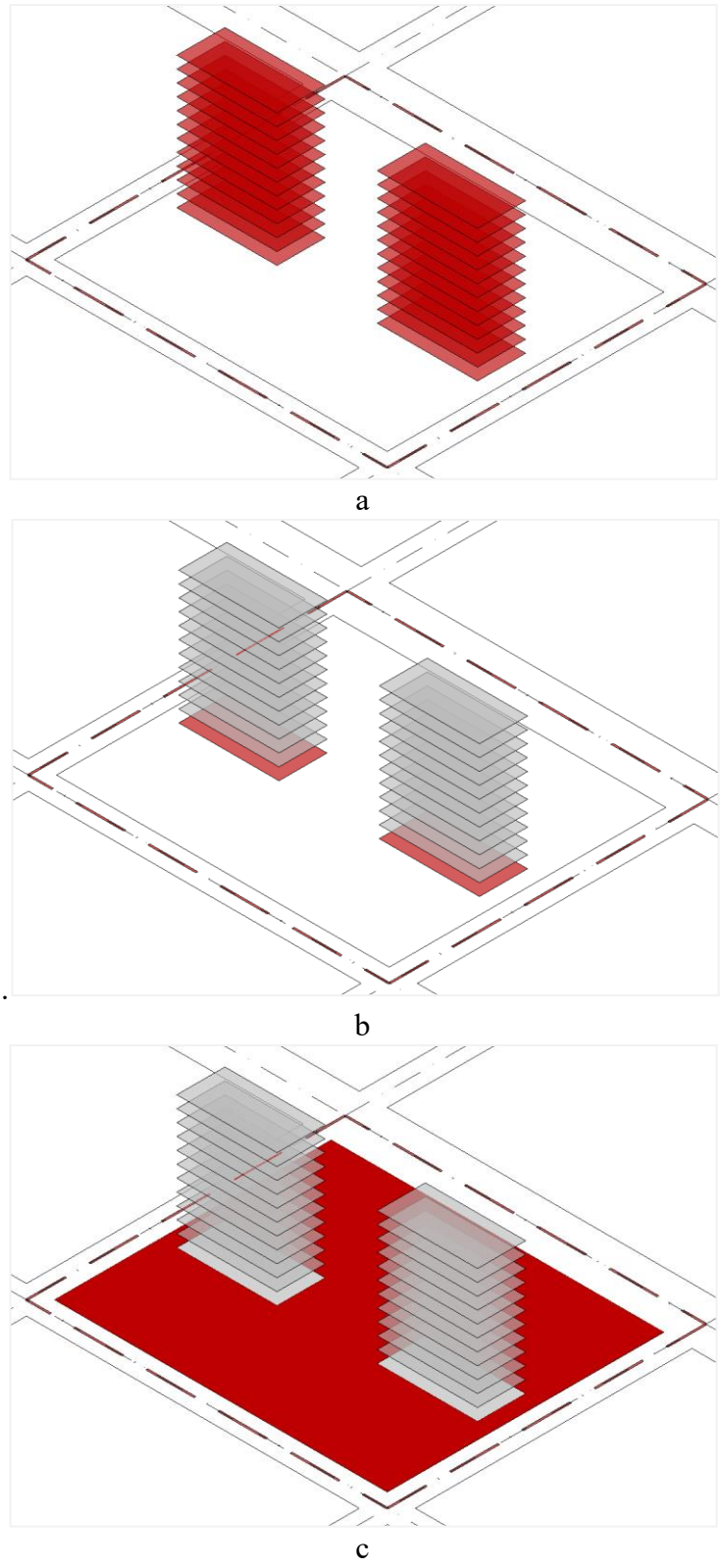

Figure 3.9 Illustration for FSI, GSI, and OSI in a basic fabric area. (a) the floor space index FSI; (b) the ground space index GSI; (c) the open space index OSR. The red dotted line indicates the out boundary of the façade area.

Three key urban morphological indices are introduced for describing the density and form of the buildings and spatial features, the floor space index (FSI), the ground space index (GSI) and the open space index (OSR) as illustrated in Figure 3.9. here are some other indicators purely measures area, height, and length, e.g. the total area of the planned area A_T, the height of the buildings in terms of storey numbers L and measured by metre H, and the perimeter of the buildings L, etc., which may not be sufficient for sake of comparing different urban forms. Thus, it is necessary to adopt or raise a series of comprehensive urban form indices.

Figure 3.9 illustrates the implication of the three indices in a basic fabric area, in which the red dotted line along the road central lines shows the boundary of the fabric area, the size of which can be regarded as the A_T of it. As can be seen in Figure 3.9 and Equation 3.4, the FSI indicates the ratio of total floor area to the total area of the planned area.

$$FSI = \frac{\sum A_f}{A_T} \tag{3.4}$$

where the A_f represents the floor space. It can be seen that the FSI considers mainly the total development intensity, and can also represent the total mass of building entities per unit land area, given that the floor height are similar. The GSI is the ratio of the ground projection of the buildings to the total planned area (Oliver-Solà et al., 2011). In Figure 3.9b and Equation 3.5:

$$GSI = \frac{\sum A_g}{A_T} \tag{3.5}$$

where A_g is the ground space of a building. It can be seen that the GSI defines the two dimensional building density of the urban area. The OSR which describes the porosity of the planned area is defined as the ratio of open space to the total planned area (Huang, Lu, & Sellers, 2007), as shown in Equation 3.6:

$$OSR = \frac{\sum A_O}{A_T} \tag{3.6}$$

where A_O indicates the open space except all building footage and road surface areas, as can be seen in Figure 3.9c.

3.4.1.2 Relationship between basic urban form density indices

Besides the GSI and OSR, the road coverage ratio (RSR) describes the density of roads in terms of the ratio of the surface area of carriageways to the total planned area. The three two-devotional spatial coverage indices have the relationship shown in Equation 3.7:

$$GSI + OSR + RSR = 1 \tag{3.7}$$

In Equation 3.8 the relationship between FSI and GSI is also demonstrated:

$$\frac{FSI}{GSI} = L \tag{3.8}$$

where the L shows the average layers of floors of the buildings.

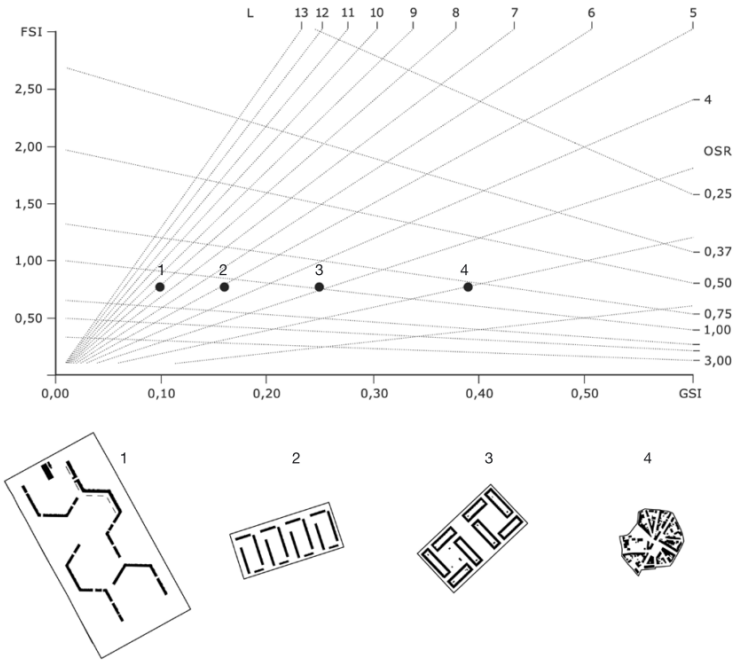

Figure 3.10 Four examples of urban forms derived from urban areas of Amsterdam with equal value of FSI (Pont & Haupt, 2005)

The relationship of the FSI, GSI, OSR and the building layers L are interrelated thus it is possible to construct an framework to demonstrate and evaluate the urban form in terms of density using a four axes framework, which is originally introduced by Pont and Haupt (2005) as the Spacemate tool, as can be seen in Figure 3.10 that, three sample areas with identical FSI has distinctive GSI, OSR, and *L*.

3.4.2 Road space and traffic related indices

- ***Daily spatial traffic density – DSTD***

The *DSTD* is proposed in this research a measured of the total vehicle density in terms of vehicles per day per unit area. It is calculated by dividing the cumulated vehicle counts in all roads in the entire planned district of an average day with the total size of the studied area, as demonstrated in Equation 3.9:

$$DSTD = \frac{Q_T}{A_T} = \frac{\sum Q_r}{A_T} \tag{3.9}$$

where Q_r is the annual average traffic flow of a single road. By setting the FSI at three levels and fixing the DSTD, the parametric study is able to be carried out by systematically changing the arrangement and height of the buildings, the pattern and density of the road network.

- ***Road network density – N***

The road network density *N* is one of the key factors describing the length density of the roads, which is also utilised in the Spacemate tool by Haupt (2005). It can affect both traffic distribution and urban fabric typology is the road density in terms of meter per square meter, as shown in Equation 3.10:

$$N = \frac{\sum l_{ir} + \frac{1}{2}\sum l_{er}}{A_T} \tag{3.10}$$

where the l_{ir} and l_{er} represents the length of the inner roads and the roads at the outer edge bordering the studied area and the external areas. In this study is the four arteries surrounding studied area and is calculated by half of their length. This rule of calculating total road length is also applicable to the calculation of other parameters that have road length involved, as the external road has only shares half of their road kerbs with the internal area.

- ***Height-to-width ratio – HWR and road width index – RWI***

The height-to-width ratio is introduced to estimate the average aspect ratio of the street spaces formed by flanking buildings and the ground surface (Schulte, Tan, & Venkatram, 2015), the calculation method of the HWR of a single road is shown Equation 3.11:

$$HWR = \frac{H_s}{w_s} = \frac{\frac{1}{n}\sum_{i=1}^{n} h_i}{w_s} \qquad 3.11$$

where H_s is the average height of the street space, w_s represents the width of the street, and h_i is the height of the flanking building façade, as can be seen in Figure 3.11. It is to note that the street width w_s here is measures the average distance between the flanking building façades rather than the road carriageway width w_r.

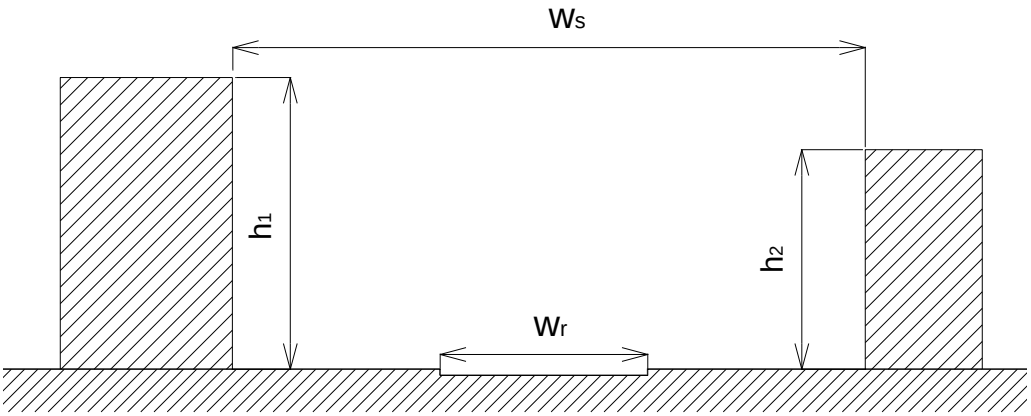

Figure 3.11 Calculation of the height-to-width ratio of a typical street section with two parallel flanking buildings

Similarly, the road width index (RWI) is proposed in this research as a geometric parameter that describes the geometry of the space from a different perspective. It reflects the ratio of the road width w_r that defined as the average distance between opposite road kerbs, to the entire width of the street canyon w_s that defined by the distance of flanking buildings, as can be seen in Figure 3.11. It can be calculated by a simple calculation as shown in Equation 3.12:

$$RWI = \frac{\sum w_r}{\sum w_s} \tag{3.12}$$

It can be seen approximately as a two-dimensional parameter that describes the proportion of the road space occupation ratio in a street canyon.

3.4.3 Building related indices

- ***Building frontal area to street index – BFASAI***

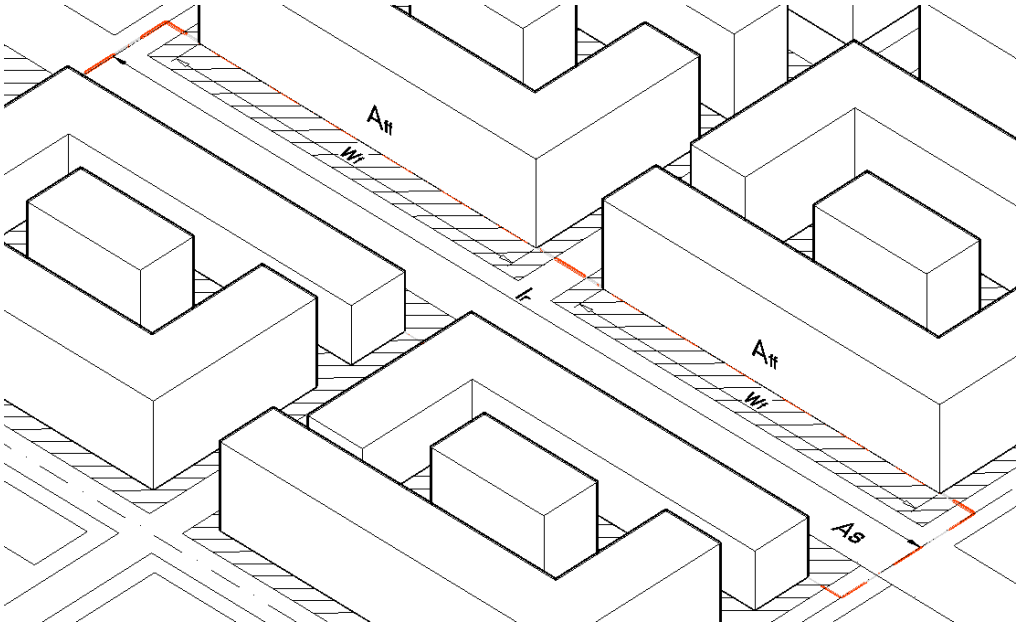

Figure 3.12 The parameters of the street space for the calculation of BFASAI and BFLI

As shown in Equation 3.13 that, the BFASAI can be seen as a more precise descriptor alternative of the HWR which is the aspect ratio of the cross section of an average street canyon. Considering that the specular reflections in the street canyon are key to the propagation of traffic noise and mainly occur between the flanking building façades

(Probst, 1998), this index may be seen as an aspect ratio that describes the shape of the street canyon more closely and may be more related to traffic noise calculation.

$$\text{BFASAI} = \frac{\sum A_{ff}}{\sum A_S} \tag{3.13}$$

- ***Building façade area ratio – BFR***

The building surface area ratio (BFR) measures the ratio of all building façade area of the buildings to the total area of the planned district (Burian, Brown, & Linger, 2002), as shown in Equation 3.14, where the A_{fa} indicates the building façade area.

$$\text{BFR} = \frac{\sum A_{fa}}{A_T} \tag{3.14}$$

- ***Rugosity index – RI***

The rugosity index (RI) is the mean height (H_m) of all built and non-built objects in the urban area, which reflects the average height of the entire urban canopy (Adolphe, 2000). It can be calculated as Equation 3.15:

$$\text{RI} = \frac{\sum (A_g \times H)}{\sum (A_g + A_o)} \tag{3.15}$$

where A_g and A_o represent the building ground space area and the non-built open space area. This urban morphological index generally describes the average height of an urban area with considering both built and non-built spaces, thus the result RI or H_m in Equation 3.12 is normally lower than the average building height H.

- ***Building frontal length index – BFLI***

The building frontal length index (BFLI) can also be defined as the street interface density (SID) (Zhou et al., 2016). The BFLI measures the ratio of the width projection of the

flanking buildings w_f to the total street length l_r both of which are also demonstrated in Figure 3.12.

The BFLI measures the average ratio of the width projection of the flanking buildings w_f to the total street length l_r, both of which are also demonstrated in Figure 3.12. The BFLI can then be calculated using the Equation 3.16:

$$\text{BFLI} = \frac{1}{n}\sum_{i=1}^{n}(\frac{w_f}{l_r})_i = \frac{\sum w_f}{2(\sum l_{ir} + \frac{1}{2}\sum l_{er})} \quad 3.16$$

where the parts below fraction line calculate the total length of roads with flanking buildings accounted in the calculation of BFLI of each individual fabric area, the l_{ir} and l_{er} represents the length of internal roads and the length of the external roads bordering the planned district.

- ***The building perimeter to road length index – BPRLI***

In this study the building perimeter to road length index (BPRLI) is another newly proposed index which can be defined as the total perimeter of all buildings to the total length of the roads, as defined in Equation 3.17:

$$\text{BPRLI} = \frac{1}{n}\sum_{i=1}^{n}\frac{P_i}{(\sum l_r)_i} = \frac{P_T}{2(\sum l_{ir} + \frac{1}{2}\sum l_{er})} \quad 3.17$$

where the i indicates the total number of basic fabrics in the planned district; P represents the perimeter of all buildings in a basic urban fabric as shown with blue lines in Figure 3.13; $\sum l_r$ shows the total length of all roads surrounding a basic fabric area. Due to reduplication of roads in-between neighbouring basic fabrics, the parts in the final formula below the fraction line $2\left(\sum l_{ir} + \frac{1}{2}\sum l_{er}\right)$ calculates the total length of roads that are accounted in the calculation of BPRLI of an individual fabric area.

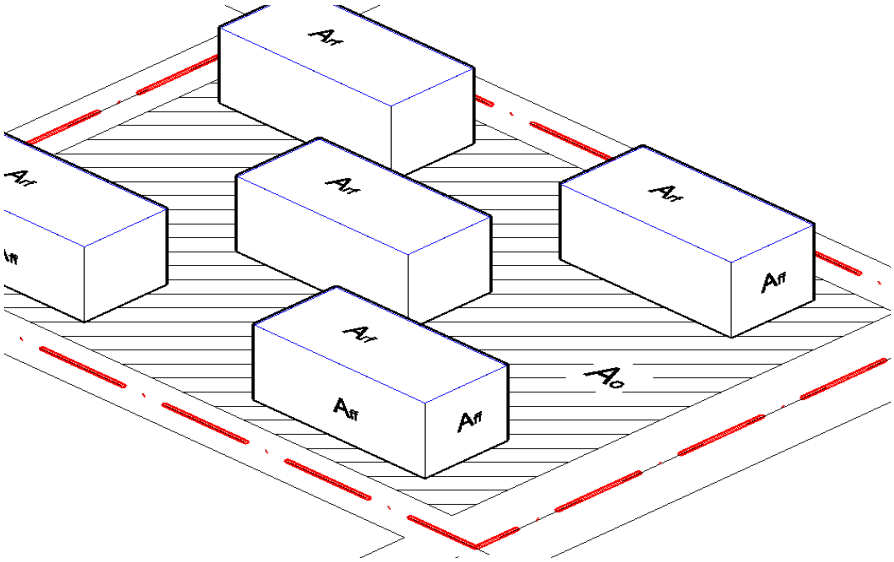

Figure 3.13 The parameters of a basic fabric for the calculation of CAR, BPRLI, and BSAPAR.

As can be seen in Figure 3.13, the red dash lines following the road centre lines, denote the boundary of the planned basic urban fabric; the blue lines indicate the perimeters of the buildings; A_{rf} and A_{ff} represent the rooftop surface and the frontal façade area respectively, $A_o$represents the open ground space.

- ***Complete aspect ratio – CAR***

The complete aspect ratio (CAR) as an concept to measure the roughness of the planned area is widely used in urban aerodynamics related studies (Burian et a l., 2002) (Edussuriya, Chan, & Ye, 2011), which measures the ratio of all roughness area plus the ground area to the total land area. As demonstrated in Equation 3.18 that the total roughness area in this study is consists of the roof and all façades of the buildings:

$$\mathrm{CAR} = \frac{\sum(A_{fa} + A_{rf}) + A_G}{A_T} \qquad 3.18$$

where the open ground area A_G in this study is all the open ground space except the buildings, and the A_{rf} is the individual rooftop area of a building as shown in Figure 3.13.

- ***The building block area index –BBAI***

The building block area index (BBAI) proposed by the author in this study calculates the ground coverage of the building block boundary. It can be calculated as the total building block boundary area to the total lot area as can be seen in Equation 3.19:

$$\text{BBAI} = \frac{\sum A_B}{\sum A_L}$$

3.19

Where A_B is the size of the external boundary of all buildings within a basic urban fabric, when there is only one building, it is equivalent to the building ground space A_g. The A_L here indicates the size of the planned lot area in a basic urban fabric, the boundary of which is the road kerbs. This BBAI reflects the coverage of the built-up areas including the space fully or partially restrained in a planned lot, which is especially important when the building layouts are confined. When there are smaller BBAI, there tend to be larger open space.

- ***Building surface area to plan area index – BSAPAR***

The building surface area to plan area ratio (BSAPAR) represents the ratio of the total surface area of all buildings to the total area of the planned district (Hao & Kang, 2014; Burian et al., 2002), as shown in Equation 3.20:

$$\text{BSAI} = \frac{\sum(A_{fa} + A_{rf})}{A_T}$$

3.20

Where the A_{rf} represents the building roof area as can be seen in Figure 3.13, which can be calculated using the value equivalent of building ground space area A_g.

3.4.4 Calculation of spatial noise indices

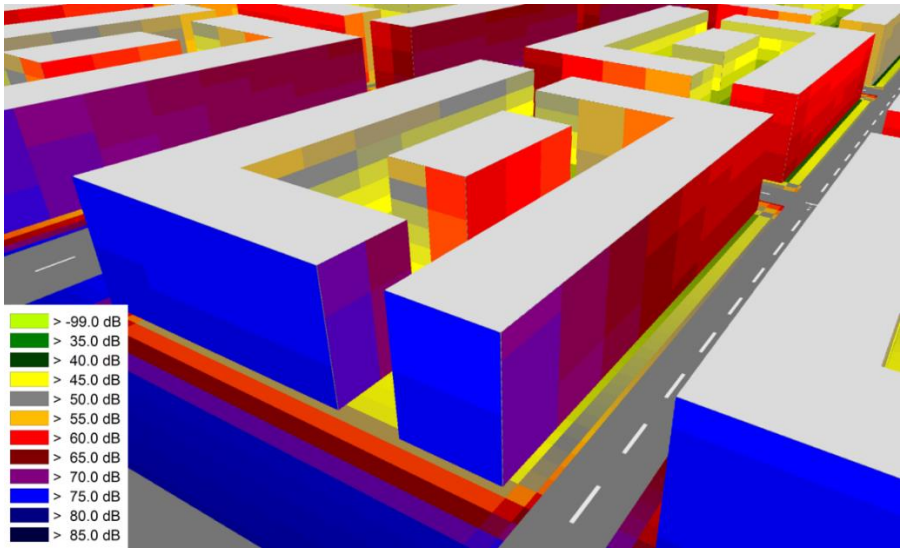

Figure 3.14 Noise calculation on the building façades, the building evaluation can then help to estimate the noise level at the building façade level of all buildings.

The calculation of noise is conducted using the calculation method defined in CRTN and ISO 9613-2 method. The general ground spatial noise indices and the ground façade spatial noise indices are derived from the grid noise maps calculated above the ground level. Meanwhile as shown in Figure 3.14 that the SPL on the building façades can be calculated using the building evaluation function (DataKustik, 2012a), a series of statistical spatial noise indices can also be derived from the database using the same statistic measure as that used on the ground level spatial noise indices. Due to the lack of indoor noise calculation method in the urban scale, the façade spatial noise indices can in some extent be seen as an approximate indicator of the impact to the indoor environment caused by the outdoor the traffic noise.

With the Matlab programme and the building evaluation option in the noise mapping package, there are three types of spatial noise indices to be derived from the noise maps: the ground levels (GL_n) which only measures the noise levels at the ground level, ground façade levels (GFL_n) that represents the noise level distribution close to all the building façades at the ground level, and the total façade levels (TFL_n) which considers the noise distribution on the third dimension by measuring the noise distribution on the façades of all buildings. Six basic statistical spatial noise indices that represent the spatial noise distribution of each type of noise levels, including the L_{max}, L_{avg}, L_{min}, L_{10}, L_{50} and L_{90} and a series of attenuation indices are calculated based on basic subtractions using two of the

spatial noise indices to describe the overall attenuation between the two spatial noise indices. The spatial noise indices and their implication can be seen in Table 3.6.

Table 3.6 Statistical implication of the spatial noise indices.

Indices	Indication
Spatial noise indices	
L_{max}	Spatial maximum noise level
L_{avg}	Spatial average noise level
L_{min}	Spatial minimum noise level
L_{10}	Spatial intrusive noise level
L_{50}	Spatial median noise level
L_{90}	Spatial background noise level
Spatial noise attenuation indices	
L_{max} -L_{avg}	Total attenuation from the quietest to the noisiest
L_{10}-L_{90}	Total attenuation from intrusive and background noise level
L_{max} -L_{50}	Attenuation in the noisier half space
L_{50}-L_{min}	Attenuation in the quieter half space
L_{max} -L_{10}	Attenuation in the 10% noisiest area
L_{10}-L_{50}	Attenuation in the relatively noisier space
L_{50}-L_{90}	Attenuation in the relatively quieter space
L_{10}-L_{90}	Attenuation in the 10% quietest area

It is to note that, the ground noise level GL_n denotes the general noise impact to all the ground space in the studied area except that covered by road and buildings, and the variety of GL_n represents different statistical measure of the overall traffic noise distribution, and is ideal for further application in all forms of large scale strategic noise maps; similarly the GFL_n and the TFL_n reflects the noise impact to the urban inhabitants at the overall ground level and on all the vertical façades of the buildings.

The various forms statistical noise indices in Table 3.6 are derived using the same Matlab program as shown in Section 3.4.4, and could both be derived from other forms of strategic noise maps. Thus, the methods and findings in this chapter can be deployed as strategic measures for large scale noise assessment and prediction, especially the relatively low-rise built-up areas without considering the distribution of noise on the vertical level.

3.4.5 Selection of idealised urban morphology types

In the real-world situation, the structure of the road network and the building form varies depends on a variety of factors, e.g. the planning scheme, land-use, development strategy, population and culture etc. Nonetheless, in this study some of the representative features of existing urban morphology types are defined based on typical features abstracted from real-world cases and are reflected and constrained by predefined indices.

3.4.5.1 Traffic distribution

In this research, the scale and traffic pattern of the idealised urban area cases are predefined. As described earlier, Q_T and DSTD are fixed. The structure of the road network and hence the traffic distribution pattern are defined first, based on which the texture and pattern of the city are defined later. A series of idealised transportation network types are defined. The main approach of designing a series of abstracted road network in this study is to reflect the traffic distribution pattern and the road network density and topology.

Based on empirical analysis of the urban road network scale found in previous chapters, it is found that there are fundamentally two types of road network systems in existing cities and metropolitan areas. The road hierarchy of most of the cities in the east and west have the high-speed archery road system with a network density of 1000–1500 m, which serves as the major thoroughfare connecting one district or urban area to another. In which the values of DSTD are identical, i.e. there are the same number of vehicles passing through each square kilometres.

3.4.5.2 Road network selection

Three fabric types are set in this study accordingly with relatively high, medium and low road network density *N;* corresponding road network typology could be seen in Figure 3.15. The road networks are defined correspondingly into four types, one with high *N* (network density) as can be seen in Figure 3.15a, one with low network density as can be seen in Figure 3.15b, two cased with medium *N* of the same value but different network type as can be seen in Figure 3.15c and Figure 3.15d. It is to note that the cases with

medium road density as can be seen in Figure 3.15c and Figure 3.15d have the same value *N*, while are slightly different in the distribution of the branch roads.

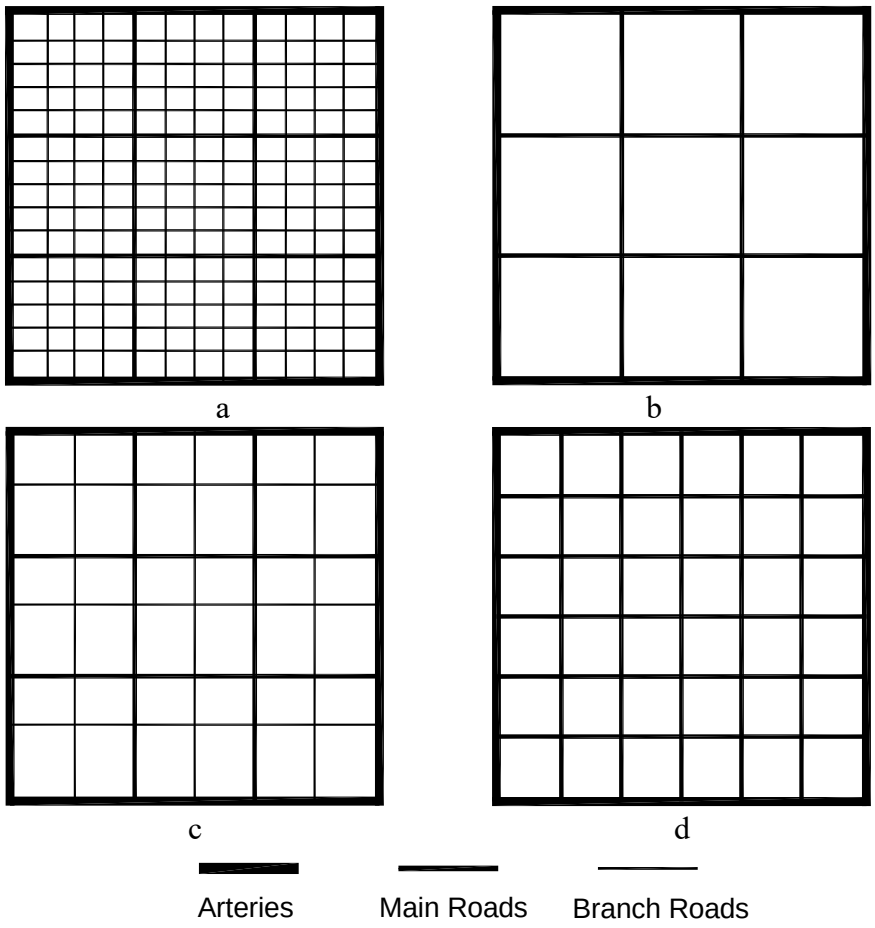

Figure 3.15 Four pre-defined idealised road grid network patterns. (a) High network density; (b) Low network density; (c) Medium network density set 1, with unevenly distributed small branch roads; (d) Medium network density set 2, with evenly distributed branch roads.

The main roads and branch roads in Figure 3.15d is evenly distributed with an identical width of 14 m and divide the entire district evenly into 36 square-shape blocks covering approximately 37056 m^2 each. The four idealised cases also represent three typical urban fabrics with an average size of 90 m × 72 m, 375 m × 375 m and 187.5 m × 187.5 m respectively.

In each case, the gap between the arteries is fixed at 1155m, and 4 basic main roads are set evenly with a gap of 385 m from each other. The density of the branch roads is set individually into 3 categories. In the highest density case, 21 branch roads together with

the arteries and main roads divide the entire district into 180 blocks with an average area of 7411 m^2. The lowest density area has 9 large urban fabrics with 3.7 hectares on average.

The two cases with medium road density are designated the same value of in terms *N*, while the distribution of the branch roads is slightly different. Both cases have six branch roads, while for the cases with smaller the branch roads, the branch roads distributed unevenly with smaller road width of 7 m, is a typical scenario in modern Chinese real estate developments or *Danweis*.

3.4.5.3 Classification of pre-defined urban morphological indices

In each road network type, nine sets of urban forms with different combination of FSI and GSI, as well as building height *L* in terms of storeys are planned. 36 idealised cases spread are introduced with nine sets of FSI and GSI values, and with the same GSI or FSI, the building height in terms of *L* are distinctive; the change of GSI also leads to varying porosity in terms of OSR values.

3.4.5.4 Building arrangement and forms

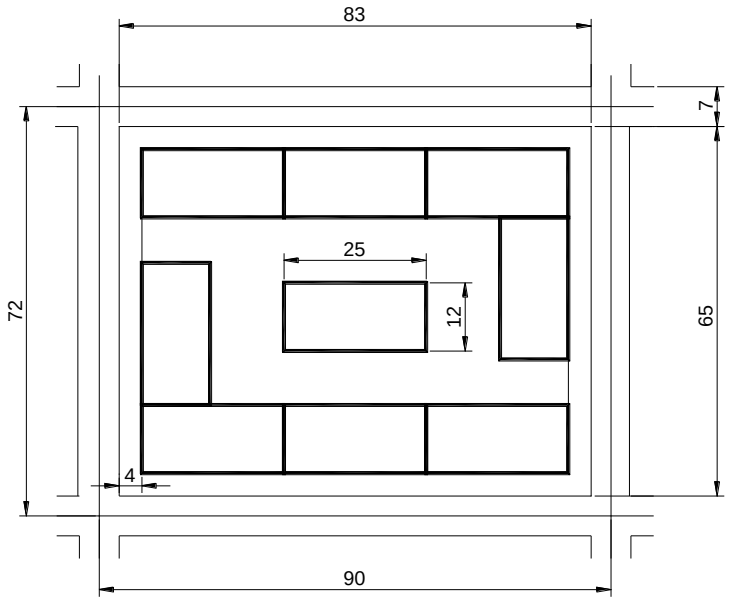

Figure 3.16 The scale and plan of a building block with high GSI using the combination of the basic building unit (unit: m)

To ensure the consistency and comparability of the cases, the building blocks are planned using a basic building unit of 25 m × 12 m as shown in the example in Figure 3.16. In

most of the cases, the buildings are designed using integer times of the basic unit. The building forms are planned uniformly the planned road network according to the pre-defined urban form indices. The idealised building forms have a variety of urban morphological indices combinations, which together with the combination of nine different types of road networks represents a series of typical features of subsistent urban forms in both eastern and western cities.

3.4.6 Statistical analysis methods

The relationship between the urban morphological indices and spatial noise indices are systematically analysed with the help of a statistic software, the SPSS 22 (IBM Corp., 2011). A group-wise comparison is conducted between different case groups with three different urban density-related indices. Then the correlation is systematically analysed using the bivariate correlation analysis. A series of prediction models are developed based on a multiple linear regression process in a hierarchical fashion, only the independent variables, i.e. the urban morphological predictors with acceptable collinearity and exhibits strong prediction power are reserved in the final prediction models. The implication of the predictors and the dependent variables i.e. certain spatial noise indicators are discussed. It is to note that the prediction models have limited prediction power and applicability in the real urban noise planning practice considering the limitation of the idealised sample cases analysed in this study. It is still of great significance to explore that how certain characteristics of the urban form that can be regulated during the urban planning process, can significantly have affect the traffic noise distribution.

3.4.6.1 Basic comparisons

To demonstrate the general trend of the influence of some key urban morphological features on the traffic noise distribution, a series of preliminary comparisons of the spatial noise indices are conducted between different case groups according to the urban-density-related indices, the FSI, GSI and road network *N*.

- ***Group-wise general noise level comparison***

The values of the indicators that indicating the general noise level in the idealised case are compared across case groups of different urban density. The cases groups are divided based on the difference in urban density weighing by three indices, the FSI, GSI and road network density *N*. The spatial noise indices L_{avg} and L_{50} that representing the spatial average and median noise level are compared in bar charts to demonstrate the how the change of urban density in terms of each density-related index affects the spatial average noise level. The general noise level of each density group is also compared with the 55 dBA threshold according to noise standards of EU (EEA, 2010) and China (MEP China, 2008).

- ***Variation of noise level***

It is also essential to understand how the traffic noise levels distributes spatially in the urban space. A further analysis on the spatial distribution and variation of traffic noise levels are conducted. For each case group of low medium or high urban density, five statistically important indices of each spatial noise index type, the L_{max}, L_{10}, L_{50}, L_{90} and L_{min}, are selected to demonstrate the noise levels at the road source end, the top 10% nosiest space, the median values, the lowest 10% space, and the quietest zones, the maximum, mean and minimum values of each types of noise levels are highlighted, for the sake of indicating the range of distribution.

- ***The difference in standard deviations***

In the meantime, dot charts are drawn to present the standard deviations (SD) of all six indices of each spatial noise index type. The SD represents the tendency of each index differ from the mean value. Hence for each index, the higher the SD value, the higher variation the values. The low, medium and high-density groups are collectively compared for each index type.

- ***Noise attenuation***

The spatial noise attenuation is also compared. A number of stacked bar charts are demonstrated for each case group. Differently coloured sections of the bars represent the noise distribution from the nosiest zone to the quietest zone, divided by five key spatial

noise indices, L_{max} to L_{10}, L_{50}, L_{90} and L_{min}. The stacked bar chats graphically demonstrate how the road traffic noise attenuate in general and in each noise zone divided.

3.4.6.2 Multiple linear correlation analysis

A general multilinear correlation is conducted between all the urban morphological indices tested, and the spatial noise indices as well as some calculated indices that representing the spatial attenuation in certain areas. Only the two-tailed Pearson correlation coefficient R with Pearson Sig. value of $p < 0.01$ are high-lighted, with considering the nature of this parametric study. The implications of the significant correlations are interpreted in detail from the perspectives of both urban noise transmission and urban planning.

The urban morphological indices are divided into three different groups, the urban density related indices which are mainly predefined to represent typical urban morphological modalities based on empirical values of real-world cases. The building and street geometric indices (Edussuriya, Chan, & Ye, 2011), which are mostly related to the building layout and the street interface morphology; and the urban geography related indices, which are mostly related to the three-dimensional characteristics of urban settlements and the general geographical features of the built-up area.

Six spatial noise indices of the open ground, the ground façade level and on all façades level are tested. The average noise attenuation from the spatial intrusive noise level to the background noise level measured by L_{10}-L_{90}, the average attenuation in the quieter half and the noisiest 10% space measured by L_{50}-L_{min} and L_{90}-L_{min}; the average attenuation in the quietest 10% space; and the attenuation in the noisier half and quieter half measured by L_{max}-L_{10} and L_{max}-L_{50} are also tested representatively.

3.4.6.3 Multiple linear regression modelling process

Based on the results of the multi-linear correlation analysis, correlation between a series of urban morphological indices and spatial noise distribution indices, it can be seen that there are strong indications that the change of certain urban morphological characteristics

can significant affect the general level and distribution of traffic noise impact in the open ground and to the indoor environment.

To further test the effectiveness of the variables and providing a practical tool for urban noise estimation and abatement in the earliest stage of urban planning process, prediction models with strong prediction power of measured by R^2 of over 0.5 are produced through a series of multiple linear regression analysis. The independent variables (IV) of the predictors of the models are the urban morphological indices that are found in the multi-linear regression process with Pearson correlation Sig. values of $p < 0.01$; the dependant variables (DV) are the L_{avg}, L_{10}-L_{90} of three types of spatial noise indices.

- ***Hierarchical linear regression***

The selected IVs are thereafter inserted into the regression model in a hierarchical fashion. The Hierarchical regression analysis refers to a prediction model development process in which the user is allowed to specify the entry of IVs with a pre-fixed order based on relevant theory and the user's judgement rather than pure statistical indicators, through which the most interested variable can be examined (UCD Denver, 2016). In a typical hierarchical linear regression process, one or more IVs of interests could be tested to compare the change in prediction power (Kim, 2016). It is to note that Hierarchical linear regression is different from a Hierarchical Linear Modelling (Woltman et al., 2012) process.

The statistical principles of a hierarchical multiple regression are similar to a standard or stepwise method, the difference is that the IVs are input, and theoretically important IVs can be tested individually, hence the overall prediction model and relative contribution of each block of variables can be assessed, more importantly it gives the user more freedom to test the prediction power of IVs that matters the most in reality (UCD Denver, 2016).

- ***Collinearity and elimination of independent variables***

The collinearity among IVs could reduce the prediction power and applicability of the model, as it implies that the IVs with high collinearity may indicate the same concept. Thus, a process of cut-off shall be implemented in order to remain the most influential

IVs based on the tolerance value, or its reciprocal, the Variance inflation factor (VIF) (Jesshim, 2003).

The commonly used VIF cut-off value of 10 (Cohen et al., 2003; Myers, 2000) is not adopted in this research. A more strict collinearity diagnostic method of removing the IVs with Variance Inflation Factor (VIF) higher lower 5 is adopted, with both statistical and substantial considerations (Heiberger & Holland, 2004). Akinwande, Dikko, & Samson (2015) also proposed the elimination process targeting on a VIF $\leq$ 5 for better identification of suppressor variables to be remained in the prediction model.

3.5 Conclusions

In this chapter, the methodology adopted in each major parts of the study is systematically described. The main logic that threads through the four major chapters is the quest of the potential relationship lies between urban morphological indices and spatial noise indices through applying the EU noise mapping method in a variety of sample areas, both in the real-world urban environment in the UK and China, and a series of idealised sample areas. The state-of-the-art EU noise simulation package Cadna/A with applying the calculation method CRTN and ISO 9613-2 is chosen as the main tool for the noise simulation in all chapters. In the first part in Section 3.2 the methods adopted in Chapter 4 and Chapter 5 for the optimisation of the default calculation configurations, and the method for the applicability test are interpreted in detail. A series of novel tools and concepts are introduced in Section 3.3 for the comparison study conducted in Chapter 6, including the grid map processing programme using Matlab, and the method for a series of spatial noise indices that characterises the general noise level and the distribution of noise. The basic case selection criteria, data acquisition method for the noise mapping calculation are also introduced. In Section 3.4 a parametric study approach is introduced for Chapter 7, by abstracting a series of representative urban morphological indices reflected in 36 idealised cases. The fundamental notions, calculation methods and implications of the sixteen tested morphological indices are explicitly introduced. The meaning and calculation method of the spatial noise indices and the spatial attenuation indices are also introduced, the statistical principles and processes of the correlation analysis and the production of prediction models is also introduced in detail with reference.

Chapter 4 A pilot study on the optimisation of EU noise calculation method in Chinese urban environment

4.1 Introduction

In previous studies in the EU, a variety of notable calculation errors is found when using current calculation methods, the gap between calculation and measurement can be as large as 6-11 dBA depending on the location of the receiver points. (Hepworth, 2006; Nijland & Van Wee, 2005).

The primary aim of this chapter is to test the feasibility of utilising the optimised calculation configurations and modelling method in a sampled case are selected in a case with typical Chinese urban sound environment features. Based on a series of parametric tests by changing the default configurations, a set of optimised calculation configuration settings can then be introduced.

The first objective of this chapter is to conduct a series of pilot test to verify and find a set of optimised calculation configurations through systematically tuning the default configurations recommended by representative EU traffic noise calculation methods and mainstream noise-mapping packages. The second objective is to test the effectiveness and accuracy of the EU method in the selected case study area with a series of spatial and acoustical features found in urban sound environments typical to China. Further analysis and discussions are then conducted on the inaccuracies found in certain locations and urban scenarios, suggestions of improvement are given.

The chapter consists of three major parts: Firstly, in Section 4.2 the method for the case selection and the characteristics of a selected area with relatively simple urban morphological and urban sound environment features is introduced. The topography, urban morphology, building, road and traffic features are introduced. In Section 4.3, a series of calculation settings based on default configurations are tested. The measurement results at a variety of receiver points locating both on the ground level and approximate

to the building surfaces on different altitudes are collected for the applicability analysis. By utilising the in-situ data collected, a series of noise calculations are conducted using sets of optimised calculation configuration settings, the total A-weighted SPL of most of the receiver points and the SPL at the central frequencies of eight major octave bands of smaller sets of receiver points are conducted. The validity of the default ground absorption settings, the opposite façade correction calculation setting and the increased maximum reflection order are discussed. In the further applicability test in Section 4.4, the observable disparities between the calculation and measurement results are systematically analysed to validate the patterns and the potential causes of the disparities in a variety of scenarios. The calculation accuracy of both the A-weighted noise levels at each receiver point and the noise spectrum analysis of a series of receiver points selected at sensitive locaitons are discussed.

4.2 Studied case selection

In this section, to test the adaptability of the selected noise mapping calculation method in typical Chinese urban sound environment, a case study area with relatively simple urban sound environment and morphological features in Wuhan is selected. A series of calculations are implemented on a variety of receiver points in the area. By systematically adjusting the default configuration settings, the calculation results are then compared with the in-situ measurement results. Further analysis and discussions are then conducted on the inaccuracies found in certain locations and urban scenarios, suggestions of improvement are given.

The area is selected for its simple acoustic environment features and representativeness of Chinese urban sound environment features: a large plain square surrounded by a group of multi-storey and high-rise buildings, and there is only one dual-carriage way, the Donghu Road, with large traffic flow. The Donghu Road is a lakeside road dividing the Donghu Lake and the Wuhan University. As can be seen in Figure 4.1, due to its relatively closed form and isolated location, it is less interfered by other traffic noise sources, therefore a series of calculations can be better conducted to verify the performance of the state-of-the-art EU noise calculation method using the default configuration settings.

4.2.1 Topography and urban morphology

The terrain enclosed by the pair of arc-shaped buildings is slightly uneven and has several gradually ascending steps from the Donghu Road to the south side square of a high-rise building, each step is approximately flat, and the roadside square is nearly 1.1 m lower than the ground bases of the buildings. The rectangular square locating in the south of the high-rise buildings is 7.9 m higher than the ground base of the high-rise buildings.

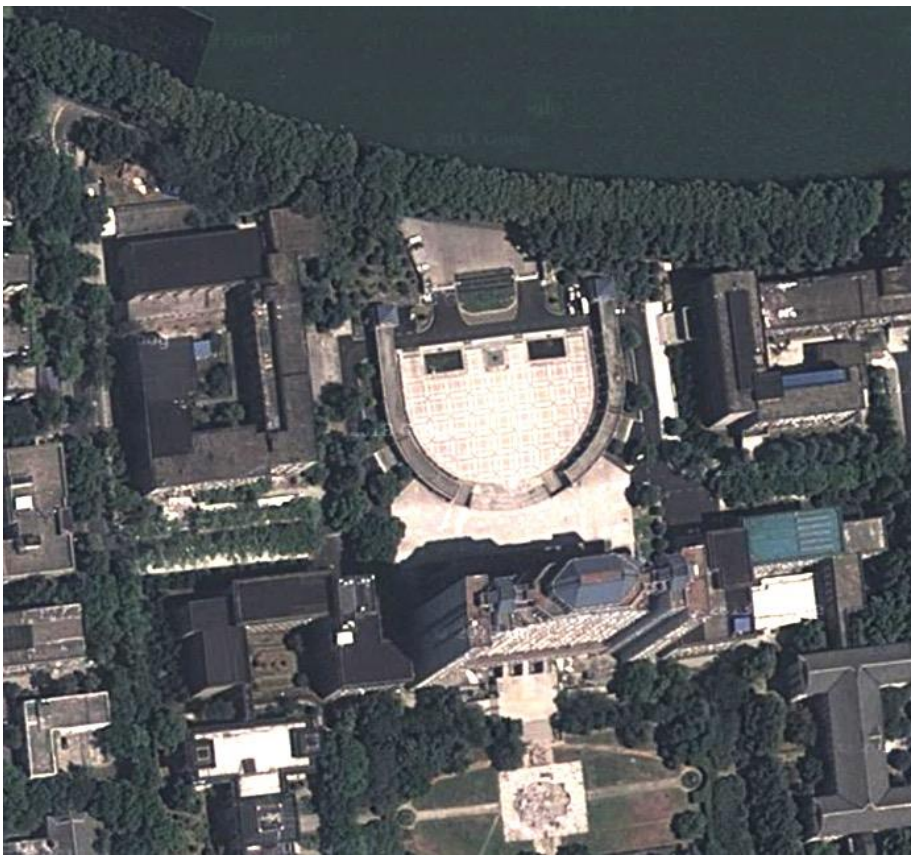

Figure 4.1 Donghu Road with open square and high-rise building. Source: Google Maps (Google Inc.)

The selected area is part of the Wuhan University with an exclusive campus of 3.4 km^2. The enclosed campus together with similar types of urban settlement units or building agglomeration is common in major cities in China like Wuhan, which serves as one of the most unique self-contained urban units (Huang, 2006). The traffic accessibility is strictly managed, thus this site close to an external main road — the Donghu Road — is ideal for a pilot study with the simplest elements: main road, open space, and high-rise building.

The dual-carriageway Donghu Road is the only road source in this case, which runs alongside the Donghu Lake with large open water and no noise sources. In the centre of the sampled area between the road and the main building, the open square surrounded by a small road and a group of education buildings, including the 21-storey major building, is as large as nearly 6000 m^2. The square is a medium version of its kind, comparing with many large urban squares of this type in major Chinese cities. The urban open squares in China are mainly constructed for political and public activity purposes; and normally planned close to one or more main roads facing one or a group of massive-scale public buildings; having hardened surface little or no vegetation (Gaubatz, 2008).

4.2.2 Building features

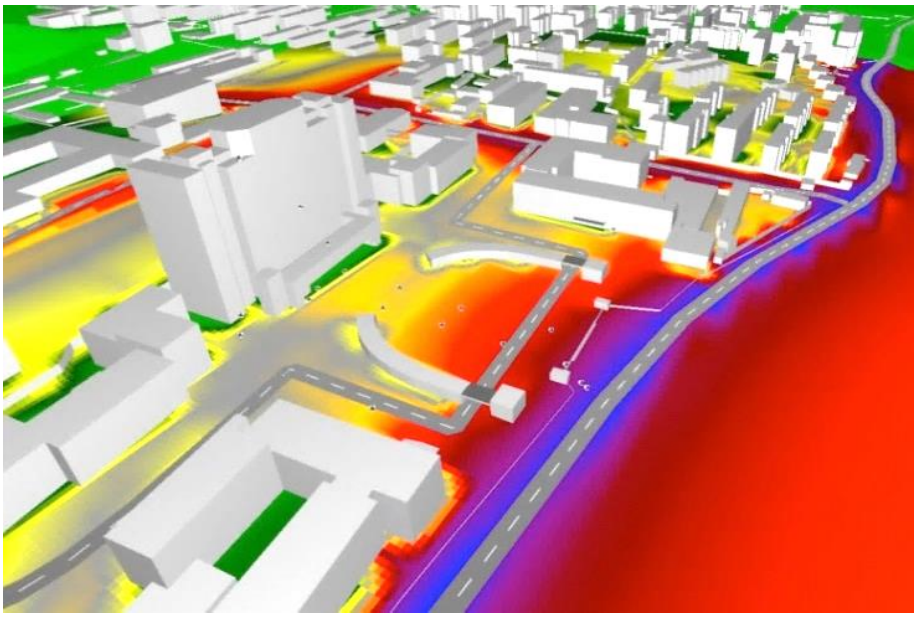

Figure 4.2 3D model – Donghu Road with open square and high-rise building

The buildings form of the surrounding the selected case study area is also relatively simple, which may thus benefit the noise calculation accuracy. The buildings in and around this sampled area are mostly education buildings, classroom, and library, etc. These multi-storey buildings mostly have rough, naked concrete façades and flat roof and are mostly built between 1950's to 1980's.

The 21-floor high-rise building facing the square and the lake with an annexed 4-storey podium is the tallest building in this area, which was built in the late 1990's. The façades are decorated with ceramic tiles, and the windows ratio is also larger than those traditional

buildings around. There is a separate podium of four storeys annexing with the main building, which has an accessible flat roof and partially suspended ground floor opening towards the square.

As can be seen in Figure 4.2 that, there is one pair of mirrored arc-shape buildings for exhibition purpose that locate in both sides of the square with reflecting glass façades. Both buildings are only 1-storey and about 3.5 m high. The façade absorption/reflection coefficients were set accordingly.

4.2.3 Road and traffic conditions

The Donghu Road is a dual-carriageway road connecting the city centre to the west side and the outskirt parts of the city on the east side. As part of the campus in which all vehicles and passengers need to enter and exit through a handful of entrances with security guards, the vehicle access through this area is also strictly controlled. Special external vehicles like empty taxis and trucks without vehicle permits are not allowed to enter or pass through.

The above urban form and traffic management means have two consequences that make this normal width road stuffed with heavy traffic. Firstly, it makes the Donghu Road close to the lake embankment the only path that connecting a wide range of urban districts lie on the east and west side of the south lake bank. Therefore, although only with two carriageways, the Donghu Road has a much larger traffic flow than the normal roads with a similar width. The traffic per hour in measured period is 1528 veh/h with 3% heavy vehicles. The second consequence is that most of the roads inside the campus are much quieter comparing with the Donghu Road except the ones that connecting to the entrance gates. The small road gate on the west side of the site which connects the Donghu Road through the gate has a traffic flow of 270 vehicles per hour with 7% heavy vehicles during the measurement period; while it locates more than 50 m from the square and is shadowed by large building blocks hence the influence of the traffic noise of it to sampled area is limited. There is a negligible number of small vehicles on the small road trespassing the square.

During the measurement period, except for the two roads with traffic mentioned above, there is background noise from farther areas caused by the traffic of remote roads and the community noise from the campus behind the high-rise building.

4.3 Test on default calculation configurations

In typical EU environmental calculation methods, a series of corrections for environmental attenuations are considered in the calculation of the noise propagation from road source to the receiver points. It includes the correction of geographic divergence calculated based on the slant distance from the road segments to the receivers; the screening effect caused by equivalent barriers obstructing the source and the receiver points; the correction for the attenuation due to the ground effect; and the correction due to reflection from various reflective surfaces especially the building façades, etc. (UK DfT, 1988)

4.3.1 Selection of receiver points and default calculation configurations tested

The locations of all receiver points including the reference point are shown in Figure 4.3. As shown in the 3D perspective view that there are a series of façade point on the surface of the building and the podium selected and measured in order to validate the accuracy of the noise simulation on the façade of the building on different heights. Point B04 is locating beneath the elevated part of the podium while Point E05 is locating on the surface of the podium with a height of 12 m relative to the ground. Point E06 and E07 were measured close to the building façade at the 9^{th} Floor and 18^{th} Floor respectively.

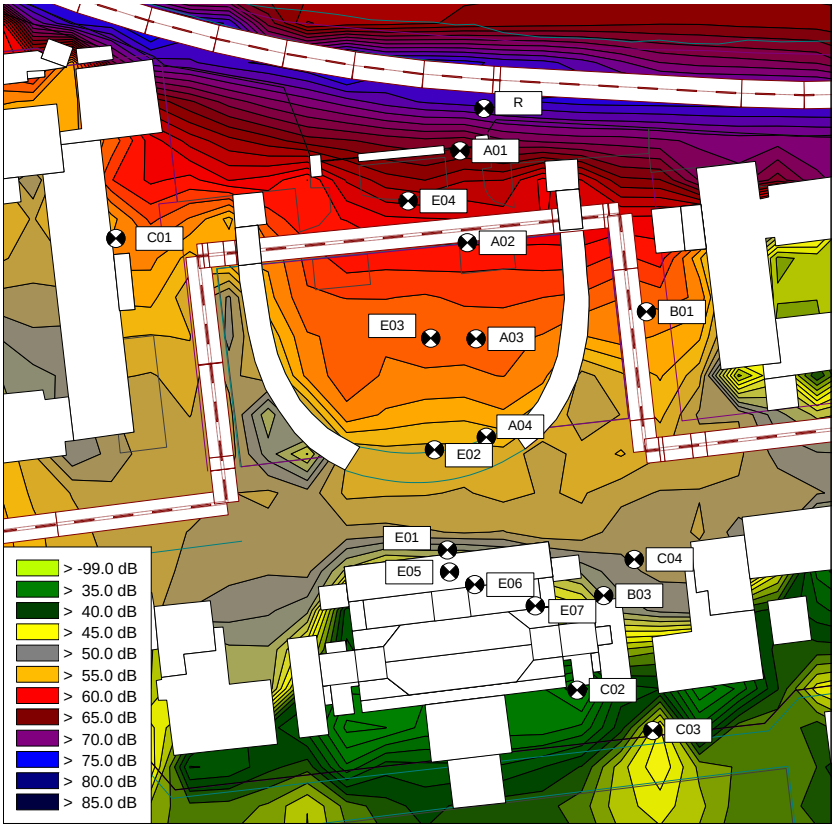

a

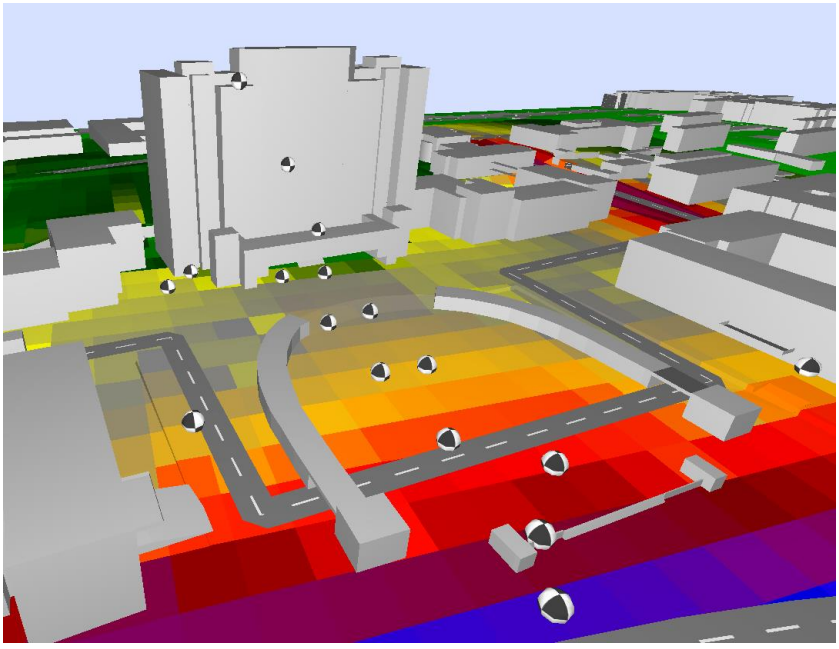

b

Figure 4.3 Location of the measured receiver points in the Donghu Road area. (a) locations of the receivers on the noise map (b) perspective view. It can be seen that the receivers have varied heights.

Table 4.1 Configuration tests conducted in the Donghu Road area case

Max. Rf. Order	Correction for opposite reflection	Max. Rf. searching radius (m)	General settings	Ground absorption coefficient
0	Max.1.5dB	100	Default [a]	0.4[b]
	No	100		
1	Max.1.5dB	100	Default	0.4
		500		
	No	100	Default	0.4
				0.4
		200		0.4
		500		
2	Max.1.5dB	100	Default	0.4
		500		
	No	100	Interpolation = 17×17	0.4
			Max Error = 0.5	
			Max Error = 0.5, Max Dist. = 1	
		100	Default	0.4
		100	Default	0.4
				0.4
		200		0.4
		500		
3	Max.1.5dB	100	Default	0.4
	No	100	Interpolation = 17×17	0.4
			Max. Error = 0.5	
			Max Error = 0.5, Max Dist. = 1	
		100	Default	
		100	Default	0.4
				Default [c]
		200		0.4
		500		

[a] Default general configuration of Cadna/A v4.3:
Max. Error = 0 dBA; Max. Search Radius = 2000 m; Min. Distance Source to Receiver = 0 m; Grid interpolation = No; Ground absorption coefficient = 1.0. (DataKustik, 2012a)
[b] Set according to the in-situ ground condition.
[c] The default value of ground absorption coefficient is set to 1, which is tested in the configuration setting group with the maximum reflection order set to 3.

It is to note that, by maneuvering most of the coefficients in the general calculation configurations, e.g. the grid interpolation methods, the Max error, Minimum distance from the source to receiver, have merely no observable effect on the calculation results.

For the sake of testing and finding applicable configuration settings for typical Chinese urban environment, a series of configuration combinations are tested as can be seen in Table 4.1, which are adjusted on the basis of the default calculation configurations (DataKustik, 2007). The configurations that found to have a significant impact on accuracy level including the maximum reflection order, the maximum 1.5 dBA of correction for mirror source reflection, the maximum reflection-searching radius, the maximum error, the maximum distance to the source line, and the grid size, etc.

For instance, when the max reflection searching radius is increased to higher than the default value of 100 m, the accuracy of the receiver locating more than 100 m from the road source could gain 0.1–0.2 dBA of enhanced accuracy, while if take other sources of inaccuracy into consideration, these improvement is negligible.

4.3.2 Ground absorption coefficient

4.3.2.1 Test on the ground absorption coefficient settings

The ground absorption correction Δ_{GA} in the calculation of noise attenuation is mainly determined by the input of ground absorption coefficient. As described in CRTN, if the ground in between the noise source and the receiver is partially or fully absorptive, then a correction for the ground effect is needed. The correction is greater when the receiver point is closer to the ground and is progressively weaker with distance increasing. The absorption correction is determined by *I, d* and *H*, which are the proportion of the absorbing ground surface, the horizontal distance to the road kerb and the average height of the propagation line. (UK DfT, 1988) Where the coefficient *I* indicates the proportion of absorbent surface of the ground, which is equivalent to the absorption coefficient *G*.

- ***General accuracy level***

A series of noise calculations are conducted by adjusting the default ground absorption coefficients. Three typical *G* values are employed, including: $G = 0$ which indicates that

no noise absorption is occurring on the ground surface; G = 0.4 which is estimated according to the real site condition, which is an approximated value of the default setting for structured façade; and G = 1 which indicates that the ground is totally absorptive as being covered by soft soil or grass. The maximum reflection order is set to 3 and the opposite façade correction is disabled. All other configuration settings are set as the default value in Cadna/A(UK DfT, 1988). The results can be seen in Table 4.2 and Figure 4.4.

Table 4.2 Comparison between different ground absorption settings [a], errors with absolute value equal to or smaller than 3 dBA are highlighted.

Point	$H \geq (d+5)/6$ (Y/N)	Slant Distance(d') (m)	Horizontal Distance(d) (m)	h [b] (m)	H [c] (m)	*Calculation error*		
						I=1 [d] (dBA)	I = 0.4 (dBA)	I = 0 (dBA)
R	N	7.7	4.1	1.1	1.1	-0.5	0.3	0.9
A01	N	18.8	15.3	1.3	1.1	-1.6	-1.5	-1.5
E04	N	32.7	29.2	1.5	1.3	2.2	3.3	4.3
A02	N	42.1	38.6	1.8	1.4	-1.2	0.4	1.4
C01	N	56.0	52.4	3.3	2.1	0.2	1.2	2.0
B01	N	57.1	53.6	2.4	1.7	-0.5	1.2	2.0
A03	N	66.3	62.8	2.0	1.5	-2.7	-0.7	0.1
E03	N	67.1	63.6	2.0	1.5	-1.1	0.9	1.8
A04	N	91.3	87.8	2.0	1.5	-5.9	-3.7	-3.6
E02	N	95.4	91.9	2.0	1.5	-1.7	0.4	0.4
E01	N	120.1	116.6	3.2	2.1	-4.0	-2.0	-0.5
C04	N	120.4	116.9	3.1	2.1	-5.3	-3.4	-3.1
E05	N	127.2	122.8	15.2	8.1	-0.7	-0.1	-0.1
B03	N	130.1	126.6	3.2	2.1	-6.4	-4.5	-4.1
E06	N	140.1	132.6	33.2	17.1	0.0	0.4	0.7
E07	**Y**	145.3	130.1	57.2	29.1	1.5	1.6	1.7
C02	N	154.6	151.1	3.2	2.1	-11.8	-11.8	-11.8
C03	N	163.8	160.3	3.2	2.1	-9.1	-7.4	-7.4

[a] Maximum reflection order is set to 3, opposite façade correction of 1.5 dBA is disabled.
[b] The relevant height from source to receiver point.
[c] Average height of the propagation line. H=(h+1)/2, according to CRTN (UK DfT, 1988).
[d] The proportion of the absorbent surface of the ground, which is equivalent to the absorption coefficient G.

Firstly, as shown in Table 4.3, when the ground absorption coefficient is set to 0.4 according to the estimation of the actual site situation, the accuracy level is the most desirable among the three sets. The MAE is 1.6 dBA and the mean error is -0.4 dBA with an SD of 2.0 dBA, which is both the lowest among all three tested scenarios. It indicates

that the calculation result is sensitive to the setting of the ground absorption coefficient, though the effect is relatively small in general.

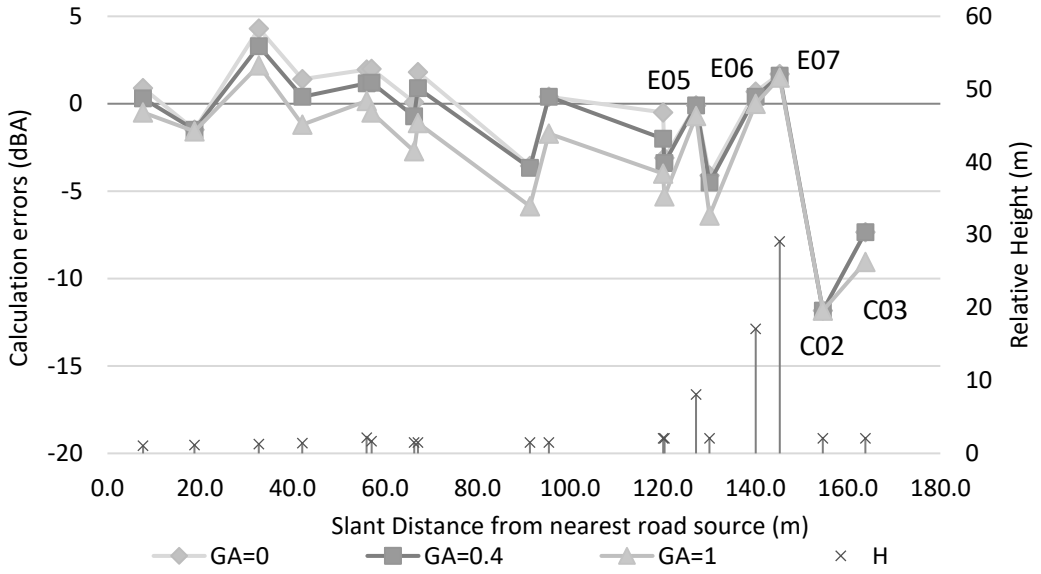

Figure 4.4 Configuration test on ground absorption setting – Donghu Road area, when the *G* is set according to the real site condition, the MAE tend to be the smallest.

It is notable that, when the ground absorption coefficient is changed, the calculation results at the only shadowed point C02 are unaffected, while that of all other receiver points without being shadowed by the main buildings are affected more significantly. Including the point C03 that locates approximately 9.2 m farther away from the road than the C02, where the calculation results is still significantly affected when the ground is changed from fully-absorptive to partially and non-absorptive, the calculation error at which drops for 1.7 dBA when *I* changes from 1 to 0.4 and 0. It indicates that the change of ground absorption coefficient has no little effect on the calculation of receiver points shadowed by large buildings, as the noise calculation at which is mainly the lateral reflections, etc.

Table 4.3 Error statistics for the directly exposing receiver points – Donghu Road area

I / *G*	0	0.4	1
Mean (dBA)	0.2	-0.4	-1.7
SD (dBA)	2.2	2.0	2.4
MAE (dBA)	2.2	1.6	2.2

It can be also seen that the effect of changing the ground absorption coefficient also reduces with distance, while the effects on receiver points with higher altitude are limited.

As can be seen Table 4.3 that, for the sixteen receiver points without being screened by the main building, the variation of results caused by the change of ground absorption coefficient generally increase with distance, while for the three receiver points locating approximately to the building façade at higher altitude, the variation of the errors is relatively smaller.

As can be seen that, the results variation due to the increasing in ground absorption coefficient have limited impact on the overall inaccuracy level, and the variation increase with distance but has no effect for the receiver points locating in the shadowed area. The receiver points at relatively higher altitude also merely not affected by the change of ground absorption.

- ***Analysis and implication***

From the brief comparison above, it can be seen that the change of ground absorption coefficient has less effect on the receivers above a certain altitude. As shown in Figure 4.4 and Table 4.2, for the six points on the front side of the main building with the horizontal distance ranging from 116.6 m to 130.1 m, the variations of the calculation errors on three elevated points E05, E06 and E07 is relatively smaller than all other receiver points on close to the ground level within this range.

This is due to that according to the current calculation methods the ground absorption has no impact on points locating higher above the ground. As can be seen at E07 that the results of three ground absorption settings remain almost merely the same, with only a tiny difference of 0.1 dBA amongst the results. According to CRTN (UK DfT, 1988):

$$H = (h + 1)/2 \tag{4.1}$$

$$\Delta_G = 0 \quad if \quad H \geq \frac{d+5}{6} \text{ or } h \geq \frac{d+2}{3} \tag{4.2}$$

Nevertheless, in this sampled case as shown in Table 4.2 that only the point E07 which locates on the balcony on the 18th floor with a relative height of 57.2 m compare with the source line which meets the condition described in Equation 4.2. At point E07, the

horizontal distance to the road kerb is d = 130.1 m. Therefore, it can be calculated that at E07 and or points with the same horizontal distance between the source and the relative height h of above 45.2 m, the correction of ground effect for the traffic noise from the corresponding road segments is not calculated. The slight variation of the results found in Table 4.2 may be caused by road segment at a farther distance.

4.3.2.2 Discussion on the ground effect calculation

- ***Typical Chinese urban form***

To further test the influence of the default calculation method for the ground absorption correction, a test is conducted in an idealised urban form with typical Chinese street space features. For a typical major street canyon in which between the flanking buildings to the nearside road kerb the horizontal distance d = 15 m, as shown in Figure 4.5, the highest value of h that can be affected by ground effect is 5.7 m. For the façades with height above $\frac{d+2}{3}$, only the corrections due to geometric divergence and surface reflection are considered in the calculation, the ground absorption and potential reflection from the ground surface is not taking into consideration.

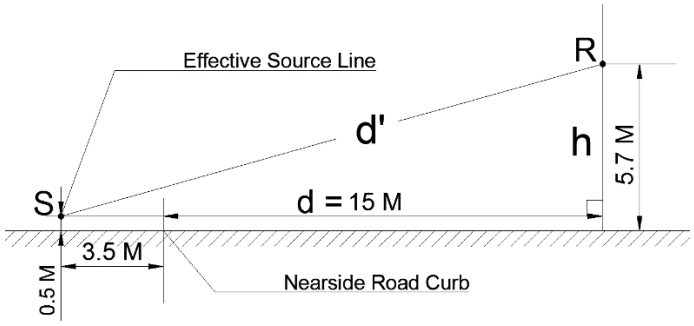

Figure 4.5 Calculation of ground absorption in a typical Chinese major road canyon with wide kurb-to-building distance of 15 m, point R is a representative receiver point.

According to CRTN (UK DfT, 1988), the source line locates at 3.5 m from the road kerb and 0.5 m above the road surface. In this specific case, the perpendicular slant distance *d'* from the effective source line S to the receiver point R is 19.2 m. With precluding any reflections and screening effect from any nearby objects, for the receiver point R with the height of 5.7 m, the distance correction and the correction due to the influence of the

ground surface are the two major corrections to be accounted in the final calculation, as shown in Equation 4.3:

$$L_R = L_E + \Delta_d + \Delta_G \tag{4.3}$$

where L_E is the SPL of the emission source, i.e. the road source level, the Δ_D and Δ_G are the attenuation correction caused by distance and ground absorption, respectively. In this idealised case, the distance correction Δ_d for point R can be calculated as:

$$\Delta_d = -10log10\left(\frac{d'}{13.5}\right) = -10\log_{10}(19.2/13.5) = -1.5\ dBA \tag{4.4}$$

Then according to the typical ground absorption calculation method in CRTN:

$$\Delta_G = 5.2Ilog_{10}\left(\frac{6H-1.5}{d+3.5}\right)\ dBA\ if\ 0.75 \le H < \frac{d+5}{6} \tag{4.5}$$

The coefficient *I* is calculated as a value equivalent to the ground absorption coefficient *G* of the ground surface between the road and the receiver point. Considering the relationship between *H* and receiver height *h* described in Equation 4.1, the Equation 4.5 can be converted to:

$$\Delta_G = 5.2Glog_{10}\left(\frac{3h+1.5}{d+3.5}\right)\ dBA, if\ 0.5 \le h < \frac{d+2}{3} \tag{4.6}$$

Therefore, for point R with a height of 5.7 m, if the ground effect is not considered in the calculation using Equation 4.6, the potentially neglected ground absorption correction at receiver point R is 0.01 dBA, which is apparently negligible. It indicates that around the upper-boundary height i.e. 5.7 m of the ground effect calculation method, there is only a negligible amount of ground absorption correction considered in the SPL calculation using current method. Above this boundary height, no effect of the ground absorption and reflection is counted in the calculation.

Due to the unique urban planning system, in the high-density urban area of Chinese major cities like Wuhan the flanking buildings along the wide main roads, may have the road-kerb-to-façade distance similar to the idealised case (Wen, 1991) and with the height much higher than 5.7 m. The potentially neglected reflections from the ground may affect a large amount of façades and indoor environment. There are also many open squares with hardened surface and high flanking buildings similar to the one in the Donghu Road case, where the amount of neglected ground reflection to the building façades at heights can be evident.

Thus, neglecting the potential ground reflection from the scattering ground surface of the pedestrian area in-between road and buildings might cause potential inaccuracy when estimating noise impact on the residents in general. It would therefore be interesting to test if the correction for ground reflection and absorption can be calculated using alternative ways rather than the height-restricted method. It can thus be helpful to test the adaptability and accuracy of current EU methods in the façade noise calculation of the high-rise buildings along the wide street canyons.

- ***Parametric analysis***

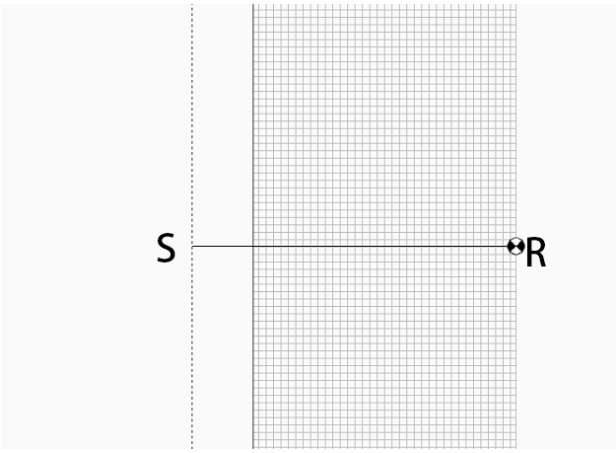

Figure 4.6 Test on the the ground absorption calculation method, the thin dash line denotes the centre of the nearest lane, S and R represents a typical source and receiver points, respectively.

Calculations with and without the solid reflector are conducted on five representative receiver heights. A free field scenario without the influence of the ground and any other surfaces is calculated to determine the total attenuation purely due to geographical divergence. The contribution to total attenuation from the ground absorption correction

and the real reflective ground surface at point R on different heights can then be obtained and compared.

A quantitative comparison was conducted between the calculation of real reflection and the default method based on the ground absorption coefficient adopted in current method. As can be seen in Figure 4.6 that the ground is covered with the object type of 3D reflector (DataKustik, 2012a), the surface of which can have both absorption effect and reflection effect despite the default way of calculating the ground effect in CRTN (UK DfT, 1988) and ISO 9613-2 (ISO, 1996). The surface of the 3D reflector is defined with the absorption coefficient *G'* that is equivalent to the ground absorption coefficient *G*. A series of receiver point R is placed at a series of different heights in the same horizontal location, from the lower-boundary height *h* from 0.5 m to the height of a typical Chinese multi-storey residential building of 20 m, and a reference height of 100m at which the absorption and reflection of the ground surface may have little impact.

Table 4.4 The contribution to total attenuation from the ground absorption correction and the reflective ground surface

G/*G'* [a]	1	0.4	0	1	0.4	0
Receiver height *h* (m)	Contribution of the ground effect [b] (dBA)			Contribution of the 3D reflector [c] (dBA)		
0.5	4.1	2.0	0.0	4.1	2.0	1.1
1.5	3.2	1.6	0.0	3.2	1.1	0.2
4.0	1.0	0.5	0.0	1.0	-1.1	-2.1
5.7	0.2	0.1	0.0	0.2	-1.9	-2.8
20.0	0.0	0.0	0.0	0.0	-2.0	-3.0
100.0	0.1	0.1	0.1	0.0	-2.1	-3.0

[a] The absorption coefficient of the ground or the solid reflector.
[b] Calculations are conducted using the default setting of Cadna/A and CRTN, with the opposite façade correction activated.
[c] To ensure the noise reflection from the solid reflector on the ground surface is counted in the calculation with the highest accuracy, the max reflection order is set to 20.

From the test results, it is found that the reflection from the ground surface is potentially neglected by up to 3.0 dBA. As can be seen in Table 4.4 and Figure 4.7 that, for the scenario of using the default absorptive ground and the scenario of the reflective ground surface, the contribution of the ground surface decreases with the increasing height. When the ground absorption coefficient is set to 1 or fully absorptive, the ground effect is the

highest in both scenarios due to the strong influence of the ground surface to the sound wave on both the source side and the receiver side (ISO, 1996).

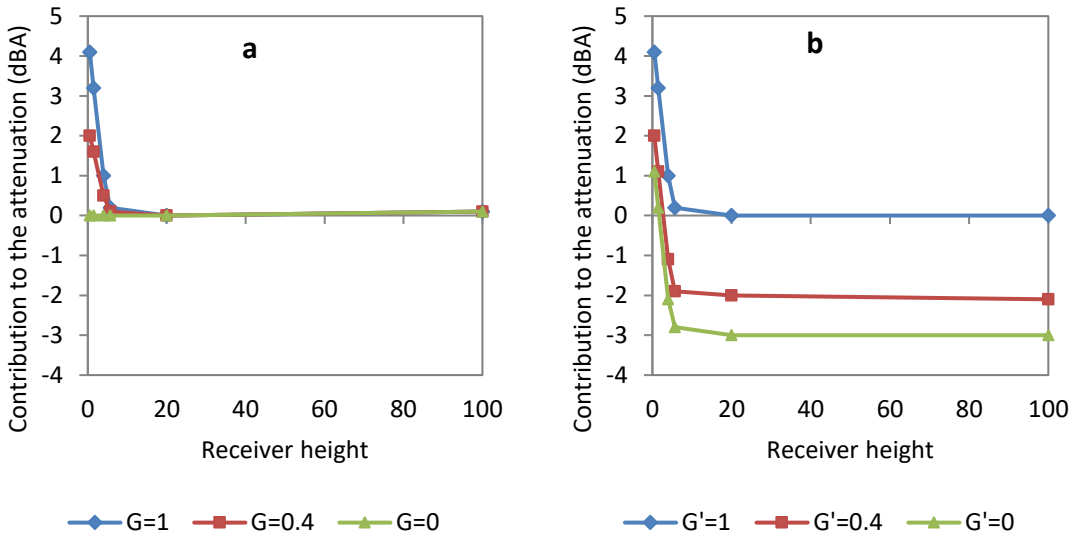

Figure 4.7 The contribution to total attenuation from the ground absorption correction and the reflective ground surface

It can be seen that when the ground absorption coefficient keeps decreasing, the contribution of the ground to the total attenuation decreases in both scenarios. As can be seen in Figure 4.7a that by solely adopting the default calculation method of ground effect, the contribution of the ground to the total attenuation drop to approximately 0 at the threshold height of 5.7 m and remains around zero at higher altitude. Nevertheless, as can be seen in Figure 4.7b that, the reflection of the ground surface starts to have a negative contribution to the total attenuation, and it reaches 2.0 dBA when the ground reflection coefficient equals to 0.4, and reaches 3.0 dBA when the ground is totally reflective. It is also notable that when the ground is totally reflective, the default calculation method for the ground effect ignores all possible reflections from the ground and there is no contribution from the ground surface to the receivers at all altitudes. It can be seen that the current mainstream methods for the calculation of ground effect may have neglected the effect of ground surface reflection.

- ***Implications***

Kephalopoulos et al.(2014) also found that the current noise-mapping methods are not capable of coherently combining the calculation of the ground effect of the direct waves

and the reflected waves. In another word, it can be seen that when applying the current EU strategic noise mapping technique in typical Chinese urban environment consists of tall buildings and large open space, there is a certain amount of neglected reflections from the ground surface need to be taken into consideration.

For typical low-rise street canyons with a relatively lower value of *d*, e.g. the streets in typical European residential areas, neglecting the ground reflection is not as problematic as the typical Chinese street canyon case. In smaller streets with low-rise buildings, the relatively closer distance from road source to the boundary surface of the street canyon, i.e. the building façade or barriers, makes the reflection from the building and barrier surface prevail and the ground reflection at a lower height near the ground is therefore almost negligible.

Nevertheless, in typical high-density Chinese cities like Wuhan, typical high-rise street canyons with wide pedestrian space, and some extreme cases with large open space and high-rise buildings similar to the Donghu Road area with a massive open square adjoining the main road and the high-rise buildings, are both very common in major Chinese cities (Gaubatz, 2008). As discussed earlier that the reflection from the normally hardened ground surface in these urban space is neglected, and only the correction due to direct propagation, screening effect and vertical façade reflection are considered in the calculation. To ensure the applicability of typical noise mapping calculation methods on the effect of ground absorption and reflection, some supplementary corrections may be needed in the mentioned types of urban scenarios when the current EU method is adopted; and further study and potential improvement to combine the ground reflection is necessary.

4.3.3 Opposite façade correction

For the sake of reducing calculation time, a correction for the opposite façade reflection is defined in some calculation methods, For instance, in the German method RLS-90 (Germany FMoT, 1990), only the first time of reflection is calculated using mirror image method, higher order of reflections are calculated using a correction value which was found to be slightly overestimated in research by Probst (2010). It is defined in the paragraph 26 of CRTN that when there is a row of buildings or barriers on the other side

of the road with a height of over 1.5 m, a reflection correction of maximum 1.5 dBA is required for reducing the calculation time consumption, and it is also depending on the view angles of the buildings subtended to the receiver point. In contrast, when the mirror source method is used, the façade reflections are calculated on each reachable effective façade for the sound rays, which is relatively more time-consuming especially when the reflection order is high and in large-scale calculations. (UK DfT, 1988)

As shown in Figure 4.8 that two groups of calculations with the reflection correction option activated and deactivated are both conducted, both of the maximum reflection order is set to 3, although actually when the option of opposite façade correction is deactivated, it is equivalent to set the maximum reflection order to 0. All the rest configurations are by default. The results are then compared and analysed.

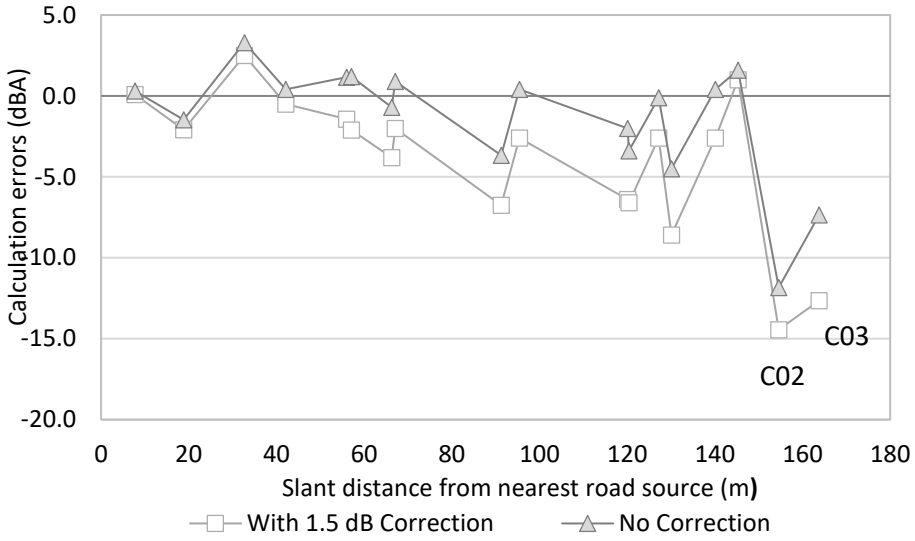

Figure 4.8 Calculation errors with the setting of maximum opposite façade correction of 1.5 dB on and off – Donghu Road area, the errors without the 1.5 dB correction is generally smaller.

It is found that with the correction setting for opposite façade correction deactivated, the accuracy level generally is increased dramatically, especially when the distance is farther from the road source and closer to the façade of the main building tower. For points locating approximately within 40 m from the source line where the reflection from the building façade is not prevailing, the gap between the two sets is negligible as can be seen in Figure 4.8. It can also be seen that at a further distance the calculation error greatly increased when the default 1.5 dBA correction for reflection is activated.

When the calculation with the opposite reflection correction is activated the calculation time is greatly reduced, thus this option is still necessary for larger scale grid noise calculations. In later part of this chapter, for the sake of testing the applicability of typical traffic noise calculation method in the typical Chinese urban environment, as well as for ensuring all the reflection calculations are conducted using the default mirror image method, especially for the calculation of SPL spectrum on major octave band central frequencies, the option of opposite façade correction is deactivated.

4.3.4 Test on the maximum reflection order

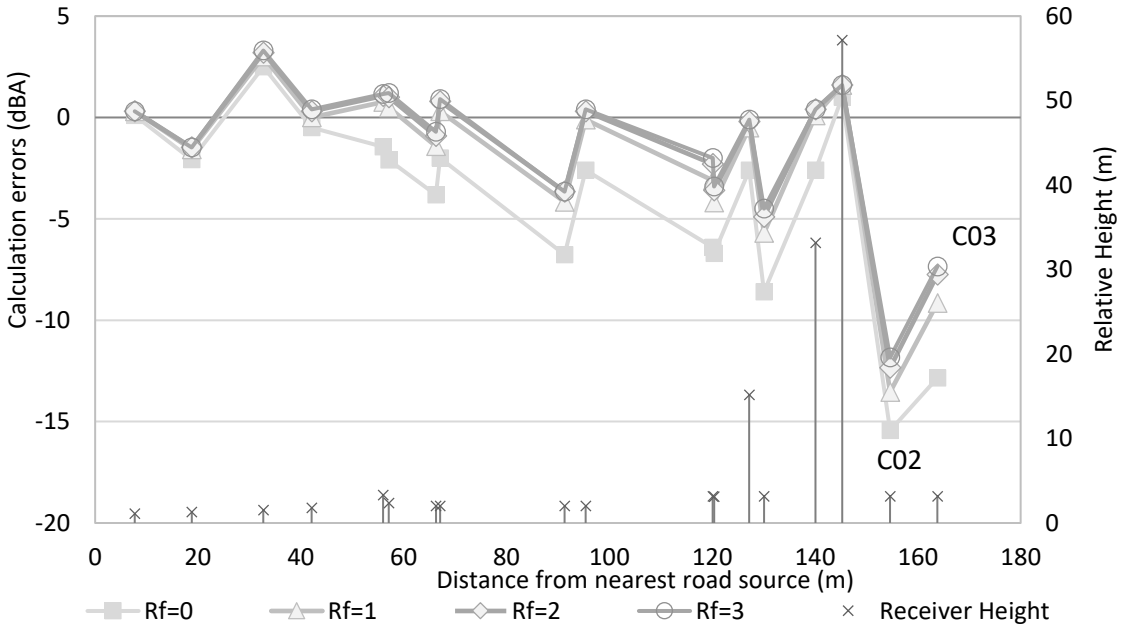

Figure 4.9 Errors with different reflection order settings – Donghu Road area, the calculation error is generally smaller when the max. refleciton in creases.

By conducting a series of calculation using increasing maximum reflection orders, it is found that by increasing the maximum reflection order, the calculation error generally decreases. The calculation results are systematically demonstrated in Figure 4.9 and Table 4.5, together with the slant distance and relative height information of the receive points, in Table 4.5 the favourable error of smaller than 3.0 dBA are highlighted. It can be seen that the errors are the largest when the maximum reflection order is set as 0, which means no reflection from any surface is considered in the calculation. When the maximum reflection order increases from 1 and 2 to 3, the effect of error reduction becomes less obvious.

Table 4.5 Calculation errors with different reflection orders – Donghu Road Area[a], errors with absolute value equal to or smaller than 3 dBA are highlighted.

Point	Distance [b]	Height	Rf=0 (dBA)	Rf=1 (dBA)	Rf=2 (dBA)	Rf=3 (dBA)
R	7.7	1.1	0.1	0.3	0.3	0.3
A01	18.8	1.3	-2.1	-1.6	-1.5	-1.5
E04	32.7	1.5	2.5	3.0	3.2	3.3
A02	42.1	1.8	-0.5	0.0	0.3	0.4
C01	56.0	3.3	-1.4	0.8	1.1	1.2
B01	57.1	2.4	-2.1	0.5	1.0	1.2
A03	66.3	2.0	-3.8	-1.4	-0.9	-0.7
E03	67.1	2.0	-2.0	0.3	0.8	0.9
A04	91.3	2.0	-6.8	-4.2	-3.7	-3.7
E02	95.4	2.0	-2.6	-0.1	0.3	0.4
E01	120.1	3.2	-6.4	-3.1	-2.3	-2.0
C04	120.4	3.1	-6.7	-4.2	-3.6	-3.4
E05	127.2	15.2	-2.6	-0.5	-0.2	-0.1
B03	130.1	3.2	-8.6	-5.7	-4.9	-4.5
E06	140.1	33.2	-2.6	0.1	0.4	0.4
E07	145.3	57.2	1.0	1.6	1.6	1.6
C02	154.6	3.2	-15.4	-13.5	-12.3	-11.8
C03	163.8	3.2	-12.9	-9.2	-7.8	-7.4

[a] The ground absorption coefficients is set to 0.4 and reflection correction are set to off.
[b] Slant distance from source line to receiver points.

Specifically, by comparing the errors occurring on all receiver points locating in different distance from the road source, it can be seen from Figure 4.9 that, by setting the maximum reflection order to 3, the error is relatively smaller when the distance is less than 80 m; and the absolute calculation error tends to be generally much higher when the distance is over 80 m. The worst accuracy occurs at the two receiver points locating over 140 m behind the high-rise main building, although the increasing of maximum reflection order also has significant for these two points.

It can also be seen that for the series of receiver points measured close to the podium and the high-rise main building with various altitude, the distribution of the errors tends to be more vibrant than that of the receiver points on the ground level. The causes of errors are to be examined in sections below.

4.4 The effect of urban morphological features

4.4.1 Distance from the road source and building

The noise attenuation of a series of receiver points exposing to direct traffic noise are statically compared, it is found that the calculation of noise attenuation tends to be more accurate at a closer distance from the road source. In the selected area the open square between the Donghu Road and the main building, the noise from the main road freely propagates from the effective road source line through a longer distance than in normal street space before it reaches the building façades. The distance from the effective traffic noise source line to the podium of the main building is approximately 120 m. The inaccuracy level between the calculation and the measurement results of the selected points varies due to the specific situation of the points, especially the increasing distance from the source line. In addition, it is necessary to consider the potential reflections from the surrounding building façades. Two sets of calculations with different configurations for the façade reflection calculation are conducted. The difference and the causes of the increasing inaccuracy are discussed below.

Two sets of calculation results using multiple orders of reflection are compared and analysed. The calculation configuration adopted including the default option of opposite façade correction of maximum 1.5 dBA activated and deactivated, in which the latter the reflection correction is instead calculated via the mirror source method for potentially better accuracy.

The statistics of the results using two sets of calculation configurations are shown in Table 4.6. Table 4.6a shows the results of which the default reflection correction of maximum 1.5 dBA is activated, the Table 4.6b shows the results when maximum reflection order is set to 3 and the calculation of reflection is conducted using mirror source method.

4.4.1.1 Calculation errors at different distance from the road source

When using the default CRTN method for reflection calculation as shown Table 4.6a, the accuracy level is relatively worse than that of using combined method shown in Table 4.6b. For all sixteen receiver points directly exposing to the road source spreading from

0-150 m and within different distance ranges, including 0-60 m. 0-120 m and 120-150 m, the MAE and SD of the former are all higher than the latter.

Table 4.6 Statistics of calculation errors – the Donghu Road area [a] (a) calculation using default CRTN method [b]; (b) calculation using combined method [c]

a

Position	Distance range (m)	Points amount	Mean error (dBA)	SD (dBA)	MAE (dBA)
Front only	0–60	6	-0.6	1.6	1.5
Front only	0–120	10	-1.9	2.3	2.4
Front and side	120–150	6	-4.3	3.2	4.6
Front and side	0–150	16	-2.8	2.9	3.2

b

Position	Distance range (m)	Points amount	Mean error (dBA)	SD (dBA)	MAE (dBA)
Front only	0–60	6	0.8	1.4	1.3
Front only	0–120	10	0.2	1.8	1.4
Front and side	120–150	6	-1.3	2.2	2.0
Front and side	0–150	16	-0.4	2.0	1.6

[a] Configuration was adjusted based on the default settings in Cadna/A 4.3 when using CRTN. Maximum reflection order is set to 3, ground absorption is set to 0.4 based on the actual ground situation. No reflection correction was set.
[b] The option of opposite reflection correction of maximum 1.5 dBA is activated.
[c] The opposite façade correction of maximum 1.5 dBA is deactivated; the maximum reflection order is set to 3.

The calculation results using mirror source method for the reflection can be regarded as accurate which is shown in Table 4.6b. It can be seen that for all sixteen receiver points spreading 0-150 m from the road source the overall mean error is -0.4 dBA, with an SD of 2.0 dBA and the MAE is only 1.6 dBA, which is all lower than 3.0 dBA and can be regarded as relatively accurate (ISO, 1996). Meanwhile, the errors using default CRTN calculation method got clearly higher disparities, with a mean error of -2.8 dBA, an SD of 2.9 dBA and the MAE of 3.2 dBA. It indicates that although the buildings locate relatively far from the road source, if taking multiple reflection orders from the façade and barriers into the calculation, the general accuracy level can be greatly enhanced.

It is also shown that in the typical large open space the disparities between the calculated and measured results generally increases along with the increase of source-receiver distance. As can be seen in Table 4.6b that, by taking maximum reflection order of 3 into the calculation, the six points locating within 60 m from the source line has relatively

better accuracy level than that of all ten receiver points locating within 120 m from the source line.

It is also interesting to notice that when the calculation is based on real reflection using mirror source method, the calculated noise level tends to be overestimated at a closer distance with a positive mean error. As shown in Table 4.6b that, the mean error generally tends to be positive within 120 m from the road source line. When the slant distance is less than 60 m the average calculated results is even 0.8 dBA higher than the average measured results, with an SD of 1.4 dBA and MAE of 1.3 dBA.

When the receiver point locates even farther from the road and closer to the high-rise main building and its annexed podium, the accuracy level can be even lower. For the six receiver points spreading from 120 m to 150 m, the calculated SPL of which are averagely 1.3 dBA lower than the measurement results, with an SD of 2.2 dBA and MAE of 2.0 dBA.

4.4.1.2 Discussion

It can be seen that the receiver points locating in the open space which is directly exposing to the effective road source have generally acceptable accuracy level, disregard the calculation method adopted, while as being pointed out in section 4.3.3 that when taking the multiple orders of reflection into calculation the accuracy level is generally more desirable than that of the calculation using default method of reflection correction. It indicates that although the distance between the road and the high-rise building in this relatively open urban form is far, the reflection from buildings still has a slight influence on the calculation accuracy.

It is also notable that the calculation method and noise mapping package have limitations at a certain distance. For both of the calculation groups, despite the method adopted for reflection calculation, the increasing of slant distance, say, from 60 m to 120 m can generally raise the error between calculation and measurement. The similar phenomenon is also discovered in a research by Jian and Huang (2005) that, in an idealised urban environment, the noise level can be underestimated for 3–4 dBA when the distance increases. It is also notable that when the slant distance keeps increasing, the accuracy level of the receiver points around the high-rise building gets even worse.

Considering the findings in previous sections, it can be seen that for receiver points locating at a relatively farther distance from the road source, the noise calculation is prone to be affected, mainly by the calculation of ground absorption and the calculation of reflection from the building façades and barriers. The influence of the buildings to the noise propagation is further studied in next section.

Another finding is that when the real reflection is accounted, at a closer distance the calculated noise level is even slightly overestimated, where the errors of the results considering the default reflection correction tend to be negative. This may be due to the default mirror source calculation method for the façade reflections of multiple orders, which can cause overestimation in the calculation of reflections from surrounding vertical surfaces, and the potentially underestimated ground absorption.

4.4.2 Hypothetical scenario analysis on effect of façade reflection

To further test how the façade reflection affects the calculation, a set of comparative calculations are conducted and the results are demonstrated in Figure 4.10. Relevant location of some of the receiver points is illustrated in the cross-section view in Figure 4.11. The results are also listed in Table 4.7.

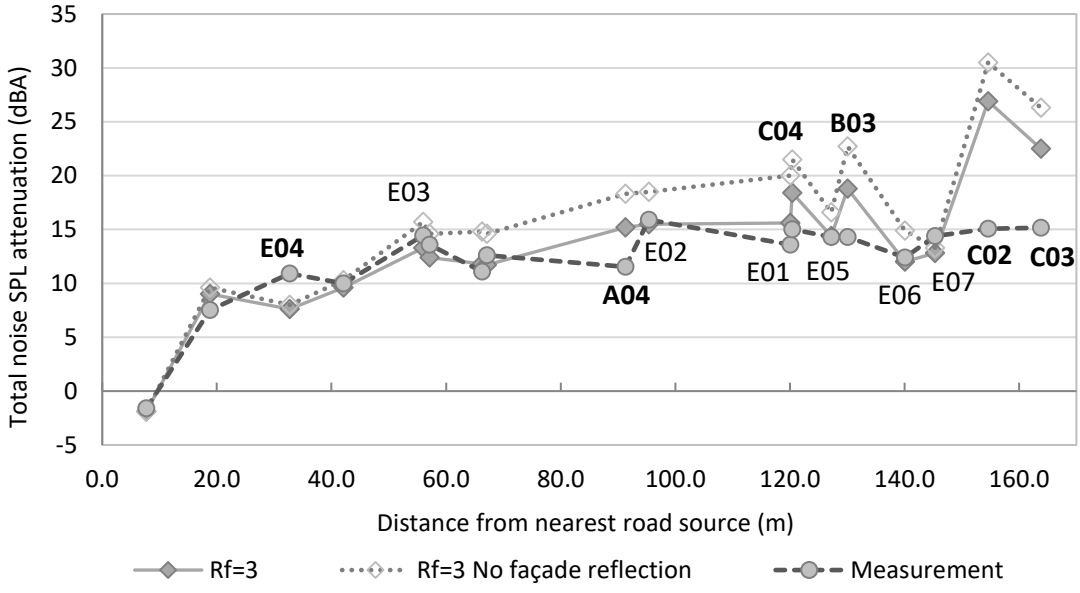

Figure 4.10 Hypothetical scenario analysis on the façade reflection settings – Donghu Road Area, it can be seen that turning off the façade reflection could increase the calculation error globally.

Table 4.7 Hypothetical tests on the façade reflection settings – Donghu Road area, the rows with errors greater than 3 dBA are highlighted.

Point	d' (m)	*h* (m)	Measured Attenuation (dBA)	Calculated Attenuation (No Correction) *			
				Rf=3; With Reflection		Rf=3; No Relection	
				Attenuation (dBA)	Error (dBA)	Attenuation (dBA)	Error (dBA)
R	7.7	1.1	-1.6	-1.9	0.3	-2.2	0.6
A01	18.8	1.3	7.5	9.0	-1.5	9.6	-2.1
E04	32.7	1.5	10.9	7.6	3.3	7.2	3.7
A02	42.1	1.8	10.0	9.6	0.4	9.4	0.6
C01	56	3.3	14.5	13.3	1.2	14.9	-0.4
B01	57.1	2.4	13.6	12.4	1.2	14.6	-1.0
A03	66.3	2.0	11.1	11.8	-0.7	14.0	-2.9
E03	67.1	2.0	12.6	11.7	0.9	13.7	-1.1
A04	91.3	2.0	11.5	15.2	-3.7	18.1	-6.6
E02	95.4	2.0	15.9	15.5	0.4	18.5	-2.6
E01	120.1	3.2	13.6	15.6	-2.0	20.0	-6.4
C04	120.4	3.1	15.0	18.4	-3.4	21.1	-6.1
E05	127.2	15.2	14.3	14.4	-0.1	16.6	-2.3
B03	130.1	3.2	14.3	18.8	-4.5	22.1	-7.8
E06	140.1	33.2	12.4	12.0	0.4	14.7	-2.3
E07	145.3	57.2	14.4	12.8	1.6	13.3	1.1
C02	154.6	3.2	15.1	26.9	-11.8	30.5	-15.4
C03	163.8	3.2	15.2	22.5	-7.4	26.3	-11.2

* Maximum reflection order is set to 3. No opposite reflection correction is set.

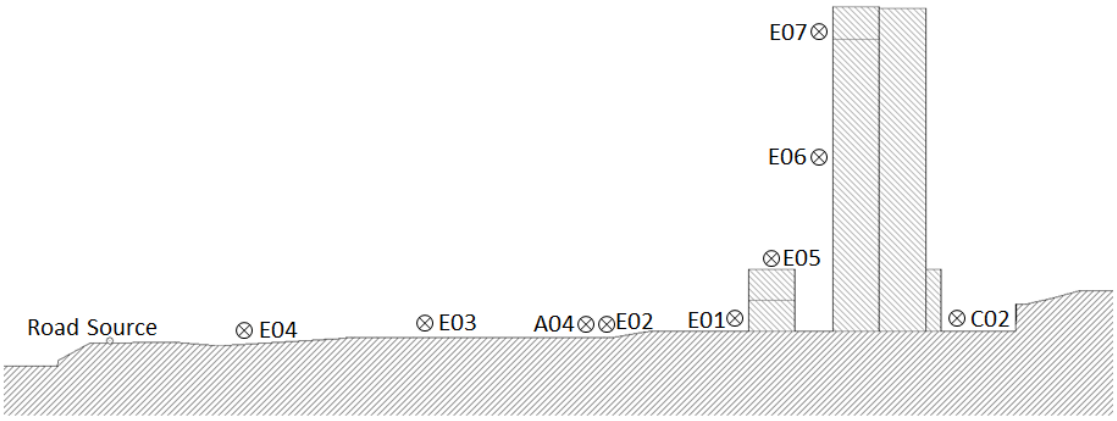

Figure 4.11 West to east cross-section view – Donghu Road area

In Figure 4.10 the solid line with diamond points demonstrates the calculated noise attenuation of all receivers by setting the maximum reflection order to 3; the darker dashed line connecting round dots shows the measured attenuation by calculating the gap

between the received SPL and the SPL of the road source line. To test how the noise reflection from building façades affects the calculation of noise attenuation, a hypothetical scenario with all the reflection coefficient of the building façades set to 0 is calculated and demonstrated with lightly dotted line.

It can be seen firstly that at a closer distance, say less than 50 m, the total calculated and measured noise attenuation generally coincides with each other. As described in the previous section, it is also worth noticing that there are clear disparities between the measured and the calculated results for the points locating around or more than 100 m from the road and close to the main buildings. The highlighted rows in Table 4.7 mark the points at which the errors are greater than 3.0 dBA. For the scenarios of without considering the surface reflections by setting the reflection coefficient to be 0, the lightly dotted results line in Figure 4.10 has a clear gap from the other two scenarios, especially when the distance is farther than 50 m, which indicates the significant importance of the façade reflection calculation as demonstrated in Figure 4.11. The causes of the disparities on some key points are further discussed below.

4.4.2.1 Ground point in the open square close to low-rise building

The reflection from the smooth façade of the arc-shaped exhibition building as well as the other buildings increases the received SPL value and hence reduced the calculated noise attenuation on point A04. As shown in Figure 4.12, the receiver point A04 locates at 91.3 m from the road source and close to the arc-shaped exhibition building in the outer part of the square.

As can be seen in Figure 4.10 and Table 4.7 that when the façade reflection is considered the calculation error on point A04 is -3.7 dBA; when building façade reflection is neglected, the calculation error at A04 is almost doubled to -6.6 dBA. For the point E02 locating at a similar distance of 95.4 m but farther from the exhibition building and all surrounding buildings, it can be seen that the calculation error is only 0.4 dBA, which is relatively smaller, even when the façade reflection is set off, the absolute error on point E02 is still within 3.0 dBA. It can be seen that on the ground level in the typical open space, the building façade reflection plays a significant role in affecting the calculation accuracy even if the distance to the road is relatively far.

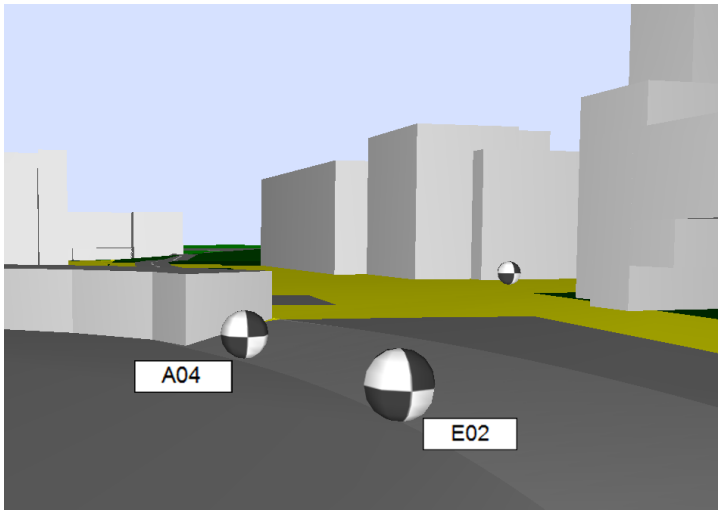

Figure 4.12 Perspective view of the receiver point A04, B02 and C03 – Donghu Road area

4.4.2.2 Similar distance, different surrounding

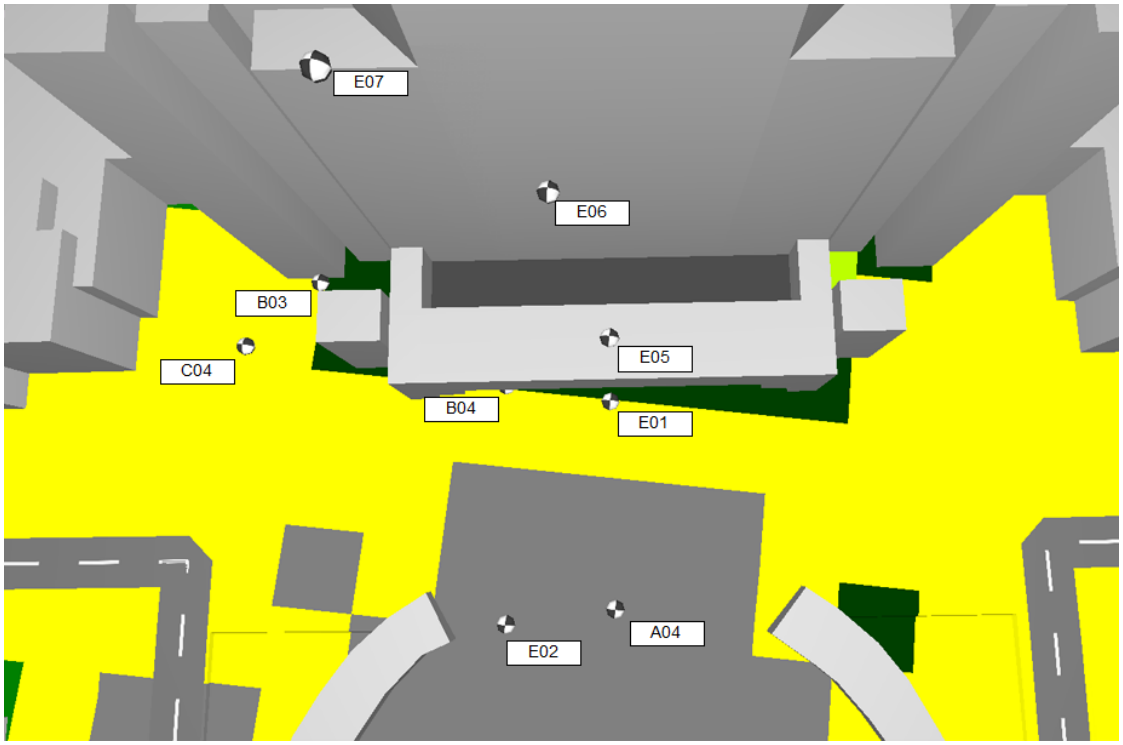

Figure 4.13 Perspective view of the receiver points on the front side of the main building – Donghu Road area

For the two receiver points E01 and C04 with similar height and similar slant distance to the source line, the cancellation of façade reflection have distinct effects due to the difference in the transmission path and distance to surrounding buildings. As can be found in Figure 4.10 and Table 4.7 that, when the maximum reflection order is set to 3and all

actual reflections are calculated without using the setting of 1.5 dBA correction, the total attenuations occurred at E01 and C04 are 2.0 dBA and 3.4 dBA higher than the measured attenuations respectively. When the façade reflection is globally switched off, the calculation errors both greatly enlarged to -6.4 dBA and -6.1 dBA respectively, which are increases of 4.4 dBA and 2.7 dBA in absolute calculation errors respectively.

From the comparison of the calculation errors, it can be seen that the avoidance of façade reflection has more impact on the point E01, considering the nearest distance to the road source and the relative height of both points are similar. As shown in Figure 4.13 that the point E01 locates at the foot of the 4-storey podium building, while the point C04 locates at the centre of a small open space to the east side of the main building and surrounded by neighbouring building façades. Nevertheless, although the point C04 is surrounded by a group of neighbouring buildings, the noise transmission path to it is partially screened, and the distance to the nearest façade is larger than that of the point E01. On the contrast, the point E01 as a façade point locating just over 1 m from the foot of the podium building, the noise propagation path from the road source is relatively free and unblocked. The noise level on point E01 is hence affected by stronger façade reflection from the podium building. Therefore, once the façade reflection is globally disabled, the decrease of noise attenuation on Point C04 is relatively limited and smaller than that on point E01 due to the larger distance to surrounding façades and the screening of other buildings on the noise propagation path.

4.4.2.3 Remote façade points partially screened

In this typical Chinese urban environment, the calculation error of some remote ground receiver points is relatively much higher than normal due to the complicated effect caused by the surrounding buildings. As shown in Figure 4.14, B03 as a façade point locates 130.1 m from the road source line and just above 1 m from the foot of the main building. With setting the maximum reflection order to 3, the gap between calculated and measured attenuation is -4.5 dBA. When the noise reflection from the surrounding façades is disabled, the calculation error jumped for 3.3 dBA to -7.8 dBA.

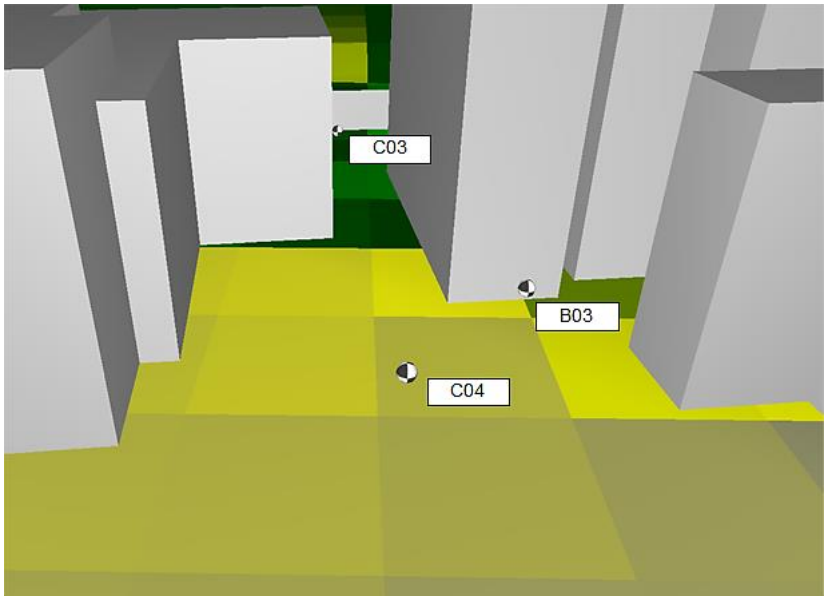

Figure 4.14 Perspective view of the receiver point C04, B03 and C03 – Donghu Road area

The noise attenuation on point B03 is also greatly affected by the surrounding building environment. Firstly, although similar to point C04, the point B03 also locates in the relatively remote and sealed space rather than open to direct noise impact as point E01 and other receiver points spreading on the front side of the main building and the open square. Because the noise propagation path is partially blocked, due to more complicated calculation of screening effect the calculation error on B03 is relatively large despite the façade being considered or not. Secondly, the point B03 is locating relatively farther in the small open space shared with point C04 and closer to the façades of the buildings. It can be seen that the façade noise reflection contributes 3.3 dBA in the total noise attenuation at the location as remote as where B03 locates.

4.4.2.4 Fully screened points besides or behind the main building

The more extreme case of the effect of façade noise reflection is the point C02 and C03 which merely have no direct path from the noise source. For these two points locating near the main building with slant distance of over 150 m from the road source line, the error between the calculation and the measurement results are much higher due to the existence of the group of neighbouring buildings including the high-rise main building.

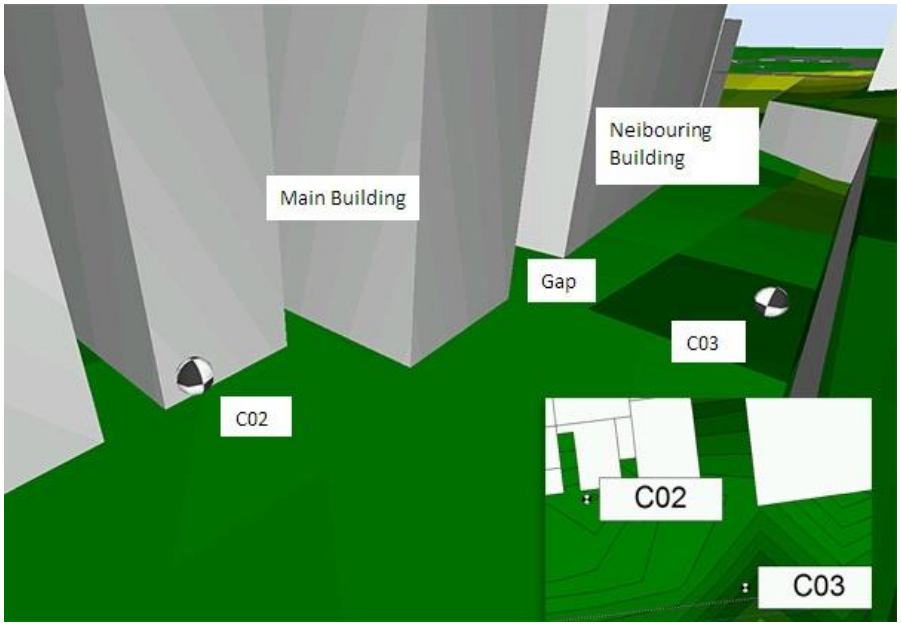

Figure 4.15 The position of two special points – Donghu Road area

The biggest error of -11.8 dBA occurs at point C02 locating 154.6 m from the effective road source line, at which as can be seen in Figure 4.15 that the main building screens the direct noise transmission path from the source. Similar but smaller discrepancy of -7.4 dBA occurs on point C03 at 163.8 m locating between the buildings. On point C03 the noise reflection and diffraction from the road source can reach through the gap between the two neighbouring buildings, the error at point C03 is hence reasonably smaller than that of the C02 which is entirely blocked by the main building. When all façade noise reflection is neglected, the calculation errors on point C02 and C03 rise to -15.4 dBA and -11.2 dBA respectively. It further indicates the important influence of the façade noise reflection on the calculation of noise in the remotely located and partially or fully blocked locations.

It is also to note that the calculated noise attenuation at point C02 is almost doubled in both scenarios. The huge error occurred at point C02 disregarding the façade reflection is on or off also implicates that the calculation of noise transmission loss through the main building at point C02 may have been overestimated in the calculation. Considering the scale of the main building, the lateral diffraction effect may also be hugely underestimated and causes the overestimation of the noise attenuation at point C02.

4.4.3 *Receiver points on different heights of the building surface — influence of the high-rise building and the annexed podium*

As can be seen in Figure 4.3b that the high-rise main building has relatively large surface area facing the road without any screening barriers or buildings, it is of great importance to examine how the high-rise main building and the annexed podium affect the calculation of noise with height increasing. Point E01, E05, E06, and E07 are selected to test the effect of increasing height on the accuracy of the calculation. Two hypothetical scenarios with the podium and the main building removed are introduced for comparative analysis.

In the perspective view of the Donghu Road area in Figure 4.9 as well as the section view in Figure 4.11 it can be seen that the south side of the main building is facing the open square, E01 and E05 locate at the foot and on the rooftop of the annexed podium building with a height of 3.2 m and 15.2 m respectively, while receiver points E06 and point E07 are selected at the 9th floor and 18th floor with heights of 33.2 m and 57.2 m respectively. Point E06 locates just over 1 m from the façade of the building and point E07 locates at the edge of a small balcony at the 18th floor and approximately 2.5 m from the building façade.

4.4.3.1 *General results*

Table 4.8 Errors between calculation and measurement at different heights – Donghu Road area, errors with absolute value equal to or smaller than 3 dBA are highlighted.

	Slant Distance (m)	Horizontal Distance (m)	Relative Height (m)	Rf.=3 with Reflection (dBA)	Rf.=3 No reflection (dBA)	Rf.=3 No podium (dBA)	Rf.=3 No main building (dBA)
E01	120.1	119.9	3.2	-2.0	-6.4	-3.2	-2.0
E05	127.2	125.6	15.2	-0.1	-2.3	-2.8	0.1
E06	140.1	135.4	33.2	0.4	-2.5	0.5	-0.5
E07	145.3	133.5	57.2	1.6	1.1	1.6	2.3

Calculation results of three scenarios are compared and the results are shown in Table 4.8 and Figure 4.16, including the calculation with default settings and the maximum reflection order of 3, the calculation with façade reflection deactivated and two hypothetical scenarios with the annexed podium building and the main building removed respectively. The selected four points spread around the front side of the main building

with horizontal distances spreading within a range of 15 m, although the slant distance to source line varies.

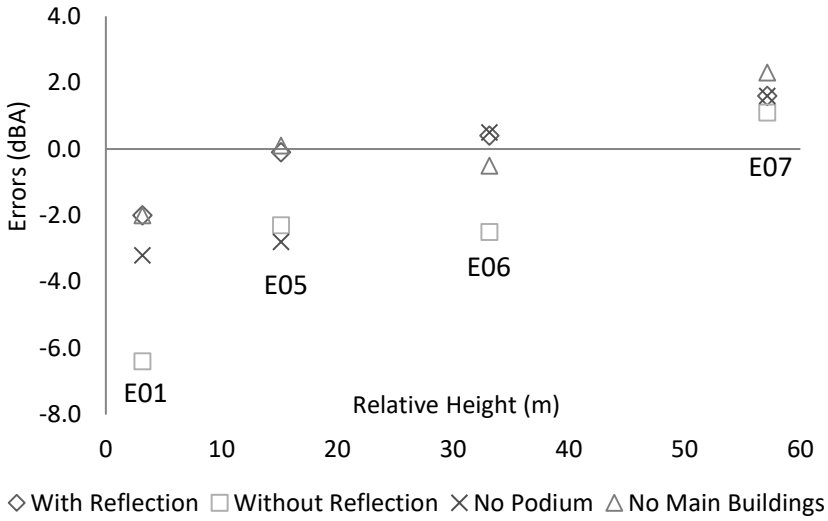

Figure 4.16 Errors at different heights in a series of hypothetical tests – Donghu Road area

It can be seen that when the receiver points are at a higher altitude without being affected by low-rise neighbouring buildings, the errors tend to be closer to 0 despite the change of scenarios. When the façade reflection of all buildings are disabled, the gaps between the calculation and measurement tend to increase negatively especially at lower heights. With the podium and main building removed respectively, the gaps generally tend to become smaller, while the change tendency of discrepancies varies depending on the specific situation of the points.

4.4.3.2 E01 and E05 – Points at lower attitude

- ***Effect of façade reflection***

As can be seen in Figure 4.17a that, point E01 locates on the ground level with a relative height of 3.2 m, 120.1 m from the road source line and just over 1 m away from the façade of the annex podium building. Point E05 locates at the centre of the rooftop with a relative height of 15.2 m and slant distance of 127.2 m from the road source line. The point E05 is relatively clear from the surrounding building façades with a minimum distance of 12.1 m from the south side of the main building.

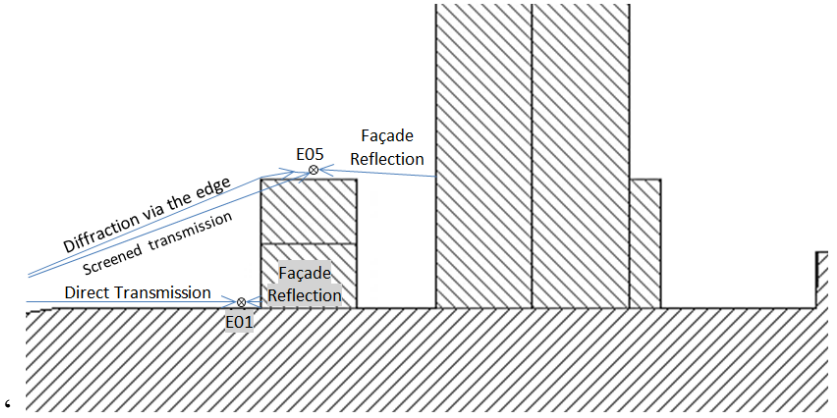

a

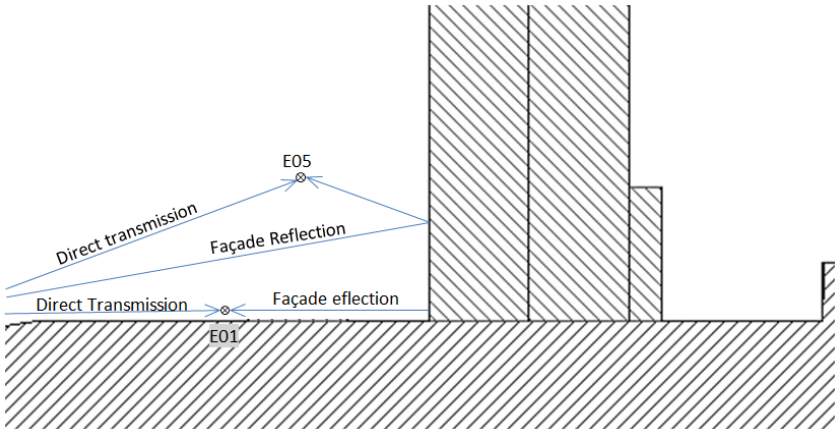

b

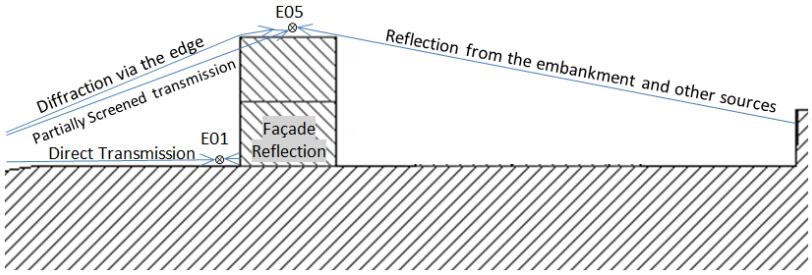

c

Figure 4.17 Major corrections calculated at point E01 and E05 – Donghu Road area. (a) The original scenario with all buildings; (b) Hypothetical scenario without the podium; (c) Hypothetical scenario without the main building.

On the ground level at point E01 the noise calculation is affected by strong reflection of the building façades, thus the accuracy level is generally the lowest among the four points. It is interesting to note that at point E01 and E05 that both locating closely around the 4-storey podium building with different heights, the calculation error at point E01 is evidently larger than that of the point E05. When the maximum reflection order is set to

3 with normal façade reflection settings, the calculation errors on the two receiver points are -2.0 dBA and 0.1 dBA respectively, which are both acceptable; while in the scenario of façade reflection being switched off, the gap between calculation and measurement increases due to the lack of reflection correction. Nevertheless, the error at point E01 increases 4.4 dBA negatively to -6.4 dBA, while the calculation error of the point E05 only increases half as that of point E01 for 2.2 dBA negatively to -2.3 dBA.

Point E01 as a ground receiver point close to the building façade, the direct façade reflection as well as the noise reflection from the surrounding buildings plays a major role in the calculation of total noise attenuation. Thus, when the façade reflection is disabled, consequently the calculated SPL at point E01 decreases evidently.

In contrast, at point E05 the influence of the façade reflection tends to be less than that at point E01 due to larger distance towards the nearest façade. As can be seen in Figure 4.17a that point E05 locates at a higher position with more open surroundings. Although multiple sources of influence including the direct noise transmission from the source and the diffracted noise from the edge of the roof have a certain impact on the calculation, due to its relatively larger distance to the nearest main building, the influence of façade reflection calculation is also limited. Therefore, when the façade reflection is disabled, the increase of calculation error is only half of that at point E01.

- ***Test on hypothetical scenarios***

In the scenario with the podium building remove as can be seen in Figure 4.17b, that when the podium is removed, the discrepancy between calculated and measured SPL at point E01 and E05 increased negatively to -3.2 dBA and -2.8 dBA respectively, which are at a similar level. It indicates that when the podium building is removed, the strong façade noise reflection at point E01 and the diffraction from the roof edge at point E05 are both suppressed accordingly, thus direct transmission and the façade reflection from the façade of the main building at a similar distance become two major sources of correction at both points.

In the hypothetical scenario of the main building being removed as shown in Table 4.8 and Figure 4.16 that at point E01 and point E05, the calculation is merely not affected. Only at Point E05, due to the removed façade reflection from the main building, the

calculated result is raised 0.2 dBA and the discrepancy turns from -0.1 dBA to 0.1 dBA. As shown in Figure 4.17c that, at point E01 the façade reflection from the podium dominates, and at point E05 due to the openness of its surroundings, the main building brings little façade reflection to it; when it is removed, the second third order of indirect reflection from other sources behind the main building is also negligible.

4.4.3.3 E06 and E07 – Façade points at higher altitude

At point E06 and E07, as shown in Table 4.8 and Figure 4.16 that due to the relatively higher position, these two points are less affected by the reflections from surrounding buildings except the main building itself. With building façade reflection cancelled, the calculation result of E06 dropped for 2.9 dBA and the error increased negatively to -2.4 dBA. At Point E07 due to its relatively higher altitude, the reflection from all the building façades including the main building only contributes 0.5 dBA to its calculation results. The error dropped from 1.6 dBA to 1.1 dBA cancellation of façade reflection.

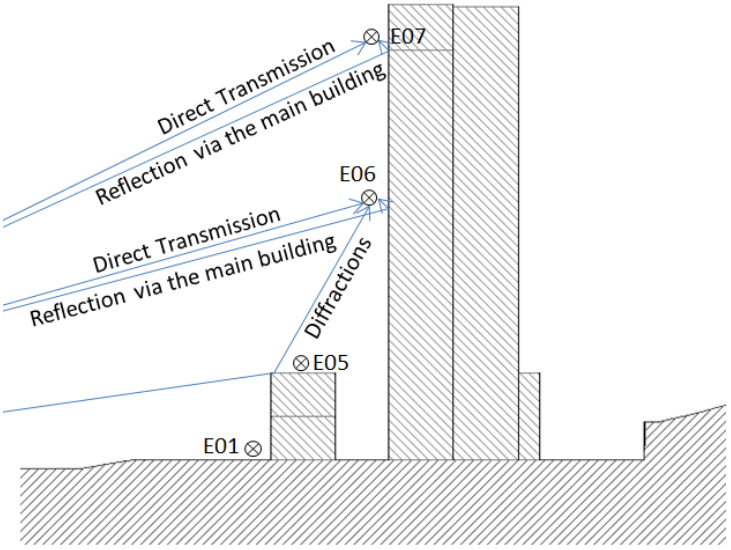

Figure 4.18 Major corrections calculated at point E06 and E07 – Donghu Road area

As illustrated in Figure 4.18 that the major source of correction for the attenuation calculation at point E06 are E07 are both direct transmission and façade reflection. It may because the average building height of the surrounding buildings are much lower than the height of both E06 and E07, the 2nd and 3rd order of reflection and the diffracted noise from the edge of the podium is negligible. Thus, when the podium has been removed the discrepancy of calculation and measurement at point E06 changed for only 0.1 dBA, and

no change occurred at point E07. In contrast, it is interesting to note that when the main building is removed, the calculated noise level at point E06 decreased 0.9 dBA while that of the point E07 increased 0.7 dBA.

As can be seen in Figure 4.13 that point E06 locates more closely to the façade of the main building, hence it is more affected by the façade reflection of the main building. As the point E07 locates outside the balcony of the top floor, the distance towards the nearest façade of the main building is larger than that of point E06, which causes less façade reflection from the main building façade. In this hypothetical scenario, when the main building is removed, the screening effect of the main building is also deactivated, thus there may be a series of direct or indirect reflections from the neighbouring buildings reach it freely, thus raises the noise level as well as the discrepancy between calculation and measurement.

4.4.3.4 Implications

At the ground level, the noise calculation is greatly affected by the influence of façade reflections of surrounding façade, especially when the receivers are locating at a height lower than surrounding buildings. The effect is strongest close to the surface which is under the direct impact of the traffic noise.

It could be seen that at the distance of more than 120 m from the road source, the annex podium of the building has merely no effect on affecting the noise level at higher altitude. At the same time, the vertical façade of the main building facing the road source, the sound transmission in between it and the road is affected hugely. Though due to the large distance created by the open square, mainly the façade points at the surface of lower height is strongly affected by the façade reflection from the main building. The screening effect of the main buildings may cause more influence to the non-façade points around it.

4.4.4 Calculation error at different frequencies

The section examines the SPL calculation accuracy of the SPL at the central frequencies of eight major octave bands. The calculated SPL at the eight frequencies are then collected and compared with the measured results; results are shown in Figure 4.19. Detailed errors

between the measurement and the calculation can be seen in Table 4.9, MBA equivalent r lower than 3 dBA are highlighted.

Table 4.9 SPL spectrum calculation errors at major octave bands central frequencies – Donghu Road area, errors with absolute value equal to or smaller than 3 dBA are highlighted.

	Calculation errors (dBA)								
	31.5 Hz	63 Hz	125 Hz	250 Hz	500 Hz	1 kHz	2 kHz	4 kHz	8 kHz
E01	-4.6	-4.8	-6.9	-4.4	-1.8	0.6	0.7	-1.6	-11.2
E02	-5.2	-3.7	-4	-0.5	0.7	1	1.6	1	-6.3
E03	-5.8	-4.6	-3.8	-2.1	0.6	1.9	1.4	0.2	-9.5
E04	-1.6	1.2	2.5	4.3	5	4.5	5.2	5.9	4.5
E05	-4.9	-3	-6.5	-6.8	-1.5	-0.1	0	-0.5	-12.7
E06	-1.8	-4.2	-4.1	-3	-0.8	0.4	0.8	-0.5	-10
E07	-7.1	-1.2	-3.1	-1.7	-1.2	-0.9	-0.9	-5.3	-18.7
Mean	-4.4	-2.9	-3.7	-2	0.1	1	1.3	-0.1	-9.1
SD	1.9	2	2.9	3.2	2.2	1.6	1.8	3.1	6.6
MAE	4.4	3.3	4.4	3.3	1.6	1.4	1.5	2.1	10.4

The errors of central frequencies of all major octave bands are shown in Figure 4.19, it can be seen that the alignment of the calculated and measured are generally well-fit, with some small gaps spreading at various frequencies in each diagram. The absolute errors equivalent or smaller than 3.0 dBA are highlighted in Table 4.9. As can be seen that, the error of most of the receiver points except E04 at 8000 Hz is exceptionally high, with an overall MAE of 10.4 dBA, the mean error is -9.1 dBA with an SD of 6.6 dBA.

The accuracy level is generally acceptable in the spectrum ranging from 500–4000 Hz, where the MAE of all points at these frequencies is smaller than 3.0 dBA. The errors are slightly larger at lower frequencies ranging from 31.5 Hz to 250 Hz, with the MAE of 3.3–4.4 dBA, which is also where most of the sound energy concentrate. It may be caused by the unique propagation properties of low-frequency noise. In a research by Can et al. (2010), it was also found that there is systematic underestimation in the calculation of traffic noise when using current static traffic noise calculation methods. The potential causes of inaccuracy in these frequencies at some receiver points are discussed below.

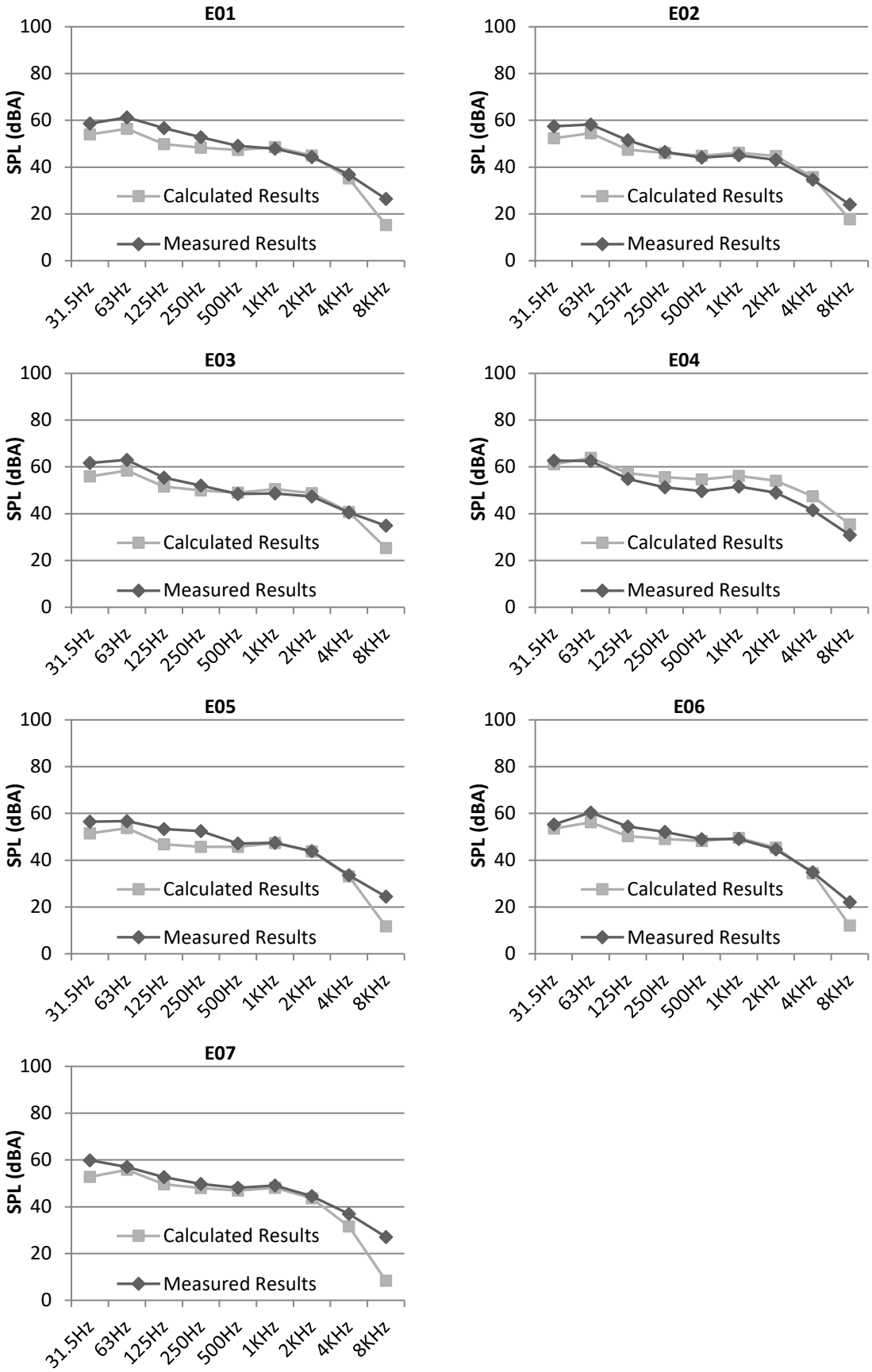

Figure 4.19 SPL spectrum analysis of the Donghu Road area

4.4.4.1 Receiver points closer to the source

The ground receiver points E02, E03 similarly have more evident errors at lower frequencies, in the meantime, the ground point E04 generally has a higher error at higher frequencies. These three points locate with an interval of 20-30 m from each other in the open space close to the road source. The distance from the high-rise building is also longer than the façade points.

For E02 and E03 the errors in frequencies from 31.5 Hz to 125 Hz is also high, nevertheless, at 250 Hz the errors are more acceptable than those of E01 and E05. The problem of the overestimated decay of lower frequency noise seems to be not a problem for point E04 which may be due to its close location from the road source and the direct transmission dominates, while in the calculation of ground effect the SPL at higher frequencies from 250 Hz to 8000 Hz appears to be overestimated. As shown in Figure 4.3 that there is a patch of soil ground absorber in-between E04 and the road, the higher frequency noise may largely be absorbed in the transmission in the c situation.

Another potential reason of the reversed alignment of errors at E04 in higher and lower frequencies comparing with other receiver points is that it is relatively much farther from the high-rise main building; the potential inaccuracy of reflection calculation in lower spectrum range at the long distance from the source may need to be considered as well.

4.4.4.2 Remote receiver points at lower altitude

According to the previous discussions about the point E05, as can be seen in Figure 4.17a that the potential error in the calculation of the screening effect and the diffraction caused by the podium edge may both have influences on the calculation accuracy. The point E01 and E05 locating on the ground close to and above the podium building has relatively longer slant distance from the source line, and the correction of ground effect at which is counted in the calculation based on the relative heights.

It can be seen that at both E01 and E05, the actual attenuation of the energy-concentrated lower frequency noise levels from 63-250 Hz is not as high as calculated. As can be seen in Figure 4.17a that the transmission route from road source to E01 is relatively more affected by the ground; at point E05 the transmission route from the source is partially

screened by the edge of the podium. Although the lower frequency noise with longer wavelength and higher sound energy has less loss in long-distance attenuation (Leventhall, 2003), it generally shows that relatively lower altitude the noise attenuation in lower frequencies is slightly overestimated due to the more complicated surroundings and the potential inaccuracy in the calculation of ground effect. In the other hand, considering the two points are both close to the building surface, the overestimation of the loss in the façade reflection of lower frequencies may also be counted.

4.4.4.3 Remote receiver Points at higher altitude

The errors at the two façade receiver points, E06 and E07 at higher altitude shows the most acceptable accuracy level in middle range frequencies, while the accuracy level at both ends, especially the higher frequencies, are less desirable than average.

It is worth noticing that for point E07 that locates close to the top of the main building, although the accuracy level at the middle-frequency range is relatively desirable, the overall calculation accuracy level at which is the worst among all seven points measured. As can be seen in Table 4.9 and Figure 4.19 that, at point E07, in the low to middle frequency range from 63 Hz to 2000 Hz the accuracy level is desirable with absolute errors mostly within or only slightly above 3.0 dBA. Nonetheless, at the lowest frequency of 31.5 HZ, the noise level is overestimated for 7.1 dBA. At the high-frequency end, the calculation accuracy is even worse: the calculation result at point E07 is overestimated for 5.3 dBA at 4000 Hz and 18.7 dBA at 8000 Hz respectively.

In one hand this may be the contribution of the same reason mentioned earlier that for lower frequency noise the ground situation may affect the propagation evidently. In another hand, the atmosphere noise attenuation at higher frequencies, say, 8000 Hz may have been greatly underestimated. It can also be seen from Table 4.9 that, this is a global phenomenon among all receiver points despite their relative height. For all receiver points the MAE at 8000 Hz is 10.4 dBA, and the mean error of which is -9.1 dBA with an SD of 6.6 dBA, which is significantly higher than the MAE of all other frequencies.

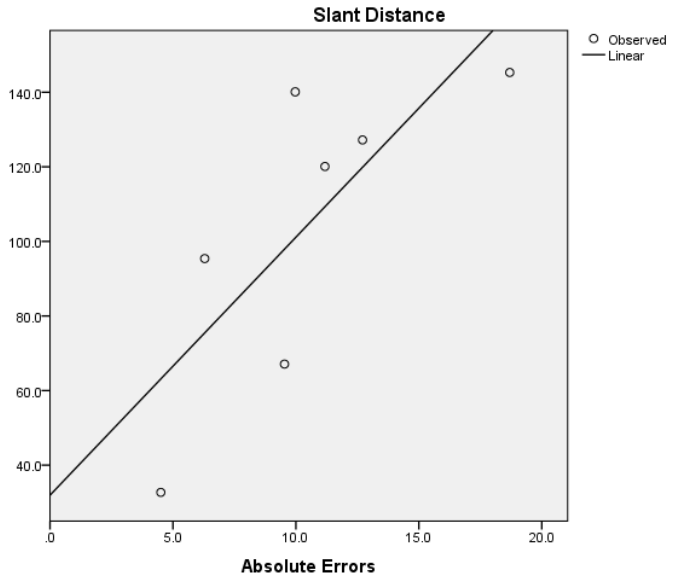

Figure 4.20 Relationship between the absolute errors at 8000 Hz and the slant distance of seven receiver points – Donghu Road area (R^2 = .590, $p < 0.05$).

In fact, it is found that for the seven points with the SPL spectrum measured and calculated, the errors at 8000 Hz are increasing with the slant distance. As can be seen in Figure 4.20 that, the slant distance of seven receiver points has a significant positive correlation with the absolute errors occurs at 8000 Hz (R^2 = .590, $p < 0.05$). From Figure 4.19 it can be seen that the errors are mainly due to the underestimation in the calculation of the high-frequency noise. The potential cause of the increased inaccuracy at high frequencies may because of the overly estimated atmosphere absorption.

4.5 Conclusions and discussions

4.5.1 General findings

In previous studies in the EU, a variety of notable calculation errors is found when using current calculation methods, the gap between calculation and measurement can be as large as 6-11 dBA depending on the location of the receiver points. (Hepworth, 2006; Nijland & Van Wee, 2005). In this chapter, a sample case in Wuhan, China was selected for simple road, building and spatial features. Controlled tests are then conducted to verify the effect of the adjustment of default calculation configuration settings on the calculation accuracy. The results indicate that the most of the recommended configurations used in the selected

typical EU noise mapping methods and packages are sufficient in the simulation of the relatively open and simple urban area with typical Chinese urban sound environment characteristics. A series of noise calculations and in-situ measurement are implemented on a variety of receiver points in the sampled area, although disparities of up to 11.8 dBA between the calculated and the measured results are found, the general accuracy of the calculation using CRTN is acceptable, and the specific error varies depending on the specific locations of the receiver points. Some essential adjustment for the sake of the optimisation of the default settings and modelling method are suggested. It is also noted that despite the efforts of optimising the configurations, the calculation error at some receiver points are difficult to be eliminated or reduced, the potential effects of the unique building and urban form features on the calculation accuracy are preliminarily analysed.

4.5.2 General tests on default configurations

The calculation accuracy of a series of default calculation configurations setting are verified systematically. The settings of the ground absorption coefficient are tested. Most of the default settings in the selected EU noise mapping packages seems has no or very limited effects on the calculation accuracy.

It is found that the in the studied case, setting the ground absorption coefficient to 0.4 based on the actual site condition can ensure better calculation accuracy comparing with that of using the default value of 0 or 1. Then a parametric test is conducted on the effect of the potentially ignored ground reflections by using the reflective surface modelling method on the ground level instead of ground absorption. It is found that up to 3 dBA of ground reflection effect may have been neglected; although it is also found that the effect occurs within a limited height range.

The configurations related to the calculation of reflection are also tested. It is found that increasing the maximum reflection order is helpful for control the inaccuracy, but only to a limited extent, the maximum reflection order of 3 is sufficient to ensure acceptable accuracy level without severely prolonging the calculation time. It is also noted that the method of 1.5 dBA correction for the opposite reflections (DataKustik, 2007) that can largely reduce the calculation time may not be suitable for receiver points locates far from

the source, say, farther than 40m from the road source in this sampled area. As the calculation error is increased significantly when the setting is activated.

4.5.3 Tests on the effects of urban morphological features

Specific effects of the typical Chinese urban sound environment feature on the performance of EU noise calculation methods are examined. It is noticed that with the optimised calculation settings, the mean calculation error is generally acceptable, for the sixteen receiver points spreading 0–150 m from the road source on the front side of the main building is -0.4 dBA, with an SD of 2.0 dBA and the MAE of only 1.6 dBA. Through the analysis of the effect of the7 slant distance on accuracy, it is also found that the accuracy level drops along with increasing slant distance, and has better calculation accuracy within 0–60 m than within 0–120 m. The error is the largest when the receiver point locates at further than 150 m and entirely shadowed by the main building.

It is also found that the total attenuations at the distance range from 60-120 m on the front side of the high-rise main building are significantly increased, indicating the direct contribution of the building façade reflections to the calculation results. Through a series of Hypothetical scenario test, it is found that the higher inaccuracy level at a further distance are more prone to be influence of surrounding façades at a further distance from the road. The effect is stronger for façade points close to the high-rise main building, especially at lower height.

Furthermore, the full-spectrum noise levels measured at seven receiver points are systematically tested and analysed. The general statistics at each central frequency of all receiver points shows that the accuracy level at a middle-range frequency from 500-4000 Hz are generally desirable; while the SPL of the lower frequency range from 31.5 to 250 Hz are more or less underestimated. The calculated SPL at 8000 Hz is globally the most underestimated, the absolute errors occurred at which is also found to be significantly correlated to the increase of slant distance.

4.5.4 Optimisation of default calculation configurations

Based on the tests conducted in this chapter, some default settings of the default calculation configurations and modelling method manifest potential of being adjusted to

improve the general calculation accuracy, according to the specific location and condition of the sound environment simulated. Some of the suggestions of optimisation are displayed in Table 4.10.

Table 4.10 Optimised calculation configurations settings and modelling method

Options	Settings / Improvement	Applicable scenarios
Maxi. order of reflection	1	Open space, no or little screening occurs
	3	Any multi-story buildings or tall barriers exist
1.5 dB reflection correction	Yes	Large scale noise mapping or relatively space
	No	Complicated urban space with buildings / barriers
Calculation of ground absorption	0	Fully-reflective surface.
	1	Soft pervious soil
	Set accordingly	Estimated based on the dominating condition of the ground surface
	3D Reflector	For receiver points locate close to the road edge and with reflective-ground surface
Façade reflection coefficient	Set according to façade conditions	For receiver points close to buildings that locate far from road kerbs. Points close the façade of high-rise buildings
Atmosphere divergence	Improvement need for the calculation of noise of higher frequencies.	For receiver points locate far from the road source.

It is to note that, for the receiver points located in relatively open space at the ground level close to the main road, say within 40 m, the default calculation configurations can ensure rather accurate results. Optimisation of configuration settings are recommended to be adopted in the scenarios that locates farther from the road and affected significantly by the façade reflections of surrounding building facades. It is to be mentioned that, the calculation inaccuracy of some scenarios is difficult to be improved by simply improve the configurations settings and modelling method, e.g. screening effect of the high-rise building at a distance of 120 m, the systematic increasing error increasing of the high-frequency noise, etc. Further studies are needed to find the potential causes and methods of improvement.

Chapter 5 Applicability examination of EU traffic noise calculation method in typical urban environment of China

5.1 Introduction

This chapter focuses on the examination of the applicability of EU noise mapping calculation methods in the typical high-density urban environment that is common in China. The accuracy of the calculation methods using optimised calculation configuration is systematically tested. The aim is to test how certain urban morphology features influences the performance of representative EU noise mapping calculation method and package.

Following the Chapter 4, four more cases with typical urban morphological and acoustic features are selected in Wuhan. The case selection is based on distinctive urban morphological characteristics of representative urban areas selected in Wuhan, China, based on both urban morphology features and road traffic conditions. There is at least one representative urban form feature, and one to two main roads with heavy traffic in each one of the cases.

General comparisons of the A-weighted sound pressure levels are made to all receiver points measured a variety of locations with different slant distances to the road source and relative height. In each case, a variety of receiver points representing different scenarios with certain spatial and acoustic features are studied using representative EU noise mapping package and road noise calculation method. The correlation between the observable calculation errors is analysed. A series of noise calculation with both general A-weighted and the central frequencies of eight major octave bands are conducted. The results are compared with the measurement result using the optimised configuration in all five cases. Detailed analysis is then made according to the patterns and the potential causes of the errors in specific typical Chinese urban acoustic and morphological features.

The main part of the chapter consists of three parts. Section 5.2 explores the noise calculation accuracy in a comprehensive area comprised of a typical urban village and multi-storey residential area, the emphasis is put in the urban village close to the main road with heavy traffic. Due to the planning system of China, the urban form of the street canyon is prevalent in major cities; where the traffic concentrated main roads are normally flanked with multi-story and high-rise buildings. The form of the street canyons and the road structure varies. Section 5.3 discusses how the traffic noise propagates and in a typical main-road street canyon with flanking high-rise complex comprised of high-rise towers and long belt-shaped podiums, both the calculation accuracy on the ground on the façade at a different height, inside and outside the street canyon are analysed. Section 5.4 analyses the propagation of the double layer roads running through two street canyons with distinct urban form. In both cases one main road with an elevated high-speed road, runs across a relatively wider and a relatively narrower street canyon, the elevated part of the latter is fitted with confined noise barriers, the simulation and the effect brought by the barrier is also analysed.

5.2 Urban village close to heavy-traffic main road

5.2.1 General description

5.2.1.1 Topography and urban morphology – an urban form typical to China: The Urban Village

The south part of this area with high density and low-rise residential buildings can be categorised as a typical type of urban form of China, the urban village. The urban villages are gradually shaped in the rapid process of urbanisation since early 1980's, which are former rural villages that were locating amongst urbanised districts or in the outskirt of the metropolitans. (Song & Zenou, 2012)

The urban village has two distinctive features: The building density is exceptionally high, and the alleys separating the buildings are pedestrian dominated and non-accessible to large vehicles even domestic cars. Current urban villages mainly are agglomerations of the low-income population, including previous agricultural population and domestic

migrants from the rural area and small towns who pursue low-rent accommodations (Li et al., 2014).

Figure 5.1 Typical pedestrian dominated alleys and paths within Chinese urban villages, photo taken by author

5.2.1.2 Building features – Mixture of low-rise and high-rise buildings

The buildings adjacent to the main road the Renghe Road are mostly converted into commercial uses, e.g. small restaurants and hotels, etc. At the same time, the ground floor of the buildings facing the only vehicle-accessible alley in this area is crowded with grocery stores and street food stalls as can be seen in Figure 5.1.

Figure 5.2 Satellite map – Renghe Road area. Source: Google Maps (Google Inc.)

As shown in Figure 5.2 and Figure 5.3 that although in the north part of the selected area close to the main road the Youyi Avenue which locates in the north of the area, the buildings are mainly department stores with large masses, and multi-storey and high-rise buildings of 7–20 storeys. Nevertheless, the buildings only occupy an area ranging from 60–120 m on the south side of the Youyi Avenue. The relatively larger scale and higher height high-rise buildings may act as huge noise barriers, and evidently block the traffic noise from the Youyi Avenue on the north side.

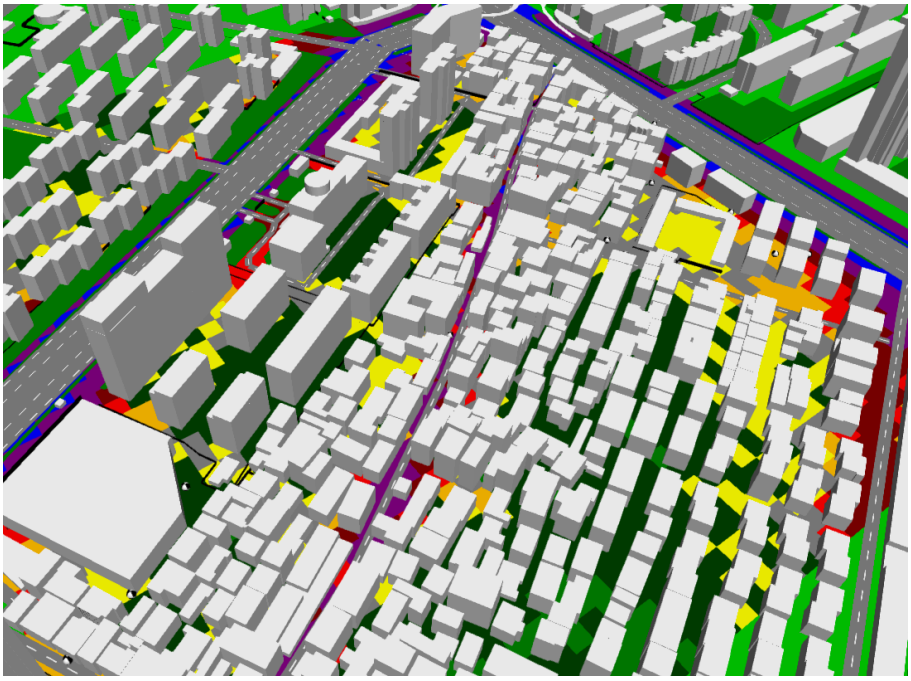

Figure 5.3 3D perspective view of the urban village close to Renghe Road

5.2.1.3 Road and traffic conditions

There are two main roads surrounding the selected area, the Youyi Avenue locating in the north and the Renghe Road locating in the east. Both of the two main roads are planned as major traffic pathways with six carriageways with heavy traffic flow each day. In the measured period, the hourly traffic flow counts of the two roads are 3424 veh/h with 8% heavy vehicles and 1344 veh/h with 18% heavy vehicles, respectively.

There are pedestrian-dominated alleys spread across the urban village area. Vehicle access to the inner part of this area is greatly limited to one single road across the area in the middle starting from the Renghe Road on the east side across this village. The main traffic of this road consists of a relatively small number of electronic bicycles. All the small

roads and alleys scattering within the area amid the low-rise residential buildings are mainly pedestrian and bicycle dominated.

5.2.1.4 *Noise sources*

There are three roads measured: Youyi Avenue, Renghe Road, and a 5-metre-wide alley across the area, the noise level spectrum was measured using high definition sound level metres. The three road sources have the general noise level in terms of L_{Aeq} measured with the values of 76.6 dBA, 76.5 dBA, and 71.0 dBA, respectively, although it needs to be noticed that the noise measured inside the small 5-metre-wide small alley is mainly domestic noise rather than traffic noise.

It is also notable that due to lack of traffic access, the major noise source inside the urban village area is commonly domestic and community activities, including cooking, talking, music playing, TV, ventilation and air conditioners, etc.

5.2.2 *General measurement result and applicability examination*

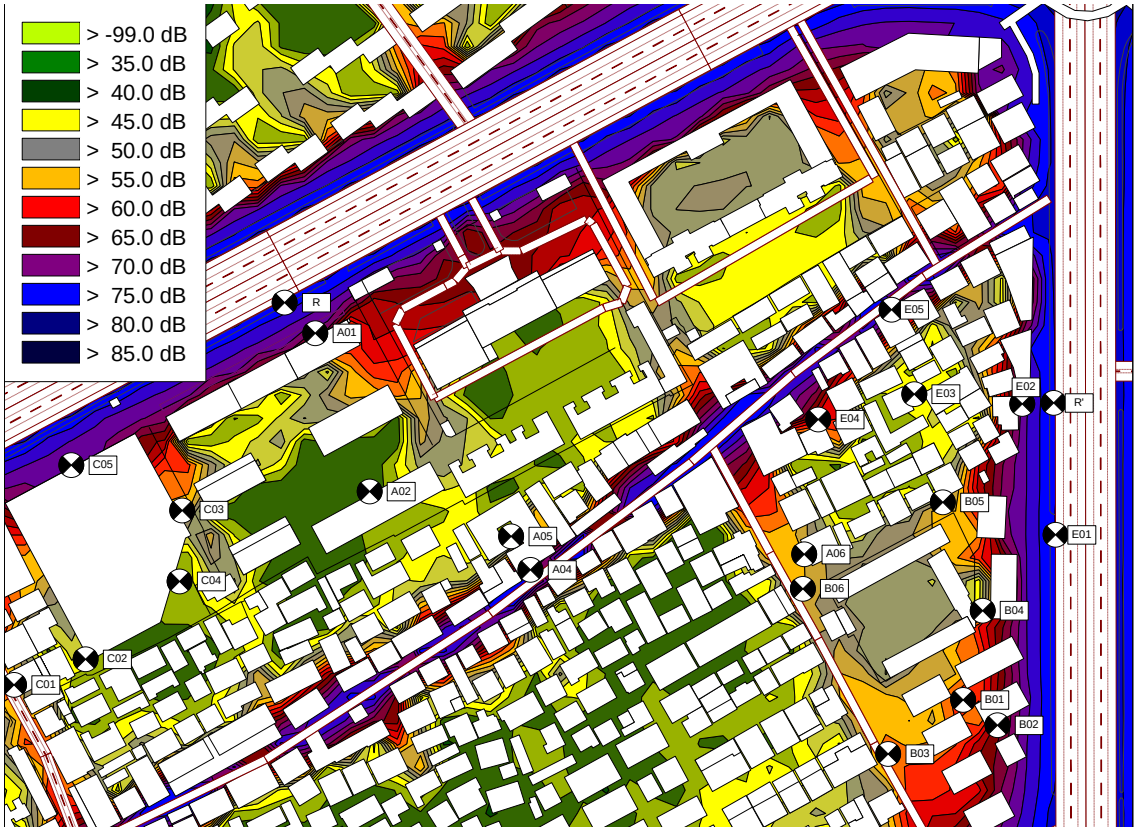

Figure 5.4 Noise map and receiver locations – Renghe Road area

This section compares the simulation results and the in-situ measurement results. By systematically comparing the major disparities, a further attempt is made to explore how certain typical urban morphological characteristics in the selected area affect the noise calculation accuracy.

A series of receiver points are measured across the selected area. The calculation and measurement results at the receiver points as shown in the map are demonstrated and systematically compared. The locations of the receiver points are selected based on the relative distance to the major noise sources, as well as the relative distance to the building façade.

Based on the location of the receiver points as shown in Figure 5.4, the receiver points are divided into two groups that are close to the Renghe Road and close to the Youyi Avenue respectively. By comparing the disparities between the measured and calculated results, a series of parameters and factors are considered in the calculation and specifically analysed below.

5.2.2.1 Distance from the nearest road source

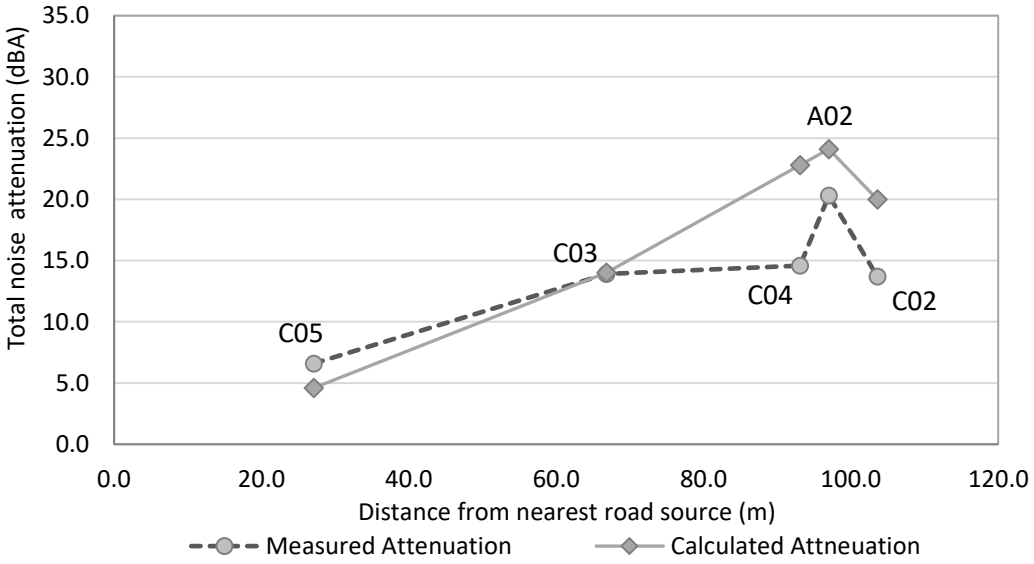

Figure 5.5 Measured and calculated traffic noise attenuation from the Youyi Avenue – Renghe Road area, the attenuation is generally more overestimated for receivers over 80 m away from the road source.

Firstly, the changes of noise attenuation with distance increasing from the road source are tested by. In this case, two groups of receiver points are selected based on the dominant

road noise source, i.e. the two main roads in the tested area. The noise attenuation at each receiver points are calculated and compared.

In Figure 5.5 it can be seen that both the measured and calculated attenuation from the Youyi Avenue in the north increases along with distance, the attenuation of the calculated generally coincide with the measured at a closer distance within 70 m at point C05 and C03. For points locate more than 90 m from the road source, the calculated attenuation is much higher than the measured ones. The attenuation at receiver point C04 and C02 are overestimated by 6.3 dBA and 8.2 dBA respectively, the large inaccuracy may mainly attribute to the screening effect of the single large building block as can be seen Figure 4.9.

Figure 5.6 shows the comparison between measured and calculated attenuation at the receiver points locating close to the Renghe Road in the urban village area. It can be seen that both the calculated and measured noise attenuation increase dramatically when the receiver points situate amid the low-rise residential buildings without direct transmission from the main road source. It is also notable that the gap between the calculated and measured results increases when the distance from road source increases.

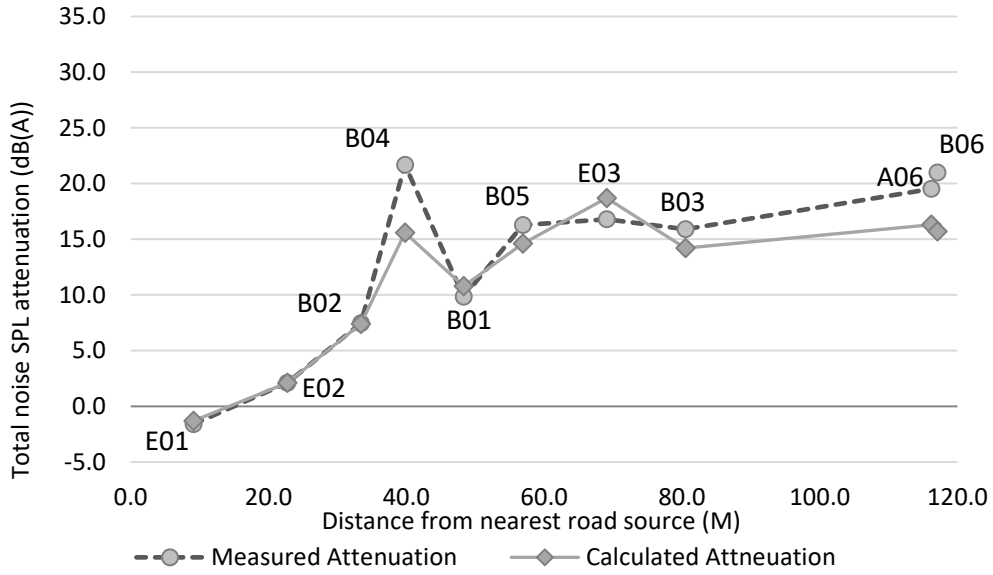

Figure 5.6 Measured and calculated traffic noise attenuation from the Renghe Road, the attenuation at farther locations tend to be underestimated.

The complicated façade conditions may bring accumulated errors in the calculation of multiple façade reflections. According to the simplified top-side and lateral calculation

method adopted in this study (DataKustik, 2012a), the high-density and random building scatter may also cause more inaccuracy in the calculation of roof diffraction and lateral diffraction. It is also notable that the general gap between the measured and calculated attenuation are not as big as those points close to the Youyi Avenue as shown in Figure 5.5, it may due to the relatively open space in the urban village area as can be seen in Figure 5.7.

5.2.2.2 Effect of the increasing maximum reflection order

- ***Receiver points in the urban village area***

Normally by increasing the reflection order, the general calculation accuracy can be improved accordingly. Nonetheless, it is found that simply by increasing the reflection order, in this high-density and low-rise urban village the calculation accuracy is not significantly improved.

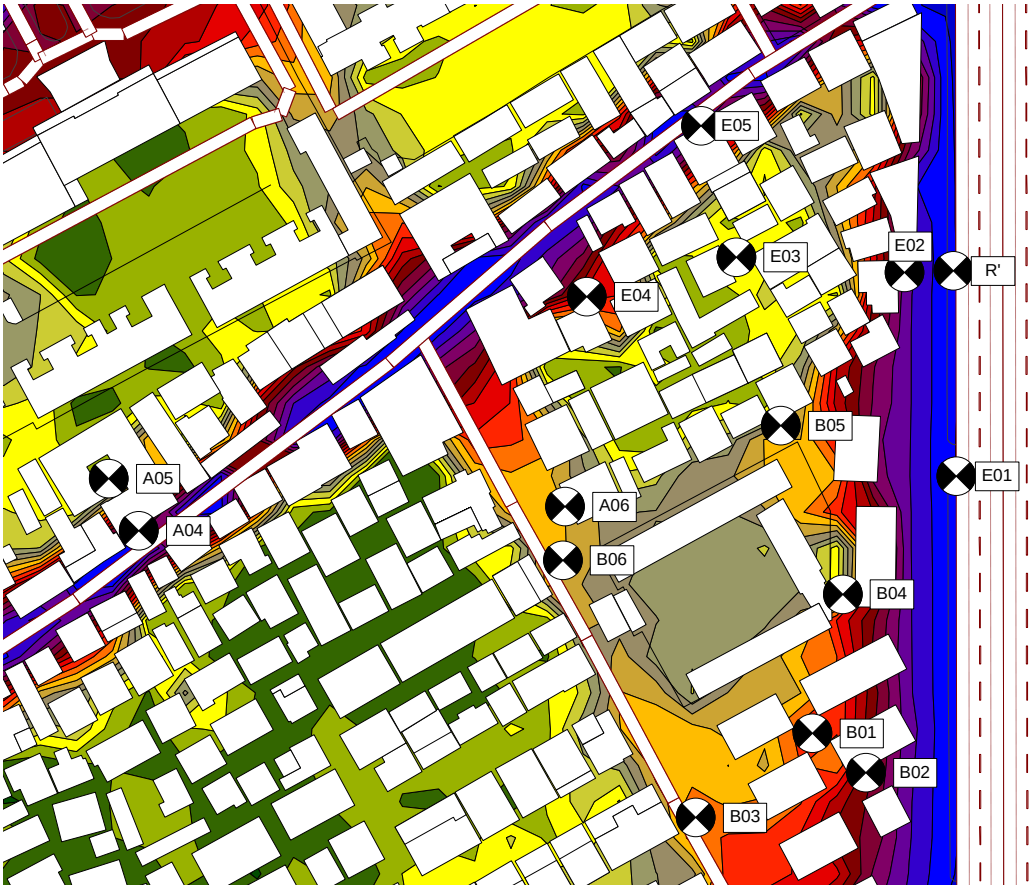

Figure 5.7 Receiver points locating among the urban village area near the Renghe Road

To further determine the cause of the calculation errors occurred at the receiver points amongst the low-rise residential buildings in the urban village as can be seen in Figure 5.7, a series of calculation is conducted on receiver points locating in the low-rise urban village area as can be seen in Figure 5.8, using a series of increasing reflection orders from 0 to 4. The calculation results are shown in Table 5.1 below.

Table 5.1 Error statistics with different maxium reflection order settings – receiver points in the multi-storey residential area near the Renghe Road

	Rf =0	Rf=1	Rf=2	Rf=3	Rf=4
Mean (dBA)	-5.6	-2.2	-1.0	-0.3	0.0
SD (dBA)	8.4	7.7	7.4	7.3	7.3
MAE (dBA)	8.7	6.9	6.7	6.7	6.6

It can be seen in Table 5.1 that with the increase of maximum reflection orders, the noise level at the receiver points in the urban village area generally increases with the increasing of reflection order. Meanwhile, the MAE (Mean Absolute Error) decreases from 8.7 dBA to 6.7 dBA when maximum reflection order increases from 0 to 2 and remains around 6.7 dBA and has limited improvement when it is higher than 2. The SD of the errors also has a similar trend of change, which remains 7.3 dBA when reflection order is set higher than 3.

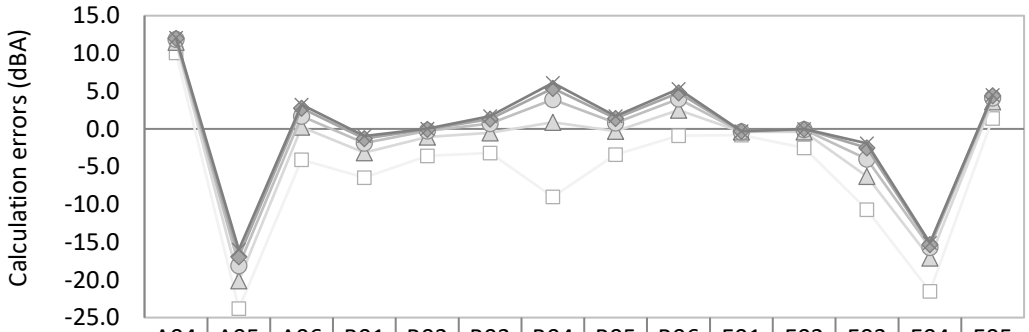

	A04	A05	A06	B01	B02	B03	B04	B05	B06	E01	E02	E03	E04	E05
Rf=0	10.1	-23.8	-4.1	-6.5	-3.6	-3.2	-9.0	-3.4	-0.9	-0.8	-2.5	-10.7	-21.5	1.4
Rf=1	11.5	-20.1	0.2	-3.2	-1.1	-0.5	0.9	-0.3	2.5	-0.4	-0.4	-6.3	-17.1	3.6
Rf=2	11.9	-18.1	1.7	-1.9	-0.3	0.7	3.9	0.8	4.0	-0.4	-0.1	-4.0	-15.7	4.1
Rf=3	12.0	-16.9	2.7	-1.3	0.0	1.3	5.4	1.4	4.8	-0.3	0.0	-2.5	-15.3	4.4
Rf=4	12.1	-16.0	3.2	-1.0	0.0	1.7	6.1	1.7	5.3	-0.3	0.0	-1.9	-15.1	4.5

Figure 5.8 Calculation errors of the receiver points in the urban village area with different reflection order settings – Renghe Road area, the error reduction effect of increasing the reflection orders seems to be not obvious.

Although it is found in the previous chapter that generally increasing the calculation reflection order is in favour of improving the calculation accuracy, the result above indicates that the complicated building arrangement in the urban village area may significantly reduce the effect. When the noise reflection order is set to higher than 2, the effect of accuracy improvement is merely negligible.

It is notable that, large and calculation errors are found in some receiver points at A04, A05 and E04, despite the increase of reflection orders. It may mainly due to the relatively enclosed surrounding space at these points especially at point A05 and E04. As can be seen in Figure 5.9, that both of which are closely surrounded by low-rise residential buildings of 2-3 storeys. The small pedestrian alley going through the surveyed area may also bring uncertainty and extra influence to these receiver points.

- ***Receiver points in the area with multi-storey building blocks***

As can be seen in Figure 5.10 and Table 5.2, in the multi-storey residential area with lower building ground space coverage, there are similar but more evident improvements of calculation accuracy found in most of the receiver points when reflection order increases.

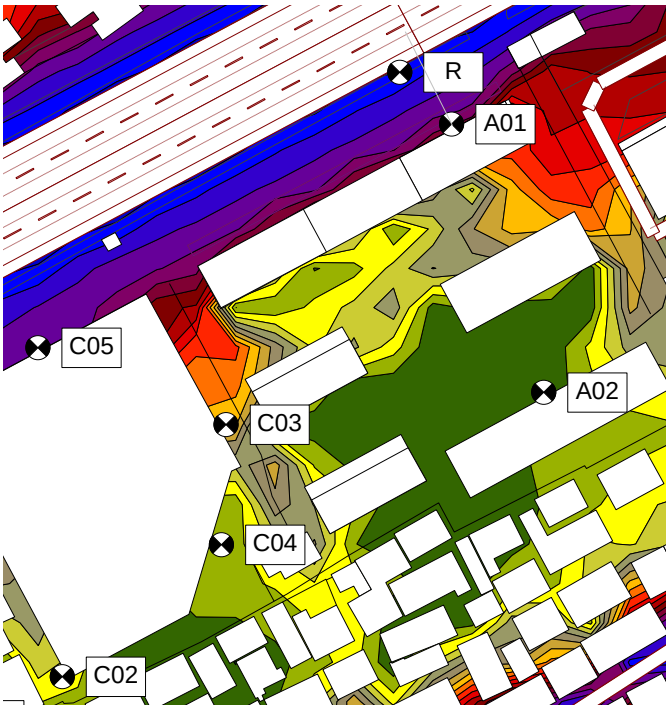

Figure 5.9 Receiver points locating amid the multi-storey residential buildings – Renghe Road area

Regarding the morphologically features, as shown in Figure 5.9 that these multi-storey residential buildings, as well as the 2-storey large scale building block close to the Youyi Avenue, are planned and constructed according to current Chinese planning system (Huang, 2006). Amid the buildings are large accessible space that are spared to ensure sufficient natural lighting, and there is also a distance of 15 m from the road kerb to the nearest building. Given the relatively open space for noise transmission, the increasing of reflection orders in the calculation allows more improvement comparing with that of the high-density and low-rise urban village area.

Table 5.2 Error statistics with different reflection order setting – receiver points in the multi-storey residential area near the Youyi Avenue

	Rf=0	Rf=1	Rf=2	Rf=3	Rf=4
Mean (dBA)	-7.5	-4.2	-2.6	-1.3	-0.5
SD (dBA)	8.9	7.6	6.5	5.7	5.1
MAE (dBA)	8.7	6.5	5.2	4.2	3.6

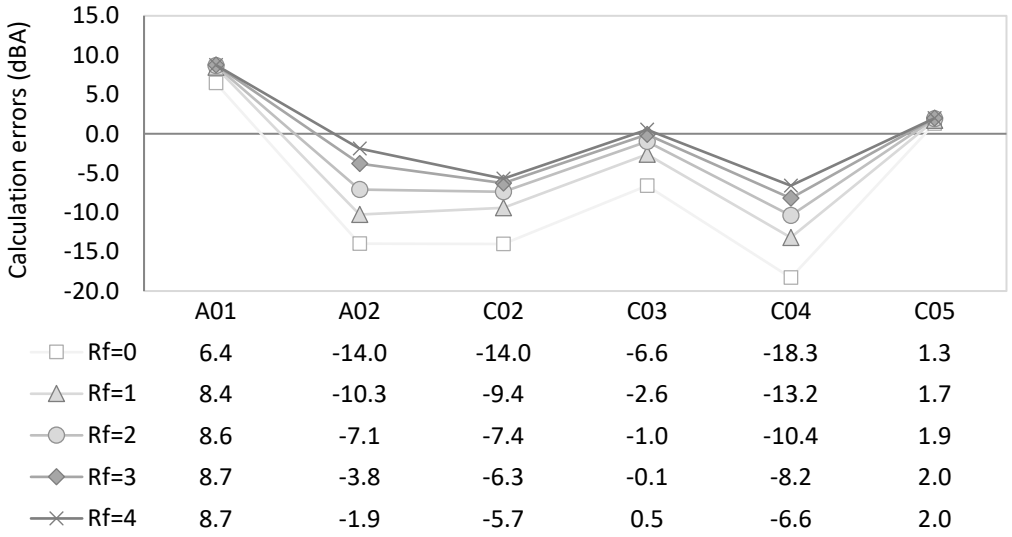

Figure 5.10 Calculation errors of the receiver points in the area with multi-storey building blocks with different reflection order settings – Renghe Road area, the effect of error reduciton is evident.

From Figure 5.10 it can be seen that the receiver points C03 and C05 have the least changes when the reflection orders are changed. As the direct noise transmission from the Youyi Avenue can reach these three points and the extra order of reflection from façades has merely no impact on the results. At the same time, it could be seen that the improvement of calculation errors at A02 and C04 are relatively large, where these two points are blocked by other buildings and have no direct emission from the road source.

It may because that the distance in between the surrounding buildings is large enough to allow the increased reflection order to have a distinct impact on the calculation accuracy.

- ***Comparison and analysis***

It is notable that the noise reflection order increasing can greatly enhance the calculation accuracy, while in the case of the urban village the overly compact low-rise residential buildings only allow very limited façade reflection to transmit through the accessible space. Thus, the typical EU calculation method may need to be improved to adapt to the calculation of façade noise reflection in the typical high-density and low-rise Chinese urban from, e.g. the urban village.

5.2.3 Calculation error at different frequencies

5.2.3.1 Roadside receiver points

For the receiver points close to the noise source with direct exposure, i.e. point E01, E02 and E05, the accuracy level is generally acceptable. As can be seen in Table 5.3 and Figure 5.11 that, the result at point E05 is most desirable as it locates just within the small alley containing the small pedestrian dominated road, what being input to the line source simulating the road does not get big disturbance in the direct transmission and reflection in such small scale.

Table 5.3 SPL spectrum calculation errors at major octave bands central frequencies – Renghe Road area, errors with absolute value equal to or smaller than 3 dBA are highlighted.

	Calculation errors (dBA)								
	31.5 Hz	63 Hz	125 Hz	250 Hz	500 Hz	1 kHz	2 kHz	4 kHz	8 kHz
E01	3.4	2.8	0.8	0.9	-3.5	-3.4	-4.1	-2.6	-3.4
E02	-2.1	1.2	0.8	-1.6	-3.6	-4.9	-3.2	-0.3	0.0
E03	-0.9	-0.2	-5.7	-8.4	-11.5	-8.3	-6.4	-6.1	-9.5
E04	-2.8	-1.8	-17.6	-19.3	-26.1	-17.6	-18.4	-10.6	-11.5
E05	2.1	1.2	0.4	0.1	0.0	0.0	0.0	0.0	-0.8

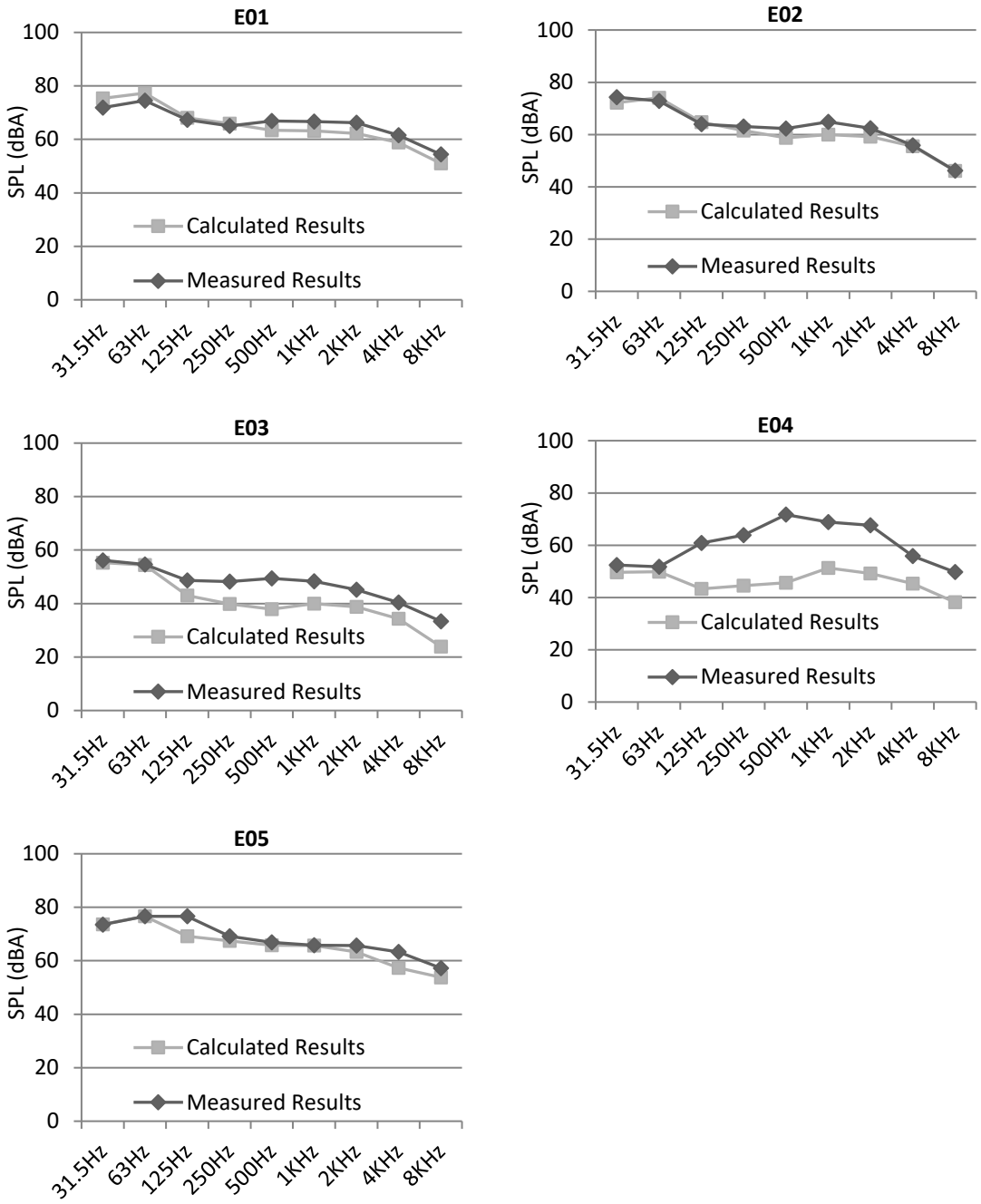

Figure 5.11 Measured and calculated noise level spectrum of the Renghe Road area

Comparing with that of the point E05, point E01 locates close to the Renghe Road with larger width and more complicated building façade conditions close to the road; it allows intricate façade reflections that may have caused the larger errors, only at 125 Hz and 250 Hz the errors are relatively small. The result at receiver point E02 is also generally accurate except at the frequencies from 500 Hz to 2000 Hz where the calculation results are over 3.0 dBA lower than that of the measured results, while at the lowest and the

highest frequencies, the calculated results generally coincide with that of the measured ones.

For point E01 and E02 next to the Renghe Road at different locations, the errors from 500 Hz to 2000 Hz are both slightly larger than other points. It indicates that there may be some mutual environment factors affecting the noise propagation on these frequencies at both points. The potential factors may include the façade condition of the roadside buildings, the ground absorption coefficient or even the parking cars and trucks which are impossible to simulate accurately in the software.

5.2.3.2 Receiver points locating amid the residential dwellings

Figure 5.12 Perspective view of the point E02, E03, and E04 in the Renghe Road area

At receiver point E03, it can be seen in Figure 5.11 that the calculated noise level at central frequencies of over 125 Hz are all deviated evidently from those of the measured noise level, while at the same time the level at the most energy concentrated frequencies of 31.5 Hz and 63 Hz are both coincide with the measured perfectly. As can be seen in Figure 5.12 that Point E03 locates in a quiet alley amid the densest part of the urban village, there is no direct transmission path from the Renghe Road towards the point E03.

Although as demonstrated earlier in Figure 5.8 that by increasing the reflection order the general calculation accuracy at point E03 can be improved evidently, the noise of higher frequency from Renghe Road is still underestimated as can be seen in Figure 5.11. Which may due to the more complicated transmission of sound rays across multiple low-rise buildings including the paths of diffraction and reflection, at higher frequencies, the sound energy is more easily aborted in the prolonged propagation paths comparing with that of the noise with lower frequencies.

5.2.3.3 Receiver points affected by event noise from pedestrian and local community

Similar but stronger error occurs in the SPL spectrum distribution at point E04, especially in frequencies of higher than 63 Hz. In the relatively lower frequency range, say, at 31.5 Hz and 63 Hz the calculated noise level is coherent with that of the measured ones, while at middle and high frequencies the calculated noise level at each central band frequencies are much lower than the measured ones.

The location of point E04 can be found in Figure 5.12. For point E04 there are two major noise sources, the Renghe Road and the small pedestrian road. The latter is closer to the point E04. For lower frequencies, the coherence of calculation and measurement levels may due to the same reason as the point E03, that, the noise at lower frequencies with higher sound energy tend to transmit further despite the screening effects of the buildings and walls. For the noise level at middle and higher frequencies, the incoherence of calculated and measured noise level at locations close to the vibrant community noise sources, say, point E04 may be caused by relatively more vibrant community noise from the small pedestrian dominated road locating 20 m from the point E04, which is measured and input into the line source for the calculation; as well as other potentially higher frequency community noise from the surrounding residential buildings.

5.2.4 Further analysis on typical urban morphology feature

From the results above, it can be seen that as predicted that the receiver points close to the main noise sources which are mainly affected by the direct noise and the first order of reflection has generally higher accuracy level in most of the major frequencies. Nonetheless, for receiver points locating amid the high-density and low-rise buildings in

the urban village area as points E03, there is a potentially larger chance of inaccuracy, especially in the frequency range of higher than 125 Hz. Nevertheless, as can be seen in Figure 5.11 and Table 5.3, at Point E03 in the energy-concentrated lower frequencies at 31.5 Hz and 63 Hz, the calculation errors are acceptable. For frequencies higher than 63 Hz the tendency of noise level changes is close to that of the measured results, although the errors are much higher than that of the lower frequencies.

For point E04, due to the potentially remarkable influence from the community noise, it has relatively much larger errors in higher frequencies compare with that of point E03, and the tendency of noise level changing of the calculated and the measured noise level are distinct. It indicates that at frequencies higher than 63 Hz at point E04, the transmission of the traffic noise from the main road is mostly screened and more affected by miscellaneous noise sources except the traffic noise. Nevertheless, considering the accuracy in the lower frequencies of point E03 and E04 are both relatively desirable, it is reasonable to infer that by optimising the calculation configuration and considering more about the miscellaneous community noise sources and other factors, the calculation accuracy in higher frequencies could potentially be improved.

5.2.4.1 Calculation of diffraction

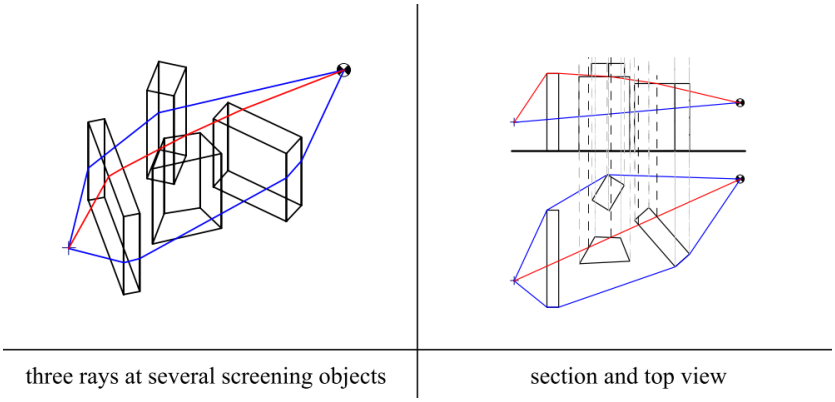

Figure 5.13 The lateral calculation method adopted in Cadna/A (DataKustik, 2012a)

The calculation of lateral diffraction may be insufficient in the urban village case in general. According to the default calculation method adopted, when there are multiple buildings screening in between the source and receiver, only one roof-top and two lateral diffraction sound paths would be calculated, as being demonstrated in Figure 5.13 that the diffraction are calculated through three convex paths around the top and each side of

all screening obstacles. Then the sound contributions of all diffractions are added energetically to get the total diffraction as demonstrated in Equation 5.1:

$$E_{dif} = E_{top} + E_{sideA} + E_{sideB} \quad 5.1$$

This calculation method as an approximation is effective with respect to reducing the time consumption of calculation, while considering the relatively low building height as well as the existence of multiple gaps among the buildings in between the receiver and the source line, there is potentially a number of sound propagation paths neglected in the calculation, thus it may cause the underestimation of total noise level received at the receiver point in the shielded zone.

5.2.4.2 Acoustical transparency of the buildings

Another potential cause of the evident disparities between the measured and calculated noise of higher frequency at point E03 and E04 may lie in the method of screening calculation of the high-density buildings. In this typical urban village case, similar to the simulation of industrial acoustical environment, the actual noise emission through the building blocks may actually be higher than that of when the buildings are regarded as 100% non-transparent, as the low-rise residential buildings are mostly made of think bricks and with large windows opening on the walls.

By default, in the calculation of the screening effect, most of the calculation methods treat the building as a solid and fully screening object, the noise in the shielded zone behind the buildings are mainly calculated via fraction and reflections. In some packages alternative ways are introduced to calculate the screened noise transmission through the receiver points lying behind the partially transparent buildings or industrial structures. For instance, in Cadna/A (DataKustik, 2012a), a factor of acoustical transparency is designated to each building and is used to calculate the total transmission factor τ, i.e. the collective transparency factor of all shielding buildings. As shown in Equation 5.2 that if only consider the effect of the building to the direct noise transmission from the source to the receiver in an ideal free field, the received sound energy E_{rcv} at receivers in the shielded zone behind the buildings is calculated by adding two contributions together. The first is the diffracted noise level via the top and side of the buildings; the second

contribution is calculated based on the direct noise which is calculated by assuming the building is removed or 100% transparent, and a total transmission factor τ by combining transmission factors of all screening buildings.

$$E_{rcv} = E_{dif} + E_{dir} \times \tau \tag{5.2}$$

where the τ indicates the total transmission factor which is the collective transparency factor of all shielding buildings. This equation is based on the assumption that the building and the source are in a free field without reflection from other buildings and the ground is totally absorptive.

A simplified test is carried out to find that if the low-rise and small size residential buildings in the urban village are partially transparent and the noise emission could go through the walls, will there consequently be any improvement in the calculation accuracy at point E03 and E04. The acoustical transparency of the low-rise buildings surrounding the point E03 and E04 as well the buildings in between the two receiver points and the nearest noise source are set to 50%. The disparities between the calculated and the measured noise level spectrum of both points are demonstrated and discussed below.

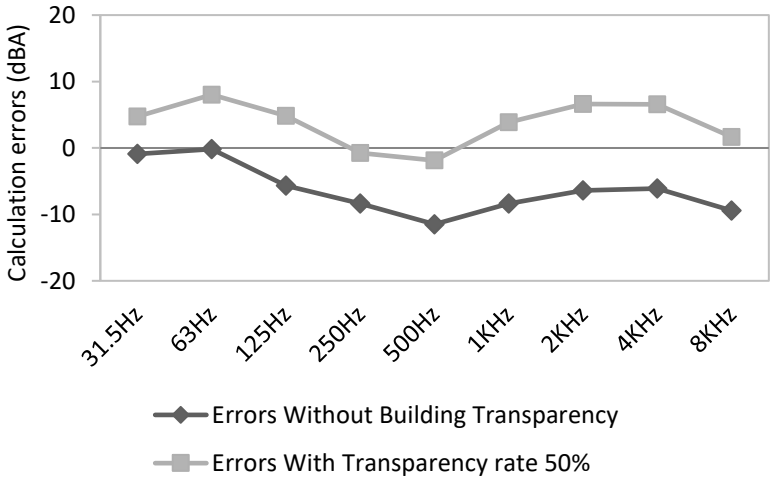

Figure 5.14 Test of the building acoustical transparency – point E03 in the Renghe Road area, increasing the the transparency ratio of buildings decreases calculation errors in some hihger frequencies.

Table 5.4 Error statistics of acoustical transparency test at all major frequencies – point E03 in the Renghe Road area

	Mean	SD	MAE
Errors without building transparency	-6.3	3.5	6.3
Errors with transparency ratio 50%	3.7	3.2	4.3

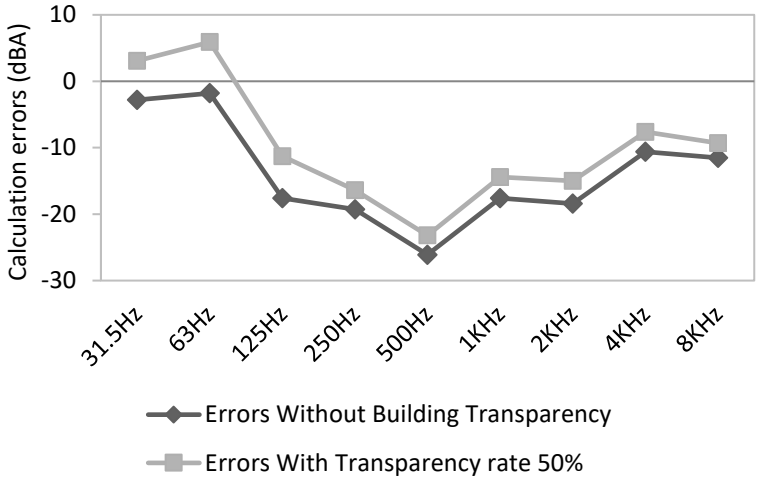

Figure 5.15 Test of the building acoustical transparency – point E04 in the Renghe Road area, the error reduction effect of increasing the transparency ratio is not evident.

Table 5.5 Error statistics of acoustical transparency test at all major frequencies – point E04 Renghe Road area

E04	Mean	SD	MAE
Errors without building transparency	-14.0	7.5	14.0
Errors with transparency ratio 50%	-9.8	8.8	11.8

The results suggest that at the point E03, the calculation accuracy is improved evidently when the acoustical transparency is introduced. As can be seen in Figure 5.14 and Table 5.4 that when all the surrounding buildings and the buildings in between point E03 and the main road source line are using the default acoustical transparency factor of 100% without considering the buildings as partially transparent, the calculated results at eight octave band central frequencies are generally much lower than those of the measured with a standard deviation (SD) is 3.5 dBA and the mean error of -6.3 dBA, the mean absolute error of which is 6.3 dBA.

Nevertheless, when the acoustical transparency is introduced with a median level of 50%, the SD of the calculation errors of all eight frequencies reduces to 3.2 dBA and the mean

error becomes less too, to 3.7 dBA, with a mean absolute error of 4.3 dB, which are still under a satisfactory level but the improvement of calculation accuracy is apparent.

At point E04, because of the influence from the small pedestrian dominated road, the general accuracy improvement with setting a 50% acoustical transparency is as distinct as at point E03. As shown in Figure 5.15 and Table 5.5 that generally the calculated noise level at most of the central frequencies of eight main octave bands is still much lower than those of the measured results. The mean absolute error shrinks from 14.0 dBA to 11.8 dBA, while the SD increases from 7.5 dBA to 8.8 dBA, the mean error is -14.0 dBA and -9.8 dBA before and after the introduction of acoustical transparency respectively.

Above results indicate that the importance of considering the factor of acoustical transparency rate when the building condition is partially transparent and crowded closely. As can be seen in this test, in this typical high density and low-rise urban village next to the main road, potentially the default calculation configuration without taking the transmission factor i.e. the acoustical transparency of residential dwelling into account, can be a significant source of inaccuracy when calculating the noise level of receiver points locating relative far from the road source, as can be seen in E03 and E04. Although the acoustical transparency is helpful to enhance the calculation accuracy, it is also necessary to introduce relevant guidelines for certain building types and conditions.

5.3 High-rise street canyon of heavy-traffic main road

5.3.1 General description

5.3.1.1 Topography and urban morphology – high-rise street canyon with multi-storey residential areas behind

Figure 5.16 Satelite map of the Youyi Avenue area. Source: Google Maps (Google Inc.)

This site is chosen as the study area for its typical urban street canyon features. The selected site covers a cross section of the Youyi Avenue, the main road in the south part of Wuhan. The Youyi Avenue connects two sub-districts of Wuhan city, the Wuchang District and the Qingshan District, where the former is traditional residential and commercial zone, in the latter locates one of the biggest steel industrial companies in China—the Wuhan Steel Group.

As can be seen in Figure 5.16, the long-belt-shape high-rise buildings alongside the Youyi Avenue from typical high-rise street canyons. Behind the flanking high-rise buildings alongside the Youyi Avenue, there are large areas of multi-storey residential buildings that are mainly built in the late 20th century to solve the increasing accommodation requirement of the steel industrial workers. This type of socialism collective accommodation is widely spread in urban areas in Chinese major cities (Huang, 2006).

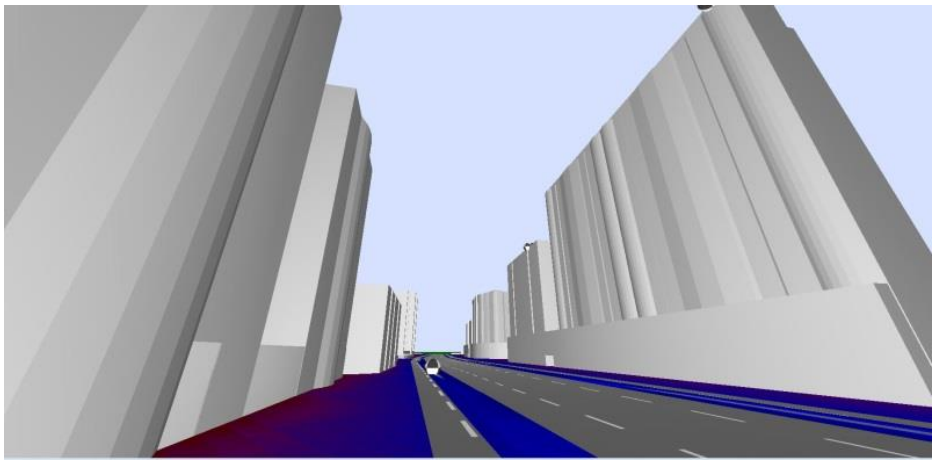

Figure 5.17 The 3D Model of the street canyon in the Youyi Avenue area

The high-rise buildings close the Youyi Avenue are combinations of 2-4 storeys podiums for commercial and office use and high-rise apartments for residential use standing above on the podium. The podiums are mostly connected together as long belt-shaped with fire extinguishing routes openings or entrance in the ground floor approximately every 90 M; while there are gaps in-between the residential towers. The flanking façades of the high-rise buildings, as well as the podium buildings, are mostly parallel to the main road, forming a partially continuous street canyon with an average height of 50–75 m high and an average width of 60–70 m as can be seen in Figure 5.17.

5.3.1.2 Building features: high-rise and multi-storey apartments

The high-rise buildings in the selected area parallel to the Youyi Avenue are typical commercial and residential mixed complex. The podiums for commercial use are 2-storey and 4-storey high in the north and south part respectively; the apartments above the podium are 16-storey and 21-storey high, respectively. The façade of the commercial podiums are mostly smooth glass or smooth coating material; the surface of the residential towers is also smoother but with enclosed balconies on all storeys. This kind of building complex with high-rise residential apartments and 2-4 storeys commercial podium are very common in most of the newly developed areas in Chinese cities, due to the convenient access to the vehicles and pedestrians on the main roads, which is very different from the European main road street canyons as can be observed in the urban area of Greater Manchester, UK.

a

b

Figure 5.18 Architecture and urban form features – Youyi Avenue area. (a) Traditional multi-storey flats for former steel industry workers (Taken by author); (b) High-rise street canyon of the Youyi Avenue; Source (Tencent Inc., 2011).

As mentioned before that the multi-storey apartments locate behind the high-rise buildings are constructed for pure residential purpose. From in-situ observation in Wuhan and Greater Manchester, the multi-storey residential buildings in the residential communities in Wuhan also have distinctive features compare with typical British residential buildings, as can be seen in Table 5.6.

Table 5.6 Typical residential building in Wuhan and Greater Manchester

Features	Wuhan	Greater Manchester
Type	Multi-storey flat	Terrace house
Heights	6–8 storeys	2–3 storeys
Balcony	With open or sealed balconies	No
Structure	Concrete and bricks	Bricks, stone, and wood
Façade	Concrete or sandstone façades	Bricks, stone or coating
Roof	Flat roof with extra additions and piles	Slope roof

The apartments outside the street canyon in the selected area are mainly 7-8 storeys with rough and complicated façade conditions. As can be seen in Figure 5.18, the façades of the multi-storey buildings are mainly comprised of rough concrete and are convex and concave with large numbers of windows and extrusive half-open balconies. Some of the balconies are sealed with windows made of PVC and glass. In the modelling process, the apartments are simplified based on the ground outline, and the overall absorption coefficient of the façades is set to 0.37 based on empirical absorption coefficient value of the surface type, 'structured façade' (DataKustik, 2012a), though the actual situation may vary depending on specific conditions of the buildings.

5.3.1.3 Road and traffic conditions

There is a large amount of traffic flow on the Youyi Avenue, for about 3640 veh/h, with 6% of heavy vehicles. The spatial features are shaped predominately by the flanking high-rise buildings close to the road, which are mixtures of commercial and residential use. The traffic flows of the smaller roads that also have impact on the selected area are also counted, the traffic flow of the Caimao Street going across Youyi Avenue in the east of the area is 102 veh/h with 1% of heavy vehicles, the small road in the south-west of the area has a smaller traffic of 41 veh/h with 2% of heavy vehicles.

5.3.1.4 Noise sources

The noise of the Youyi Avenue is measured using high definition sound level metre at the reference point R. The measured general A-weighted SPL at point R is 76.2 dBA, and the full-spectrum data is recorded. The source SPL is then calculated based on the distance from R to the effective road source line for inputting in the noise simulation.

The traffic amount of all roads affecting the measured area in the measured hour is sampled and counted as mentioned in the previous section, then input into the noise-mapping package Canda/A for simulation.

Within the measurement period near the measured receiver points there the main source of noise there is the traffic, no apparent impact from event noise, except close to the receiver points E06 and E07 that an exhaust fan hanging 2 m above the ground on the

wall of the podium building. The full-spectrum noise level is measured and the source level is then reverse calculated.

5.3.2 General measurement result and applicability examination

The noise map shown in Figure 5.19 is calculated using the default calculation setting and the maximum reflection order of 3. It can be seen that at the ground level, the noise distribution is generally unevenly distributed, most of the noise is concentrated in the main street canyon and alongside the smaller roads, there are noise leaking through the gaps in between the high-rise buildings from the main road canyon to the relatively quieter areas behind the flanking buildings.

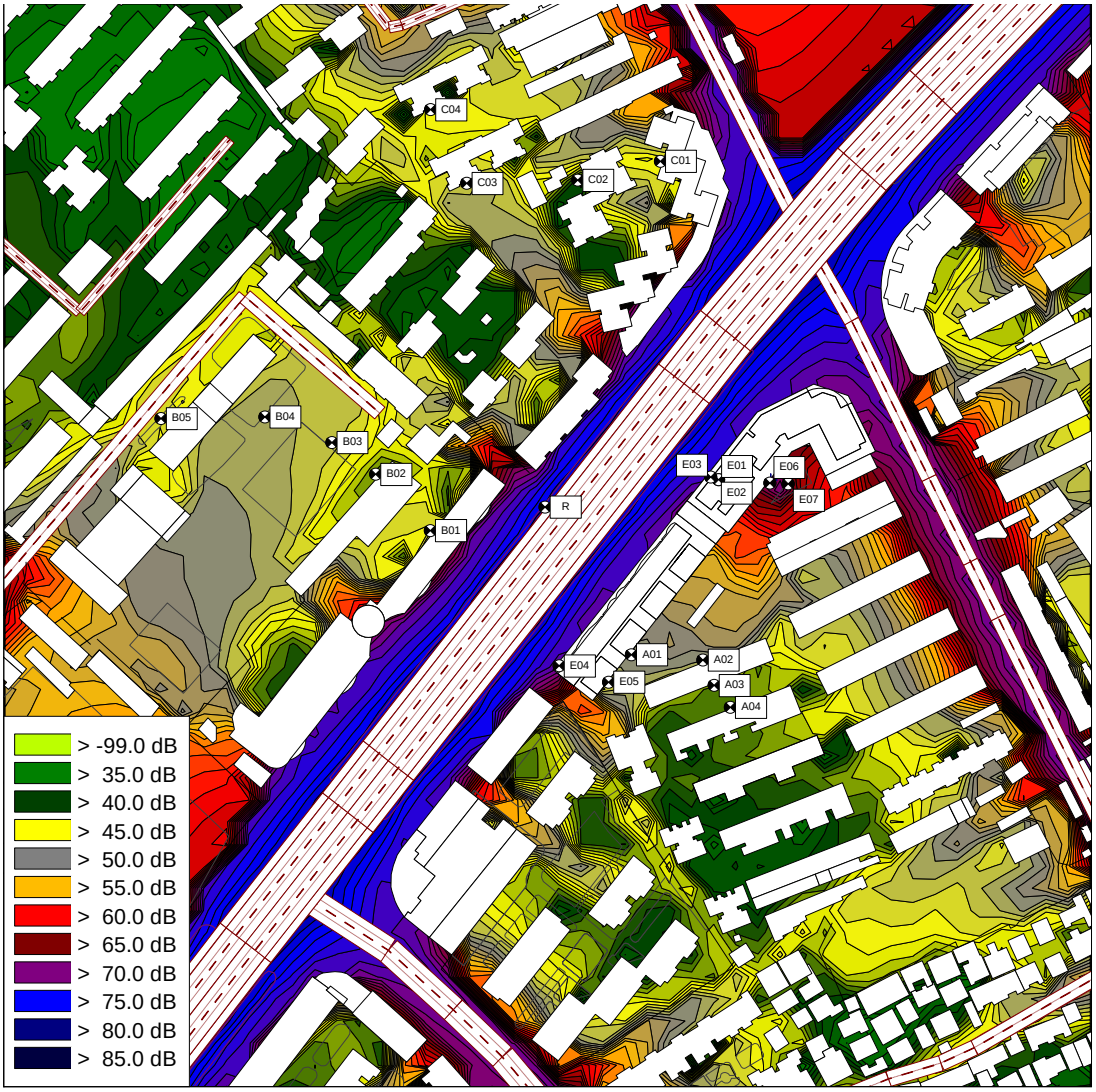

Figure 5.19 Noise map and receiver locations – Youyi Avenue area

The locations of the receiver points are shown in Figure 5.19. There are eight effective receiver points measured with high-definition sound level metres inside the street canyon and around the high-rise building at various altitudes, including one reference point R close to the main road, and two receiver points E06 and E07 in the shielded area right behind the high-rise building and close to a constant point noise source. The rest of the receiver points are spread in the residential area behind the street canyon and are divided into three groups and located by the horizontal distance from the rear of the road-side podiums to remote locations in the centre of the residential area. The locations of the receivers are mostly selected close to the façades to reflect the actual impact to the residents.

5.3.2.1 General results

In this section though observing a series of calculation results by using increasing reflection orders, it is found that in this case of the high-rise street canyon, the reflection order plays a significant key to ensuring the calculation accuracy, especially for receiver points locating relatively far from the road source and without direct exposure to the main road source.

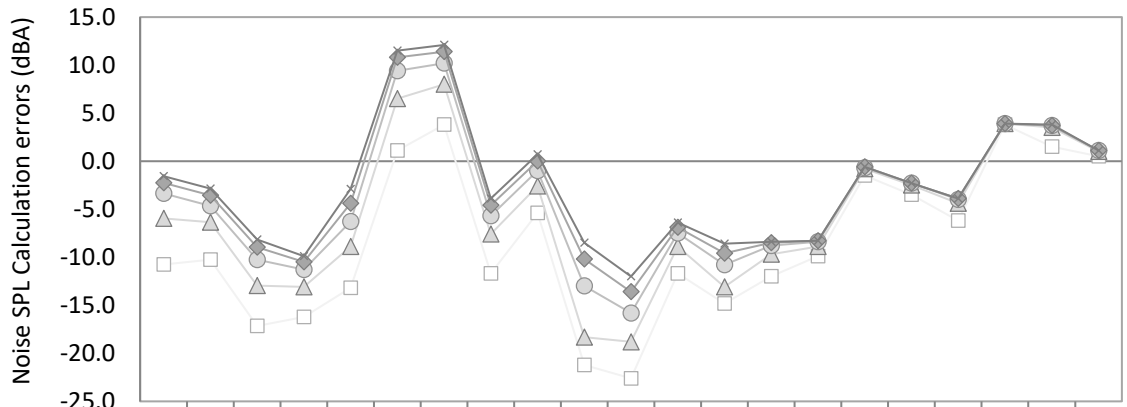

	A01	A02	A03	A04	B01	B02	B03	B04	B05	C01	C02	C03	C04	E01	E02	E03	E04	E05	E06	E07	R
Rf=0	-10.8	-10.2	-17.2	-16.2	-13.2	1.1	3.8	-11.7	-5.4	-21.2	-22.6	-11.7	-14.8	-12.0	-9.9	-1.5	-3.5	-6.2	3.8	1.5	0.5
Rf=1	-6.0	-6.3	-13.0	-13.1	-8.9	6.5	8.0	-7.6	-2.6	-18.3	-18.8	-8.9	-13.1	-9.7	-8.9	-0.8	-2.5	-4.4	3.9	3.5	1.0
Rf=2	-3.4	-4.6	-10.3	-11.3	-6.3	9.4	10.2	-5.7	-1.0	-13.0	-15.8	-7.5	-10.8	-8.8	-8.4	-0.7	-2.3	-4.0	3.9	3.7	1.1
RF=3	-2.3	-3.5	-9.0	-10.5	-4.4	10.8	11.4	-4.6	0.0	-10.2	-13.6	-6.9	-9.6	-8.5	-8.3	-0.6	-2.3	-3.9	3.9	3.7	1.1
Rf=4	-1.6	-2.8	-8.2	-9.9	-2.9	11.5	12.1	-3.9	0.7	-8.5	-12.0	-6.4	-8.6	-8.4	-8.3	-0.6	-2.3	-3.9	3.9	3.8	1.1

Figure 5.20 Calculation errors with increasing reflection order settings – Youyi Avenue area, increasing the maximum reflection orders generally reduces calculation error.

In Table 5.7 it can be seen that the increase of calculation order generally has positive effect on the calculation accuracy, the mean absolute error (MAE) decreases evidently for

3.5 dBA from 9.9 dBA to 6.4 dBA when the reflection order is raised from 0 to the 3, and the standard deviation (SD) decreases from 7.7 dBA to 6.6 dBA while the mean error changes from -8.9 dBA to -3.4 dBA.

Table 5.7 Error statistics of all receiver points with different reflection order – Youyi Avenue area

	Rf=0	Rf=1	Rf=2	Rf=3	Rf=4
Mean (dBA)	-8.9	-6.0	-4.3	-3.4	-2.8
SD (dBA)	7.7	7.4	6.9	6.6	6.5
MAE (dBA)	9.9	8.2	7.1	6.4	6.0

To furtherly test the error-reduction potential by increasing the reflection order, the maximum reflection order of 4 is also tested, it is shown that in this relatively complicated urban environment, by furtherly increasing the maximum reflection order from 3 to 4, the MAE has an extra reduction of 0.4 dBA from 6.4 dBA to 6.0 dBA, and the SD reduces for 0.1 dBA from 6.6 dBA to 6.5 dBA.

It can be seen that in the typical case of high-rise street canyon selected in China, the rise of reflection order clearly has improved the calculation accuracy by large, although the scale of changes inside the street canyon and outside the street canyon in the shielded area seems different.

5.3.2.2 Effect of increasing reflection order

- ***Receivers point in the street canyon***

Table 5.8 Error statistics of all receiver points inside the street canyon with different reflection order – Youyi Avenue area

	Rf=0	Rf=1	Rf=2	Rf=3	Rf=4
Mean (dBA)	-5.3	-4.2	-3.8	-3.7	-3.7
SD (dBA)	4.8	4.3	4.1	4.0	3.9
MAE (dBA)	5.5	4.6	4.3	4.2	4.1

It is further noticed that, for most of the receive points locating inside the street canyon, the changes of increasing the reflection order is evident but limited when the reflection order keeps rising from 1.

It can be seen in Figure 5.20 that, for the receiver points E01, E02, E03 and E04 locating in various locations close to the flanking façade, the calculation error has clear

improvement when the façade reflection is taken into account. As can be seen in Table 5.8 that, by setting the reflection order from 0 to 1, the MAE decreases for 0.9 dBA, the mean error changes from -5.3 dBA to -4.2 dBA, the SD also decreases for 0.5 dBA. This indicates that the contribution of the first order reflection from the opposite façades contributes to most of the accuracy improvement.

Nonetheless, there are only nearly negligible improvements when the max reflection order keeps increasing from 1. The MAE only drops 0.5 dBA when reflection order rises from 1 to 4, the mean error changes from -4.2 dBA to -3.7 dBA, with just 0.4 dBA drop in the SD. Actually, in the calculation method adopted the maximum correction for opposite façade reflection is set to 1.5 dBA for efficiency concern. It can be deduced that inside the street canyon by keep increasing the reflection order the accuracy improvement is small and finite; meanwhile, the calculation time may become unreasonably long.

- ***Shielded receiver points***

Table 5.9 Error statistics of all the shielded receiver points with different reflection order – Youyi Avenue area

	Rf=0	Rf=1	Rf=2	Rf=3	Rf=4
Mean (dBA)	-9.4	-6.2	-4.2	-3.0	-2.3
SD (dBA)	8.2	8.1	7.5	7.2	6.9
MAE (dBA)	10.7	8.9	7.6	6.8	6.3

In the meantime, for the rest receiver points at various locations shielded by the high-rise main buildings and have no direct exposure to the main road noise source, raising the reflection order tends to have a more evident effect on the improvement of calculation accuracy when the reflection order keeps rising. As can be seen in Table 5.9 that the MAE decreases for 1.8 dBA when the first order of reflection is turned on, the mean error changes from -9.4 dBA to -6.2 dBA, while the SD declines for 0.1 dBA. When the reflection order keeps rising from 1 to 4, the MAE keeps dropping for 2.6 dBA from 8.9 dBA to 6.3 dBA, the mean error changes from -6.2 dBA to -2.3 dBA, and the SD drops 1.2 dBA from 8.1 dBA to 6.9 dBA indicating evidently less fluctuation in the calculation errors. It can be seen that in the area shielded by the high-rise building the improvement of calculation errors by increasing the reflection order is remarkable. As can be seen in the noise map in Figure 5.19 that the high-rise flanking buildings shield most of the noise from the main road, the large scale of the flanking buildings also limits the influence of

the topside and lateral diffraction. The indirect façade reflection from various gaps between the high-rise buildings is the major source of noise receiver in the shielded area. The intricate reflection paths require higher reflection orders and more accurate settings of the façade absorption coefficient to ensure better accuracy level.

It is necessary to note that for the receiver points E06 and E07, both locate in the shadowed area that is completely shielded by high-rise building, the main noise source of these two points are the exhaust fan hanging on the wall of the podium building, thus the increasing of reflection order did not affect the accuracy of receiver points E06 and E07 as much as that of other points shielded by the high-rise building. This also indicates that the area shielded by the high-rise buildings where the direct noise transmission and lateral diffractions have relatively smaller impact, various sorts of event noise may need to be take into account in the calculation to eliminate the calculation errors.

5.3.2.3 Effect of the flanking high-rise building in the street canyon

- ***Reflection in the street canyon***

The calculation errors occurred at different altitude in the street canyon are tested. The receiver points are selected on different floors close to the façade facing the main road, for the sake of testing the calculation accuracy at the building façade of the high-rise building. Due to the limitation of the site accessibility, three façade points at the altitude of 14.4 m, 31.4 m, and 55.4 m are selected, respectively, while the lower two of which locate in a peculiar building slot space as shown in Figure 5.21 and Figure 5.22. It is found that for the receiver points locating in the street canyon at different heights, the accuracy level is generally acceptable except at the receiver point E01 and E02. A schematic diagram as shown in Figure 5.21 demonstrates the relative locations and the main paths of the propagation received by the receiver points in the street canyon.

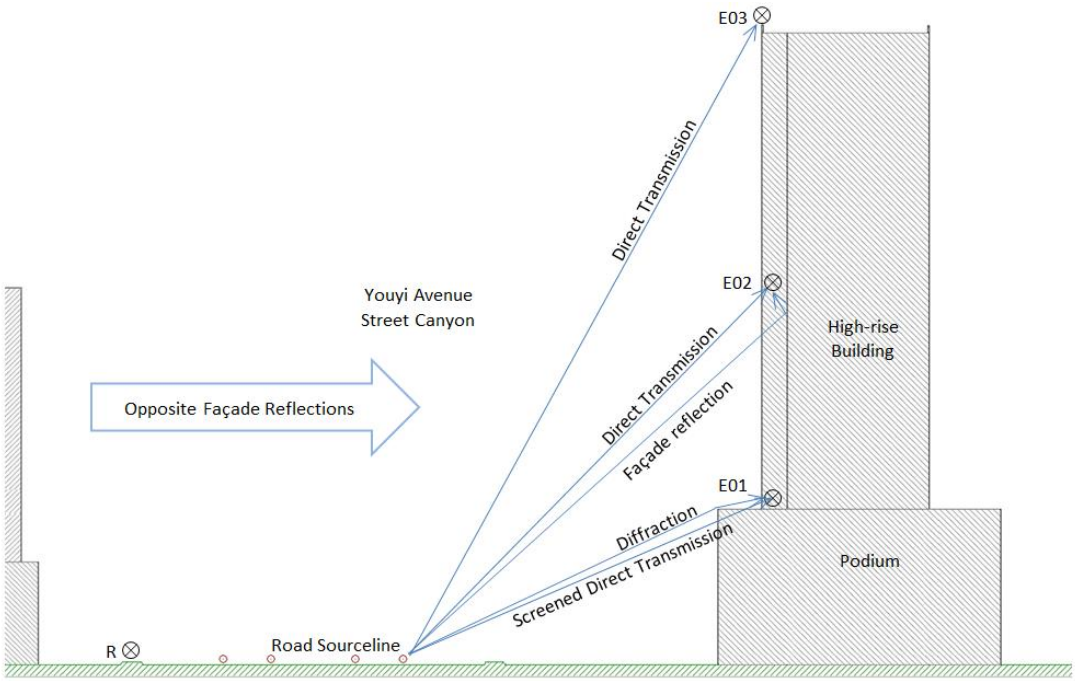

Figure 5.21 Schematic diagrams of the major corrections calculated at façade receiver points in the street canyon – Youyi Avenue area

Receiver point E01 and E02 locate in the 1.5-metre-wide and 3.5-metre-deep slot on the façade of the high-rise buildings facing the Youyi Avenue as can be seen in Figure 5.22. The slots serve as half-open ventilation wells with windows on the wall at the inner end of each floor, thus it is still of significance to evaluate the calculation accuracy in the slots. When the reflection order is set to 3, the calculation results are 8.5 dBA and 8.3 dBA lower than the measurement results at point E01 and E02 respectively, which shows relatively much higher disparities compare with other receiver points in the street canyon.

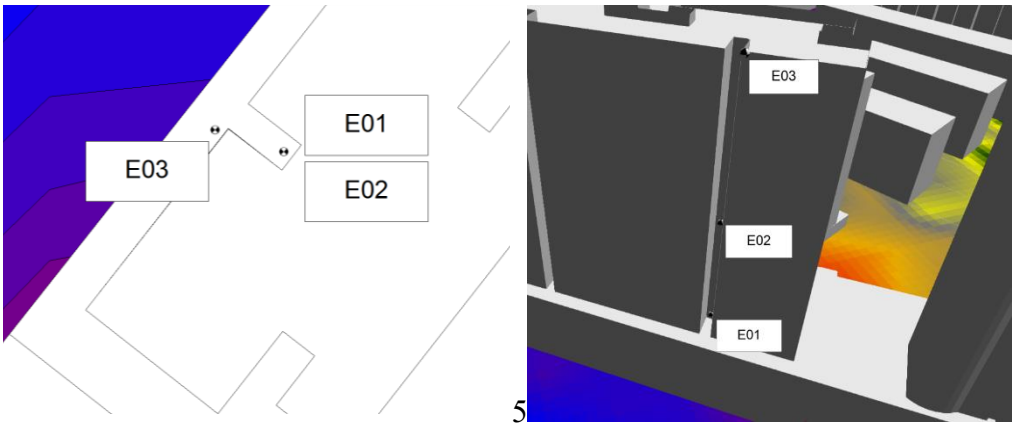

Figure 5.22 Locations of the receiver points E01, E02 and E03 in the street canyon – Youyi Avenue area

In the meantime, for point E03 that locating on top of the high-rise building above the outer edge of the façade as shown in Figure 5.22, with open exposure to the road and without reflection from the neighbouring façade, the calculation error is as small as -0.6 dBA. It is mainly due to the relatively more open location, which leads to the domination of the direct transmission, the accuracy of which can normally be ensured in traditional calculation methods.

At point E01 and E02, the peculiar building form of the slot requires relatively more complicated façade reflection orders comparing with that of the receiver points locating on relatively more exposing façade. At E01 the direct sound rays from the road segments are screened by the podium building, hence the diffracted noise from the edge of the podium is the main source of noise. At point E02 the direct transmission from the road can reach the point but the complicated façade reflections from all three sides of façades of the slot.

In the meantime, for both façade points shown in Figure 5.21 that the façades of the opposite buildings create multiple reflections and hence increase the received SPL. Nevertheless, as can be seen in Figure 5.20 that the increasing of reflection order only has a tiny effect on increasing the SPL at both points when the reflection order is higher than 2. It needs to be considered that at both point E01 and E02 the direct noise transmission from the road segments locating far from the road segment facing the slot are screened, thus the lateral diffraction from the outer edge of the slot as well as the multiple reflections in the slot space may have been underestimated in the calculation. It can be seen that a great amount of extra noise propagation is not taken into account in the calculation in this relatively more complicated urban form i.e. in the half-enclosed space where two façade receiver points locate.

- ***Noise propagation on top of the high-rise building***

In comparison with point E03, at the outer edge on the top floor of another high-rise building, as shown in Figure 5.23 and Figure 5.24, the point E04 has slightly larger calculation error of -2.3 dBA when the maximum reflection order is set to 3 and 4.

The bigger disparity at point E04 may mainly be caused due to the following two reasons. Firstly, due to the relatively more complicated building form, there are multiple façade

reflections occur at the façades close to point E04, which may not be calculated sufficiently in the calculation, while the façade reflection at E03 is relatively less complicated. Secondly, the street canyon where E04 locates is formed by two flanking buildings higher than where the point E03 locates, this may bring an extra amount of reflections from the opposite façades, and it may not have been sufficiently calculated in the calculation and contributed to the slightly larger error at point E04.

For receiver point E05 locating in the top-rear of the high-rise building, the error is -3.9 dBA when the reflection order is set to 3 and 4, which is 1.6 dBA greater than that of point E04. As can be seen in Figure 5.23 and Figure 5.24 that at point E05 the direct transmission is largely screened by the thick body of the high-rise main building, hence the main cause of inaccuracy may lie firstly in the lateral and top-side diffraction; secondly in the reflection from the shielded buildings at the rear of the high-rise building.

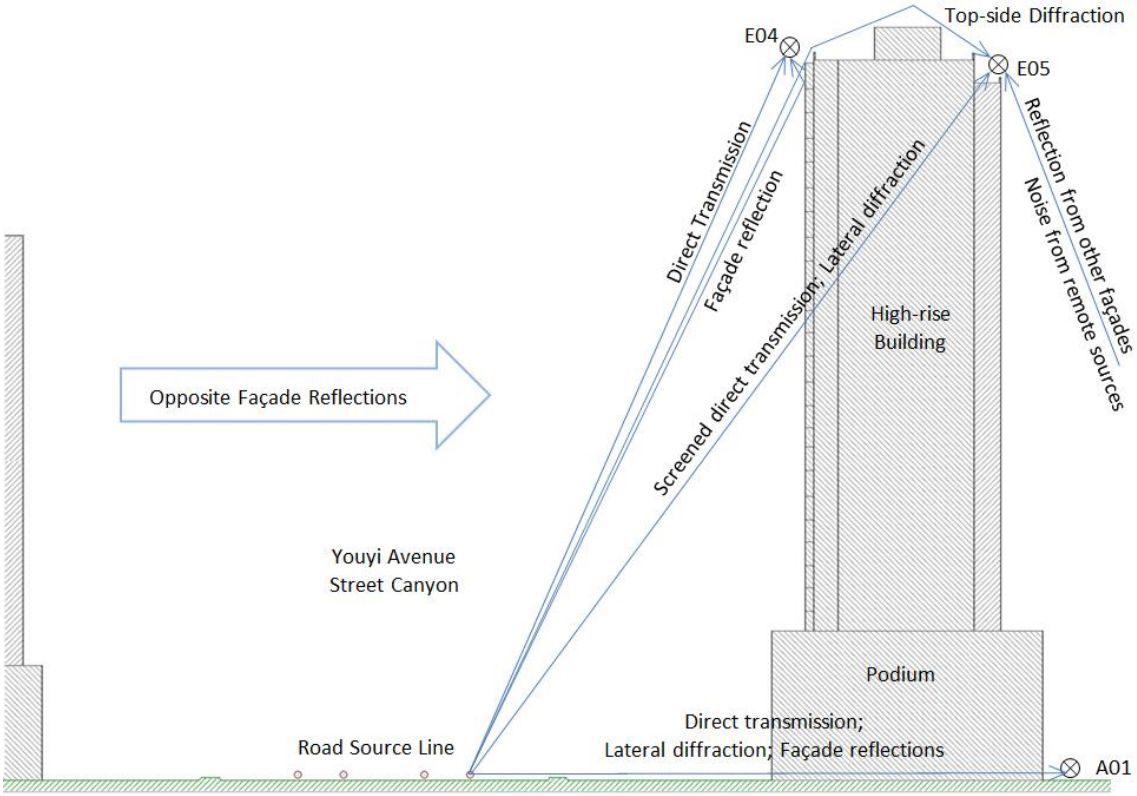

Figure 5.23 Schematic diagrams of the major corrections calculated at receiver points in the street canyon around the high-rise building –Youyi Avenue area

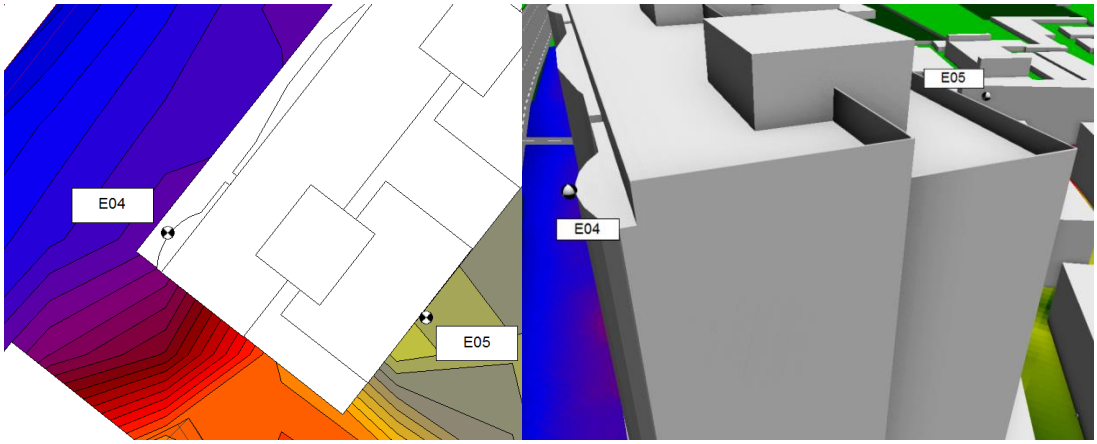

Figure 5.24 Locations of receiver points E04 and E05 above the high-rise building – Youyi Avenue area

The relatively high altitude and openness also make the point E05 prone to be affected by the background noise that is potentially neglected or the atmosphere diffraction from noise sources locating outside the measured area. As can be seen in the same map that the point A01 also locates close to the rear façade of the high-rise building, while the altitude is only 1.4 m, which is much lower comparing with that of the E05, the errors at which with maximum reflection order set to 3 and 4 are -2.3 dBA and -1.6 dBA respectively. It can be seen that the error at point A01 is much smaller than that of point E05, and with increasing reflection orders, the accuracy improvement is more evident. It may be due to the shorter slant distance from the source that makes the impact stronger, at the same time the façade reflections from the façades close to the open space between the two flanking buildings as can be seen in Figure 5.24 tend to be more accurately represented when the maximum reflection order turns higher.

- ***Summary***

As shown in Table 5.10, the effect of the typical urban and building forms in the street canyon is summarised. It can be seen that, except the obvious screening effect of the massive high-rise building, and the higher sensitivity to attenuation when slant distance is higher, there are several other noticeable unique features in the Chinese urban street canyon.

Table 5.10 Potential factors affecting the accuracy of receiver points around the flanking building of high-rise street canyon – Youyi Avenue area

Factors	E01	E02	E03	E04	E05	A01
Calculation error (dBA) [a]	-8.4	-8.3	-0.6	-2.3	-3.9	-1.6
Height (m)	14.4	31.4	55.4	72.0	70.4	70.4
Slant distance (m)	34.5	44.2	61.6	76.4	85.3	49.4
Exposure to direct transmission [b]	N	P	Y	Y	N	N
Screened by the high-rise building	P	P	N	N	Y	Y
Screened by the podium	Y	N	N	N	N	Y
Affected by top or lateral diffraction	Y	N	N	N	Y	Y
Reflection from surrounding façades	Y	Y	N	Y	P	Y
Reflection from opposite façades	Y	Y	Y	Y	N	N
Close to the ground	N	N	N	N	N	Y

[a] Maximum reflection order is set to 4.
[b] Y: Yes, or the effect mentioned does exist; P: Partially affected; N: The mentioned effect does not occur.

Firstly, the typical wide main road street canyon creates multiple reflections in between the flanking buildings lying on both sides of the main road, while due to the large width; the increasing caused by the reflection seems to be even more limited. Secondly, the high-rise building also forms peculiar building forms where the noise reflection and diffraction calculation tend to be complicated and sensitive to the calculation configuration. It is also found that, by increasing reflection order the accuracy in the shielded area of the high-rise building can get improved, especially when there are indirect lateral diffraction and reflections through the gaps between the flanking buildings as can be seen in point A01. Lastly, for receiver points locating at the top of the high-rise flanking building, such as point E03 and E04, the façade reflection only has limited effect on the accuracy, as the dominative noise source is the unscreened transmission.

5.3.2.4 Noise calculation in the shadowed area

There are three groups of receiver points measured in the shadowed area behind the flanking high-rise buildings. There are relatively more distinctive variations in the calculation errors in the shielded area at various locations, comparing with that of the receiver points inside the street canyon, as can be seen in Table 5.8 and Table 5.9.

The error changes along with distance using different reflection order settings are shown in Figure 5.25, it can be seen that with the increasing slant distance from the Youyi Avenue, the errors generally have no clear correlations with slant distance increasing.

- ***Shielded area close to the interspace among buildings – the A-series points***

As can be seen in Figure 5.25a that, the errors at the A-series points is the only group that the errors are getting smaller when the distance increases. It can be seen from the noise maps that the lateral refraction and the indirect façade reflections from the gap between two flanking building complexes are the main sources of noise received at the A-series points, the point noise source at point E06 and the noise from the Caimao street also has limited impact.

It can be seen that by simply increasing the reflection orders, the accuracy is evidently improved, but the errors at A01 and A02 are apparently smaller than the A03 and A04. It can be seen that A03 and A04 locate slightly farther from the road but are shielded by one more 7-storeys residential buildings. Nonetheless, although the A01 and A02 are shielded by the high-rise building but both points are more = influenced by the leaked reflections and lateral refractions from the gap between the two flanking buildings, and the façade of the stand-alone residential building facing the gap also acts as a strong reflector and hence by increasing the maximum reflection order from 0 to 3, the errors at the A01 and A02 are greatly reduced and much smaller than the A03 and A04.

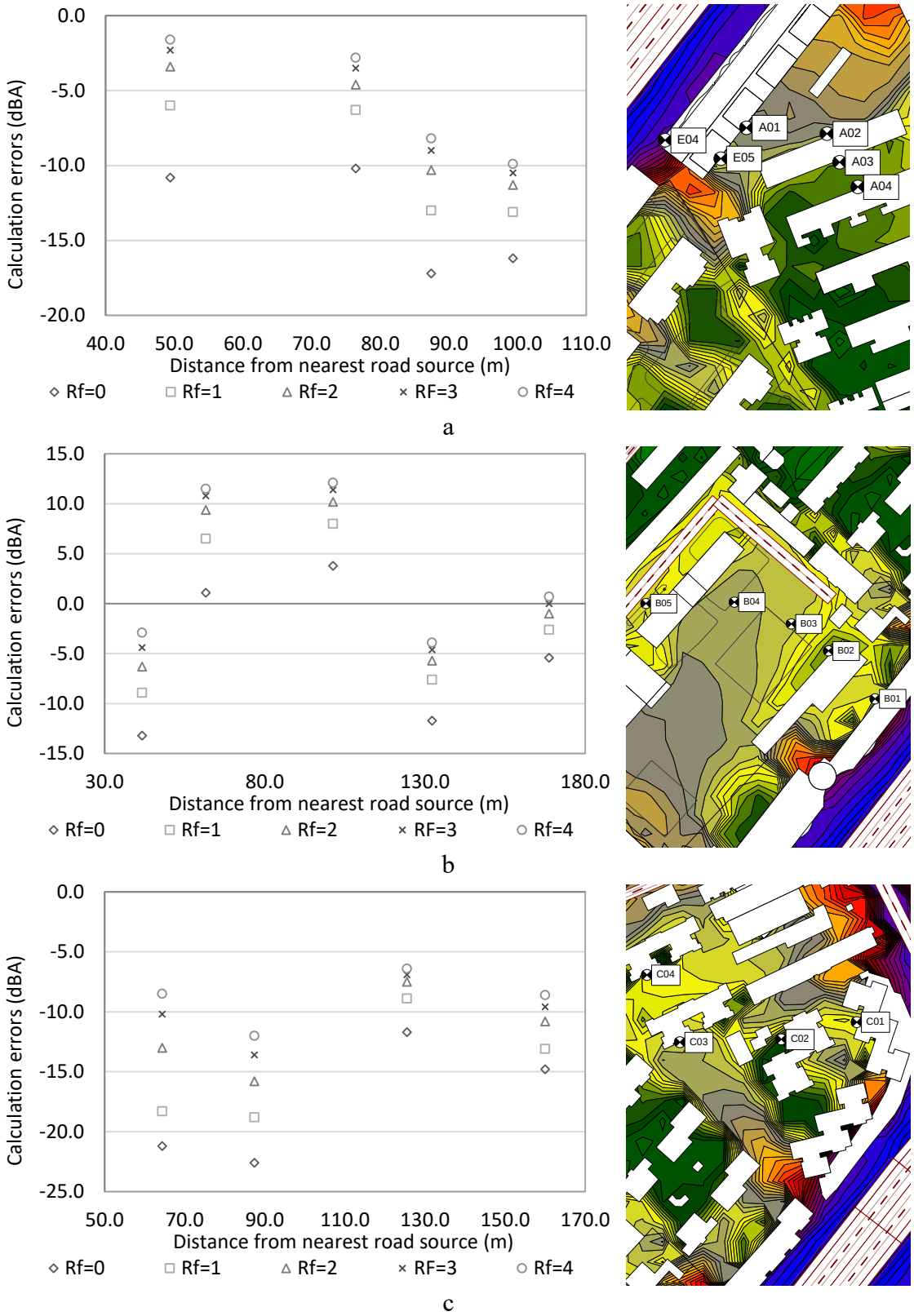

Figure 5.25 Calculation errors of the shielded receiver points – Youyi Avenue area. (a) The errors A-series points; (b) The errors change with distance at B-series points; (c) The errors change with distance at C-series points.

- ***Open space in the shielded area– the B-series points***

In Figure 5.25b it can be seen that the B series point loosely spread behind the north-side flanking buildings in a relatively more open area. The positive errors at points B02 and B03 indicate that the calculated SPL at these two points tends to be higher rather than lower than the measurement results. It can also be seen that with the increasing of maximum reflection orders, the errors at the point B02 and B03 become even larger rather than smaller. As can be seen in the noise map that although B02 and B03 locate behind the second lines buildings and closer to the main road source, the B04 and B05 are partially affected by a small-traffic-flow road outside this community thus the results are still more accurately calculated.

The cause of inaccuracy at B02 and B03 may be caused due to there are large amount of soft-soil planting field and clusters of trees with large crowns, as can be seen in Figure 5.16. In most of the current calculation methods, the potential influence of the foliages of abating the noise (Kang, 2006) is neglected largely. For instance, in Cadna/A there are foliage objects but it has no effects on the calculation, in this map, ground absorption field with high absorption coefficient is used instead but it can be seen that the effect is limited.

- ***The impact of multiple sources – the C-series points***

The C-series points as shown in Figure 5.25c has generally all negative errors which all become smaller when the maximum reflection orders increase, from 0 to 4. As shown in the noise map that in this shielded area, although most of the noise rays from the Youyi Avenue is screened by the flanking buildings, the Caimao Street, which lies on the northeast side also has relatively larger amount of traffic flow. Therefore, the errors in the C-series tend not to have a correlation with the slant distance from the street canyon.

In the C-series, it is also interesting to note that, the façade of the long-belt-shape building lying in the north of the C01 and C02 together with other surrounding façades play an important role in reflecting the sound rays from the Caimao street, although the surrounding façades close to C01 and C02 are utterly complicated. It can be seen in Figure 5.25c that with the increasing of reflection order from 0 to 4, the errors at C01 and C02 have a huge leap of 12.7 and 10.6 dBA respectively. It shows the significance of

considering more reflection orders in such complicated high-rise urban areas when the topside diffraction is largely blocked.

Point C03 has the smallest error among four C-series points due to more exposure to main road source. It can be seen in Figure 5.25c that comparing with other four points although it locates as far from both main road sources, but the sound rays of both the Youyi Avenue and Caimao Street can reach it via direct transmission and façade reflections due to two openings in between the flanking buildings.

- ***Summary***

Above results suggest that the general calculation accuracy in this urban scenario is acceptable and increasing the maximum reflection order can greatly enhance the calculation accuracy in the partially or fully shielded area behind the high-rise buildings. Nevertheless, in such high-density urban area, the current calculation methods are more effective and accurate when the direct transmission from road source is not entirely screened by the high-rise flanking buildings. In addition, in the relatively less impacted open area in the shielded community, environmental conditions such as high-density foliage and soft soil may need to be considered to ensure better calculation accuracy. The calculation accuracy in the areas that are screened by more than one row of buildings is generally worse than those that are affected by direct transmission or indirectly by the first order of reflections. It is hence essential to account all available noise sources and to consider more effective calculation methods in such unique urban form rather than simply increasing the maximum reflection orders.

5.3.3 Hypothetical scenarios tests on typical urban morphology features in the high-rise street canyon

5.3.3.1 Hypothetical scenarios tests

A series of hypothetical scenarios are proposed and calculated to test the influence of particular urban form in the street canyon on the calculation accuracy in the street canyon. The configuration of calculation is processed using the default settings without the 1.5 dBA façade correction, and the maximum reflection order is set to 4 for more accurate correction of façade reflections. A series of calculations are conducted in each scenario at

five façade receiver points that locate at various locations adjacent to the façades of the high-rise flanking buildings next to the main road. Youyi Avenue. The height and location of the five points vary while directly or indirectly impacted by the traffic noise from the main road Youyi Avenue as can be seen in Figure 5.21 and Figure 5.23.

5.3.3.2 General tests

Table 5.11 Change and absolute errors in hypothetical scenarios – Youyi Avenue area

Hypothetical scenarios		No opposite buildings (dBA)	No podium (dBA)	No high-rise tower (dBA)	No all buildings (dBA)
Change of absolute error *	E01	+1.4	-5.2	-6.9	-4.7
	E02	+0.8	+0.1	-8.1	-7.3
	E03	+0.7	0.0	0.0	+0.6
	E04	+0.8	0.0	+0.2	+1.0
	E05	+0.3	0.0	+5.9	+5.3

* It measures how the alternations made on the models in the hypothetical scenarios reduce or increases the absolute values of the original calculation errors.

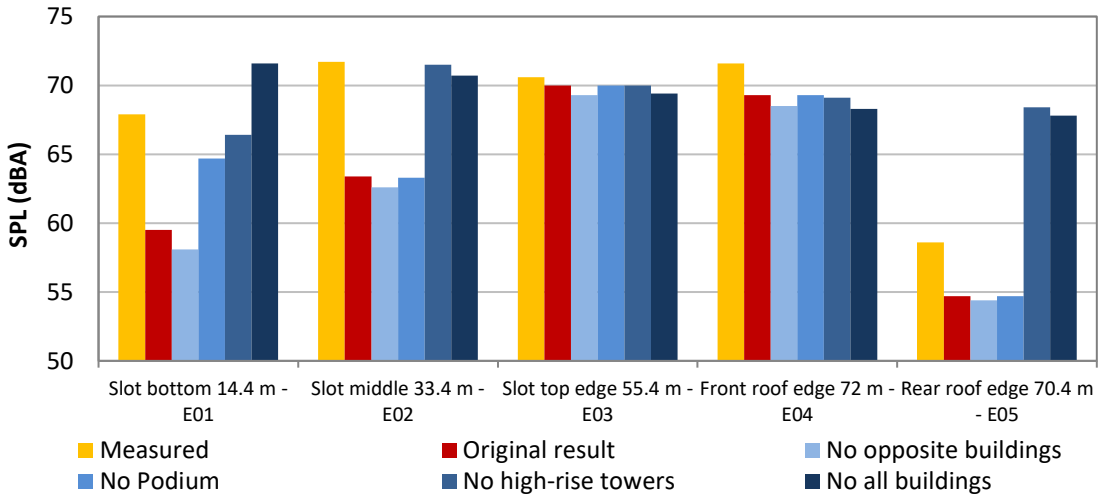

Figure 5.26 A comparison between measured and calculated results, including the original results and a series of hypothetical scenarios.

Hypothetic tests are conducted to examine how specific building form and spatial features of the street canyon may potentially influence the calculation accuracy. Four scenarios are tested for all five receiver points, the changes of the absolute values of the calculation errors are listed in Table 5.11; the results are compared with the measured results and the

original calculation results. The comparison between measured and calculated results is visually demonstrated in Figure 5.26.

Above all, it can be seen that at higher altitude on top of the flanking high-rise buildings, say, receiver points E03, E04 and E05 tend to be less affected by the alternations on the buildings due to relatively higher altitude and openness, especially the two receiver points E03 and E04 that locating near the front edge of the roof of the high-rise buildings. Some of the evidently increased SPL at point E05 are due to the cancelled screening effect of the high-rise buildings when they are removed.

Meanwhile removing the podium only has visible influence for the point E01 which locates on the surface of the podium as shown in Figure 5.21. By solely removing the opposite buildings, the specular reflections calculated are reduced at all receiver points, consequently the absolute error at most of the points become larger especially for lower points close to the flanking façade, but all within a limited range of 1.5 dBA, which justifies the default maximum 1.5 dBA correction adapted by the noise mapping package for faster calculation of specular reflections.

For receiver E01 and E02 that locate within the vertical slot on the façade of the high-rise tower at a different height, it can be seen that almost all alternations on buildings forms have more or less influenced the deviations calculated, but the extent of reduction or increasing varies in each scenario. Further analysis is made to discuss the main cause of errors at these two receiver points.

5.3.3.3 *Specific analysis on the effect of a peculiar building form*

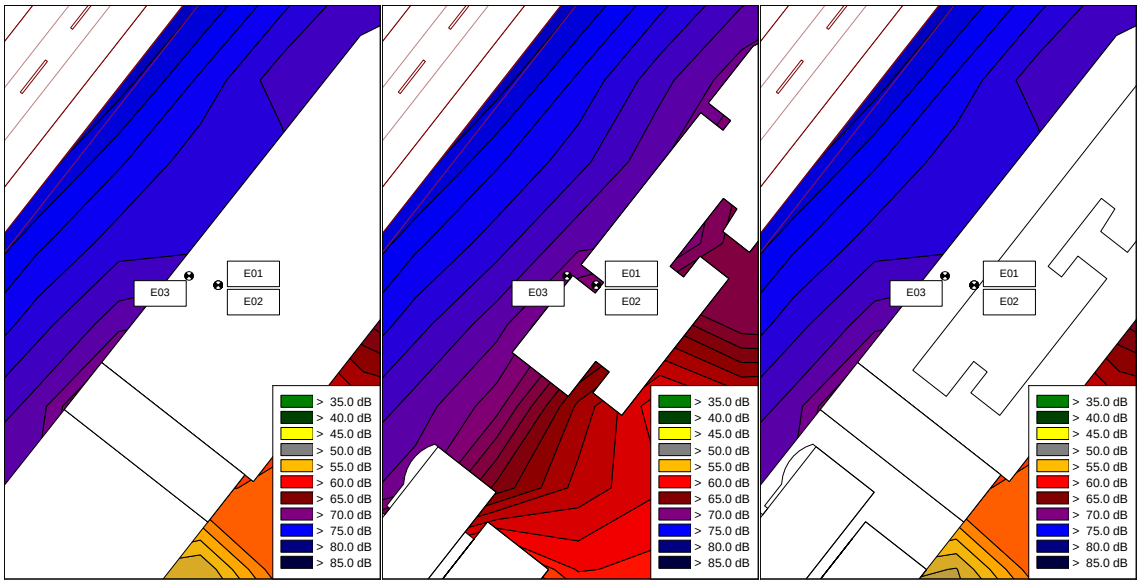

a. b. c.

Figure 5.27 The hypothetical scenarios of flattening the façade slot – Youyi Avenue area, where the figures represents the hypothetical scenarios of: (a). No towers; (b). No podium; (c). Slot flattened.

A series of hypothetical test are further conducted to examine the potential causes of the inaccuracy at point E01 and E02, which locates at 14.4 m and 34.4 m respectively inside the long slot on the front façade of the high-rise residential tower. Due to the depth of the slot, both points have limited exposure to direct noise transmission to most of the main road sections due to the depth of the slot.

Table 5.12 The changes of the absolute errors at two receiver points in the façade slot in all hypothetical scenarios

Hypothetical Scenarios	Change of AE *		Calculation elements tested
	E01	E02	
No lateral diffraction	-0.3	0.0	Calculation of all lateral diffractions
No slot	-6.7	-7.9	Screening and lateral diffraction
No opposite buildings	+1.4	+0.8	Specular reflections in the canyon
No podium	-5.2	+0.1	Any inaccuracy caused by the podium
No high-rise tower	-6.9	-8.1	Any inaccuracy caused by the tower
No podium nor towers	-3.6	-7.3	Any screening, reflections and refractions
No all buildings	-4.7	-7.3	Only the divergence attenuation

* The change of the absolute error here measures the reduction of the absolute calculation errors that triggered by the specific alternation.

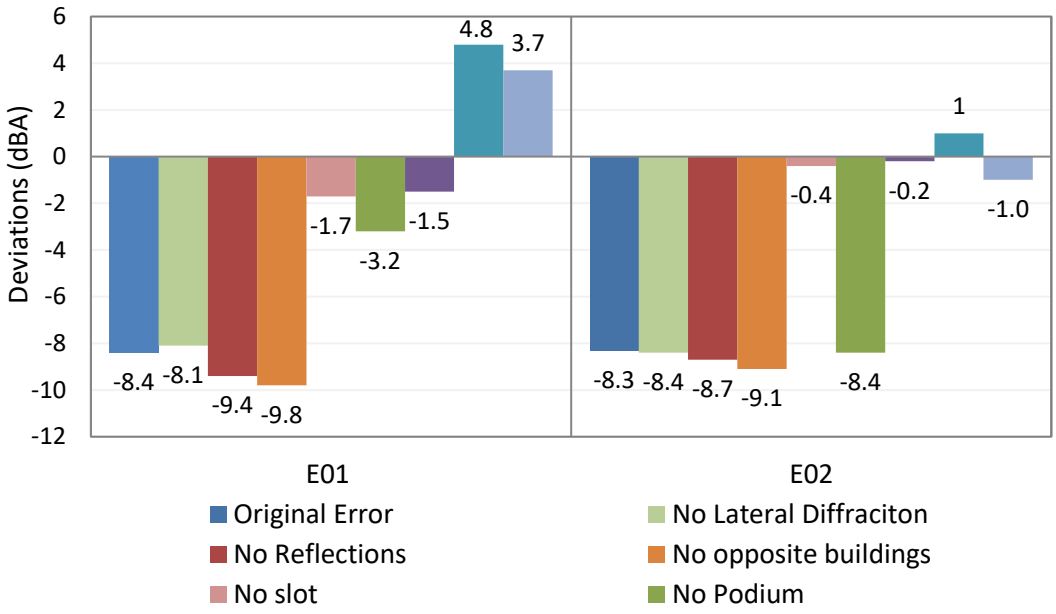

Figure 5.28 Calculation errors of two façade receiver points at different heights based derived from a series of hypothetical scenarios – Youyi Avenue area

The alternations implemented in the hypothetical tests include: turning off the calculation of lateral diffractions; an alternation on the building form by flattening the slot as can be seen in Figure 5.27c; removing the potentially influential objects, including the scenarios of solely removing the high-rise towers (Figure 5.27a), the podium (Figure 5.27b); removing both the podium and the tower; removing the row of opposite multi-story buildings that may create multiple specular reflections in the street canyon; and finally a scenario with all buildings and barriers removed. The deviations calculated in all scenarios including the original errors at E01 and E02 are demonstrated in Figure 5.28. The potential causing elements and the specific changes of absolute error at both points are listed in **Error! Reference source not found.**.

5.3.3.4 Tests on the calculation configurations

- ***Tests on the lateral diffractions***

A scenario without calculating the lateral diffractions is tested. It can be seen in the Figure 5.28 and **Error! Reference source not found.** that when the calculation of the later diffraction is switched off, there are only slight changes of calculation errors occurred at point E01 and E02. It indicates that the lateral diffraction only contributes to the received noise level to a limited extent in the calculation method adopted. It is to note that in this

scenario the topside diffractions are still calculated according to the calculation method (DataKustik, 2012a).

- ***Removing the specular reflection in the street canyon***

By removing the opposite buildings, the change in SPL and absolute error at both points are relatively small. The calculated results decreased for 1.4 dBA and 0.8 dBA respectively, the absolute errors increase the same amount accordingly. It can be seen that the change at point E01 is higher 0.6 dBA higher than that at point E02. It indicates that at lower altitude, say at point E01 that locates is more prone to be affected by the specular reflections from the opposite flanking façades.

5.3.3.5 Tests on the effect of the building complex

It can be seen that by simply flattening the long façade slot where point E01 and E02 locating the protruding parts of the high-rise towers removed leaving both receiver points exposing to the traffic noise from the Youyi Avenue, as shown in Figure 5.28, the calculated SPL at both points evidently rise by 6.7 dBA and 7.9 dBA respectively, the absolute errors are hence also reduced accordingly.

The apparent changes that occur at point E01 and E02 when the façade slot is flattened may largely attribute to the changed paths of refractions; the screening effect of the protruding parts on both sides is hence relatively limited. In the meantime, as can be seen in Figure 5.21 that the point E01 is actually largely screened by the podium, and the retreated façade of the high-rise tower allows more topside diffractions via the edge of the podium to reach. Similar effect may also occur at point E02, nevertheless, point E02 is not screened by the podium, and its higher altitude may not make it affected by the refractions from the podium edge evidently. Thus, it is possible that the extra reflections cause more increasing in the calculated SPL at E02 than E01 in this scenario, and thus it is possible that in the original calculation the reflections and diffractions inside the long and deep space of the slot are largely neglected, especially at point E02.

- ***Removing the podium***

To find how the podium affects the calculation at both points, a scenario is tested with the 4-story podium where point E01 locates on is removed. At the point E01 that locating on the surface of the podium, removing the podium contributes 5.2 dBA of reduction of absolute error, the calculated SPL also rise for 5.2 dBA. In the meantime, the calculation error at E02 only has a slight change of -0.1 dBA.

- ***Effect of the high-rise buildings***

By solely removing the high-rise towers, the errors at E01 and E02 are more evident than that when the slots are flattened. The calculated SPL rises for 6.9 dBA and 8.1 dBA at two points respectively, the absolute error reduces to the same extent. When both the podium and towers are removed, the calculated SPL at both points rise largely for 13.2 dBA and 9.3 dBA respectively and the error value both change from negative to positive. It may mainly due to wider exposure to direct and indirect noise transmissions. The change at E01 is 3.5 dBA higher than that of point E02.

- ***A free field test without all buildings***

Lastly, the extreme scenario of a free field was tested by removing all erecting buildings on the noise map, the calculated SPLs without counting all influential elements show great increase of 12.1 dBA and 7.3 dBA of increasing respectively at point E01 and E02, and the absolute error decreases by 4.7 dBA and 7.3 dBA respectively. It is to note that although the free transmission from all road sources in the surrounding area are allowed more in this scenario when all buildings are removed than in the scenario where only the podium and high-rise towers are removed, the effect of the former is slightly smaller than the latter by 1.1 dBA and 2.0 dBA at point E01 and E02 respectively. It may attribute to the extra façade reflections from all surrounding buildings when only the podium and the towers are removed.

5.3.3.6 Discussions and summary

From above results, it can be seen that, generally the calculation error using current noise calculation method are acceptable in this typical high-rise street canyon scenario at a higher altitude, given all noise sources and potentially screening and reflective objects are considered, including the multiple orders of opposite façade reflections. Nonetheless,

some peculiar urban form, e.g. the podium and the largely shielded space in the long façade slot of the flanking buildings may have exceptionally high calculation deviations.

To be specific, the main source of error at point E01 and point E02 are distinct, the podium does not affect the E02 as much as at E01 due to the higher altitude of E02 and more direct noise impact and reflections from various façades. It is found that despite the influence of the podium, the effect of simply flattening the slot where these two points locate in, the calculated SPL can gain evident rise especially at higher altitude due to more exposure to sound rays from far sources. The cause discussed previously is only partially contributed to the underestimated calculation of screening effect of the protruding parts on both sides of the slot; there may be the potentially large amount of reflections and diffractions neglected inside the slot and via both edges of the slot.

From one hand the tests show how the current noise calculation methods are capable to cope most of the calculations in the typical Chinese street canyon with relatively simple building form, from the other hand it indicates that the current method has its limit in such unique urban forms, further studies on the algorithm and calculation configuration is needed, considering the universality of these urban forms in typical Chinese cities.

5.3.4 Calculation error at different frequencies

The calculated and measured of the central frequencies at eight major octave bands of the six receiver points are demonstrated in Figure 5.29. In Table 5.13 the exact calculation errors are listed and the errors with a mean value of smaller than 3.0 dBA are highlighted.

Table 5.13 SPL spectrum calculation errors at major octave bands central frequencies – Youyi Avenue area, errors with absolute value equal to or smaller than 3 dBA are highlighted.

	Calculation errors (dBA)								
	31.5 Hz	63 Hz	125 Hz	250 Hz	500 Hz	1kHz	2 kHz	4 kHz	8 kHz
E01	-12.3	-8.0	-5.9	-6.7	-9.4	-10.7	-8.9	-7.4	-10.0
E02	-14.1	-8.2	-7.8	-5.8	-8.1	-9.4	-8.8	-7.5	-5.3
E03	-5.0	-3.3	-3.1	-2.4	-2.0	-2.7	-1.9	-3.4	-1.1
E04	-4.8	-2.2	-3.1	-3.0	-1.4	-3.4	-4.1	-2.4	-0.9
E05	-2.9	-2.4	-2.6	-5.7	-7.0	-5.3	-3.8	-6.9	-15.7
E07	-13.7	-8.7	-13.6	-13.5	-9.2	2.8	0.5	1.8	-5.5

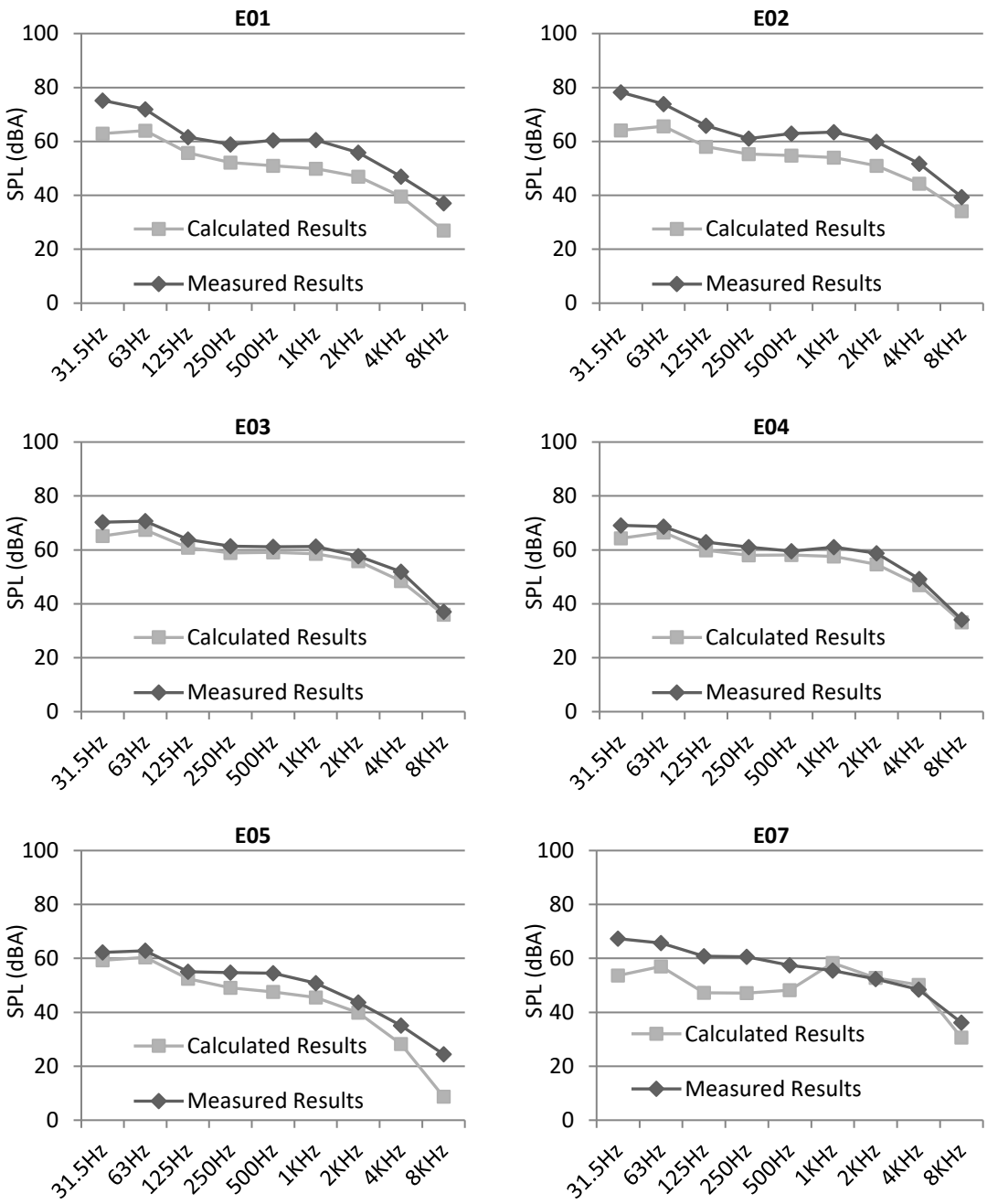

Figure 5.29 Measured and calculated noise level spectrum – Youyi Avenue area

For receiver point E01 and E02 it can be seen that negative errors of 5.3-14.1 dBA exist at all frequencies, which coincides with the results calculated using the traffic flow input shown in previous sections. It indicates that the peculiar building from where these two points locate may have a systematic effect on the calculation accuracy, regardless which calculation method is used. In the meantime, it can also be seen from Figure 5.29 and Table 5.13 that the errors occur at receiver point E03 and E04 are more acceptable. As discussed in previous sections that both points locate at the top of the flanking high-rise

buildings with direct exposures to the main road source. Therefore, the interferential factors have the relatively negligible influence on the accuracy at these two points. It can also be seen that the errors at 31.5 Hz at point E03 and E04 are much larger than those of the other frequencies, at E01 and E02 that also locates inside the canyon this phenomenon also exists. Nevertheless, at the point E05 that was locating at the top-rear side of the high-rise building, the errors at lower frequencies of 31.5-125 Hz appear to be smaller than those of the higher frequencies, and meanwhile, at 8000 Hz the absolute value of the error is as high as 15.7 dBA. Point E05 is merely not affected by the façade reflections inside the street canyon due to the screening effect of the building.

Considering that the E05, E03, and E04 are all locating at the top of the high-rise buildings, above finding hints that inside the higher SPL measured at 31.5 Hz may not be caused by the potentially neglected low-frequency background noise propagated from remote segments of the Youyi Avenue and other roads outside the measured area. Rather, at the lowest frequency of 31.5 Hz, the direct transmission, and specular reflections from opposite façades in the street canyon may be underestimated. Meanwhile, the higher errors occur at E05 in higher frequencies may be a consequence of transmission loss of higher frequency noise in the noise topside and lateral diffraction.

Due to the influence of a point noise source from the exhaust fan close to point E06 on the wall, the lower and middle-range frequency noise from 31.5-500 Hz received at point E07 are underestimated. It shows that in the real in-situ situation in the unique urban form which is entirely shielded by the high-rise buildings, the lower and middle range noise can actually reach the point E07 via other paths e.g. neglected lateral diffractions and multiple times of façade reflections, considering that there are two major interspaces lying 100 m from point E07.

5.4 Elevated roads – A comparative study

The construction of the elevated road has become a popular and debatable solution in the urbanisation process of China and for traffic congestion problems, nevertheless it may also create serious noise concerns (Lam & Ma, 2012). The elevated road is not a particularly unique urban morphology element to China, but due to the booming

population and speeding urbanisation process, the increasing demand of traffic in high-density urban areas and across metropolitan or urban sprawl areas has brought this form of road complex to Chinese cities. The peculiar urban spatial and acoustic feature created by this urban form may become a challenge to current noise calculation methods. To verify the applicability of current noise calculation method in this typical Chinese urban form, in this section, the traffic noise in two sample areas with representative urban spatial characteristics are systematically measured and simulated, the comparison reveals the performance of selected noise calculation methods in this typical urban form.

5.4.1 General description

There are two representative types of elevated main roads examined in this section, both of which have a double layer heavy traffic road running through a street canyon formed by flanking buildings. Nevertheless, there are evident distinctions in urban morphology, building form and acoustic features in each case.

5.4.1.1 Topography and urban morphology – street canyon formed by elevated roads

- ***Wide street canyon with large building blocks – Xudong Road***

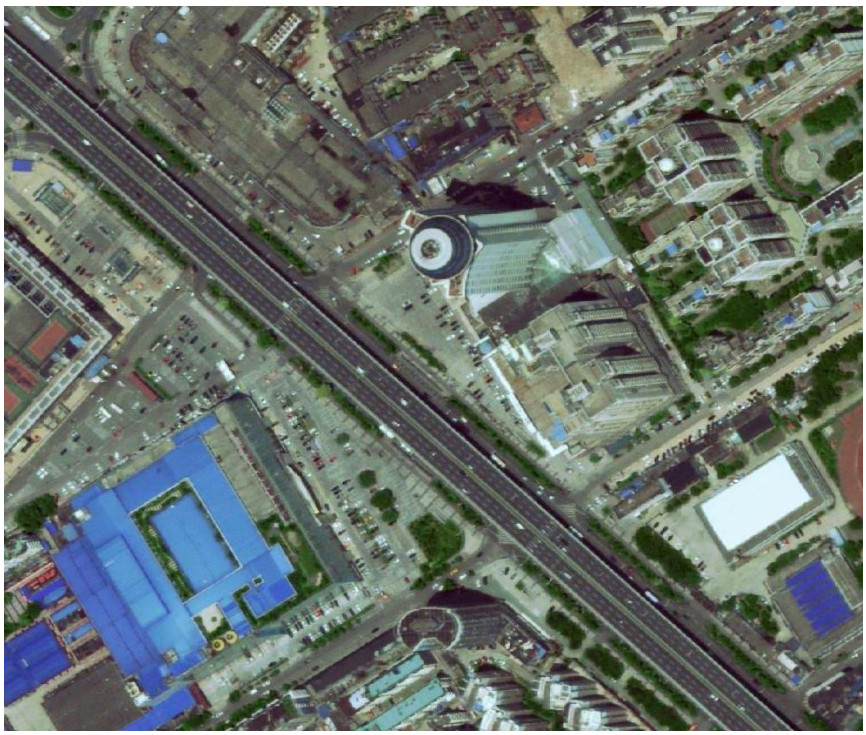

Figure 5.30 Satellite map of the Xudong Road area. Source: Google Maps (Google Inc.)

The first selected site shown in Figure 5.30 locates next to the Xudong Road and contains several large-scale building complexes. The focus in this study is concentrated on the Xudong Road together with its elevated part, and the building complex locating on the east side of the road, where a group of the high-rise hotel and apartments erect on one single large podium building which covers a rectangular field of 160 m × 80 m. The podium is 21-metre tall and nonparallel with the main Road and locates 68–26 m away from the Xudong Road.

The area next to the Xudong Road is mostly commercial or mixtures of commercial and residential use. The other three large-scale building blocks sit on both sides of the Xudong Road area as can be seen in Figure 5.30 are 10-20 m tall and with flat-roof shopping malls without high-rise buildings erecting above.

Similar to many other typical Chinese urban areas, behind the large-scale roadside buildings there are large residential areas. The residential area behind the flanking blocks on the northeast side of the Xudong Road is one of the earliest developed residential communities in the 1990's in Wuhan. Most of the residential buildings on both sides of the Xudong Road are multi-storey apartments of 7-9-storey tall and only few high-rise residential towers of 15-25 storeys close to the main road.

The terrain of this area is relatively flat and the ground is mainly hardened and covered with concrete or pavement tiles. There are a few patches of absorptive areas in the area that are covered with soft soil and plants. Thick layers of green bush in a belt shape with the height of 0.5-1 m are planted in the centre isolation strip and both sides of the Xudong Road. All planted areas are simulated in the modelling process as ground the absorption areas with an absorption coefficient of 1.

- ***Confined street canyon with high-density residential buildings – Luoshi Road area***

The Luoshi Road area is a mixed residential area that divided by one of the busiest main roads in Wuhan, the Luoshi Road, and the other two roads, the Hongshan Side Road, and the Chagang Road inside the Wuhan University on the east side. The ground in the research site close to the Luoshi Road is basically flat, although there are small hills located within 1 km to the southeast of the site. The terrain ascends slightly in the west of the Luoshi Road.

As shown in Figure 5.31 that the area is divided by the main road canyons, and the apartments around this area are loosely divided into small communities which formerly dwells the staff of government departments that forming the unique Chinese style living-and-working complex, or the *Danwei* (G. Kai, 2001). Nevertheless, they are mostly sold or rent to migrants in the process of the land commercialisation of land and real-estate market reform (Gaubatz, 1999). Therefore, the entrances to the communities are not very strictly blocked as typical Chinese residential communities, and the fences around the residential community merely have no screening effect on the traffic noise and cannot be regarded as barriers in this case.

The terrain of this area is relatively flat, except in the west side of the road the altitude of the terrain is slightly higher and a concrete embankment wall of 1-2 m tall is running along the Luoshi Road. All details of the terrain are explicitly modelled using contour lines and fault lines with precise altitude obtained from the digital map and in-situ measurement.

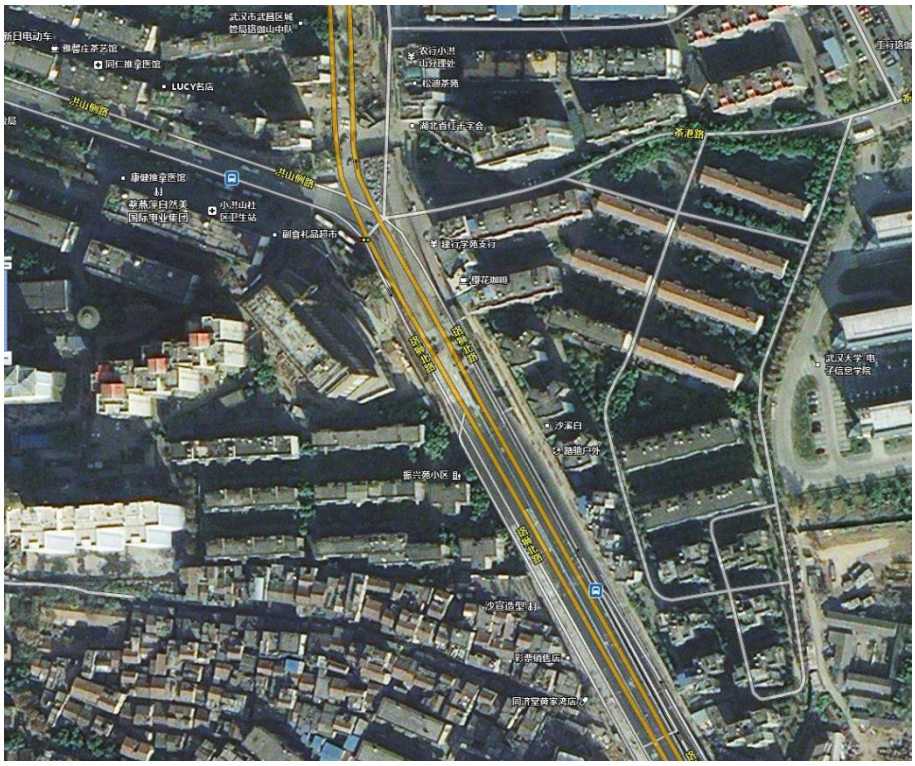

Figure 5.31 Satellite map of the Luoshi Road area. Source: Google Maps (Google Inc.)

In the Luoshi Road case, the façades of the residential buildings on both sides of the road are as close as 10 m away from the edges of the elevated road. It is hence not difficult to

understand why the construction of the elevated road is disrupted and delayed for more than one year due to the complaints about potential noise concerns that received from the local communities when the road was originally planned to be constructed. The final solution from the road planner is to seal the elevated part with galleried cantilevered barriers to ensure the best abatement of the traffic noise.

- ***Comparison of the morphological characteristics***

Table 5.14 Space features comparison of two street canyon cases

Spatial features	Xudong Road	Luoshi Road
Total road width	26 m	18 m
Kerb-to-façade distance	30-51 m	13.5 m
Road width coverage	27.1 %	59.5 %
Average width	140 m	42 m
Average height	21 m	18 m
Aspect Ratio* (H/W)	0.15	0.4

* The aspect ratio is a parameter that measures the morphology of the street canyon, equivalent to the average height of flanking buildings divided by the average distance between opposite buildings.

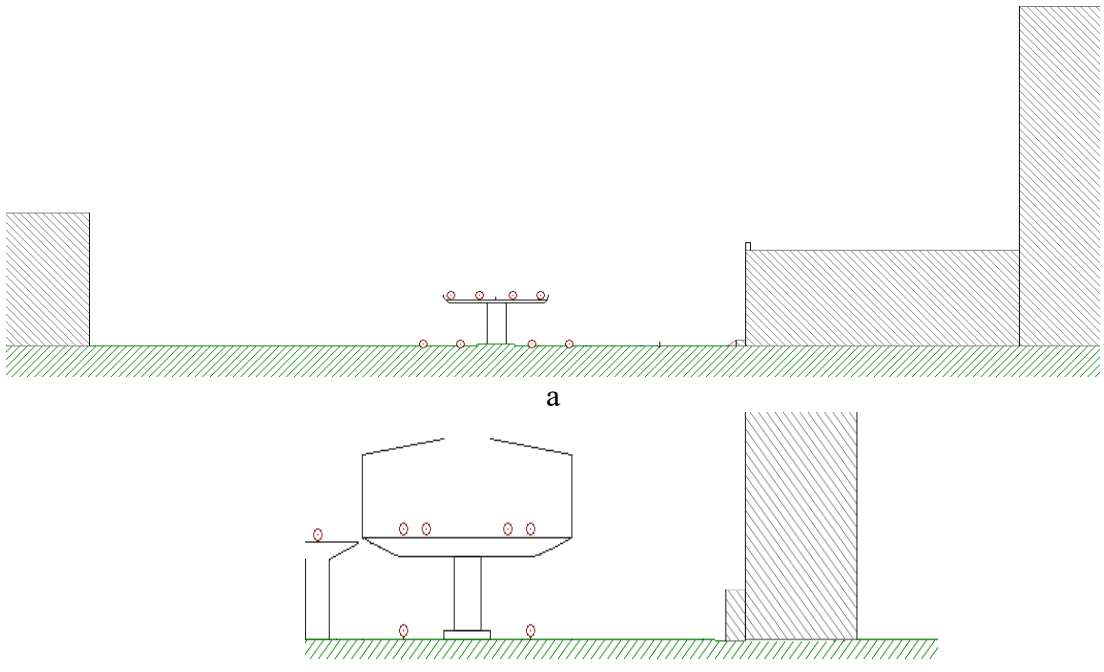

a

b

Figure 5.32 Typical cross section view of two typical street canyons with elevated roads: (a) Xudong Road street canyon (b) Luoshi Road street canyon, the latter is narrower and the elevated road is installed with partially confined noise barriers.

The urban morphological features of these two street canyons with elevated road have evident distinctions. As shown in Table 5.14 that the road of the Xudong Road street canyon is much wider than that of the Luoshi Road. Although in the Xudong Road case the flanking façades of the buildings facing the roads are doubled as those of the Luoshi Road, the aspect ratio of the former is 0.15 which is less than half of the latter.

From the section views shown in Figure 5.32, it can be seen that the scale of the Xudong Road is much larger and wider. Although in the Xudong Road case the total road width is also wider than that of the Luoshi Road, the total coverage of the road width is less than half of the latter. Due to the much larger kerb-to-façade distance from opposite flanking buildings, the effect of the specular reflections in the canyon may consequently be much less than that in the Luoshi Road street canyon.

Table 5.15 The characteristics of the elevated roads

Elevated road features	Xudong Road	Luoshi Road
Road width	26 m	18 m
Elevated road height	10.6 m	7 m
Bottom type	Flat	Curved
Parapet height	1 m	1 m
Barrier height	N/A	6 m
Barrier with cantilever	N/A	Yes
Exit ramp *	No	Yes

* There are several ramp roads connecting the elevated road in the Luoshi Road case, extra vertical barriers are installed on the outer side to avoid the strong impact of traffic noise on the flanking building.

Meanwhile, in both cases the space beneath the elevated roads may have potentially more complicated sound propagation paths as the bottom surface of the thick elevated roads may create extra reflections, while the situation may be worse in the relatively more confined space in the Luoshi Road street canyon.

Figure 5.33 The space beneath the elevated road – Luoshi Road area Source: Tencent Map service (Tencent Inc., 2011)

Moreover, as can be seen in Table 5.15 that the surface of the elevated part of Luoshi Road is 3.6 m lower than that of the Xudong Road case. The bottom surface of the elevated roads in the Luoshi Road area is curved, smooth and hence highly reflective as can be seen in Figure 5.33. Thus, it may create more reflections to wider areas on both sides of the road. It can also be seen that in this section of the Luoshi Road there are exit ramps which also has barriers installed on the outer side connecting the elevated road and the ground. Generally, the more complicated structure of the elevated road and noise barriers and appendices attached to the top of the elevated road may also cause complicated noise propagations.

5.4.1.2 Building features

The building forms and spatial features of these two sites are distinct, which are selected to represent two typical categories of elevated road canyons. The Xudong Road area is one of the types that were planned and designed from scratch during the urban sprawling in the 1990s, the elevated road is running through a large planned area with mix use of commercial and residential, due to strict plot ratio regulation and zone planning system of China, the space is relatively open and low density regarding the building coverage. In

contrast, the elevated part of the Luoshi Road area is a traditional residential with high building coverage and density and has wide varieties regarding building forms, the space of which in the street canyon and among the residential buildings are relatively narrower and confined.

- ***Xudong Road area – large scale building complex with podium***

Buildings on this site were mostly built during the economic boom in the 1990s and early 2000s. It is planned as one of the most important commercial areas in Wuhan. The main building complex is a commercial real-estate development and was one of the biggest developments of its kind when it was built in the late 1990s.

As can be seen in Figure 5.34 that the podium building itself has a height of 21 m, with a row of 1.4-metre entrance platform and steps attached to the base of the ground floor. The top of the podium is surrounded by a 1-metre-tall and 1-metre-wide parapet structure. The surface of the roof is essentially flat. One piece of long additional buildings that are 3–6 m tall in the middle separates the roof space into two parts.

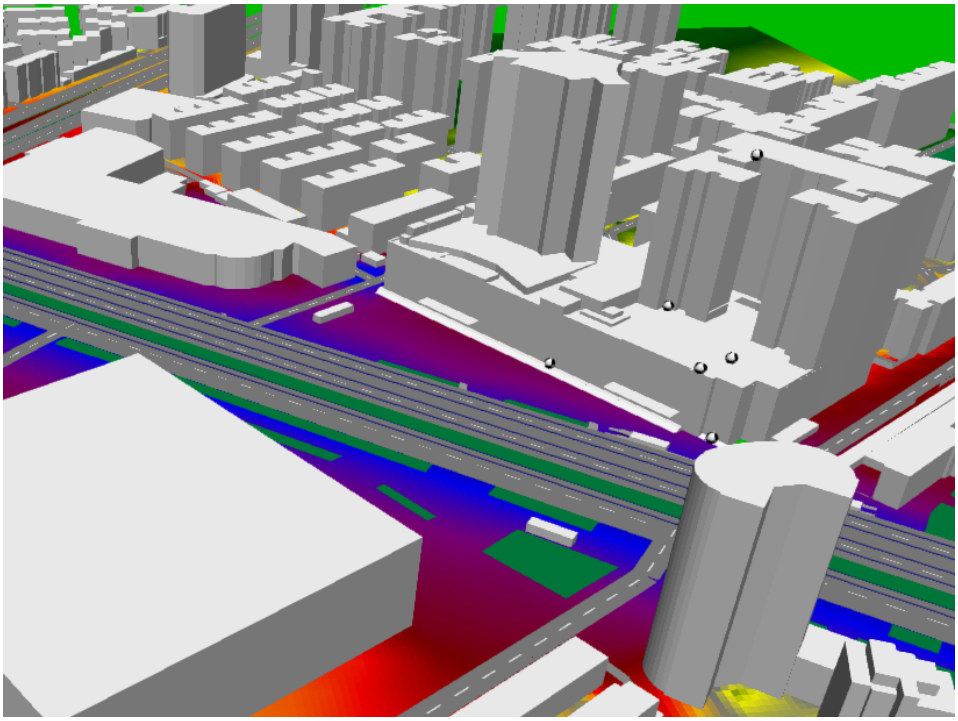

Figure 5.34 3D perspective of the large scale building complex – Xudong Road area

There are two groups of high-rise buildings erects on top of the podium. A 22-storey hotel and its annex buildings locate in the north part, and a group of apartments of up to 19

storeys locate in the south part, the latter forms a half-enclosed street canyon space at 35 m away from the edge of the podium building as can be seen in Figure 5.31.

- ***Luoshi Road area – multi-storey residential buildings with various forms***

The buildings locate in both sides of the Luoshi Road are mostly residential apartments together with several high-rise office buildings and a cluster of urban village buildings. As shown in Figure 5.35 that a group of multi-storey residential buildings sits in the Chagang Community on the east side of the Luoshi Road and the south of the Chagang Road. There is a mixture of standalone residential towers of eight storeys and terraced flats of 6 storeys. The ground floors facing the Luoshi Road are joined by a row of 1-storey podium buildings for commercial use. The residential apartments in other parts of the area are mostly old apartments of 6–8 storeys with open or enclosed balconies and are approximately built before the 1990s.

The land plots close to the main road intersection, it was planned to have higher plot ratio, therefore, the buildings are higher than average. The office buildings close the southwest corner of the intersection is of 20-storey high and has a 3-storey podium underneath it. And opposite to it stands a set of joined office buildings of 10–18 storeys high.

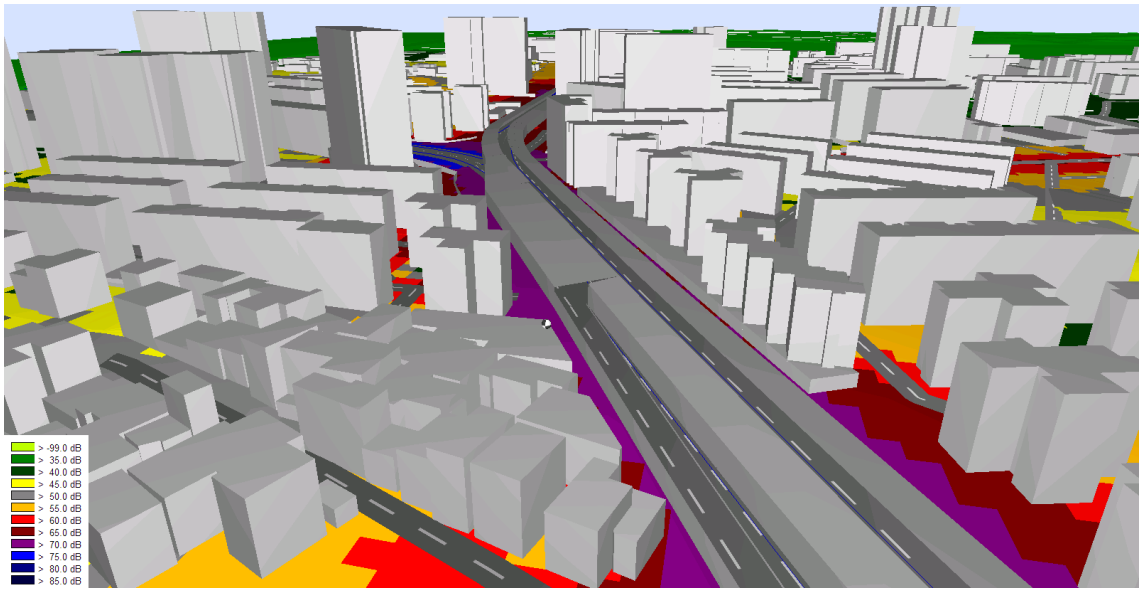

Figure 5.35 3D perspective view of the elevated road street canyon – Luoshi Road area

The small scale urban village in the southwest of the area are mainly comprised of typical 2–3 storeys traditional houses, with bricks and concrete structure, and rough façades. Some have additions on top and reach up to 12 m high. The alleys dividing the houses are

as narrow as 0.5–2 m wide. Some of the buildings are actually under major demolition during the in-situ investigation period.

- ***Comparison***

Above description shows that the average height of the flanking building façades is similar in both cases, while the overall scale and complexity are entirely different. As shown in Table 5.14 that the average height of the flanking façades in the Xudong Road area is slightly higher than that of the Luoshi Road, while the building type of the former is mainly commercial blocks with large depth and ground coverage and that of the latter is mainly lower-rise and high-density residential buildings. At the same time, the general building coverage in the Xudong Road area is also lower than that of the Luoshi Road area, which leads to much longer transmission distance and less complicated reflection and lateral reflections on the ground level.

From the perspective of building form, there are podium buildings in both cases as can be seen from the maps, but the scale and role that they play in the calculation are distinct.

As can be seen in Figure 5.32 that the distance from the outer edge of the podium buildings to the base of the residential tower standing on it in the Xudong Road case is much larger than that of the Luoshi Road case. In a certain sense due to the large depth of the podium building, the high-rise tower in the Xudong Road case, the high-rise towers standing can be seen as individual objects outside the street canyon that mainly function as huge noise screening barrier for the residential area behind them, whilst in the Luoshi Road street canyon the flanking buildings have similar height on both sides of the road.

5.4.1.3 Road and traffic conditions

In both cases, the elevated roads are built above the original main road for the sake of abating the pressure of trans-district traffic. Both the speed and traffic flow are exceptionally high in the elevated part due to less entrance and exit to the other roads of the network. Nevertheless, there are still some different in the structural and morphological characteristics.

- ***Xudong Road – high speed and heavy traffic double-layer main road***

The elevated part of Xudong Road is 10.6 m high and goes across the Youyi Avenue in the north. The Xudong Road is part of the Wuhan Avenue, one of the key arteries of the Wuhan city, which goes across the Second Wuhan Yangtze River Bridge at about 1 km away in the north of the intersection, which is one of few gigantic thoroughfares that running across the Yangtze River and connecting the two major urban areas of Wuhan divided by the river. Thus, a huge amount of traffic is concentrated on the Xudong Road.

The traffic concentration on this section of the Xudong road is considerably large due to its location. The 8-carriageway ground part has 3872 veh/h with 12% heavy vehicles, while the 6-carriageway elevated road has 3876 veh/h with 5% heavy vehicles. The traffic speed is 33km/h and 49km/h respectively. It can be seen that there is certainly massive noise emission from both parts of the road.

- ***Luoshi Road – high speed and elevated double-layer road with barriers***

The Luoshi Road is one of the busiest major thoroughfares of the transportation system of Wuhan, and in the selected area the road section has two layers with an elevated road of at least 18 m wide.

According to the in-situ statistical data, the elevated part of the Luoshi Road has a traffic flow of 3930 veh/h with 4% heavy vehicles, and the measured average speed is 60 km/h. The ground part of the Luoshi Road has a traffic flow of 2016 veh/h with 2% of heavy vehicles.

The main carriageways of the ground part of the Luoshi Road turn towards the east and connect with the Hongshan Side Road at the intersection, except the two auxiliary carriageways with very few traffic, extend towards the north, and are stopped by the green space, and ended in the residential communities.

The Hongshan Side Road has a traffic flow of 2238 veh/h with 6% of heavy vehicles, and the average speed is 22 km/h. The Chagang Road is the inner road of the Wuhan University and connects with the Luoshi Road at a T-shaped intersection. The access to the community is limited and only permitted cars can get through. But there is no fence and most of the vehicles entering have permissions and therefore, almost no vehicles will

be stopped for inspection. Hence, the speed of the Chagang Road is guaranteed at 20km/h averagely. And the traffic flow is 444 veh/h without heavy vehicles.

5.4.1.4 Noise sources

In both areas, the traffic on the elevated layer and the ground layer are the major sources of noise. In the shielded area behind the flanking buildings, there may also be some event noise, while considering the intensity of the traffic noise in the street canyon and the high-density and middle-rise buildings, the impact of the event noise is not considered when the receiver points are selected and measured. As a measure of eliminating unnecessary influences, any in-situ measurement that has been affected by irregular event noise is excluded from the examination to ensure that only the traffic noise is analysed in this study.

5.4.2 General calculation accuracy and applicability examination of the default reflection calculation method

A series of calculation is carried out to examine the applicability of current noise calculation methods in both sites, the errors occur in the calculations are then systematically compared and analysed. The calculation is conducted using the optimised configurations with no correction for opposite reflection. Due to the hardened ground surface in both sites, the absorption coefficient of the ground is both set to 0, and individual patches of ground absorption areas with higher absorption coefficient are set individually, e.g. soft soil ground and plant green isolation belt between the road lanes, etc. The locations of the receiver points are selected in the Xudong Road area based on both the acoustical and morphological features. The locations of the receiver points are shown in the two noise maps seen in Figure 5.36 and Figure 5.37.

It can be seen that in the both cases the receiver points are selected surrounding the flanking building and inside the street canyon. In both areas, there are also some points measured further inside the built-up area fully or partially shielded by the flanking building. To examine the performance of the current package on the simulation of the elevated part of the road, some receiver points are selected approximately at the same horizon and at higher altitude on the façade of the flanking buildings. In the Xudong Road

area, the focus is given to the large-scale building complex, where point E03 above the edge of the parapet wall is measured to calibrate the traffic noise from the elevated road. A series of receiver points are selected on the roof of the podium and in the partially shielded area close to the façade of the erecting residential tower from the podium to the rooftop of the tower. In the Luoshi Road case, the point E07 at the roof edge of a low-rise building and just 5 m next to the noise barrier of the elevated road. To study the noise transmission beneath the concrete base of the elevated road, some receiver points are also measured close to or under the elevated road in both case.

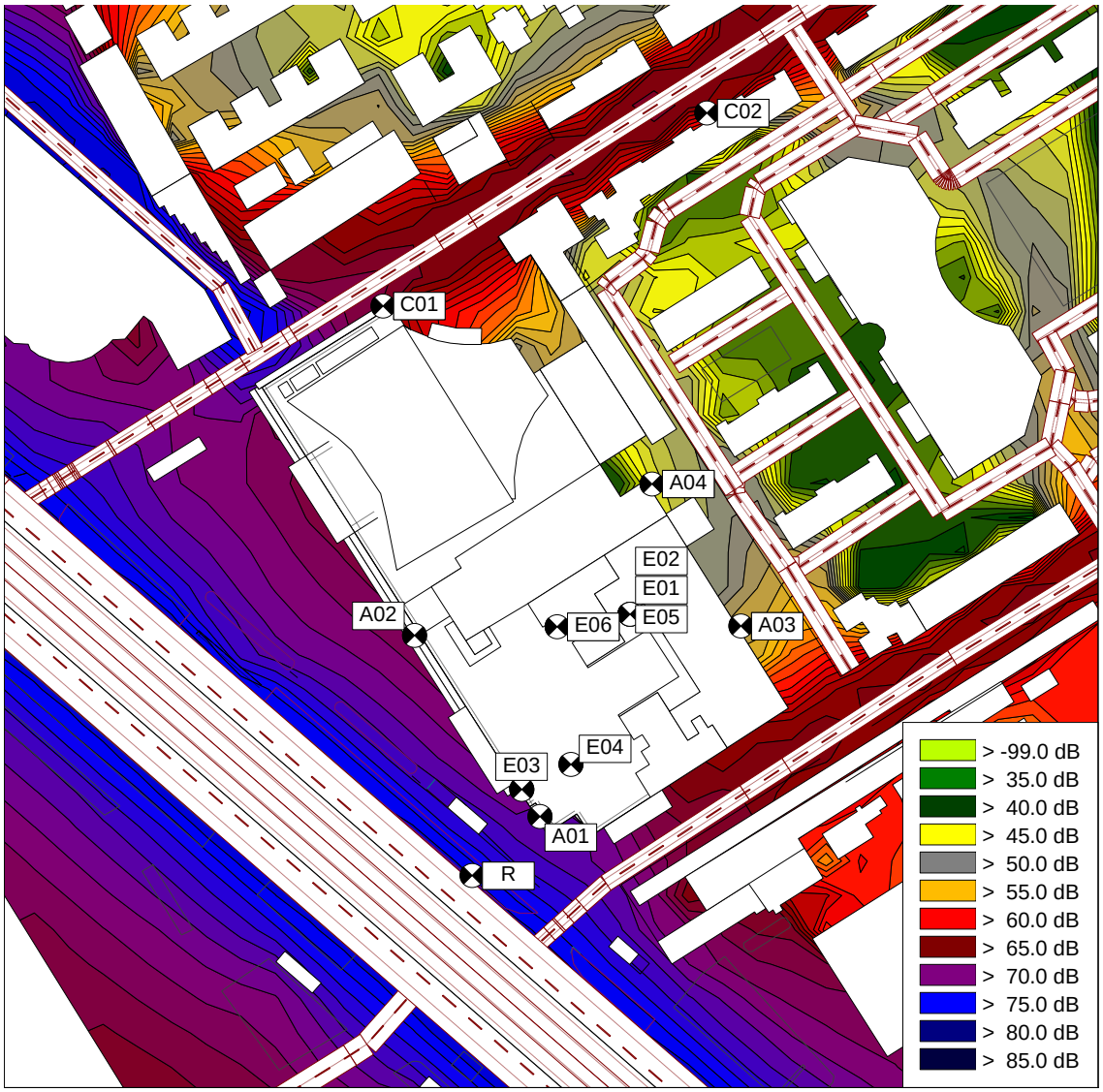

Figure 5.36 Noise map and receiver locations in the relatively open street canyon – Xudong Road area

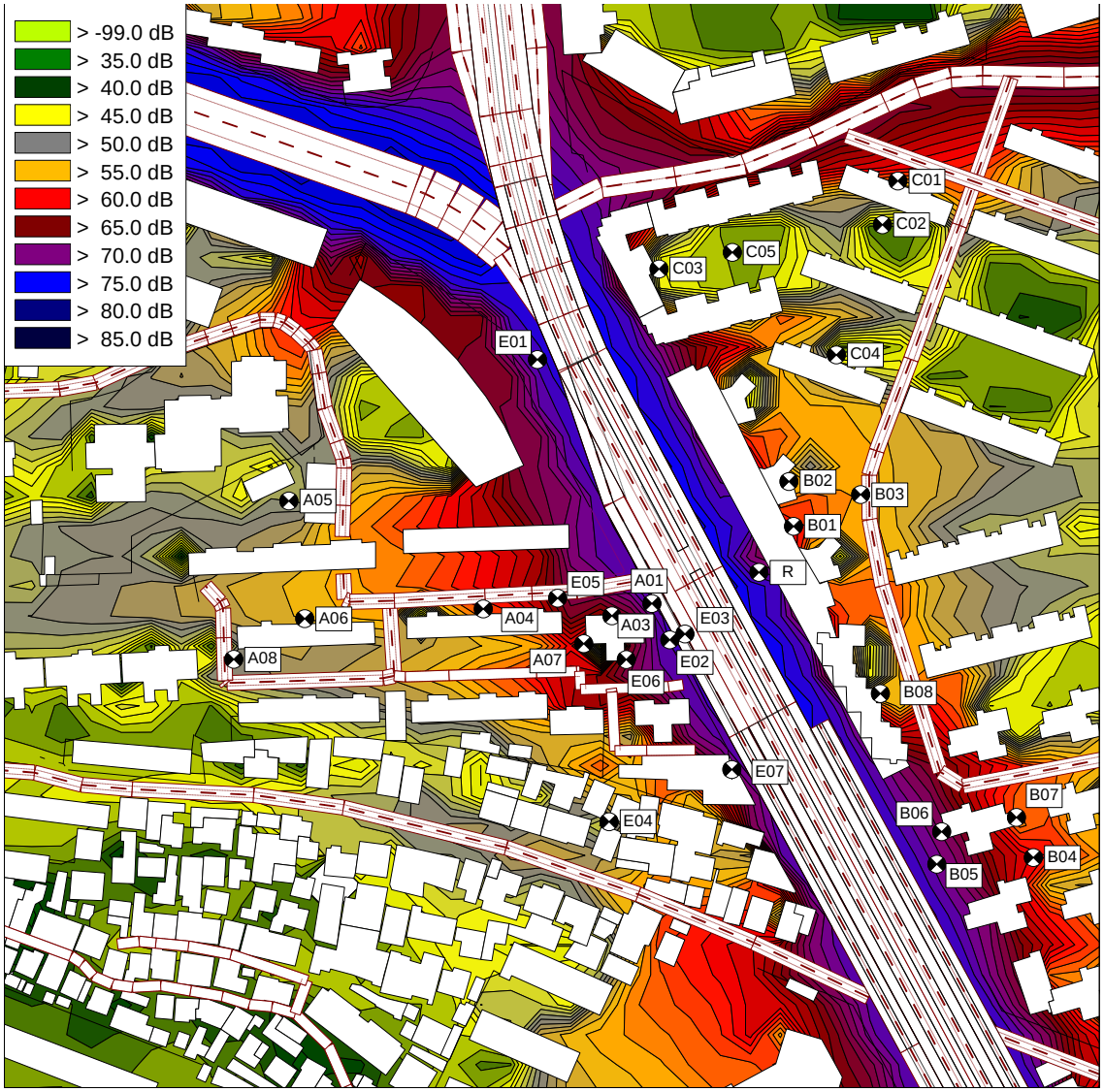

Figure 5.37 Noise map and receiver locations in the relatively confined street canyon – Luoshi Road area

5.4.2.1 General calculation accuracy level

A series of calculation are conducted using the optimised configuration for façade reflection calculations, due to the complicated spatial features in both cases, the calculation is conducted using increasing maximum order from 0 to 4. The results and the statistical parameter of each set of calculation are demonstrated in Table 5.16, Table 5.17, Figure 5.38 and Figure 5.39. The errors of the calculation using maximum reflection order of 4 are compared below. It is found that the calculation accuracy in the relatively more open space in the Xudong Road area is generally better than that in the confined and more

complicated space of the Luoshi Road case, as can be seen in Table 5.16 and Table 5.17 that the MAE of the former is 0.7 dBA lower than that of the latter.

Table 5.16 Error statistics of all receiver points – Xudong Road area

	Rf=0	Rf=1	Rf=2	Rf=3	Rf=4
Mean (dBA)	-4.7	-1.3	-0.1	0.4	0.7
SD (dBA)	7.4	5.5	4.5	4.2	4.1
MAE (dBA)	6.5	4.5	3.6	3.4	3.4

Table 5.17 Error statistics of all receiver points – Luoshi road area

	Rf=0	Rf=1	Rf=2	Rf=3	Rf=4
Mean (dBA)	-8.3	-5.2	-4.2	-3.7	-3.4
SD (dBA)	5.7	4.6	4.0	3.8	3.7
MAE (dBA)	8.6	5.7	4.8	4.3	4.1

It is also notable that generally in both cases the performance of the calculation method is more desirable on the receiver points inside and around the street canyon than those that are either shielded behind the flanking buildings or screened by major obstacles and barriers. Nevertheless, due to the peculiar morphological characteristics shaped by the elevated road, there are also some exceptions beneath or close to the elevated road.

5.4.2.2 Xudong Road area

In the Xudong Road case, the calculation accuracy is generally acceptable. When the reflection order is set to 4, the MAE is 3.4 dBA with a mean error of 0.7 dBA and an SD of 4.1 dBA. As can be seen in Figure 5.38, the highest absolute error of -7.0 dBA occurs at point E05 that locates far from the road source on the rooftop of the podium building and being shielded by the extruding parts of the residential tower.

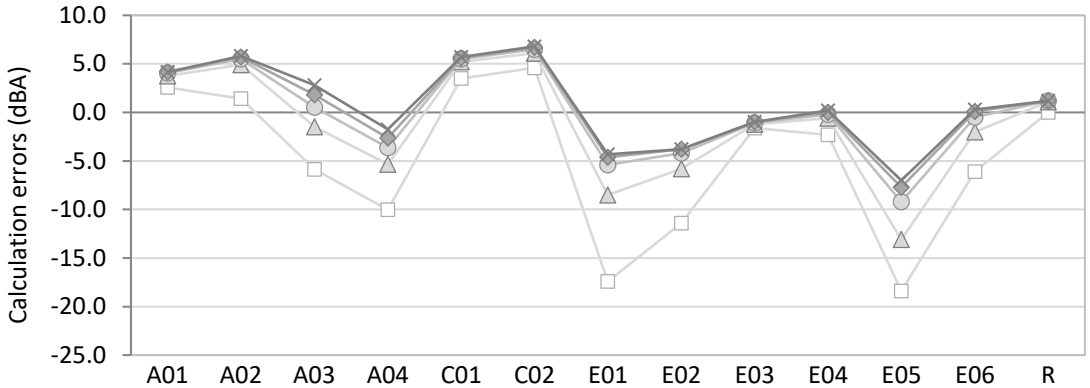

	A01	A02	A03	A04	C01	C02	E01	E02	E03	E04	E05	E06	R
Rf=0	2.6	1.4	-5.9	-10.0	3.5	4.6	-17.4	-11.4	-1.6	-2.3	-18.4	-6.1	0.0
Rf=1	3.8	4.9	-1.5	-5.3	5.2	6.1	-8.5	-5.8	-1.2	-0.6	-13.1	-2.0	1.1
Rf=2	4.1	5.5	0.5	-3.6	5.5	6.5	-5.4	-4.2	-1.1	-0.2	-9.2	-0.5	1.2
Rf=3	4.2	5.7	1.8	-2.6	5.6	6.7	-4.6	-3.8	-1.0	0.0	-7.7	0.1	1.2
Rf=4	4.2	5.8	2.8	-1.7	5.7	6.8	-4.3	-3.8	-1.0	0.2	-7.0	0.3	1.2

Figure 5.38 Calculation errors with increasing reflection order – Xudong Road area, increasing maximum reflection orders has limited error-reduction effect when Rf is higher than 1.

Some ground receiver points with direct exposure to the noise sources also have high errors. The two ground façade receiver points A01 and A02 that being measured close to the flanking façade of the podium block as well as the two receiver points C01 and C02 that being measured along the smaller road perpendicular with the Xudong Road, also have relatively higher errors ranging from 4.2 dBA to 6.8 dBA.

The error occurred at six receiver points locating above the podium building varies. The three points E03, E04 and E06 locating on the podium surface have the smallest errors among all points. The three receiver points E05, E01 and E02 locating inside the shielded corner close to the façade of the residential tower on different heights have relatively higher errors and which decreases with height increasing.

5.4.2.3 Luoshi Road area

For the Luoshi Road case, the level of accuracy is less desirable in general comparing with that of the Xudong Road case. The SPL at the selected receiver points is mostly underestimated: the MAE is 4.1 dBA, with a mean error of -3.4 dBA and an SD of 3.7 dBA. From Figure 5.38 it can also be seen that the distribution of errors fluctuates evidently. There are six receiver points having the absolute error of over 6.0 dBA among all 24 measured receiver points, especially the receiver points that locates in the shielded

areas behind the flanking buildings along the street canyon. The highest error occurs at point A05 and C03 that are completely screened by one or more buildings from the road noise source as can be seen in Figure 5.37, at both points the calculated SPL are underestimated for over 10.0 dBA.

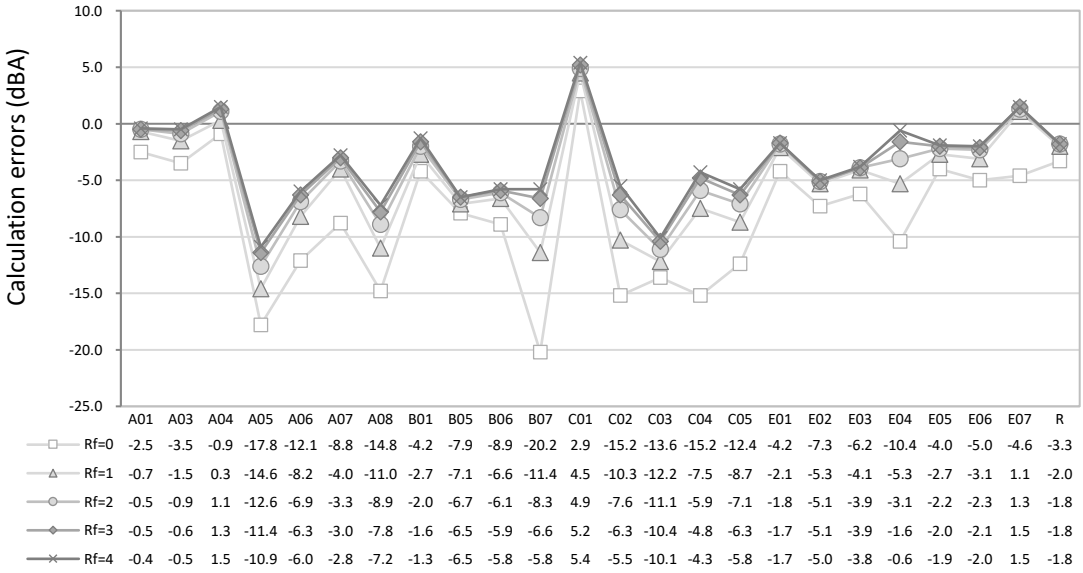

	A01	A03	A04	A05	A06	A07	A08	B01	B05	B06	B07	C01	C02	C03	C04	C05	E01	E02	E03	E04	E05	E06	E07	R
Rf=0	-2.5	-3.5	-0.9	-17.8	-12.1	-8.8	-14.8	-4.2	-7.9	-8.9	-20.2	2.9	-15.2	-13.6	-15.2	-12.4	-4.2	-7.3	-6.2	-10.4	-4.0	-5.0	-4.6	-3.3
Rf=1	-0.7	-1.5	0.3	-14.6	-8.2	-4.0	-11.0	-2.7	-7.1	-6.6	-11.4	4.5	-10.3	-12.2	-7.5	-8.7	-2.1	-5.3	-4.1	-5.3	-2.7	-3.1	1.1	-2.0
Rf=2	-0.5	-0.9	1.1	-12.6	-6.9	-3.3	-8.9	-2.0	-6.7	-6.1	-8.3	4.9	-7.6	-11.1	-5.9	-7.1	-1.8	-5.1	-3.9	-3.1	-2.2	-2.3	1.3	-1.8
Rf=3	-0.5	-0.6	1.3	-11.4	-6.3	-3.0	-7.8	-1.6	-6.5	-5.9	-6.6	5.2	-6.3	-10.4	-4.8	-6.3	-1.7	-5.1	-3.9	-1.6	-2.0	-2.1	1.5	-1.8
Rf=4	-0.4	-0.5	1.5	-10.9	-6.0	-2.8	-7.2	-1.3	-6.5	-5.8	-5.8	5.4	-5.5	-10.1	-4.3	-5.8	-1.7	-5.0	-3.8	-0.6	-1.9	-2.0	1.5	-1.8

Figure 5.39 Calculation errors with increasing reflection order – Luoshi Road area, the effect of error reduction by increasing the maximum reflection orders is obvious.

In the Luoshi Road area, due to the limited building height, most of the receiver points are selected on the ground level near or inside the street canyon. As can be seen from Figure 5.37 and Figure 5.39 that most of the receiver points that locate inside the small-scale street canyon or in the close-by area with exposure to the direct noise from the Luoshi Road, the disparities between the calculation and measurement are relatively small. Meanwhile, the receiver points that are shielded by flanking buildings or locate far from the main road source have much larger errors. For instance, the point A05, A07 and A08 which are direct impacted by the main road but locating far from it; and all the C-series receiver points and part of the B-series points which locate close to the main road, while the emission from the road source to which are largely screened by the flanking buildings.

For receiver points which mostly locate inside the street canyon space and close to the Luoshi Road, it is interesting to notice that point E02 and E03 which locates the closest to the road source have the highest calculation errors, which is potentially caused by the particular morphology of the confined street canyon that causing more reflections.

5.4.2.4 Summary

Generally, in both cases, the increasing of maximum reflection order is helpful for improving the calculation accuracy but only to a limited extent when the maximum reflection order is raised approaching 4 as can be seen in Figure 5.38 and Figure 5.39.

Nevertheless, it is also noticeable that the improvement of accuracy level in the large-scale street canyon with the wide and open elevated road is less obvious than that in the small-scale street canyon with confined elevated road. As can be seen inTable 5.16 and Table 5.17 that when maximum reflection order is raised from 0 to 4, the total deduction in MAE in the Xudong Road case is 3.1 dBA, and that in the Luoshi Road case is 4.5 dBA. Moreover, in the Xudong Road case the MAE remains 3.4 dBA when the maximum reflection order is raised from 3 to 4, meanwhile in the Luoshi Road case, the MAE keeps decreasing for 0.2 dBA, it indicates that in the Luoshi Road case there can be potentially more improvement in the calculation accuracy by raising the maximum reflection order.

It is also found in both sites that at some receiver points the improvement brought by the increasing of maximum reflection order is more distinctive. The potential causes are discussed in the sections below to find which particular urban form and acoustic characteristic may have caused the differences.

5.4.3 Test on the calculation configurations and modelling method beneath the elevated road

For receiver points were locating lower or right beneath the elevated roads in the street canyon, the errors vary depends on the particular location of the point locates. The modelling method of the elevated road by default is to apply the self-screening option to the elevated roads to simulate the screening effect as can be seen in Figure 5.40 (DataKustik, 2012a). By applying this setting, the surface of the elevated road will only entirely screen the direct noise transmission through the road slab.

The issue lying in the calculation using the default option is that the reflection caused by the bottom of the elevated road is not calculated, given the fact that there are actually two extra road sources beneath the elevated road. At the same time, the diffraction via the edge of the road slab is also ignored by default (DataKustik, 2012a).

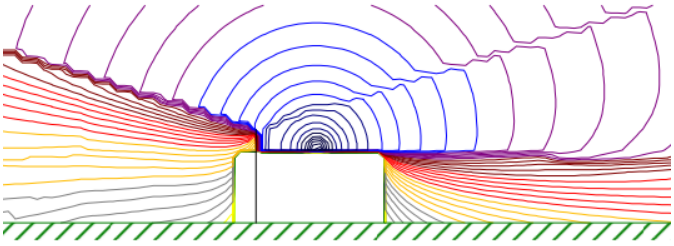

Figure 5.40 The sound level distribution in a vertical plane when the road is elevated with a vertical barrier installed on one side. Source: Cadna/A Reference Manual (DataKustik, 2012a).

Therefore, the object type 3D reflector is introduced in the modelling process to substitute the default recommendation of self-screening roads or bridges. The 3D reflector as an object type is a flat plane without thickness and a certain absorption coefficient could be configured on both sides of it. Another feature of the 3D reflector is that the refraction at all edges can be calculated or switch off while the objects of the bridge and the self-screening roads without barrier both cannot have the diffractions calculated (DataKustik, 2012a). As can be seen in Figure 5.41 that by attaching 3D reflectors right beneath an elevated road with extra road source beneath it, there is an apparent difference in noise transmission patterns occur on both sides of the elevated road. (DataKustik, 2012a)

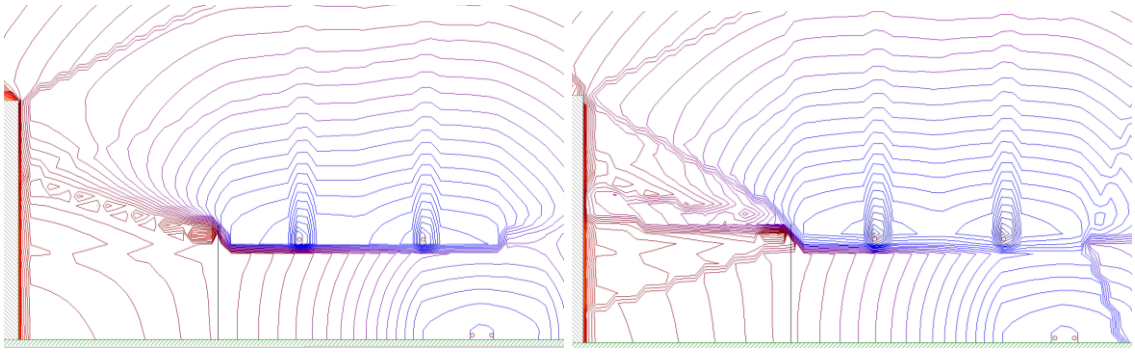

a b

Figure 5.41 Cross section view of a case for demonstration without (a) and with (b) consideration of the bottom reflection when there is one extra source beneath an elevated road – Luoshi Road area, the bottom refleciton effect seems to be largely neglected in the default modeling method.

Moreover, the structure of the concrete slabs is as thick as 2 m with surface shape beneath both of the Xudong Road and the Luoshi Road elevated part, as can be seen in Figure 5.32. The object type of the bridge is not suitable to use to simulate the base of the elevated road, as there will also be no underneath reflection and diffraction considered. Thus, the

3D reflectors together with reflective barriers are combined to model the elevated road base. It is to note that the barriers here attached to the side of the elevated road base are set to be reflective rather than absorptive. The cantilevered barriers installed upon the parapet of the Luoshi Road elevated part are modelled according to its shape and absorption coefficient.

As can be seen in Figure 5.41 that with the 3D reflector installed beneath the elevated road base instead of using the bridge, the noise distribution in the space in-between the building and the road kerb is evidently changed.

5.4.4 Calculation error of the receiver points below the elevated road at different distance

In each case, there are a series of receiver points selected locating inside the street canyon, and below the elevated road, the effect of the peculiar urban environment on the calculation accuracy of these receiver points are analysed.

In the Xudong Road area on the ground level below the elevated road, the increase of maximum reflection order has evident negative effects on the calculation accuracy of receivers and is more profoundly at a further distance from the road and close to the building façade. There are three receiver points measured on the ground level at a different distance from the road kerb: point R, A01 and A02 as can be seen in Figure 5.42. From Figure 5.43 it can be seen that the roadside point R has the most desirable accuracy level, the error of which only rises for 0.1 dBA when the maximum reflection order rises from 1 to 2 and higher. It may mainly due to that the direct noise level at point R is already relatively high and the reflections from other surfaces have very limited impacts on its result.

5.4.4.1 The Xudong Road area

For point A01 and A02 that both locate further away from the road edge with different slant distance, the negative effect of the increased maximum reflection order on the calculation accuracy is more evident. When the maximum reflection order rises from 1 to 2, the error at point A01 rises for 0.3 dBA and remains steady when it keep rising. Meanwhile, the error at the A02 rises for 0.6 dBA and keeps rising slightly for 0.2 and

0.1 dBA when the reflection order rises higher to 3 and 4. It can also be seen that the error at point A02 is 1.1–1.6 dBA higher than that of the point A01when the reflection order is higher than 1.

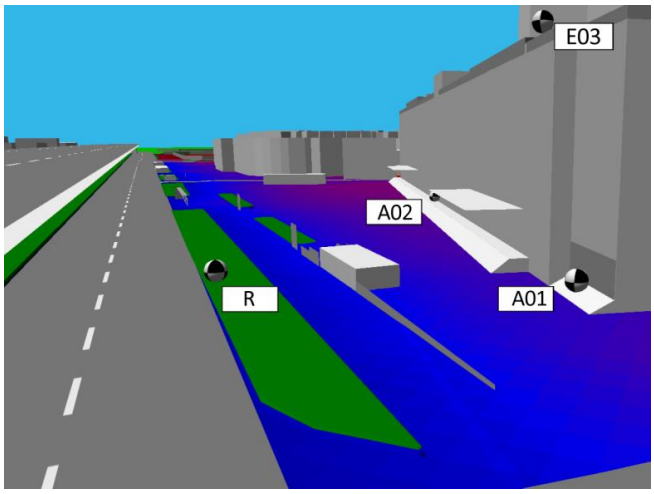

Figure 5.42 The receiver points below the elevated road – Xudong Road area

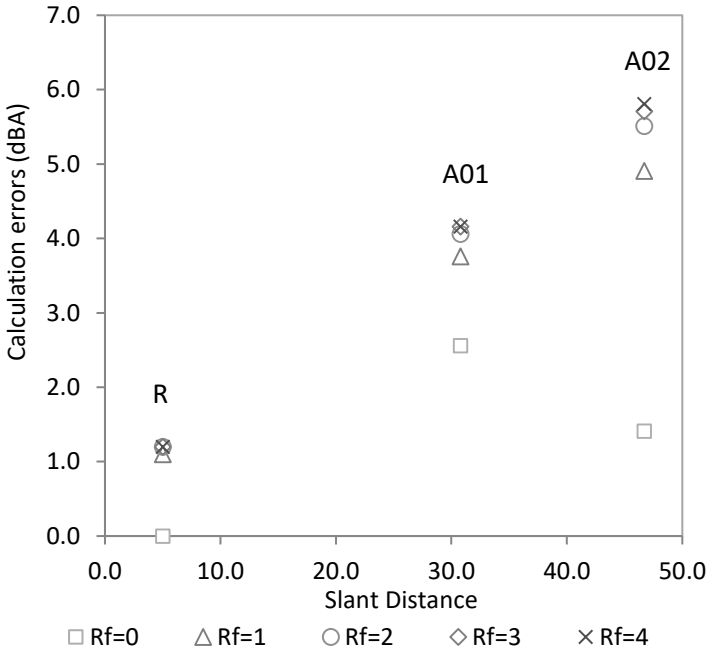

Figure 5.43 Calculation errors of the receiver points below the elevated road at different distance – Xudong Road area

As can be seen in Figure 5.42 that both point A01 and A02 locate close to the façade of the façade of the podium building. Nonetheless, the slant distance from road source at A02 is 15.9 m further than that of A01, which makes the point A02 and the neighbouring façade exposed to the traffic noise from the elevated road more than A01. This may

suggest that the increase of reflection orders may cause overestimate of noise impact from the elevated road to the ground in general when the street canyon is much wider than the elevated road.

It is also notable in Figure 5.43 that when there is no specular reflection calculated the absolute error at point A02 1.2 dBA lower than that of the A01. Nonetheless, when the reflection order is just turned on from 0 to 1, the calculation error at point A2 leaped for 3.5 dBA from 1.4 dBA to 4.9 dBA; that of the A01 only rises for 1.2 dBA from 2.6 dBA to 3.8 dBA. It is possibly caused by the overestimated reflections from the bottom surface of the elevated road slabs, as it is closer to the road kerb.

5.4.4.2 The Luoshi Road area

In the Luoshi Road area, there are six points locate below the elevated road in the street canyon, the locations of which are shown in Figure 5.44. The calculation errors and slant distance from the road source of these six points are demonstrated in Figure 5.45. Point E03 locates just beneath the base slab of the elevated road on the west side of the Luoshi Road, which also has the closest slant distance of 7.5 m to the source line among all points. Point E02 locates outside the shadow of the elevated road but still within a very close distance and there is a small stone embankment wall next to the pedestrian road and the space is relatively confined. As can be seen in both Figure 5.37 and Figure 5.44 that, other ground receiver points, e.g. point A01, R, B05 and B06 mostly locate in the relatively more open area and the slant distance from which are close.

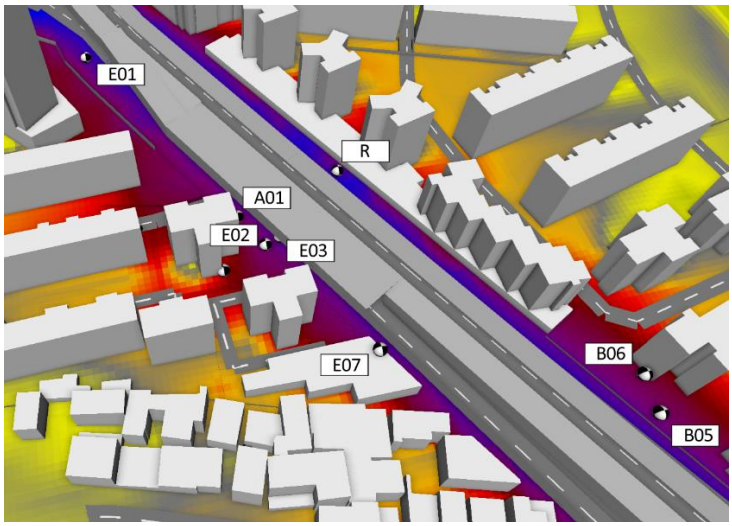

Figure 5.44 The receiver points below the elevated road – Luoshi Road area

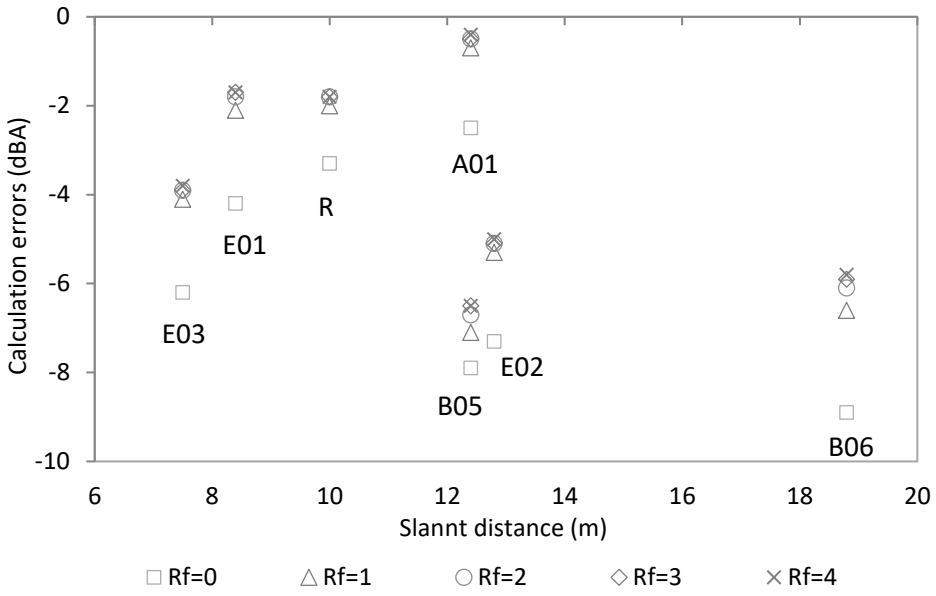

Figure 5.45 Calculation error and slant distance of the receiver points below the elevated road – Luoshi Road area

It can be seen in Figure 5.45 that at all points the results rise evidently when the reflection order increases, generally the errors hence become smaller. Nevertheless, at point E02 and E03, the largest errors of -5.0 dBA and -3.8 dBA occur when the reflection order is set to 4. The bigger error at these two points may be the consequence of multiple reflections occurred in the relatively confined space created by the ground, the elevated road, and the reflective façades of the flanking buildings and stone walls next to the pedestrian path next to the road.

The absolute error at point R, A01 and E01 are all smaller than 3.0 dBA. The slightly larger errors at B05 and B06 are potentially due to the closer distance to the exit ramp of connecting the elevated road. The declining slope and the attached barrier make it difficult to model it accurately hence increase the chance error.

Generally, in both cases, it can be seen that the calculated SPL is raised evidently when the maximum reflection order is increased, the calculation errors also change correspondingly. Nonetheless, at the relatively confined Luoshi Road area, there are larger errors in the relatively more confined spaces beneath the elevated road and close to the surrounding reflective façades.

5.4.5 *Effect of the large podium and the high-rise building*

A series of receiver points are chosen on the large-scale podium building and close to the façade of the high-rise residential buildings that are erecting on the podium, to study how the traffic noise from the elevated road propagates through the edge of the podium and impacts the residential buildings.

As can be seen in Figure 5.46, the point E03, E04, and E06 locates closer to the road and spreading at different locations on the open surface of the podium. The receiver points E05, E01 and E02 locates in the partial shield area close to the building façade at 5th, 12nd, and 24th floor, with the height of 22.4 m, 42m and 75.6 m respectively. The calculation results at all six receiver points using different maximum reflection order settings are shown in Figure 5.47.

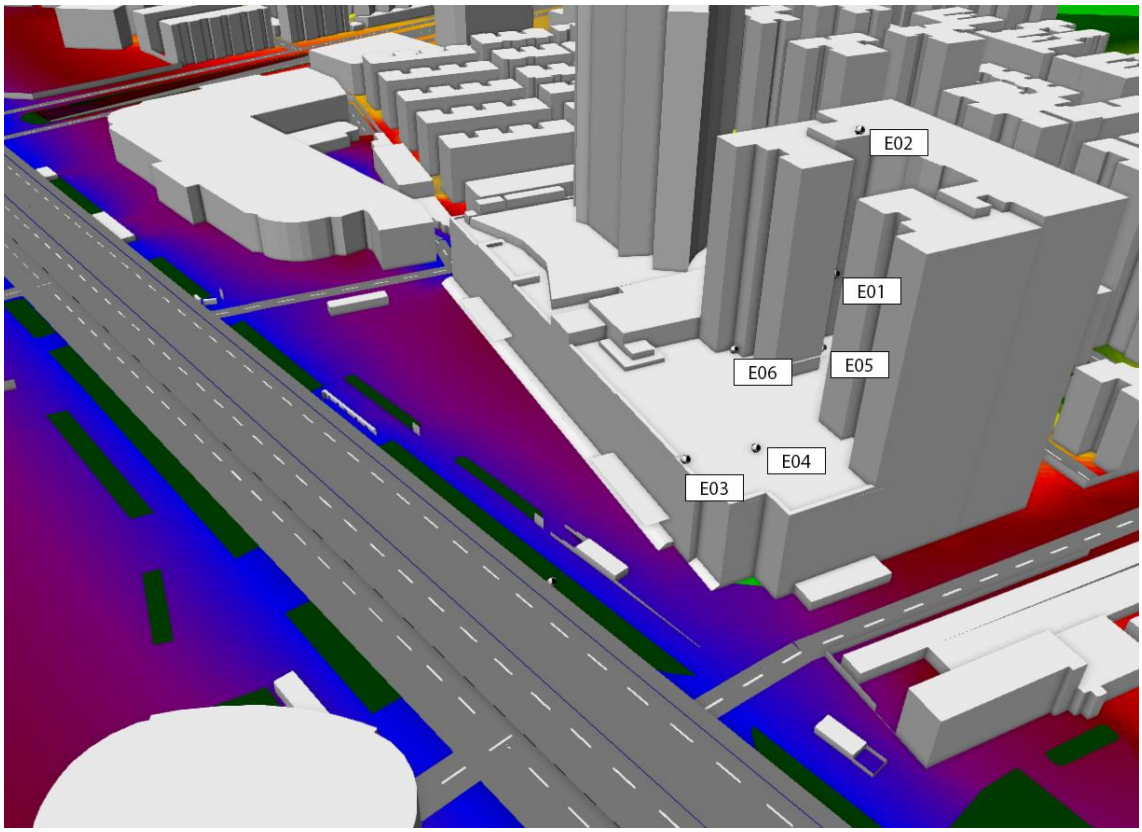

Figure 5.46 Locations of receiver points above the podium – Xudong Road area

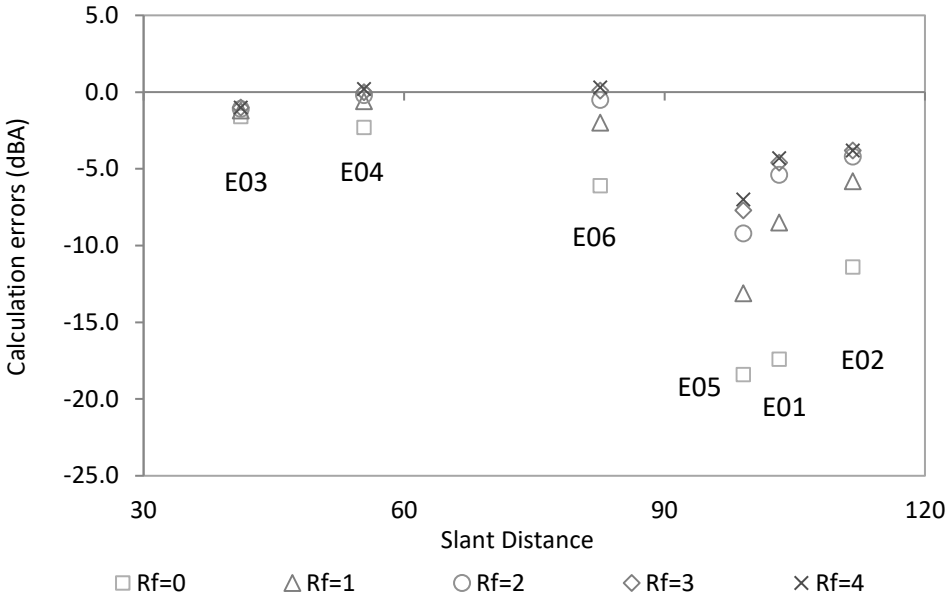

Figure 5.47 Calculation error and slant distance of the receiver points above the podium building – Luoshi Road area

Firstly, from the calculation results in Figure 5.47 it can be seen that when the maximum reflection order increases, the calculation error decreases rapidly except at point E03, at which the error does not change along with the increasing reflection order. At point E04 that locates in the centre of the podium, the absolute error improves for 1.7 dBA when the maximum reflection order rises from 0 to 1, and then remains relatively lower than 1.0 dBA.

Secondly, it is noted that the errors of the receiver points tend to be much larger in at E05, E01, and E02 in the corner that is hugely shielded by the extruding part of the residential building. Especially at point E05 that locates 1.5 m above the podium building and the direct transmission from all road sources are screened by the surrounding façades, where the error is as big as -7.7 dBA when the maximum reflection order is set to 3. In the meantime, the errors at point E01 and E02 are slightly better than that of point E05, which is potentially due to the higher altitude that allows the topside diffractions from remote segments of the elevated road via the top edges of the residential building to reach and be calculated, as can be seen in Figure 5.48. The error at the point E02 of -3.8 dBA is the smallest among these three shielded receiver points, it may because that the point E02 locates on the top edge of the residential building hence the diffractions from multiple sources could reach more easily and the calculation can be more accurate.

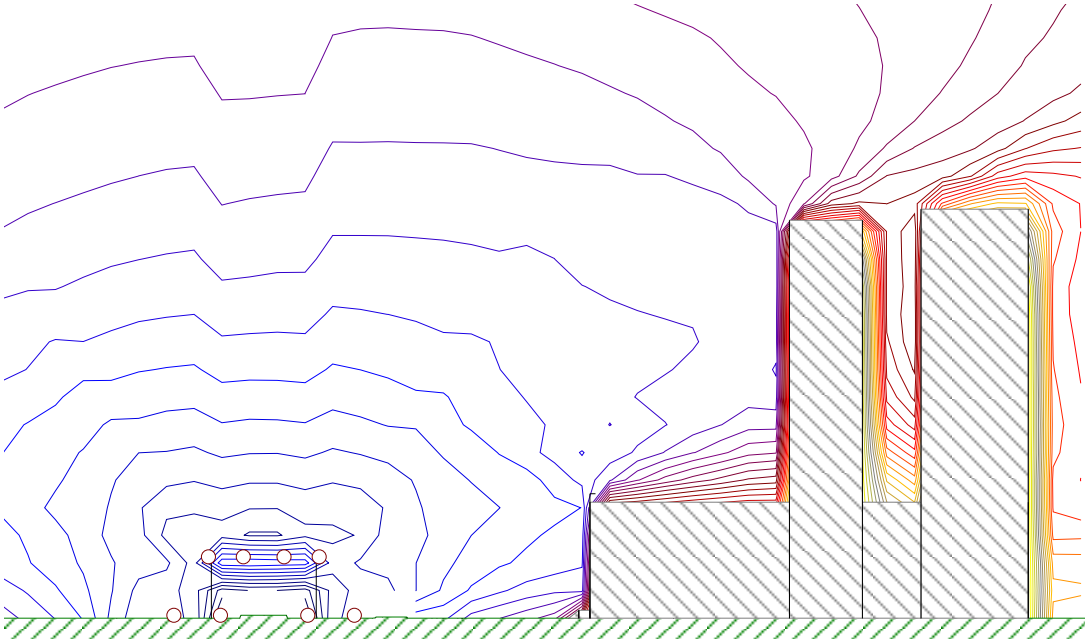

Figure 5.48 Cross section view for the propagation of traffic noise from the elevated road – Xudong Road area

Generally, the noise transmission above the podium in the Xudong Road area is relatively more accurately simulated comparing with that of the similar scenarios in the non-elevated Youyi Avenue street canyon as mentioned in Section 5.3 of this chapter. As can be seen in Figure 5.48 that the elevated part of the main road raises the noise source lines and reduces the screened direct transmissions through the podium. In the meantime, the relatively larger podium surface area allows more freely noise propagation and less influence from specular reflections from the façades of the high-rise residential buildings and flanking façades on the opposite side of the main road. Hence, the propagation of noise from multiple noise sources of the ground and elevated part of the Xudong Road can be simulated relatively more accurately.

5.4.6 Effect of the Noise Barrier

There are noise barriers installed on both sides of the elevated part of the Luoshi Road and its adjunctive exit ramps, the effect of the noise barrier is studied in the Luoshi Road area. Due to the small distance from the road to the building façades, the barriers play a significant role in screening the impact from the heavy traffic noise towards the residential buildings flanking to the elevated road.

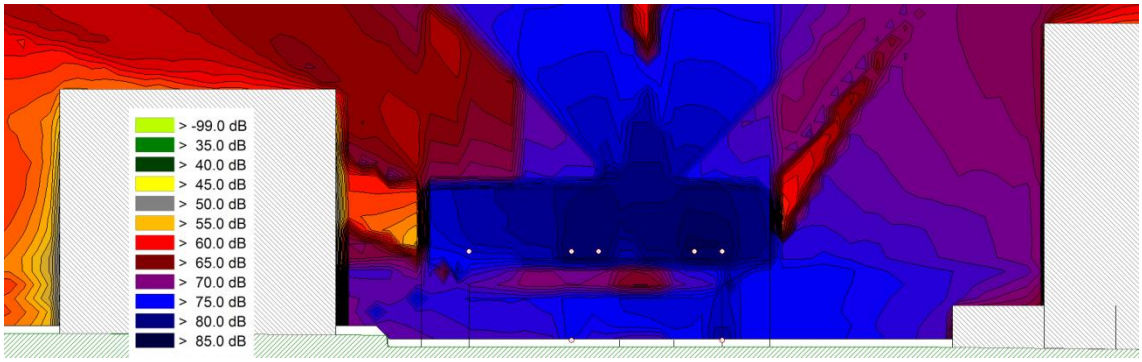

Figure 5.49 Cross section view of the elevated road with barrier – Luoshi Road area

Nevertheless, the barriers also bring issues in the simulation accuracy using current noise calculation method. For instance, in Cadna/A there are explicit instructions of how to simplify the barriers into the real model but there is also limitations in the calculation, especially when the shape and condition of the cantilevered barriers are relatively complicated which is common in the noise barriers design for roads with high traffic noise (J. Kang, 2006). As can be seen in the cross-section view of the Luoshi Road area in Figure 5.49 that the transparent noise barrier of 6-m tall with galleried cantilever nearly seals the topside of the elevated road, the noise distribution is hence largely confined inside the narrow space created by the elevated road and the cantilevered barrier.

To test the applicability of the current noise mapping method in the given acoustic environment, there is one receiver point the point E07 in the Luoshi Road area are measured next to the barrier on the roof of an adjacent building. It can be seen in Figure 5.39 when the maximum reflection order is 3 the error at point E07 is -2.2 dBA, which is within an acceptable range. It indicates that the simulation of the direct screening effect of the confined barrier is acceptable.

Nonetheless, this situation in the Xudong Road case is not as complicated, because there are no barriers installed along either the elevated road or on the ground as shown in Figure 5.48, instead there are only reflective concrete parapets of approximately 1-m tall erecting on both sides of the elevated road, this may be due to the large distance from the road kerbs to the flanking building façades and cost concerns. Nevertheless, it is also seen that the noise impact to the high-rise residential buildings is quite severe due to the heavy traffic flow on the elevated road, thus, it is still interesting to know what difference it could make if similar cantilevered barriers are installed on the elevated road.

5.4.7 Calculation error at different frequencies

The measured and calculated SPL at different central frequencies of eight major octave bands are calculated using maximum reflection order setting of 3. The line sources representing the road noise are validated systematically based on the measurement results collected at relevant reference points before calculation.

5.4.7.1 Wide open street canyon – Xudong Road area

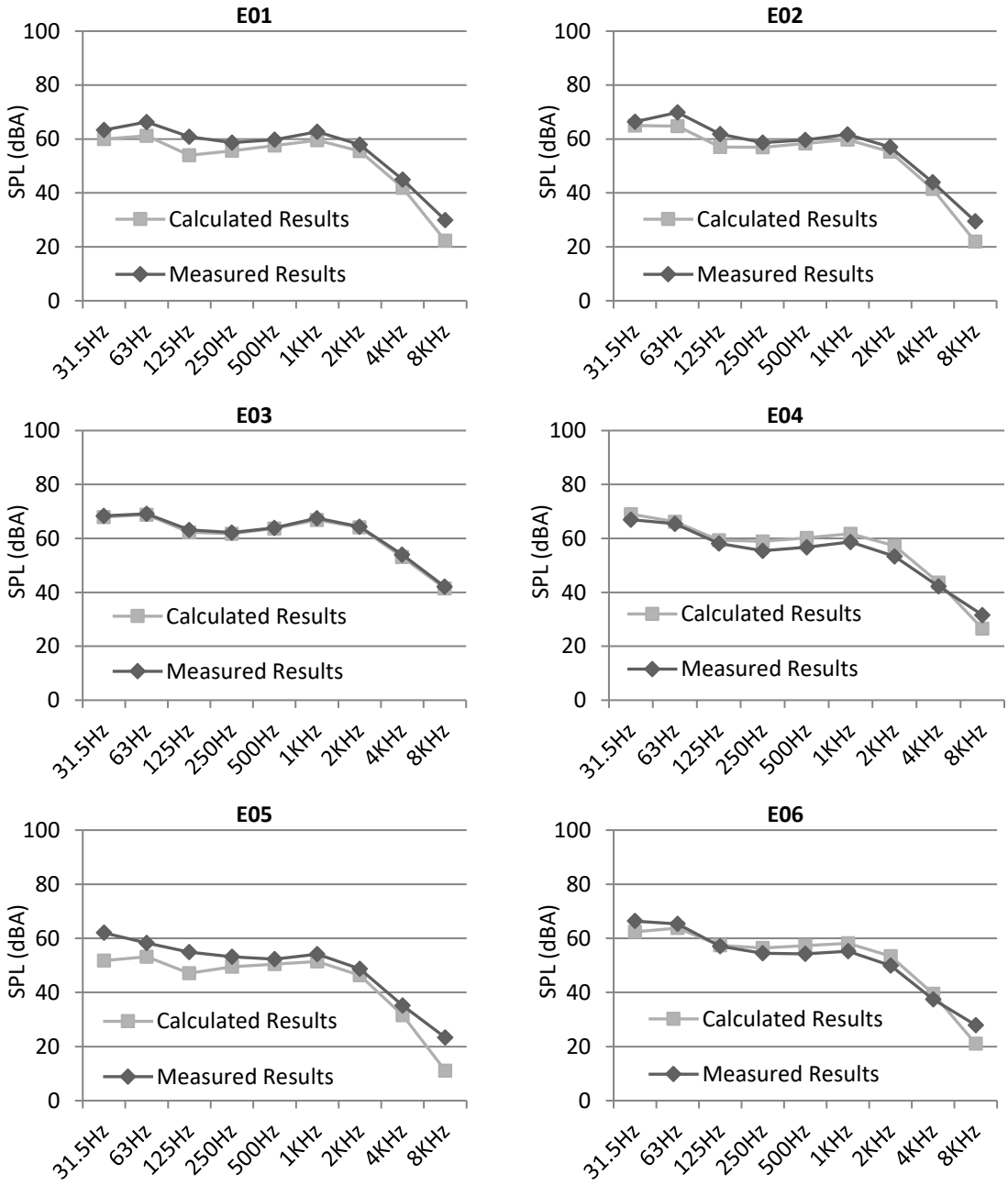

Figure 5.50 Measured and calculated noise level spectrum of the Xudong Road area

Table 5.18 SPL spectrum calculation errors at major octave bands central frequencies – Xudong Road area, errors with absolute value equal to or smaller than 3 dBA are highlighted.

	Calculation errors (dBA)								
	31.5 Hz	63 Hz	125 Hz	250 Hz	500 Hz	1 kHz	2 kHz	4 kHz	8 kHz
E01	-3.3	-5.1	-6.9	-3.1	-2.2	-3.2	-2.4	-3.1	-7.6
E02	-1.3	-5.1	-4.8	-1.7	-1.3	-2.0	-1.8	-2.5	-7.6
E03	-0.4	-0.3	-0.9	-0.5	-0.2	-0.6	-0.2	-0.8	-0.6
E04	2.0	0.7	1.2	3.5	3.5	3.0	3.9	1.4	-5.0
E05	-10.2	-5.1	-7.8	-3.7	-1.8	-2.8	-2.4	-3.5	-12.3
E06	-4.0	-1.6	0.3	1.9	3.0	2.9	3.5	2.0	-6.9

As shown in Table 5.18 and Figure 5.50 that in the Xudong Road area the errors at most of the receiver points in major frequencies are within acceptable range. Meanwhile, in the Luoshi Road area, it can be seen in Table 5.18 and Figure 5.51 that the calculation errors are less desirable comparing with the Xudong Road case. More results of the calculation are and discussed below.

In the Xudong road area, the errors at point E01 and E05 are the least favourable, among all six receiver points above the podium and close to the residential building, and the error mainly occurs at the relatively lower and higher frequencies. At both point E01 and E05, it can be seen that the errors at frequencies of 31.5–125 Hz, as well at the highest 8000 Hz are relatively lower. It may because that the direct transmission of the lower frequency noise from the elevated roads through the large-scale podium building and the extruding part of the residential towers are underestimated. Moreover, the transmission of lower frequency noise from remote road sources may also affect the result. For the higher frequency noise at 8000 Hz the errors may mainly due to the underestimated diffraction via the edge of the podium and the residential tower, as can be seen that for the other points the errors at 8000 Hz tend to be the smallest at point E03 which locates at the edge of the podium building and no diffraction need to be calculated, the E04 also has a relatively smaller error at 8000 Hz as it locates much closer to the elevated road than the rest of four receiver points.

5.4.7.2 Narrow confined street canyon with elevated road – Luoshi Road area

As can be seen in Table 5.19 and Figure 5.51 that, in the Luoshi Road area, the point E07 that locates on the rooftop of the two-storey building next to the noise barrier installed on the elevated road has the smallest errors and best accuracy among all seven receiver points. Only in the relatively higher frequencies of 4000 Hz and 8000 Hz, the errors are slightly larger. For the rest of receiver points locating lower than the elevated road, the errors tend to be larger, which indicates that the simulation of the screening effect of the noise barrier is generally acceptable. For points E01, E02 and E03 locating underneath the elevated road, the errors at most of the frequencies are lower than 3.0 dBA. It may be due to that in this relatively confined space, with the cantilevered noise barrier installed on the elevated road, the ground part of the Luoshi Road become the major source for the receiver points beneath the elevated road, thus the prediction is relatively more reliable. This is also owing to the improved modelling method, as mentioned in previous sections, by installing 3D reflector to simulate the bottom surface of the elevated road the calculation accuracy can be greatly enhanced.

Table 5.19 SPL spectrum calculation errors at major octave bands central frequencies – Luoshi Road area, errors with absolute value equal to or smaller than 3 dBA are highlighted.

	Calculation errors (dBA)								
	31.5 Hz	63 Hz	125 Hz	250 Hz	500 Hz	1 kHz	2 kHz	4 kHz	8 kHz
E01	4.0	2.8	2.3	2.9	1.5	-1.3	-0.1	4.8	4.9
E02	1.2	7.4	-0.8	1.7	2.3	2.8	3.4	3.0	-0.8
E03	-1.2	-1.4	3.3	1.9	1.7	2.6	3.2	2.0	-1.7
E04	0.9	-3.2	4.8	7.8	10.4	6.4	6.0	12.0	16.0
E05	4.4	5.3	2.8	1.3	3.9	3.8	4.7	5.1	4.6
E06	7.4	9.9	4.5	3.4	4.5	5.4	5.1	3.4	-1.7
E07	1.2	2.0	-0.9	-2.1	-1.0	0.0	1.7	3.7	-5.4

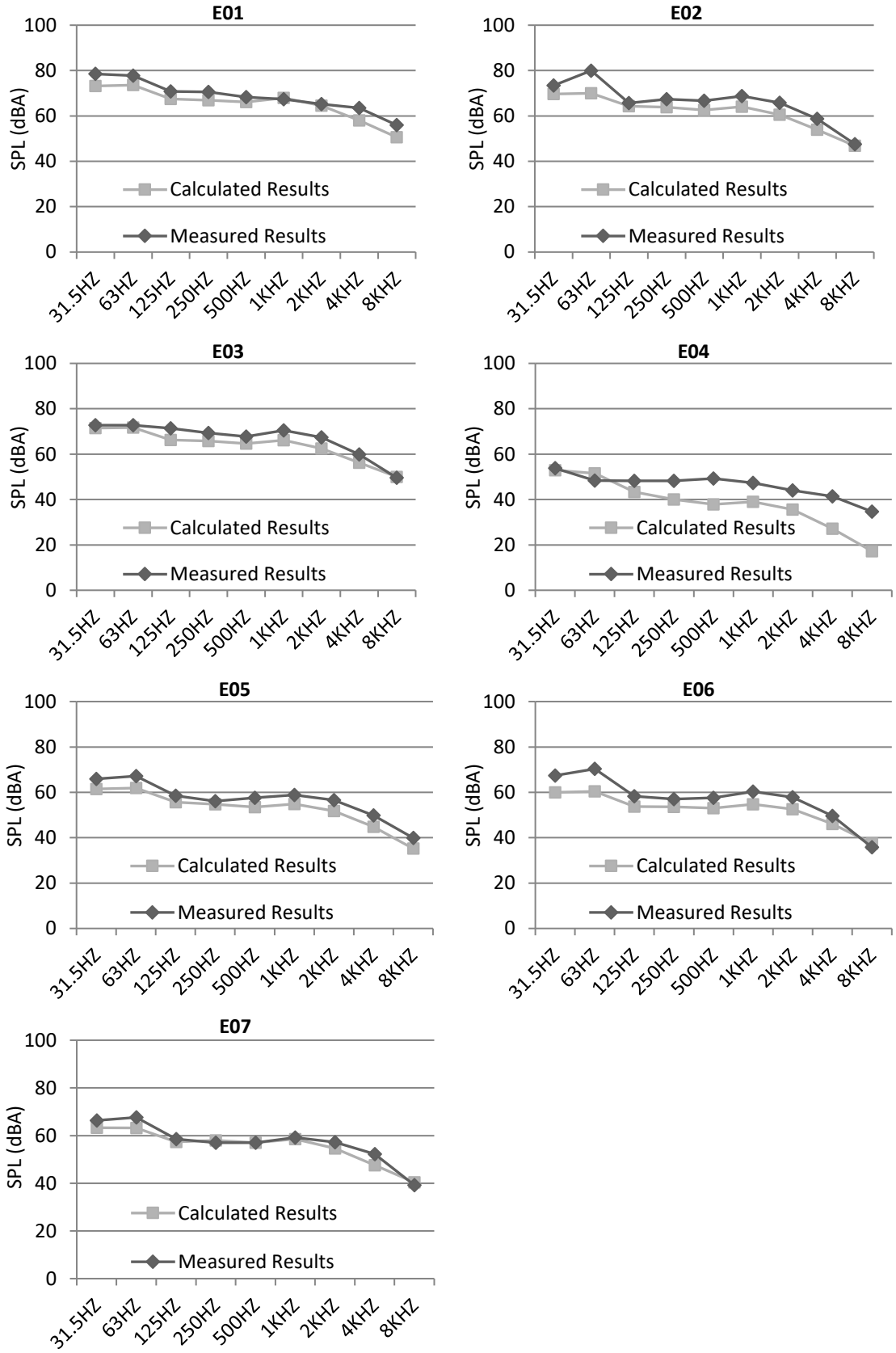

Figure 5.51 Measured and calculated noise level spectrum – Luoshi Road area

The accuracy level at the three receiver points locating farther from the road inside the residential area and the small urban village, the errors at most of the frequencies are not as desirable, especially at point E06, among all eight major frequencies only the error at 8000 Hz is within an acceptable range. It needs to be taken into consideration that the location of these three receiver points is upon a slightly uneven landform; the ground altitude is 1-2 m higher than that of the Luoshi Road ground part. For point E04, the measurement is conducted in a relatively confined space surrounded by low-rise and high-density residential buildings with low building quality. Thus, the errors of most of the frequencies may be affected by the edge of the landform, especially the stone wall dividing the residential community on the west side with higher ground altitude and the Luoshi Road with lower ground altitude.

5.5 Summary of the applicability tests

The selected case study areas menefest a series of representative Chinese urban morphological and building features commonly found in Chinese major cities. The features include high-density and low-rise urban village; the features of modern residential area with slat-shape residential flats; high-rise building towers on belt-shape podium building; main road street canyons with varying width and flanking building forms; and different forms of double-layered main roads with the elevated road, with or without confined noise barriers, etc. Some of the features can be found in different case areas.

By comparing the calculation results and the measurement results, it is found that the calculation accuracy using the selected EU noise method at most of the receiver points are within acceptable range. Nonetheless, systematic uncertainty is found in a series of scenarios that may cause higher inaccuracy level. The causes of some of the larger calculation errors are specifically analysed based on the spatial and acoustical characteristics of the urban space surrounding the receiver points. Some of the key urban morphological features and their influence in the calculation results and the recommendations of improvement measures in the noise mapping configuration and modelling process are listed in Table 5.20.

Table 5.20 Summary of typical Chinese urban morphological features influencing the compatibility of current noise calculation method

Typical urban morphology type		Cross section views	Calculation performance		Alternations to the simulation method			Improvement in max error (dBA)
Morphological type	Noise source type		Typical spatial feature / Location of the receiver	Max error[a] before the adjustment (dBA)	Configuration tuning	Change in modelling method	Max error after alternation (dBA)	
Urban village with high density and low-rise residential buildings	Main road with heavy traffic (Renghe Road)	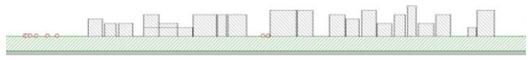	Amid the high-density and low-rise residential buildings of the urban village	-15.3 (E04)	Increasing maximum reflection order to 4	–	-15.1	0.2
				-11.5 (E03 at 500 Hz)	–	Adjusting the transparency ratio of the buildings	-1.9	9.6
High-rise Street Canyon	Main road with heavy traffic (Youyi Avenue)	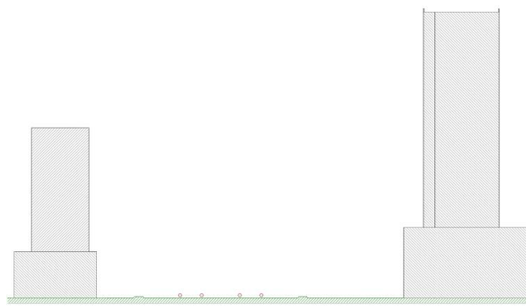	Inside the long slot on the front side of the high-rise building	-8.3 (E02)	–	Various alternations to the building form[b]	-0.4	7.9
			In the slot and screened by the edge of the podium building	-8.5 (E01)	Increasing maximum reflection order 3 to 4	Various alternations to the building form	-3.2	5.3
			On the top side of the high-rise buildings	-3.9 (E05)	Increasing maximum reflection order 3 to 4	–	-3.9	0.0
			In the area shielded by the high-rise buildings	-13.6 (C02)	Increasing maximum reflection order 3 to 4	–	-12.0	1.6
Elevated road in open street canyon	Multi-lane double-layer main road with heavy traffic (Xudong Road)	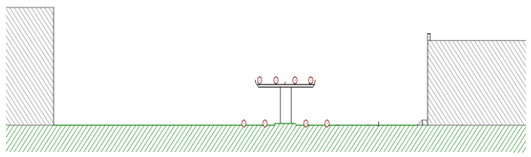	Inside the street canyon, lower than the elevated road.	5.7 (A02)	Increasing maximum reflection order 3 to 4	Modelling the elevated road slab using 3D reflectors	5.8	-0.1
			Above the large-scale podium	-7.7 (E05)	Increasing maximum reflection order 3 to 4	–	-7.0	0.7
Elevated road in confined street canyon with cantilevered barrier	Multi-lane double-layer main road with heavy traffic (Luoshi Road)	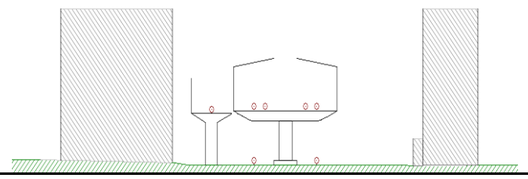	Beneath the elevated road in the confined space	-5.9 (E03)	Increasing maximum reflection order 3 to 4	Modelling the elevated road slab using 3D reflectors	-3.8	2.1

[a] The calculation configuration is subject to conditions described. The maximum reflection order is set to 3, the maximum 1.5 dB correction for opposite façade reflection is disabled. [b] Here the alternations to the high-rise residential building is to flatten the slot itself, which can only be seen as a compromise to the accurate building form modelling and cannot essentially reform the calculation accuracy in the long slot.

5.6 Conclusions

While much work has been carried out by other researchers on the noise mapping of low density cities, the techniques applicability for high density cities has been less certain (Kang, 2006). Correspondingly, in this chapter, to validate the applicability of representative EU noise mapping methods in typical Chinese urban environment, several typical Chinese urban areas with typical Chinese urban features are chosen, and a series of measurement points are chosen and measured. It is found that there are yet some limitations while calculating using the default configurations, some distinct patterns of the influential factors are systematically tested and analysed.

It is found that most of the calculation errors on the receiver points are within acceptable range. Nevertheless, there do exist distinctive errors in a certain amount of receiver points, despite the efforts of further changing the calculation settings and the modelling process.

It is also found that only in these very special locations which can be found in typical Chinese urban environment that the applicability of current calculation method and package may be affected to the certain extent. By adopting the optimised calculation configurations, especially the maximum reflection order, the accuracy level at those locations can also be improved. In some special urban form like the high-density or large-scale buildings blocking the direct transmission, or in relatively confined space, or odd objects like the elevated road with thick concrete slab, some unique modelling methodology is adapted to test the possibility of optimising the applicability of current calculation methods.

Further works may still be necessary to identify and optimise current EU noise calculation methods in relatively more complicated urban environment considering the needs of both accuracy and efficiency. Nonetheless in general especially if only the noise level at the ground level and in relatively open urban morphology are considered, the state-of-the-art EU methods is applicable in the calculation of traffic noise in most of the typical Chinese urban scenarios.

Chapter 6 Effects of urban morphology on traffic noise distribution: a comparative study between the UK and China

6.1 Introduction

There features in terms of urban density and urban morphology are distinctly different between the typical eastern and western big cities, and the difference is becoming greater considering the booming in the emerging economies like China (Gaubatz, 1999). The traffic noise distribution pattern also varies in typical major cities of China and EU, where the density of the former are generally higher than the latter (Wang, Kang, & Zhou, 2007). In this research, two representative cities, Greater Manchester in the UK and Wuhan in China, with similar structure and scale are selected, which have low and high average urban density respectively, and also have considerable differences in building form and traffic pattern. Hence the main aims of this chapter are, firstly, to find out the differences between the noise distribution in urban areas with different urban morphological features and similar urban functions in two representative cities in EU and China; and secondly to study the effect of urban morphological characteristics on the noise distribution through systematic analysis.

A comparative study is carried out between seven pairs of urban area samples in Greater Manchester in the UK and Wuhan in China. Moreover, in this chapter two special urban area with different income levels are also selected in Wuhan, which would be useful in future studies to examine whether noise level correlates with socio-economic indices in such a typical Chinese city.

The structure of this chapter can be divided into three parts: Section 6.2 outlines the background of the study, and briefs the method for case selection, data acquisition and processing. Section 6.3 lists out the noise maps and the value of the spatial noise indices and the urban morphological indices. In Section 6.4 the correlations between the indices are analysed, the effect of some distinctive factors that may influence the traffic noise level and distribution are specifically analysed.

6.2 Research background and method

6.2.1 Previous studies

This research idea in this chapter is originally initiated in a comparative study in 2007, in which two cities, Wuhan in China and Sheffield in the UK, were selected for a comparative research on urban morphological characteristics and noise distribution. Sheffield and Wuhan were chosen in the 2007 study based on the comparability of urban primacy and urban morphology. Both cities are amongst the top 10 largest in their country, and both cities have widely scattered residential areas for working class due to their industry background. As a pilot study, some interesting results are revealed. In Sheffield the spatially averaged noise level is generally higher than that in Wuhan, by 2–11 dBA, whereas Wuhan has rather high SPL along the major roadsides, about 5–10 dBA higher than that in Sheffield (Wang, Kang, & Zhou, 2007). To carry out a more systematic comparison with more typical and representative urban areas, in the current study, Greater Manchester in the UK, with a considerably larger area and more motorways across the urban area, is chosen to compare with Wuhan and was developed as one conference paper (Wang, Kang, & Zhou, 2008) and a journal article (Wang & Kang, 2011).

Using a methodology similar to the one in the 2007 study, a series of representative urban areas in Greater Manchester and Wuhan were selected to produce noise maps. A Matlab programme is then developed to transfer the noise maps into the matrices of sound level values, with which the statistical spatial noise indices including those on the ground level (EC, 2002) and on building façades could be abstracted, together with a number of urban morphological indices, to examine the differences in traffic noise distribution in different urban areas, as well as to analyse how urban morphological indices influence the pattern of traffic noise. The selection of the representative urban areas, such as public open spaces, street canyons, and typical residential buildings, are based on their urban morphologic and acoustic features (Thorsson & Ogren, 2005; De Coensel et al., 2005).

6.2.2 Case selection

6.2.2.1 Selection of typical cities

Comparing to Europe, in major Chinese cities the population density is generally higher and the total amount of vehicles is less. Based on the statistical data in 2006, calculation shows that China's vehicle ownership per capita (NBS China, 2006) is only about 1/20 of the number in the UK (ONS UK, 2001). In the meantime, the population density in Chinese cities is much higher. For example, between representative cities in the UK and China, the density of Greater Manchester's urban area is 19.5 per hectare (ONS UK, 2001), while this number in Wuhan's urban area is 48.8 per hectare (Wuhan Statistics Bureau, 2006). The differences in urban morphology between cities in China and the EU are also significant, especially in terms of the building density and traffic pattern. This is partly due to the differences in the urban planning systems (Khakee, 1996). Consequently, the noise distribution patterns may also be different. It is thus important to examine the difference in the pattern of traffic noise distribution between high-density and low-density cities, typically in China and Europe, respectively.

Greater Manchester and Wuhan are chosen as case study cities because of their typicality and representativeness as one of the biggest cities in each country. Greater Manchester and Wuhan are both situated in the centre of each country, and both are an assembling of a cluster of urban boroughs with large populations. The population of the 10 boroughs of Greater Manchester is 2,585,800 (AGMA, 2006), while the population of 7 urban boroughs of Wuhan is 5,031,038 (Wuhan Statistics Bureau, 2006), Both cities are amongst the 10 largest populated urban areas in each country (Wuhan Statistics Bureau, 2006; Pointer, 2005). The major roads going through Greater Manchester and Wuhan both have huge amounts of traffic flow, although the traffic flow on the motorways of Greater Manchester is notably lower than that on the major roads in Wuhan, despite the lower vehicle ownership per capita in Wuhan (ONS UK, 2005; WCTPDI, 2006).

6.2.2.2 Selection of urban area cases

At least 7 typical urban areas with a scale of 500 × 500 m^2 were sampled in each city with considering urban morphological characteristics and traffic pattern, the selected case categories can be seen in Table 6.1.

Table 6.1 Sampling area categories – Greater Manchester and Wuhan

Greater Manchester		Wuhan		
Wide open space and major roads		Wide open space and major roads		
Public squares in city centre		Public squares in city centre		
Street canyons and commercial blocks		Street canyons and commercial blocks		
Industry community		Industry community		
Motorway		Motorway		
Typical residential	Higher density	Residential	Typical residential	Higher density
	Lower density			Lower density
			Special cases	Low income
				High income

The space type, building density, road distribution pattern, road type, traffic flow and different land-use category are considered in the case sampling in both cities. Based on the space type and traffic statistic data obtained from local authorities (AGMA, 2006; WCTPDI, 2006), typical urban areas with wide open spaces, public squares in the city centres and motorways were selected.

It is to note that, due to different urban development context and planning system, some of the compared samples has similar urban function and land-use, while the morphology of which are sometimes distinguished in the two cities. For instance, the sampled cases of the category of the public squares in the city centre that refers to the pedestrian dominated public squares in the downtown centre in both urban areas, similarly both contain large amount of pedestrian-dominated regions and public spaces, while at the same time have huge differences in terms of building scale and spatial features in these two cites. As can be seen in Figure 6.2 that, the one in the Manchester town centre close to the Manchester central station is divided by more roads, and surrounded by large-scale public buildings; while the Jianghan Road pedestrian street is a typical Chinese downtown centre surrounded by large amount of high-density and low-rise traditional buildings, in which the traffic and public transportation are largely separated out on the wide major road bordering with the area.

In terms of different land use types, commercial areas with street canyons and areas with large industrial buildings were also selected. Two representative residential areas were sampled in each city with relatively high and low average building heights respectively. Since the maximum noise level is sensitive to the location of major roads, particular attention is also paid to sampled areas with major roads, making sure any major roads, if included, actually represent the features of the sampled areas.

Two additional areas in Wuhan were sampled, representing low and high-income residential areas respectively. The low-income residential area is a part of the old town. With low-rise residential buildings, it has a rather different urban form and traffic pattern from newly developed areas (Jin, 1993). For comparison, a typical residential area in a residential real estate development is also selected, to represent typical high-income residential areas. To validate the hypothesis, the average income data were collected through in-situ questionnaire surveys. While the average monthly income in Wuhan in 2005 is 1354.6 CNY according to Wuhan Statistics Bureau(2005), the in-situ questionnaire statistics shows that the average income in the low-income area is 1067.5 CNY and that in the high-income area is 2362.5 CNY. The independent *t*-test for equality of means showed that the mean difference is 1295.0 CNY and the significance level (2-tailed) is 0.02, indicating that a significant difference did exist between the two areas.

6.2.3 Data acquisition and processing

6.2.3.1 3D model and traffic data acquisition

For the purpose of simulation, detailed 2D vector maps in DXF format of sampled areas were obtained from EDINA ordnance survey maps in the UK (EDINA Digimap, 2008) and the Wuhan Bureau of Urban Planning in China. Then the 3D information for modelling, including the façade condition and building heights, were obtained from digital maps or from in-situ investigation by multiplying the average floor height with the number of storeys. Figure 6.1 shows the 3D building models of two sampled areas.

Due to the lack of detailed traffic data of the minor roads, in the on-site investigation, the 18 hour daily traffic flow data of the roads required by CRTN in each sampling area was calculated based on the measured rush hour count and calculated according to the

temporal distribution of the daily traffic data obtained from the local traffic statistics, the method is also described in the *Good practice guide for strategic noise mapping and the production of associated data on noise exposure* by WG-AEN (2007). For the main roads, the daily traffic flow is normally calculated as approximately 12 times as the peak hour flow, and for the smaller roads, the peak hour flow is approximately 7% of the average daily traffic flow.

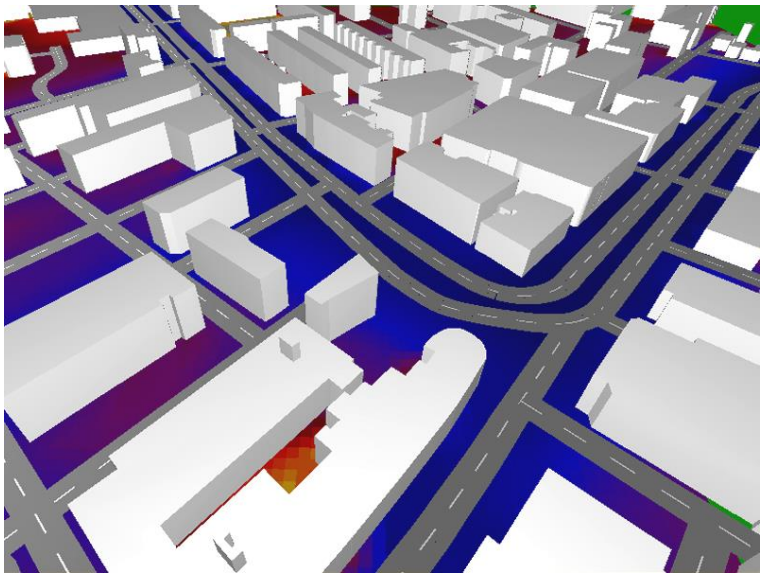

a

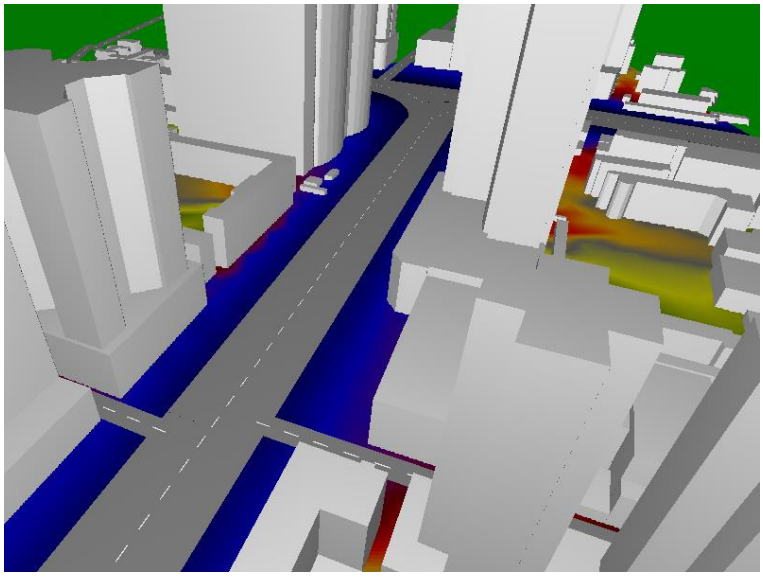

b

Figure 6.1 Two compared sampled areas with commercial blocks and street canyon (a) Oldham Street, Greater Manchester ; (b) and Jiedaokou Cross, Wuhan

6.2.3.2 Noise-mapping

For the calculation of noise maps, a widely used state-of-the-art EU noise-mapping package Cadna/A (DataKustik, 2012a) is used. Noise mapping is based on a series of algorithms specified in various standards, internationally (ISO, 1996) and nationally, for various noise sources including aircraft (ECAC, 1997), road (UK DfT, 1988), railway (UK DfT, 1995) and industry (DAL, 1987). The calculation procedures and indices can often vary in different standards (J. Kang, 2006). The calculation configuration in this study is based on default international and national standards, including ISO 9613 (ISO, 1996), CRTN (UK DfT, 1988), with the optimised calculation configurations and modelling methods based on the studies in previous two Chapters.

6.2.4 Data processing

A Matlab programme is developed to obtain a series of indices characterising noise distribution and urban morphology features based on the calculated noise maps. The programme scans the RGB-colours and translates them back into SPL values. In the scan process, the spatial resolution can be defined. Consequently, statistical SPL indicators can be calculated, including L_{max}, L_{10}, L_{avg}, L_{50}, L_{min}, and L_{90}. It is important to note that the noise level indices here are spatial, rather than temporal as conventionally defined. Both the noise level in the open ground and the general noise levels next to the building façades are derived from the noise maps. The programme can also be utilised to calculate the urban morphological indices, including the road space ratio (RSR), the building ground space index (GSI) and the open space ratio (OSR), which represent the coverage ratio of the road surface, the building ground space, and the open spaces (i.e. accessible spaces except roads and buildings) in a sampled area. The grid noise maps of all selected cases are demonstrated in Figure 6.2. Table 6.2 lists the exact values of the urban morphological indices and Table 6.3 shows the spatial noise level indices, for the sampled areas in both Greater Manchester in the UK and Wuhan of China.

6.3 Calculation results

Table 6.2 Urban morphological indices of Greater Manchester and Wuhan

	Categories of the sampling areas			Morphological indices (%)		
				OSR	GSI	RSR
Greater Manchester, UK	Wide open space and major roads			62.1	15.5	22.4
	Public squares in city centre			47.5	37.8	14.7
	Street canyons and commercial blocks			41.0	33.9	25.1
	Industry community			65.5	18.2	16.4
	Motorway and residential buildings			61.4	17.8	20.9
	Typical residential	High density		67.6	16.4	16.0
		Low density		72.1	14.7	13.2
		Residential average		69.9	15.6	14.6
	Overall average			59.6	17.2	14.8
Wuhan, China	Wide open space and major roads			70.0	17.1	12.9
	Public squares in city centre			33.1	60.3	6.6
	Street canyons and commercial blocks			53.0	33.2	13.8
	Industry community			54.7	34.7	10.6
	Motorway and residential buildings			71.0	14.8	14.2
	Typical residential	High density		60.7	26.1	13.2
		Low density		68.2	20.3	11.5
		Special cases	Low income	53.6	34.6	11.8
			High income	69.3	22.3	8.4
		Residential average		63.0	25.8	11.2
	Overall average			59.3	29.3	11.4

Table 6.3 Spatial noise indices of Greater Manchester and Wuhan

Sampling area categories			Spatial noise level indices (dBA)											
			Ground noise level indices						Façade noise level indices					
			L_{avg}	L_{50}	L_{min}	L_{90}	L_{max}	L_{10}	L_{avg}	L_{50}	L_{min}	L_{90}	L_{max}	L_{10}
Greater Manchester, UK	Wide open space and major roads		71.3	71.0	47.0	63.0	85.0	79.0	68.8	69.0	47.0	61.0	83.0	77.0
	Public squares in city centre		68.6	69.0	43.0	59.0	81.0	77.0	68.3	69.0	43.0	57.0	81.0	77.0
	Street canyons and commercial blocks		68.9	69.0	45.0	59.0	81.0	77.0	67.9	69.0	45.0	57.0	81.0	77.0
	Industry community		63.8	63.0	47.0	57.0	75.0	71.0	63.3	63.0	47.0	57.0	75.0	71.0
	Motorway		70.1	71.0	45.0	61.0	85.0	79.0	66.9	67.0	45.0	59.0	81.0	75.0
	Typical residential	High density	62.0	61.0	47.0	55.0	79.0	73.0	61.1	61.0	47.0	53.0	79.0	69.0
		Low density	54.5	53.0	31.0	47.0	69.0	63.0	55.7	57.0	31.0	49.0	67.0	63.0
		Average	58.3	57.0	39.0	51.0	74.0	68.0	58.4	59.0	39.6	51.0	73.0	66.0
	Overall Average		65.6	65.3	39.6	57.3	79.3	74.1	64.6	65.0	39.6	56.1	78.1	72.7
Wuhan, China	Wide open space and major roads		71.9	73.0	45.0	57.0	83.0	79.0	64.6	65.0	45.0	51.0	81.0	77.0
	Public squares in city centre		55.1	53.0	37.0	43.0	83.0	69.0	51.2	49.0	37.0	43.0	81.0	65.0
	Street canyons and commercial blocks		58.5	55.0	37.0	41.0	87.0	79.0	58.5	55.0	37.0	41.0	87.0	79
	Industry community		59.3	57.0	39.0	47.0	81.0	77.0	57.7	57.0	39.0	47.0	81.0	69.0
	Motorway		65.6	65.0	35.0	55.0	85.0	79.0	59.2	59.0	37.0	51.0	77.0	67.0
	Typical residential	High density	61.2	61.0	43.0	53.0	79.0	73.0	60.8	61.0	43.0	53.0	77.0	71.0
		Low density	57.5	57.0	35.0	49.0	79.0	69.0	56.1	55.0	35.0	47.0	79.0	67.0
		Special cases: Low income	53.0	49.0	37.0	45.0	83.0	73.0	50.6	49.0	37.0	43.0	81.0	59.0
		Special cases: High income	57.5	59.0	33.0	41.0	79.0	73.0	53.6	53.0	33.0	41.0	79.0	69.0
		Average	57.3	56.5	37.0	47.0	80.0	72.0	55.3	54.5	37.0	46.0	79.0	66.5
	Overall Average		60.0	58.8	37.9	47.9	82.1	74.6	56.9	55.9	38.1	46.3	80.3	69.2

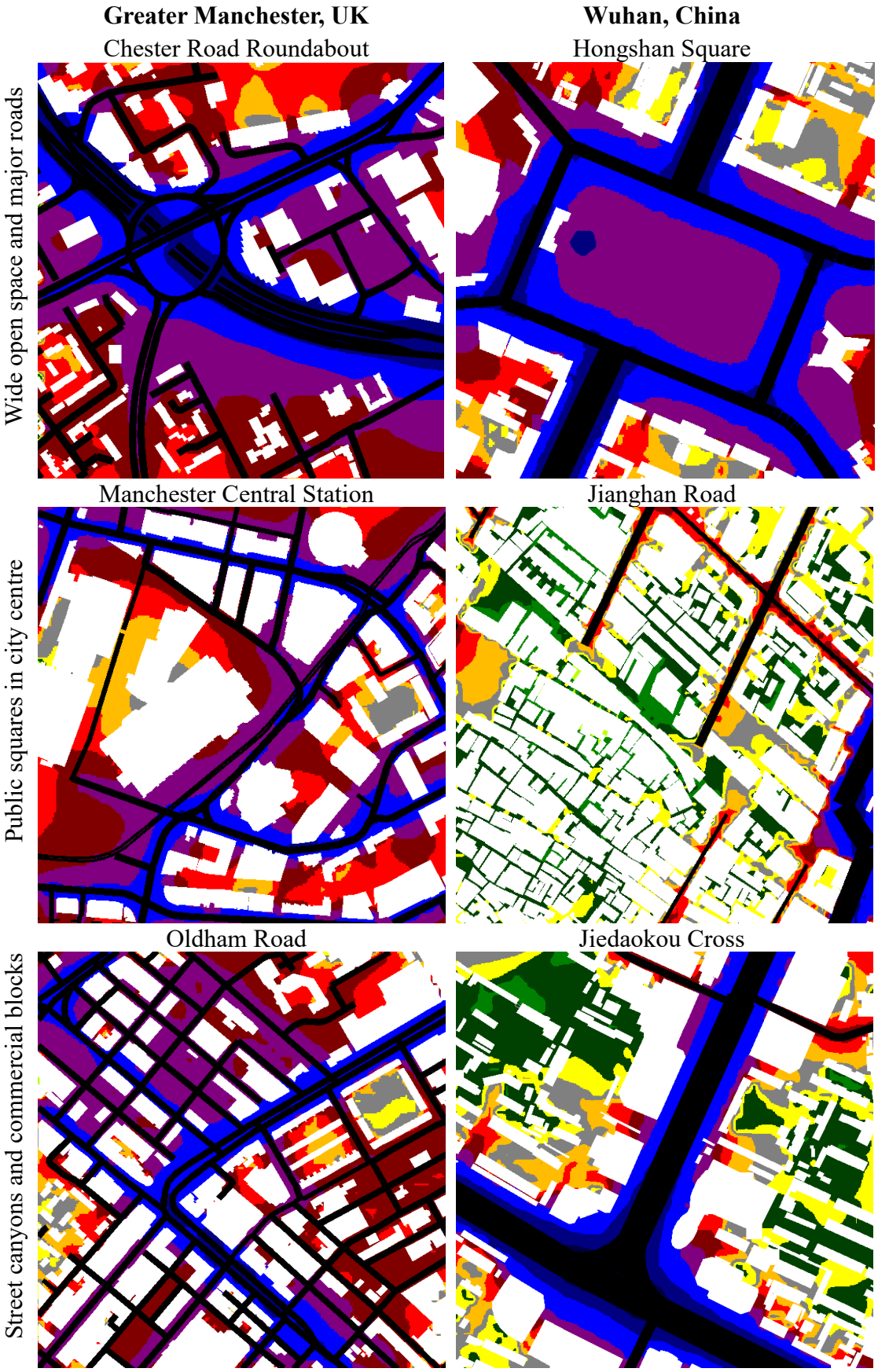
Greater Manchester, UK
Wuhan, China
Chester Road Roundabout
Hongshan Square
Wide open space and major roads
Manchester Central Station
Jianghan Road
Public squares in city centre
Oldham Road
Jiedaokou Cross
Street canyons and commercial blocks

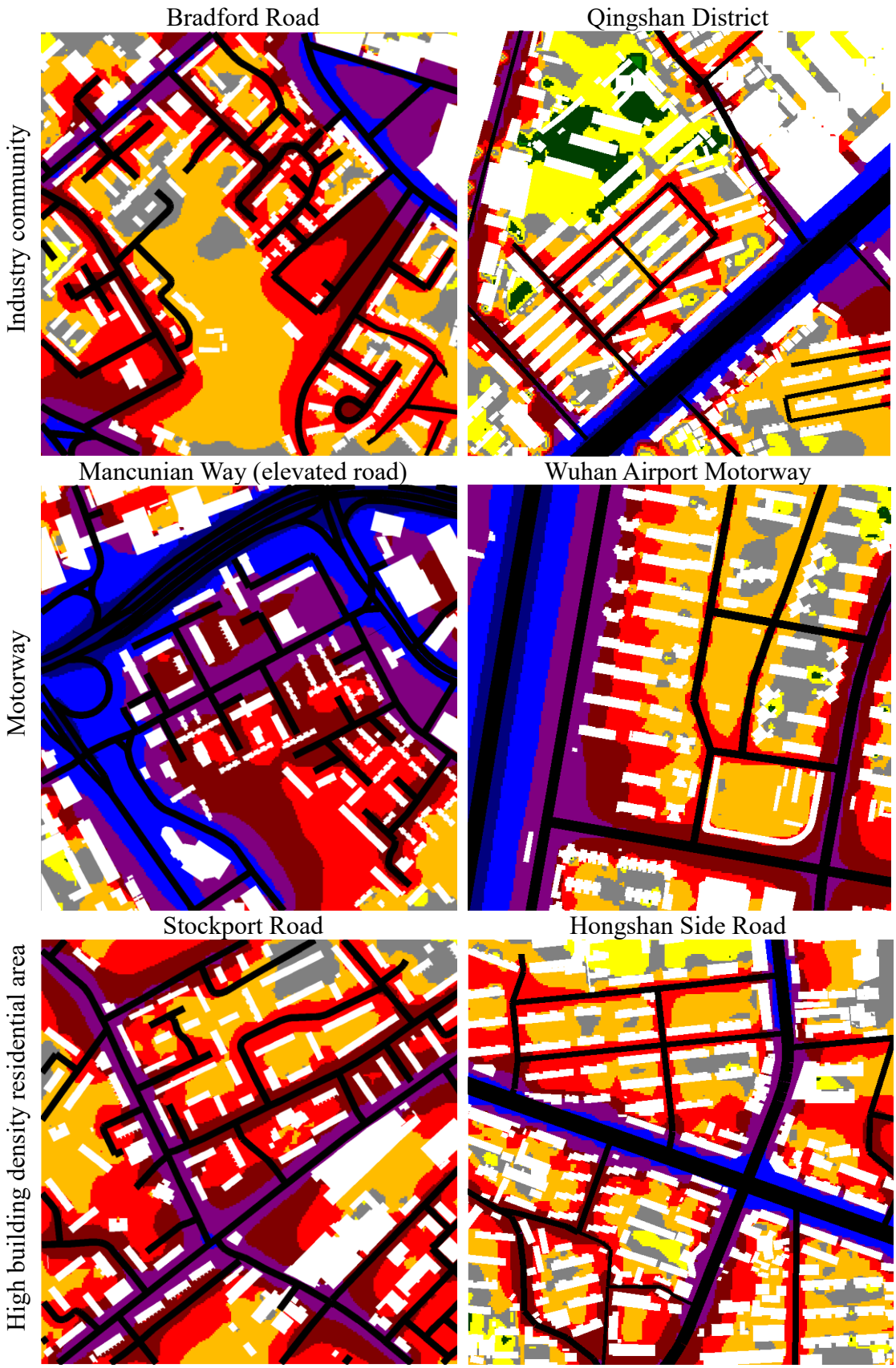
Bradford Road
Qingshan District
Industry community
Mancunian Way (elevated road)
Wuhan Airport Motorway
Motorway
Stockport Road
Hongshan Side Road
High building density residential area

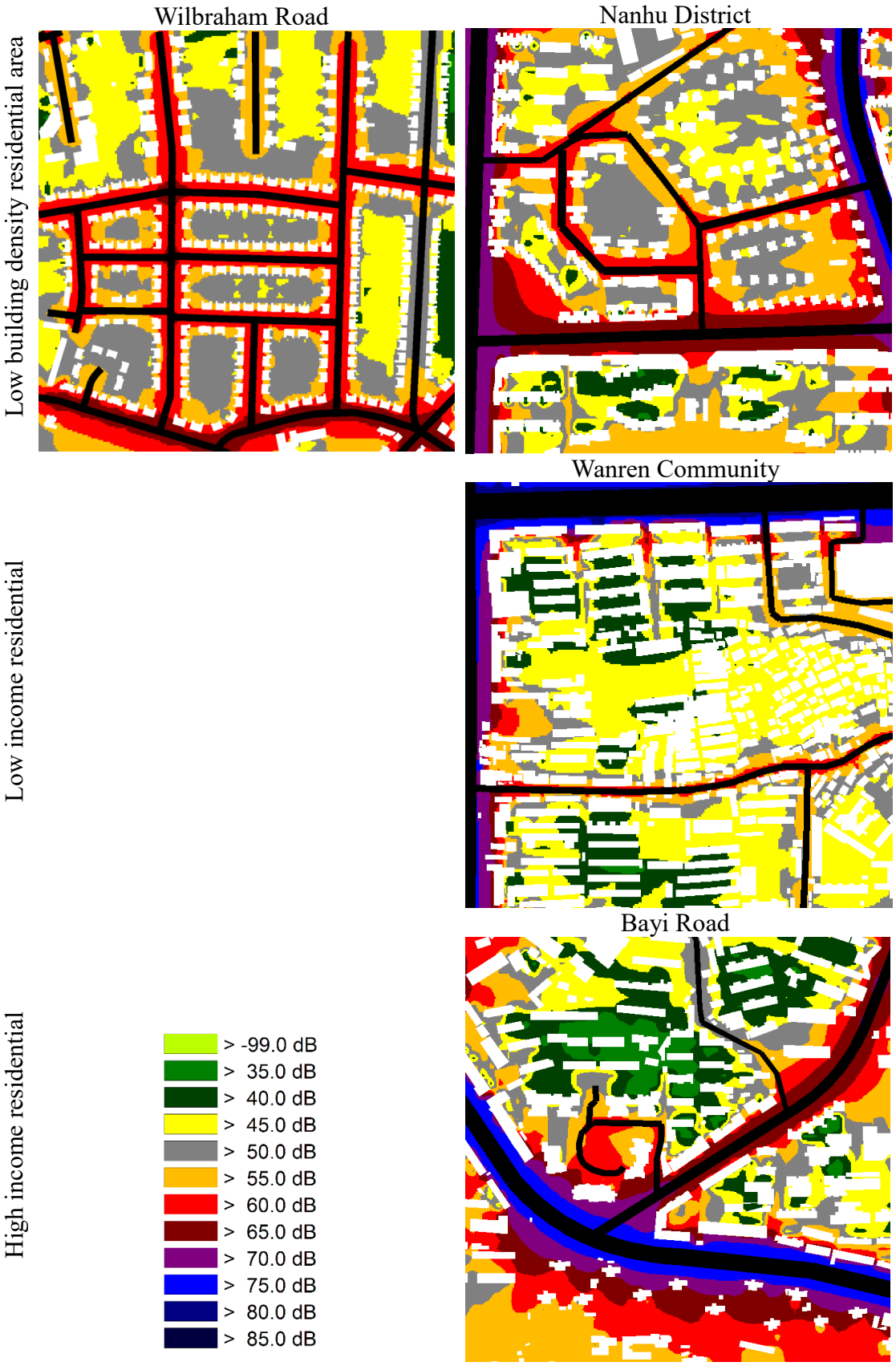

Figure 6.2 Noise maps of the selected study areas in Greater Manchester, UK and Wuhan, China

6.3.1 General comparison of spatial noise indices

Figure 6.3 shows the comparisons of ground noise level between the same category of sampling areas in Greater Manchester and Wuhan. It is remarkable that the average and spatial median ground noise level, L_{avg} and L_{50} in the Wuhan samples are generally 5.6 dBA and 6.5 dBA lower than that in the Greater Manchester samples, respectively, except for the wide and open spaces and major roads and typical low density residential cases, in which the L_{avg} and L_{50} in the Greater Manchester samples are slightly lower than those in Wuhan. In terms of L_{min} and L_{90}, the difference is also evident where the ground noise level in terms of L_{min} and L_{90} in Greater Manchester is 1.7 dBA and 9.4 dBA higher than that in Wuhan on average, respectively. Conversely, the ground noise L_{max} and L_{10} in Wuhan samples are generally higher than those in Greater Manchester, by 2.8 dBA and 0.5 dBA on average, respectively, since the maximum road traffic in Wuhan is generally higher. In the low density residential area, all the spatial noise indices in the Greater Manchester samples are lower than those in Wuhan, by 0.4–10 dBA, perhaps because the former is far from major roads and has a much lower traffic density.

Corresponding to Figure 6.3, in Figure 6.4 the façade noise levels are shown. It can be seen that the differences in façade spatial noise indices between samples in Greater Manchester and Wuhan are similar to those of the ground spatial noise indices, but the differences are generally larger. For example, the differences in L_{avg} and L_{50} between Greater Manchester and Wuhan samples are 7.7 dBA and 9.1 dBA, respectively, considerably higher than those for ground noise levels. Overall, the average attenuation of traffic noise in Greater Manchester samples is smaller than that in Wuhan, which is possibly due to the smaller average distance from building façades to the roads sides in Greater Manchester. It is noted that in Figure 6.4 the differences between the maximum façade noise level and maximum ground noise level of each area are generally rather small. This is mainly caused by the relative low resolution of receiver grid. In the calculation, the spacing of the receiver grid is set as 10 m × 10 m, whereas the road width is normally around 10–20 m in the sampled areas.

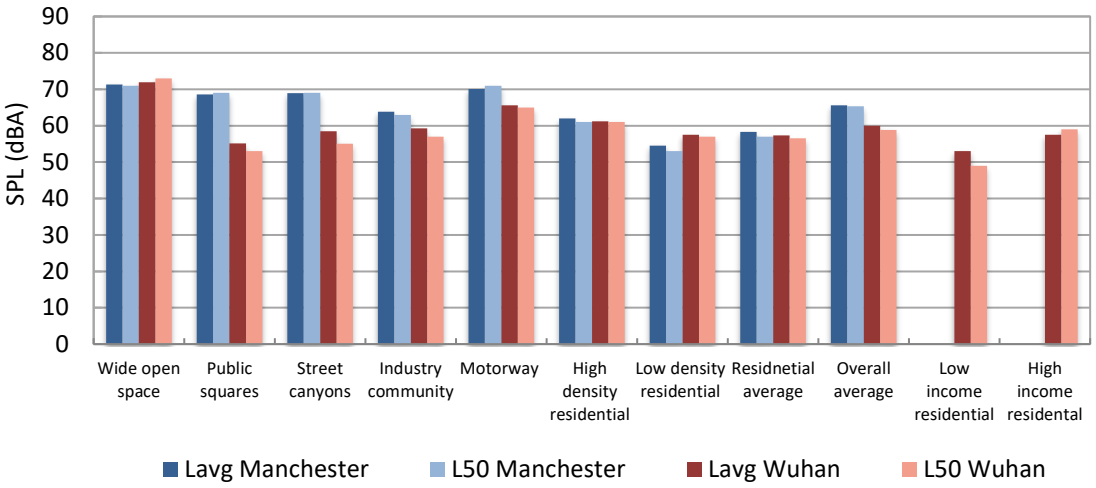

a

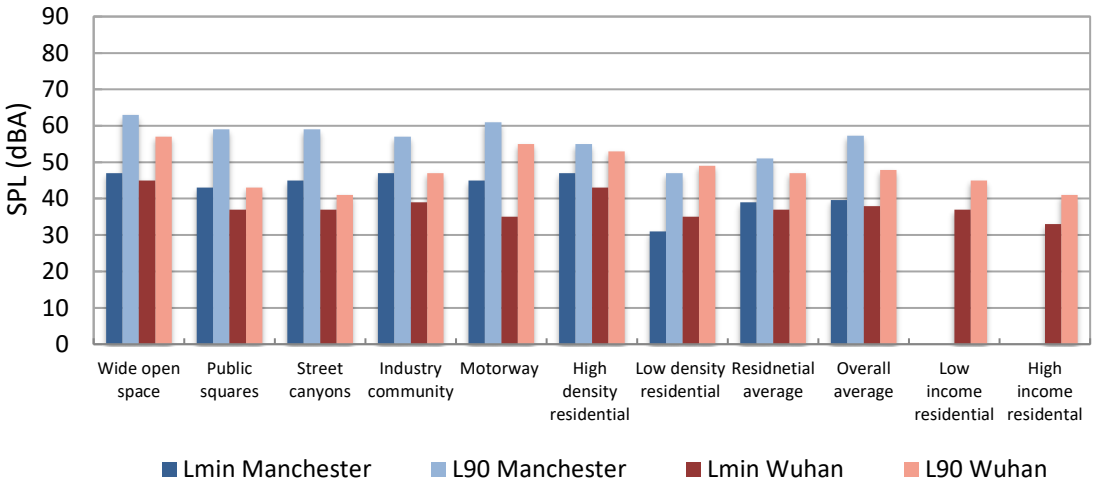

b

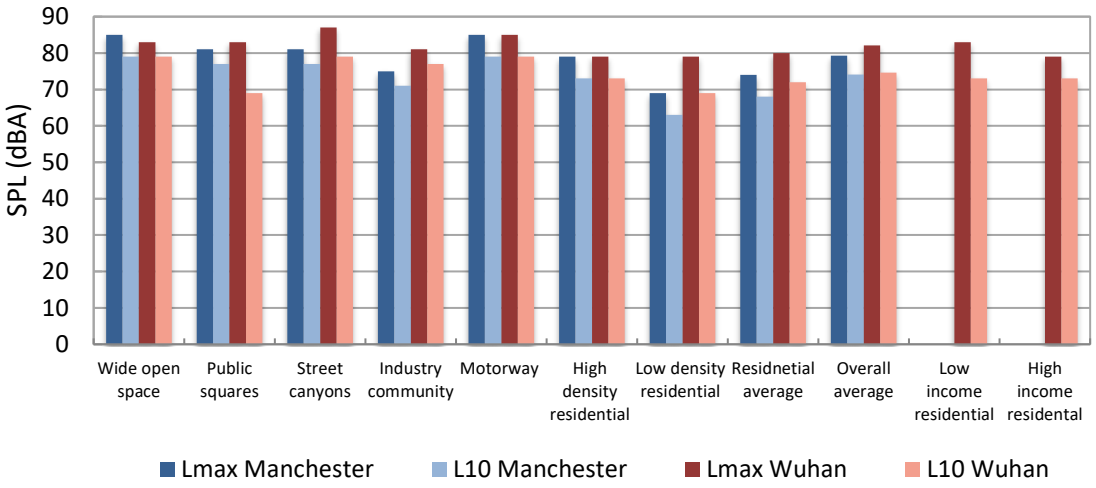

c

Figure 6.3 Comparisons of general ground spatial noise indices of (a) L_{avg} and L_{50}; (b) L_{min} and L_{90}; (c) L_{max} and L_{10} between Greater Manchester and Wuhan

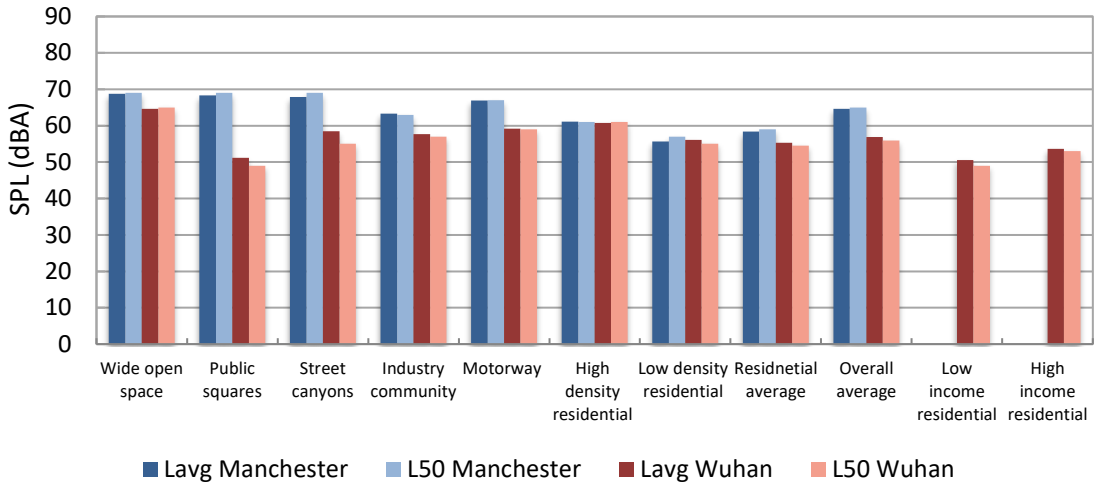

a

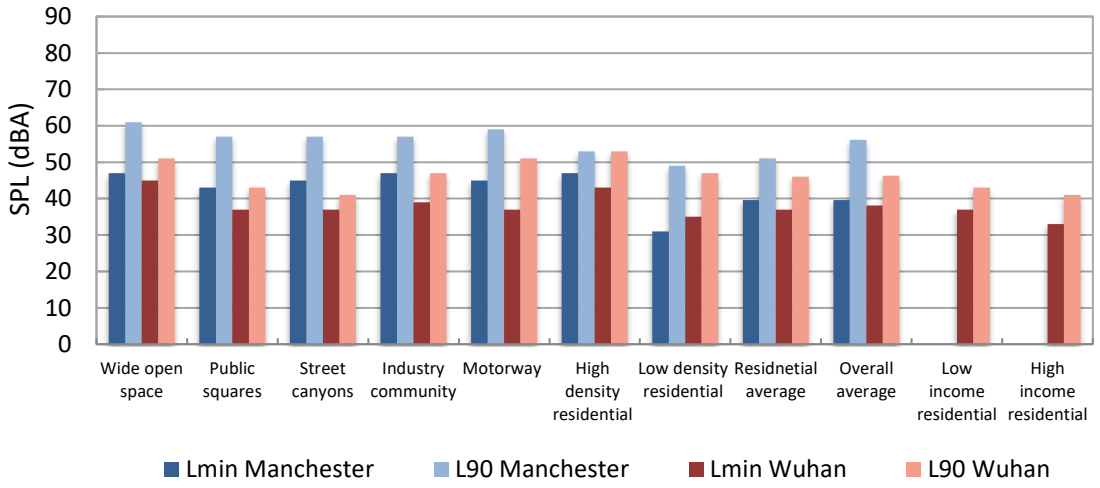

b

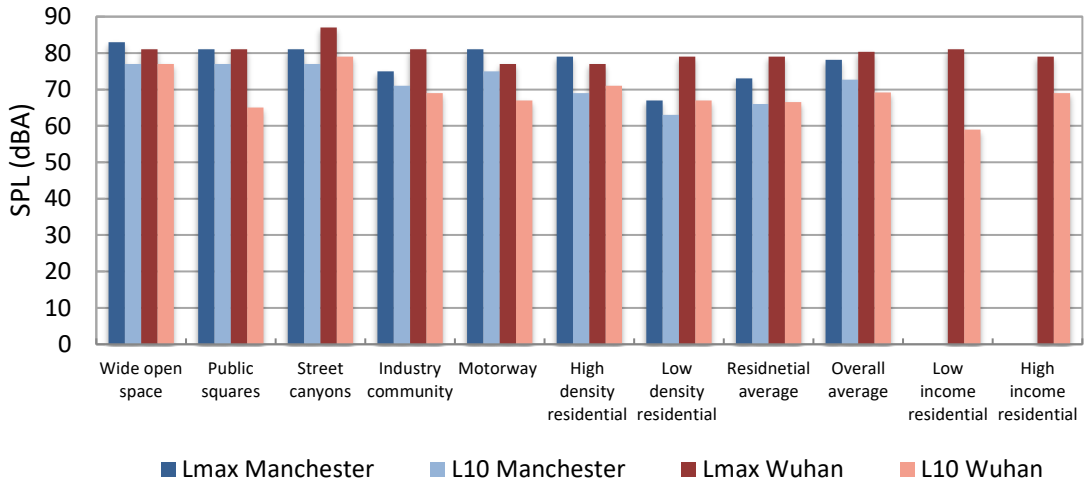

c

Figure 6.4 Comparisons of building façade spatial noise level of (a) L_{avg} and L_{50}; (b) L_{min} and L_{90}; (c) L_{max} and L_{10} between Greater Manchester and Wuhan

The more evenly distributed roads in Greater Manchester samples make the spatial intrusive noise of building façade, in terms of L_{10}, 3.5 dBA higher on average than that in Wuhan samples, although the L_{max} of façade noise in Wuhan is higher than that in Greater Manchester by 2.2 dBA. This is perhaps because, compared with Greater Manchester, in Wuhan samples, there are much higher traffic flows on the major roads, but in the minor roads behind the major road canyons the traffic density is low and also, buildings act as effective noise barriers due to their greater heights than those in Greater Manchester.

6.3.2 Comparison of urban morphologic indices

The urban morphological indices are shown in Figure 6.5 (also shown in Table 6.4). It can be seen that the GSI in Wuhan samples is 10.2% higher on average than that in Greater Manchester samples, except the street canyons and commercial blocks case and the motorway case, where the Greater Manchester samples are 0.7% and 3% higher than the Wuhan samples, respectively. In terms of the RSR, Wuhan is 3.4% lower on average than that in Greater Manchester, whereas the differences in the OSR between the two cities are not systematic, and the average OSR in both cities are close.

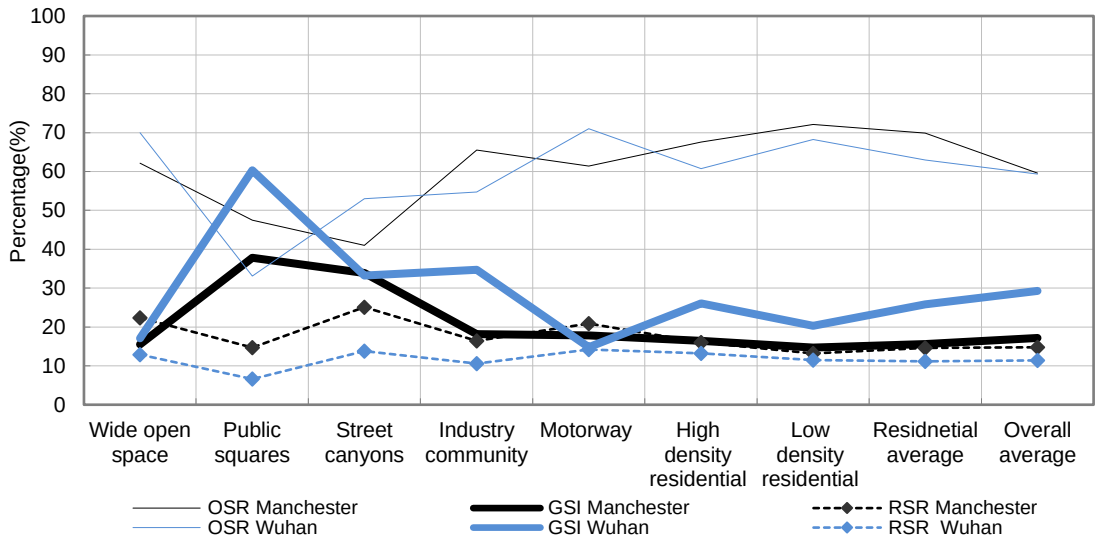

Figure 6.5 Comparisons of the three major urban morphological indices between Greater Manchester and Wuhan.

6.4 Comparison and analysis

6.4.1 Correlation between spatial noise indices and morphologic indices

By carrying out bivariate correlation analysis using the statistics software SPSS 22 (IBM Corp., 2011), the linear correlations between urban morphological indices and spatial noise indices are examined, considering both ground and façade noise levels, as shown in Table 6.4 and Table 6.5, all the correlations with a significance level of $p < 0.05$ are highlighted.

Although only 2-tailed correlations are analysed for most of the indices analysed, it is to note that, according to the calculation method of traffic noise adopted, as can be seen in Equation 3.1, the traffic noise level generally increases with the number of vehicles, the latter is closely related with the number of road lanes. Therefore, the 1-tailed Bivariate correlation between the RSR and all spatial noise indices are also analysed in order to test the hypothesis that when there are more roads, the value of all noise indices rise.

To further illustrate the general effect of urban morphological indices on the noise distribution in terms of spatial noise indices in each city, the correlations between the façade noise index L_{50} and three urban morphological indices derived from the noise maps in the two cities are shown in Figure 6.6, Figure 6.7 and Figure 6.8, respectively.

From Table 6.4 and Table 6.5 it can be seen that, when 2-tailed Bivariate correlation analyses are conducted, there are only few significant correlations found between the spatial noise indices and a number of morphological indices in the sampled cases of both cities. It is interesting to find in Table 6.4 and Table 6.5 that, the general tendency of correlation between OSR and GSI in both cities are opposite. In Manchester it seems the accessible open space coverage represented by OSR are generally negatively correlated with the noise indices, although only the correlation with L_{50} and L_{10} on façade level are found to be significant; and the rise of GSI tends to decrease all noise indices in Greater Manchester despite none of the correlations are found to be significant. On the contrary, in Wuhan, the rise of OSR increases the noise levels and the rise of GSI decrease the noise levels on both the ground level and building façades, except the maximum noise level L_{max}.

Table 6.4 Bivariate correlation between spatial noise indices and urban morphological indices of the Greater Manchester cases, where the significance level is also shown, the Pearson correlation coefficient R with $p < 0.05$ (*) are highlighted.

Pearson Correlation		L_{avg}	L_{50}	L_{min}	L_{90}	L_{max}	L_{10}
Ground spatial noise indices							
OSR	R	-0.633	-0.646	-0.305	-0.512	-0.479	-0.603
	Sig.	0.127	0.117	0.506	0.240	0.277	0.152
GSI	R	0.406	0.428	0.119	0.279	0.242	0.384
	Sig.	0.366	0.338	0.800	0.544	0.601	0.396
RSR (2-tailed)	R	0.728	0.716	0.520	0.698	0.693	0.700
	Sig.	0.063	0.070	0.232	0.081	0.084	0.080
RSR (1-tailed)	R	*0.728	*0.716	0.520	*0.698	*0.693	*0.700
	Sig.	0.032	0.035	0.116	0.004	0.042	0.004
Façade spatial noise indices							
OSR	R	-0.731	*-0.789	-0.305	-0.442	-0.600	*-0.772
	Sig.	0.062	0.035	0.506	0.321	0.159	0.042
GSI	R	0.540	0.602	0.118	0.204	0.391	0.584
	Sig.	0.211	0.152	0.800	0.661	0.386	0.168
RSR (2-tailed)	R	0.685	0.696	0.523	0.681	0.665	0.693
	Sig.	0.090	0.083	0.228	0.092	0.103	0.084
RSR (1-tailed)	R	*0.685	*0.696	0.523	*0.681	0.665	*0.693
	Sig.	0.045	0.041	0.114	0.046	0.051	0.042

Table 6.5 Bivariate correlation between spatial noise indices and urban morphological indices of the Wuhan cases, where the significance level is also shown, the Pearson correlation coefficient R with $p < 0.05$ (*) are highlighted.

Pearson Correlation		L_{avg}	L_{50}	L_{min}	L_{90}	L_{max}	L_{10}
Ground spatial noise indices							
OSR	R	0.582	0.655	0.010	0.542	-0.263	0.366
	Sig.	0.100	0.056	0.980	0.132	0.493	0.333
GSI	R	-0.613	-0.657	-0.071	-0.587	0.166	-0.447
	Sig.	0.079	0.054	0.855	0.096	0.670	0.228
RSR (2-tailed)	R	0.519	0.405	0.341	0.572	0.371	0.661
	Sig.	0.152	0.279	0.369	0.108	0.325	0.053
RSR (1-tailed)	R	0.519	0.405	0.341	0.572	0.371	*0.661
	Sig.	0.076	0.140	0.184	0.054	0.163	0.026
Façade spatial noise indices							
OSR	R	0.546	0.620	0.073	0.450	-0.433	0.244
	Sig.	0.128	0.075	0.852	0.224	0.244	0.527
GSI	R	-0.611	*-0.668	-0.144	-0.499	0.381	-0.290
	Sig.	0.081	0.049	0.712	0.171	0.311	0.449
RSR (2-tailed)	R	*0.676	0.624	0.425	0.530	0.034	0.398
	Sig.	0.046	0.072	0.254	0.143	0.931	0.289
RSR (1-tailed)	R	*0.676	*0.624	0.425	0.530	0.034	0.398
	Sig.	0.023	0.036	0.127	0.071	0.466	0.145

The analyses on the effect of road coverage shows similarly positive tendencies in samples in both cities. It can be seen from Table 6.4 that for the Greater Manchester samples, with considering the connection between the increasing of road coverage and increasing of vehicles, the 1-tailed correlation analyses reveals significant positive correlations between the RSR and almost all ground spatial noise indices, except for L_{min}. For the façade noise levels in Manchester samples, similar but weaker 1-tailed correlations are found except for L_{min} and L_{max}. In the Wuhan samples, as can be seen in Table 6.5 that, the correlations are all positive while not as significant, except for the Ground L_{10} that are normally close to the road sources. In terms of façade noise level in Wuhan, significant positive correlations do exist between the RSR and $L_{50\ avg}$ (2-tailed and 1-tailed) and L_{50} (1-tailed). Figure 6.6 demonstrated it with showing the significant positive correlations found between RSR and spatial façade median L_{50} in both cities. Above findings indicate that, in general, when the total space of the roads increases, the spatial average and median noise level on the building façade will increase accordingly, despite the variation in terms of urban forms.

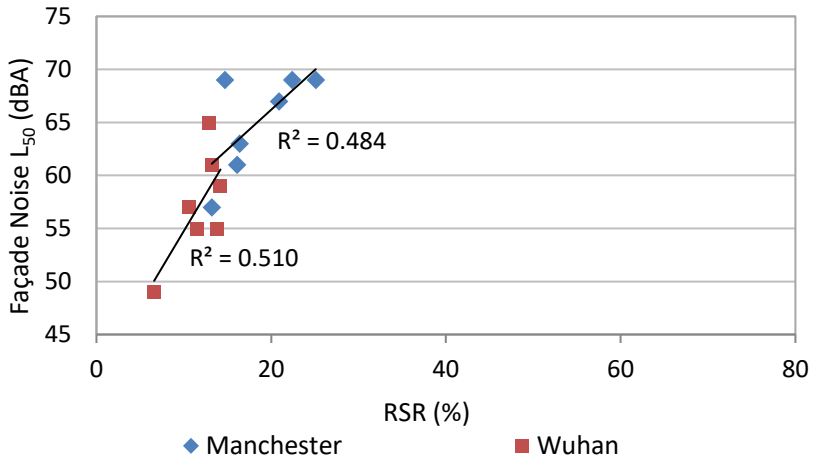

Figure 6.6 Significant correlations ($p<0.05$) found between RSR and Façade L_{50} *in* Greater Manchester ($R^2 = .484$, $p < 0.05$) and Wuhan ($R^2 = .510$, $p < 0.05$).

Figure 6.7 shows the correlation between GSI and spatial median façade noise level L_{50}. It can also be seen from Table 6.5 that in the Wuhan samples, there are negative correlation found between the GSI and the median spatial façade noise level L_{50}, while for the Greater Manchester samples the correlation tends to be positive, although not at a statistically significant level.

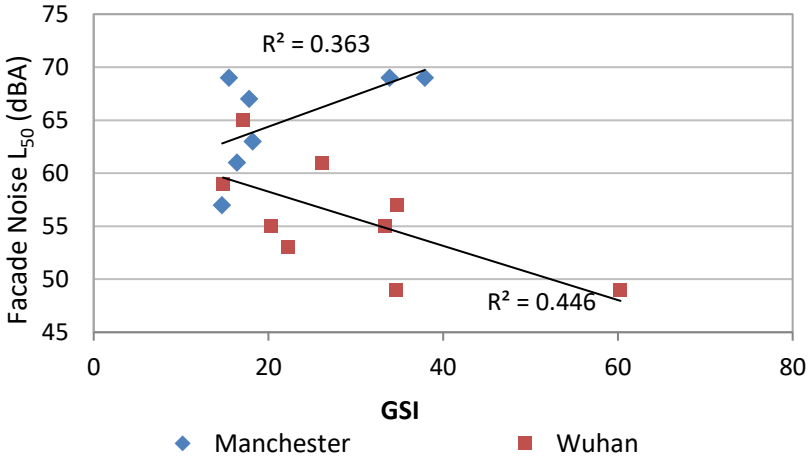

Figure 6.7 Correlations between GSI and Façade L_{50} *in* Greater Manchester (R^2 = .363, $p > 0.05$) and Wuhan (R^2 = .446, $p < 0.05$).

As shown in Figure 6.8, the tendencies in the two cities are also different. In Greater Manchester, when the OSR increases, the noise impact on building façades increases, whereas, in Wuhan, the tendency is opposite.

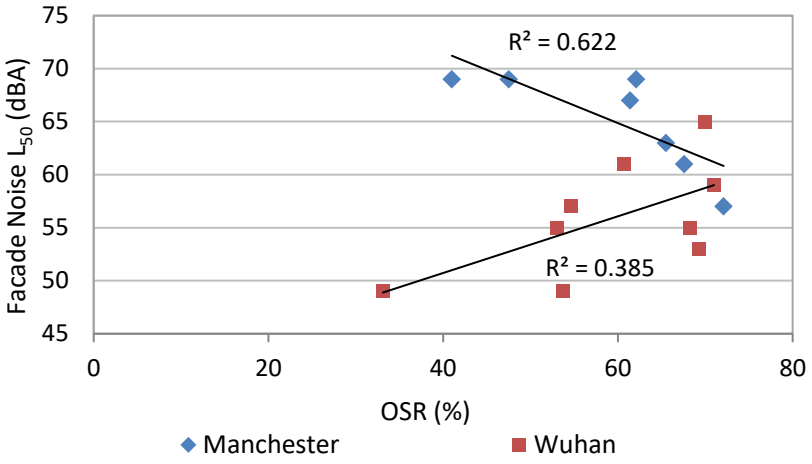

Figure 6.8 Correlations between OSR and Façade L_{50} *in* Greater Manchester (R^2 = .622, $p < 0.05$) and Wuhan (R^2 = .385, $p > 0.05$).

The correlations between urban morphological indices are tested as well, as shown in Figure 6.9. It can be seen that there is a negative correlation found between the GSI and OSR in both cities, which means when the urban density in terms of building coverage rises, the general size of the open space decreases accordingly.

A significant negative correlation ($p < 0.05$) is shown between the RSR and GSI in Wuhan samples, indicating that the increasing of road coverage, can actually decrease the space

of the buildings. In contrast, in Greater Manchester the correlation is also negative but insignificant between the RSR and GSI, which may mainly be due to the typical Chinese urban morphology with main roads distributed throughout the whole city with a typical spacing of 350–500 m (Wu & Li, 2011), thus in some cases the when small road coverage in-between the main-road grid increases, the building coverage thus decrease accordingly; whereas in a typical European city like Greater Manchester, the roads are more evenly distributed and the road density are all generally high despite functions and land-use of the urban area.

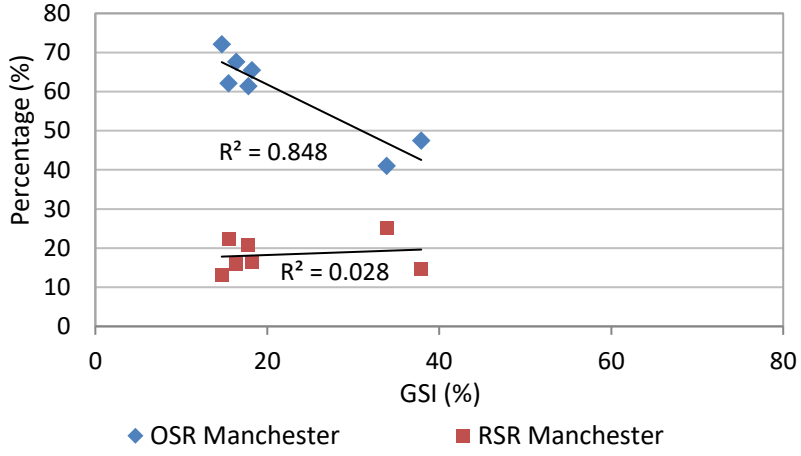

a

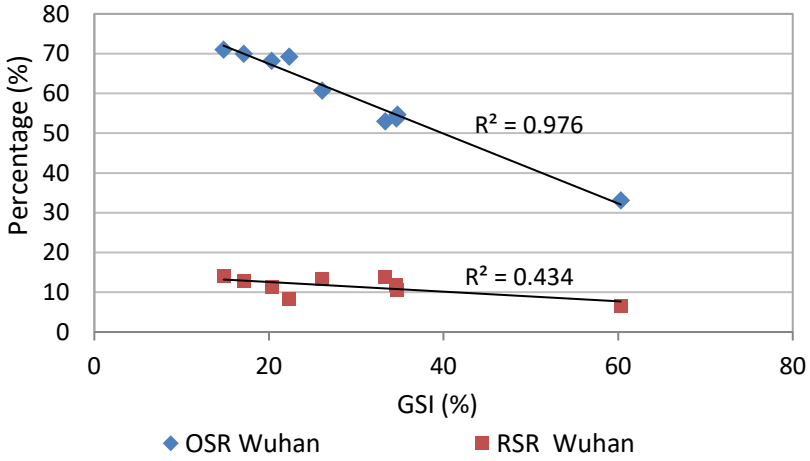

b

Figure 6.9 Significant correlations found ($p < 0.01$) between GSI and OSR, and between GSI and RSR of Greater Manchester (a) and Wuhan (b).

In each city, at least two representative residential areas, namely higher GSI areas with multi-storey flats (Wuhan) and semi-detached houses (Greater Manchester), and lower GSI areas with low storey flats (Wuhan) or detached houses (Greater Manchester), are

chosen respectively to find out more general principles of correlation between urban density and noise distribution. From the results above (e.g. Figure 6.3 and Figure 6.4), it can be observed that the higher density residential area in each city generally has higher noise levels, considering all spatial noise indices.

6.4.2 Further discussion on the case-wise differences

6.4.2.1 Public square samples

In terms of L_{50}, one of the most distinct differences occurs in the city centre public squares cases (see Figure 6.3 and Figure 6.4). The ground noise level L_{50} of the Wuhan case is 16 dBA lower than that of Greater Manchester case, as also illustrated in Figure 6.10; and in terms of the façade noise level, the L_{50} is even 20 dBA lower than that in Greater Manchester case. This is because the OSR and relative RSR in the Wuhan case are much lower than that in the Greater Manchester case, by 14.4% and 8.1% respectively, causing much lower traffic noise in terms of both ground and façade noise levels.

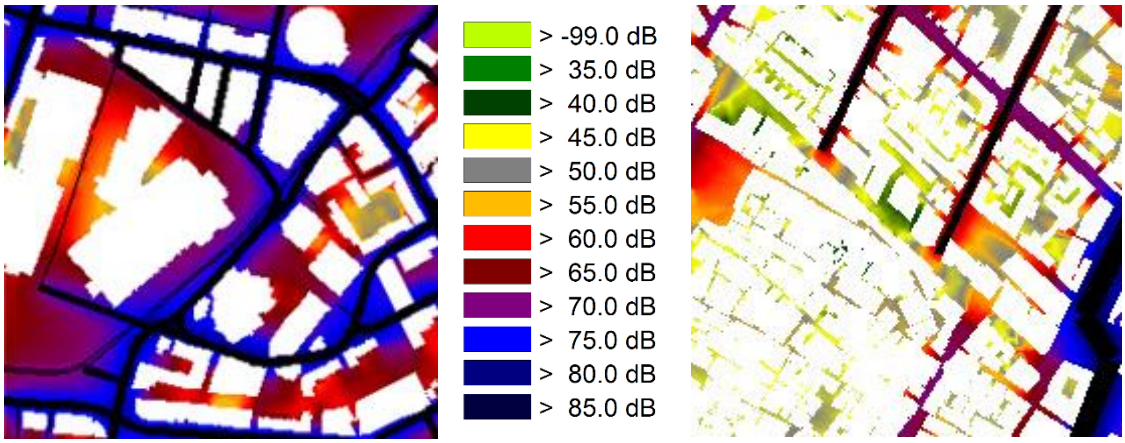

a b

Figure 6.10 Noise maps of public squares in the city centre of Greater Manchester (a) and Wuhan (b)

Both cases of public squares in the city centre of Wuhan and Manchester are pedestrian zones locates in the historical district surrounded by historical buildings that can be traced back to 19th century, while the buildings in downtown Wuhan are mainly large amount of high-density and low-rise buildings, which keeps the traffic and traffic noise outside; whereas in the Greater Manchester case, large scale individual public buildings creates

high ratio of space and lower building coverage allows the major traffic flow distributed in the whole pedestrian area, causing higher traffic noise levels.

6.4.2.2 Street canyons and commercial blocks samples

As shown in Figure 6.11, two high density commercial areas in each city are chosen, both located in the city centre. The GSI in both cities is approximately the same, with a difference of only 0.7%. However, as buildings in Wuhan are much taller than that in Greater Manchester, the actual building density in the former is still much higher than that in the latter.

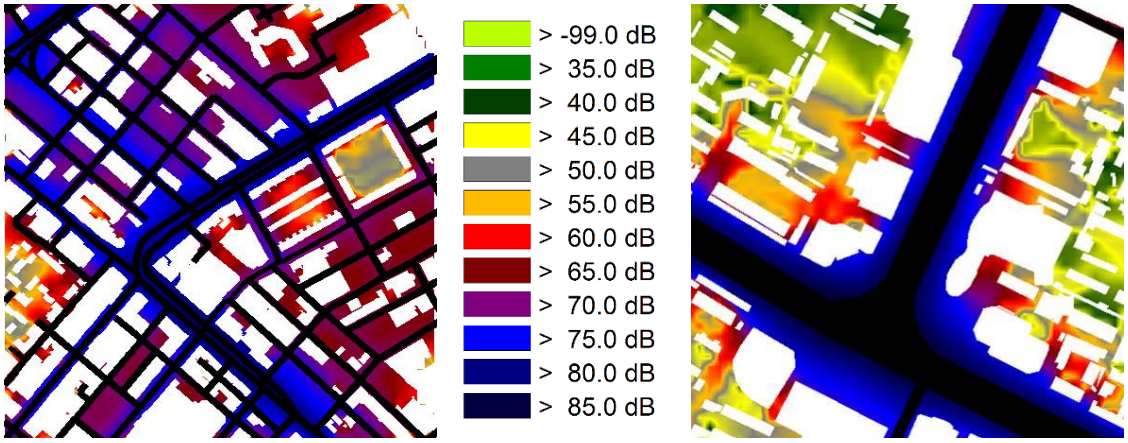

Figure 6.11 Noise maps of street canyons with commercial blocks in Greater Manchester (a) and Wuhan (b)

From the map it can be seen that the average noise in the Greater Manchester case is much higher than that in Wuhan, by 9.4–14 dBA in terms of L_{avg} and L_{50}, but the L_{max} and L_{10} in terms of ground and façade noise level in Wuhan are all higher than that in the Greater Manchester case, by 2–6 dBA. It is due to more concentrated traffic and high-rise buildings, as the RSR in Wuhan is 13.1% whereas this ratio in Greater Manchester is 25.6%. As can be seen in Figure 6.11, in Wuhan two major roads share most of the traffic, each having a traffic flow of more than 60,000 vehicles a day. Considering that buildings along the major roads are much higher than the other buildings in the same area, the street canyons actually creates a more sealed long space for isolating and attenuating the traffic noise, to protect buildings behind the canyon. Hence the result explains why the minimum and background noise level in the Wuhan case is much lower than that in Greater Manchester in terms of ground and façade noise, by 8–16 dBA.

6.4.2.3 Low and high income residential areas samples

It can be seen from Table 6.4, Figure 6.3 and Figure 6.4 that generally the noise level in the low income residential area is much lower than that of the high income area in Wuhan. The ground noise level L_{50} of the low income area is 10 dBA lower, although, in terms of the façade noise level L_{50}, the difference is only 4 dBA. It is noted, however, the maximum noise L_{max} is 2–4 dBA higher than that in the high income area. The minimum and background noise level in terms of L_{min} and L_{90} of the low income area is also higher than those in the high income area, by 2 dBA and 4 dBA, respectively.

There is one major road with heavy traffic in each area, but the one in the low income area is 10,000 vehicles/day higher than that in the high income area, which causes the higher L_{max} in the low income area. The actual building height in the high income area is much greater than that in the low income area, by 6–35 storeys. This also results in higher density in the high income area compared to that of the low income area. It is noted that in Chinese cities many people prefer living in high-rise residential buildings. The high-rise buildings obstruct the direct noise impact from the major roads more effectively than lower buildings so that as can be seen in Figure 6.12, in the high income area a quiet area inside the community is created, where the minimum noise level is lower than that of the low income one. The noise from the major roads surrounding the low income area is mostly attenuated by the high coverage of buildings, making the disparity between the façade spatial noise indices and ground spatial noise indices much smaller.

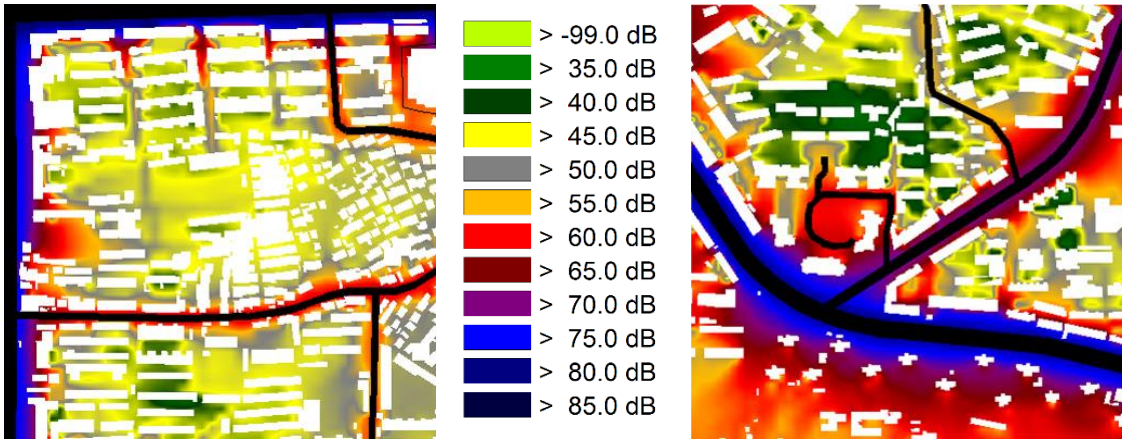

a b

Figure 6.12 Noise maps in typical low (a) and high (b) income residential areas in Wuhan

In the meantime, some potential social reasons should be considered. For example, statistics shows that, families with lower incomes own relatively fewer vehicles (Wuhan Statistics Bureau, 2006), hence the vehicle activities and noise could also be less in the low income communities.

6.5 Conclusions

There have been only few researches explored the potential influence of urban form on the distribution of traffic noise (Tang & Wang, 2007; Kang & Huang, 2005), before the comparative study in this chapter was originally initiated between Sheffield, UK and Wuhan, China (Wang, Kang, & Zhou, 2007). Further comparison between between Greater Manchester and Wuhan was conducted in this chapter with the assistant of state-of-the-art noise simulation tools and spatial noise distribution methods. It can be concluded that there are significant differences between noise distribution in high density cities as Wuhan in China and low density cities as Greater Manchester in the UK.

The highly concentrated major roads in Wuhan which normally have 2–3 times higher amount of vehicles per day than those in Greater Manchester (WCTPDI, 2006; Pointer, 2005), make the ground noise L_{max} and L_{10} in the Wuhan samples higher than that in the Greater Manchester samples, by 2.8 dBA and 0.5 dBA on average, respectively.

However, as can be seen in Figure 6.2, the unevenly distributed roads in Wuhan together with the high-rise buildings along the major roads limit the traffic noise in major street canyons, which makes the average and minimum ground noise level much lower than that in Greater Manchester. The ground noise level in terms of L_{avg} and L_{50} in the Wuhan samples is lower than that of the Greater Manchester samples by 5.6–6.5 dBA respectively. The differences in L_{min} and L_{90} are also evident.

In terms of building façade noise level, the disparities in the average and minimum noise levels are even higher. The L_{avg} and L_{50} in the Greater Manchester cases are 7.7 dBA and 9.1 dBA higher than those in the Wuhan cases. The higher difference is caused by the greater width of roads in Wuhan, which causes more traffic noise attenuation before reaching the building façades compared with that in Greater Manchester. In the meantime, the less minor roads surrounding the buildings in Wuhan make the façade noise level in

term of L_{10} much lower than that in Greater Manchester, by 3.5 dBA on average, although the L_{max} is still higher by 2.2 dBA because of extraordinary high traffic on major roads.

The analysis of correlations shows that the urban morphological indices generally have significant effects on noise levels, with different patterns in the two cities. The RSR is proved to have a significant positive correlation with most of the spatial noise indices in the Greater Manchester samples in terms of the ground as well as façade noise levels. In the Wuhan samples, it only has a significant effect on façade noise levels in terms of L_{avg} and L_{50}. The GSI has a significant negative correlation with the L_{avg} and L_{50} in the Wuhan samples in terms of both ground and façade noise levels while the correlation tends to be positive in the Greater Manchester samples. In terms of the correlations between the OSR and the noise levels, different tendencies are found again in the two cities.

It is shown that in Wuhan, the typical low income residential area has a higher maximum noise level and lower average noise level, compared with the high income residential area, although further research is needed in this aspect with more samples. Given the considerable effects of urban morphology on the traffic noise distribution patterns, it is of great significance to systematically consider more urban structures across the world. It is also important to use micro-scale simulation techniques to obtain more detailed spatial noise distribution (Kang, 2000; 2001; 2002; 2005). Finding more correlation patterns between noise distribution and urban morphology can be helpful in reducing the noise impact in a more efficient way, through better planning the roads and designing the patterns of building block arrangements (Kihlman & Kropp, 2001).

Chapter 7 A parametric study on the effect of urban morphological characteristics on traffic noise distribution

7.1 Introduction

The noise propagation in the urban environment is influenced by a variety of factors (ISO, 1996), nevertheless as found in previous chapters that the urban morphological indices has the most profound impact on the production and propagation of the traffic noise in the urban areas, amongst which the road network pattern and the building form are two of the most important influential features. The objective of this chapter is primarily to apply a semi-controlled parametric research method and discuss how urban morphological indices affect the severity and distribution pattern of urban traffic noise, and to discover the correlation between a series of urban morphological indices and the noise distribution indices. Based on the findings the chapter also focuses on the discussion of the potential of urban noise traffic noise distribution via the measures urban planning and urban design.

This chapter consists of four parts. Section 7.2 discusses the methodology to be implied in this study. Firstly, a framework of parametric study methodology is introduced, in which a group of controlled and semi-controlled urban morphological indices defining a series idealised urban forms and traffic distribution are introduced, the value of which are defined based on empirical research findings. 36 idealised urban form modalities are constructed based on a framework using controlled and semi-controlled parameters. The horizontal and vertical distribution of noise SPL in the 36 idealised cases are calculated and a series of spatial noise indices are then derived from the calculation results based on a statistical method using a Matlab programme developed. In Section 7.3, the calculation results are listed and compared briefly for the sake of comparing the traffic resistance in different case groups with distinct urban density, the variation and distribution of the spatial noise indices in case groups with identical density indices and distinct urban morphology are also compared. The Bivariate correlations between all selected urban morphological indices and a series of spatial noise indices are then systematically

analysed in Section 7.4. Furthermore, in Section 7.5 and Section 7.6, a multilinear regression analysis is conducted for the morphological indices that were found to have significant correlations with the spatial noise indices. The potential causal relationship between the variation of urban morphology and the general level and spatial distribution of traffic noise is also discussed, for the sake of potential improvement and optimisation of urban planning and designing practice and guidelines from the perspective of noise abatement.

7.2 A parametric study approach

A parametric research method with controlling key urban morphological parameters is introduced in this Chapter. The studied cases are divided into several different groups, the value of a series of density-related urban morphological indices including the *N*, FSI, and GSI are introduced, and a variety of representative urban morphological modalities with typical density, urban fabric size and traffic patterns are defined into low, medium and high groups. In each group a series of urban morphological features are designated systematically based on typical urban environment features in relatively low, medium and high density urban areas.

7.2.1 Selection of urban morphological and spatial noise indices

A series of urban morphological indices are introduced as can be seen in Table 7.1, which are classified into three groups, the pre-defined urban density related indices, the building and street geometry related indices and the urban geography related indices. Three types of spatial noise indices: the general ground levels GL_n which only measures the noise levels at the ground level, ground façade levels GFL_n that represents the noise level distribution close to all the building façades at the ground level, and the total façade levels TFL_n which are derived from 3D noise map and measures the noise distribution on the façades of all buildings. Six basic statistical spatial noise indices that represent the spatial noise distribution of each type of noise levels, including the L_{max}, L_{avg}, L_{min}, L_{10}, L_{50} and L_{90} and a series of attenuation indices are calculated based on basic subtractions using two of the spatial noise indices to describe the overall attenuation between the two spatial noise indices.

Table 7.1 Definition and calculation method of urban morphological indices adopted *

Type	Abbr.	Name	Definition	Formula
Density related indices	FSI	Floor space index	The ratio of the total floor area to the land area	$\sum A_f/A_T$
	DSTD	Daily spatial traffic density	The number of vehicles per square kilometre of an annual average day	$\sum Q_r/A_T$
	N	Road network density	The density of the road network (m/m2)	$(\sum l_{ir} + \frac{1}{2}\sum l_{er})/A_T$
	GSI	Ground space index	The ratio of total footprint of the buildings to the total land area	$\sum A_g/A_T$
Building and street geometric indices	OSR	Open space ratio	The ratio of the total open space to the total land area.	$\sum A_o/A_T$
	RWI	Road width index	The ratio of the road width to street canyon width	$\sum w_r/\sum w_s$
	RSR	Road coverage ratio	The ratio of total road carriageway area to the total land area	$\sum A_r/A_T$
	BBAI	Building block area index	The area of building block boundary to lot size ratio	$\sum A_B/\sum A_L$
	HWR	Height-to-width Ratio	The average height to width ratio of the street canyons	$\frac{1}{n}\sum_{i=1}^{n}(\frac{H_s}{w_s})_i$
Urban geography related indices	BFR	Building façade ratio	The total building façade area to land area ratio	$\sum A_{fa}/A_T$
	RI	Rugosity index	Mean height of the urban canopy	$\sum(A_g \times H)/\sum(A_g + A_o)$
	BFASAI	Building frontal area to street area index	The ratio of building façade area to street space area	$\sum A_{ff}/\sum A_S$
	BFLI	Building frontal length index	The interface density of the streets in terms of length. also known as the Street Interface Density (SID)	$\sum w_f/2(\sum l_{ir} + \frac{1}{2}\sum l_{er})$
	CAR	Complete aspect ratio	The ratio of all building surface area plus the open ground area to the total land area	$(\sum(A_{fa} + A_{rf}) + A_G)/A_T$
	BSAPAR	Building surface area index	The ratio of all building surface areas including the roof to the total land area	$\sum(_{fa}+ A_{rf})/A_T$
	BPRLI	Building perimeter to road length index	The ratio of total perimeters of all buildings to the total length of roads	$P_T/2(\sum l_{ir} + \frac{1}{2}\sum l_{er})$

* For details definition of the indices please see Section 3.4.

Both the grid noise map and the façade noise levels of all buildings are calculated following the British national standard CRTN (UK DfT, 1988) and ISO 9613-2 (ISO, 1996). Three types of spatial noise indices: the general ground spatial noise indices, the ground façade spatial noise indices, and the total façade spatial noise levels, with six indices each, are then abstracted.

7.2.2 Making of the idealised cases

The road networks are firstly defined into four types, one with high *N* (network density), one with low network density, two cases with the same medium *N* values and different network distribution types. Four basic urban fabric types with different division of road networks are also set correspondingly. With the division of the road network, four idealised cases also represent three typical urban fabrics with the average scale of 90 m × 72 m, 375 m × 375 m and 187.5 m × 187.5 m respectively, based on typical urban fabrics of real sites investigated in previous Chapters in the UK and China, as well as various form of urban grids sizes and form (Marshall, 2005). It is to note that, in one of the mid-*N* case group, the branch roads are set unevenly and with smaller road width to represent the distribution of smaller roads in typical Chinese residential area (Wu & Li, 2011), as can be seen in the illustrations of the case group mid-N set A in relevant figures.

Table 7.2 Parameter settings of the road network for four network density types

N (km/km^2)	Road Type	Q_r(veh/km^2/d)	w_r (m)	Interval(m)*
23.38	Arteries	48000	28	1155
	Main	7500	14	375
	Branch	2000	7	72
5.19	Arteries	60000	28	1155
	Main	12000	14	375
	Branch	n/a	n/a	n/a
10.39	Arteries	48000	28	1155
	Main	9000	14	375
	Branch	6000	7	187.5
10.39	Arteries	48000	28	1155
	Main	9000	14	375
	Branch	6000	14	187.5

* Minimal interval between road central lines

Accordingly, the value vehicles on each section is pre-defined based on the estimation of the empirical values of traffic flow obtained from Manchester (AGMA, 2006) and Wuhan

(WCTPDI, 2006, 2011), and the actual road traffic flow counted on site in Chapter 4 and Chapter 5. To ensure that the total occurred vehicles noise source is equal in each case, the total vehicle number Q_T is adjusted to be the same, at 168000 vehicles per day, based on approximation, (the DSTD is correspondingly can be calculated as approximately 125935 vehicles per km^2 per day). The individual traffic volume on each type of roads is distributed according to the network type and the road hierarchy of each road type as shown in Table 7.2. It is to note that, the distribution of traffic flow is majorly based on the hierarchy of the road and the total amount of roads in the same hierarchy in the planned district. For instance, for the two medium density cases, the traffic flow counts of the branch roads are set to the same, although their road width and distribution are slightly different.

7.2.3 Classification of pre-defined urban morphological indices

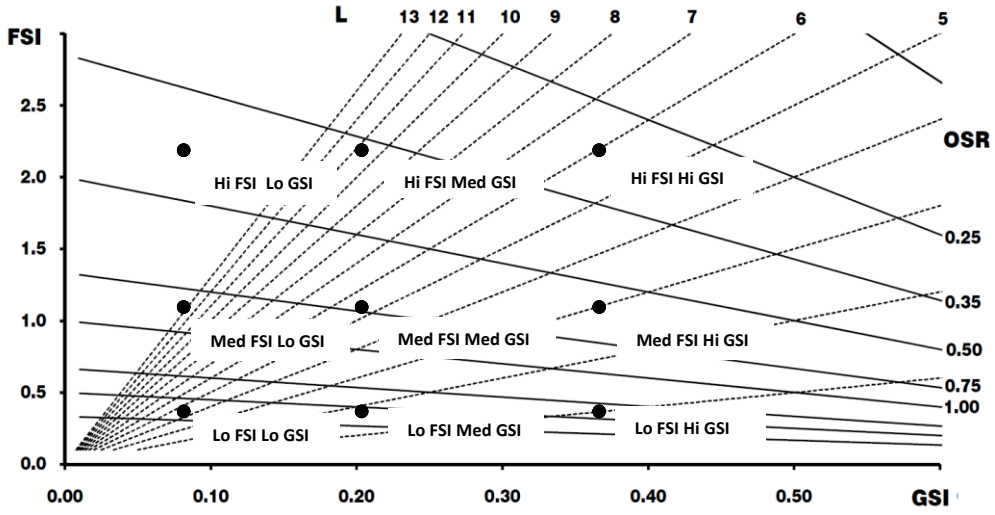

Figure 7.1 Nine combinations of FSI, GSI, OSR and *L* demonstrated based on the Spacemate chart (Salomons & Pont, 2012)

The Spacemate tool (Pont & Haupt, 2005) is introduced to demonstrate the interrelationship of the FSI, GSI, OSR and *L* as can be seen in Figure 7.1. In each road network type, nine sets of urban forms with different combinations of FSI and GSI, as well as building height *L* in terms of storeys are designated. It can be seen that the 36 idealised cases spread across nine sets of the FSI and GSI values and form a 3×3 array; the building height in terms of *L* are distinct. Correspondingly, the change of GSI also leads to a variety of OSR values.

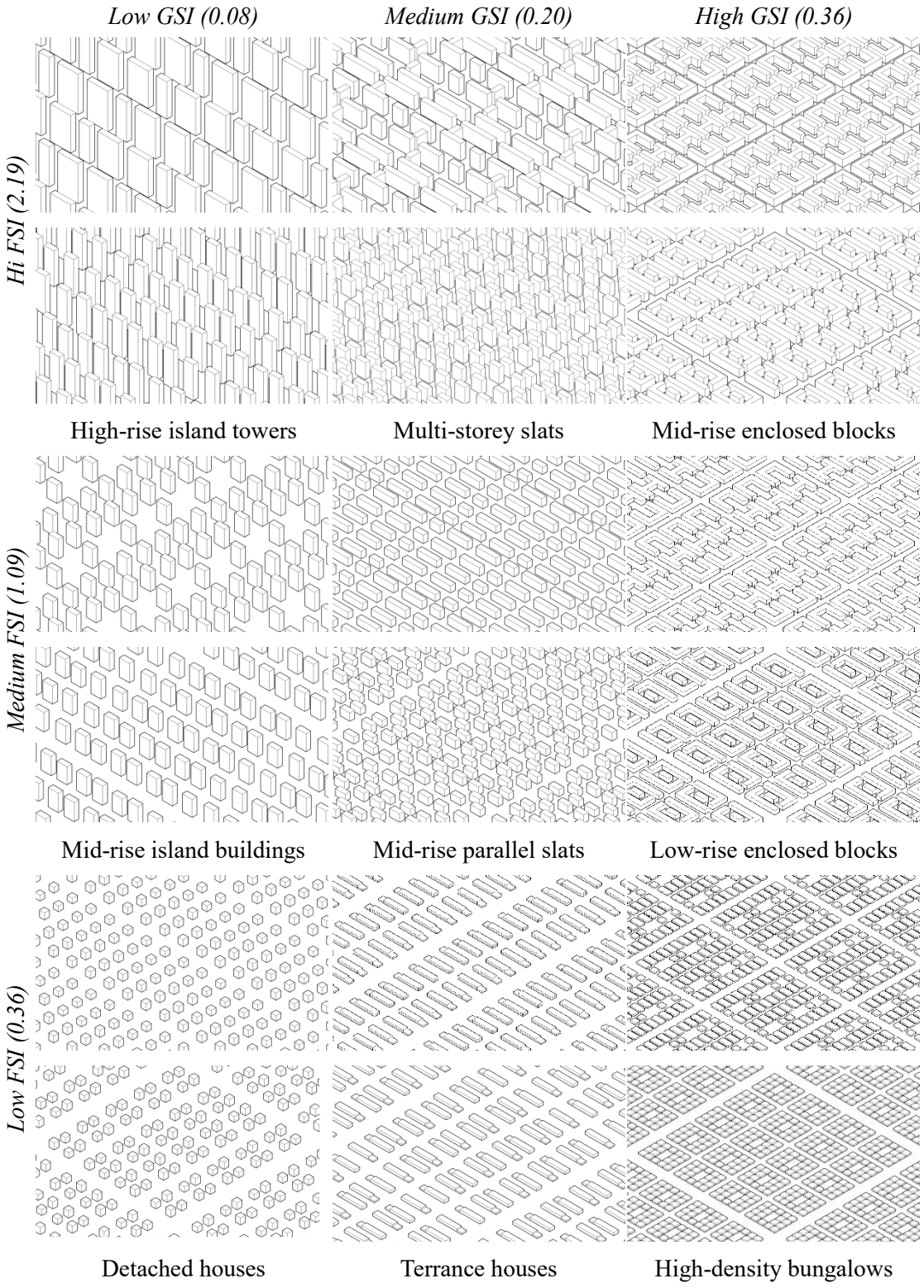

Figure 7.2 Nine examples of urban forms with different combinations of FSI and GSI

The exact values of the pre-defined urban morphological indices involved in the urban form defining are listed in Table 7.3. The building height of a single storey are defined with an abstracted value of three 3.0 m; the actual height of the buildings could then be calculated. The building forms are defined based on the four types of road networks with three levels of road network *N* by classifying the FSI to three different levels, and for each level of FSI, three level of GSI were defined accordingly.

Table 7.3 Combinations of FSI, GSI, OSR and *L* for each type of road network type

	FSI		GSI	OSR	L	H(m)
Low FSI	0.36	High	0.36	0.42	1.0	3.0
	0.36	Medium	0.20	0.59	1.8	5.4
	0.36	Low	0.08	0.71	4.5	13.5
Medium FSI	1.09	High	0.36	0.42	3.0	9.0
	1.09	Medium	0.20	0.59	5.4	16.2
	1.09	Low	0.08	0.71	13.5	40.5
High FSI	2.19	High	0.36	0.42	6.0	18.0
	2.19	Medium	0.20	0.59	10.8	32.4
	2.19	Low	0.08	0.71	27.0	81.0

The notional building forms shown in Figure 7.2 have a variety of urban morphological indices combinations, which together with the combination of nine different types of road networks represents a series of typical features of subsistent urban forms in both eastern and western cities.

As can be seen that the building to the left end of the chart have lower GSI, and tend to have more island-style arrangement with more façades exposing to the roads and adjoining open space; the building to the right end of the chart have higher GSI and tend to have more enclosed and group-style or cluster-style arrangement, and have more façades facing inwards and towards the relatively confined interspaces, and have fewer façades facing directly to the road despite the road density.

7.3 Effect of urban density indices on traffic noise resistance

By categorising the cases into different groups based on the pre-defined urban density indices, the effects of urban density are systematically observed and analysed. The statistical spatial noise indices are derived from the strategic and three vertical noise maps

calculated using Cadna/A. The cases are categorised hierarchically based on the network density, FSI and GSI respectively. The variation and distribution of traffic noise level and distribution are systematically analysed.

7.3.1 Noise calculation results and spatial noise indices

In Figure 7.3, Figure 7.4 and Figure 7.5, the noise maps of the central area surrounded by four sections of main roads with an area of approximately 14.8 hectares are demonstrated. It is to note that the grid noise maps are extracted from the overall noise maps for the sake of demonstration, the calculation of spatial noise indices are still conducted based on the whole area noise maps and building façade noise maps. The calculation areas are bordered by the central lines of the four arteries and with the area of approximately 133.4 hectares. The raster noise maps are illustrated based on a 5-dBA-step system differentiated by different colours, and the coloured pixels represent the noise levels interpolated from results of the grid receiver points. Nevertheless, the spatial noise indices are calculated based on higher resolution to ensure the accuracy of the indices. It can be observed Intuitively from the 36 noise map samples that the predefined FSI, GSI and *N* as three key factors systematically shape the urban morphological characteristics as well as the distinct noise distribution patterns in all cases.

As can be seen in Figure 7.3–7.5 that, generally, from the urban morphological perspective, the increase of GSI creates denser and more enclosed building forms. The increase of road network density *N* tends to divide the building blocks into smaller groups. From both morphological and noise distribution perspective it can be seen that the maps with fewer roads seem to have more zones with lower noise coverage, At the same time the change of road network density seems to have no obvious effect on the area around the main roads. In the meantime, it can be seen that the more confined space created by higher GSI creates more space with colours marked with lower than 50 dBA, and the increase of FSI further increases this tendency. it may because of enhanced screening effect of the higher building height. Nevertheless, above qualitative descriptions need to be further examined with more quantitative evidence. As in this parametric study, and there are three key indices pre-defined into three groups each, which are the *N*, FSI, and GSI. Therefore, some primary comparison can be made between different cases with identical *N*, FSI, and GSI.

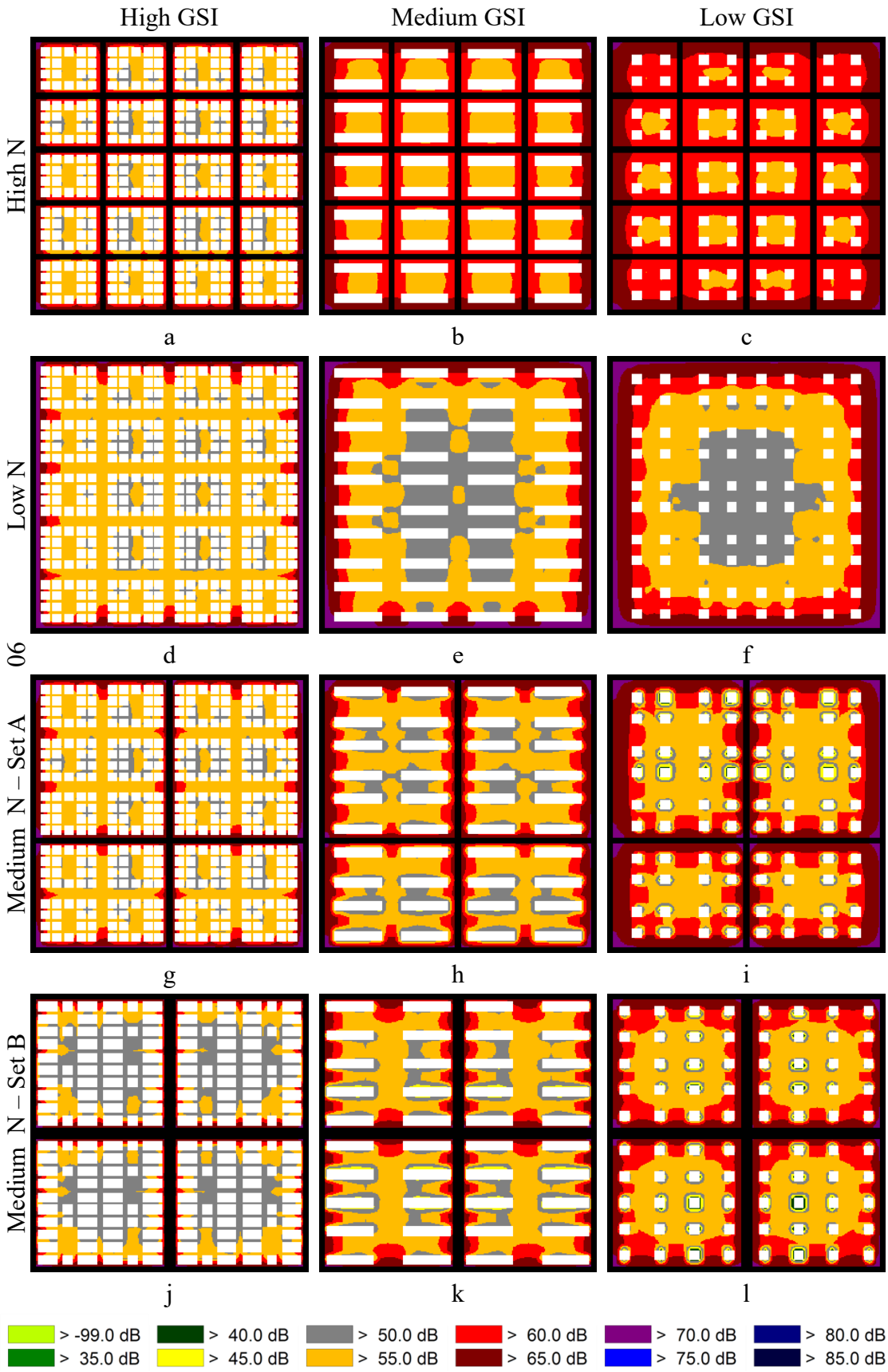

Figure 7.3 Grid noise maps of typical fabrics with relatively low FSI = 0.36

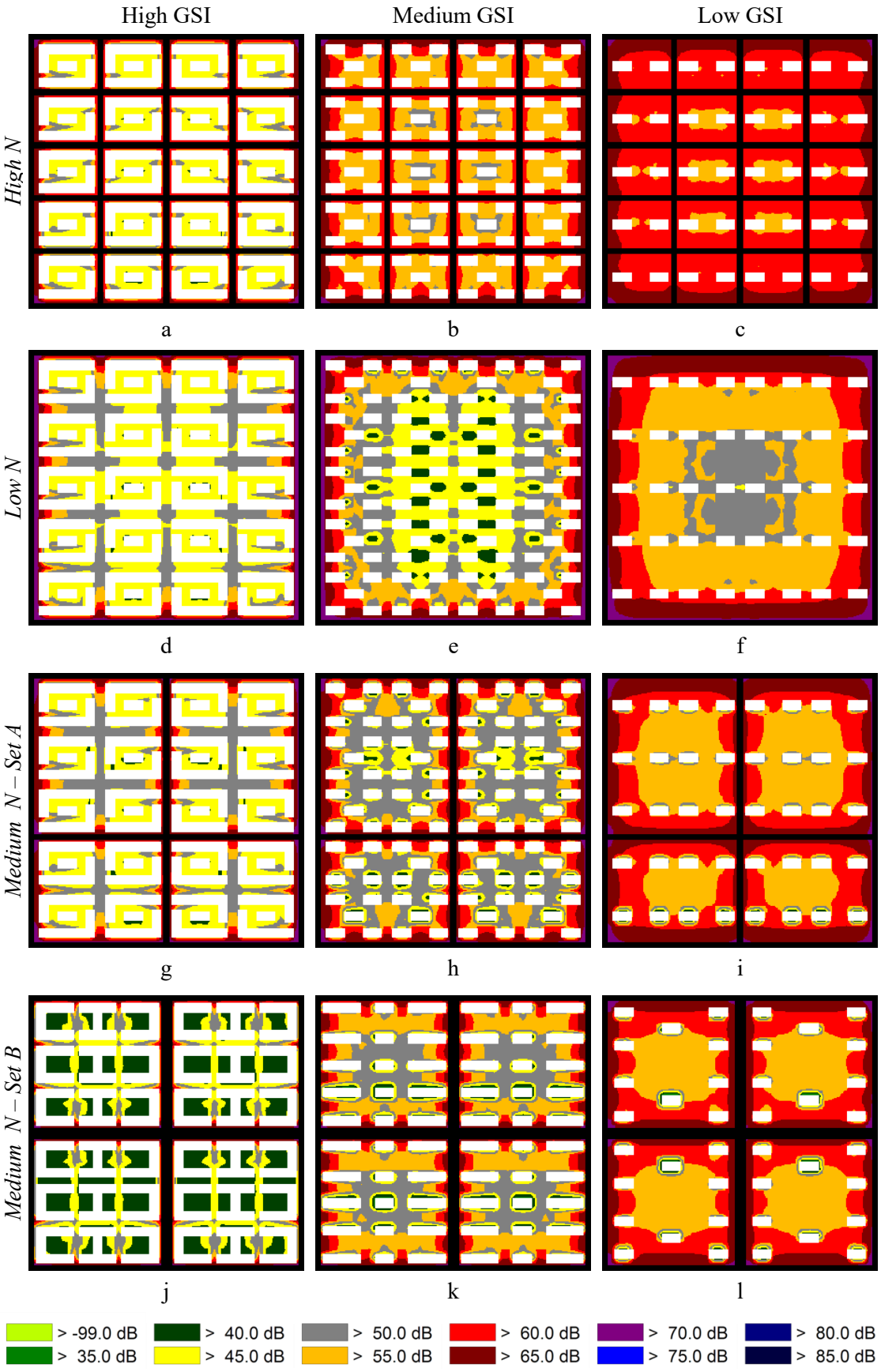

Figure 7.4 Grid noise maps of typical fabrics with relatively medium FSI = 1.09

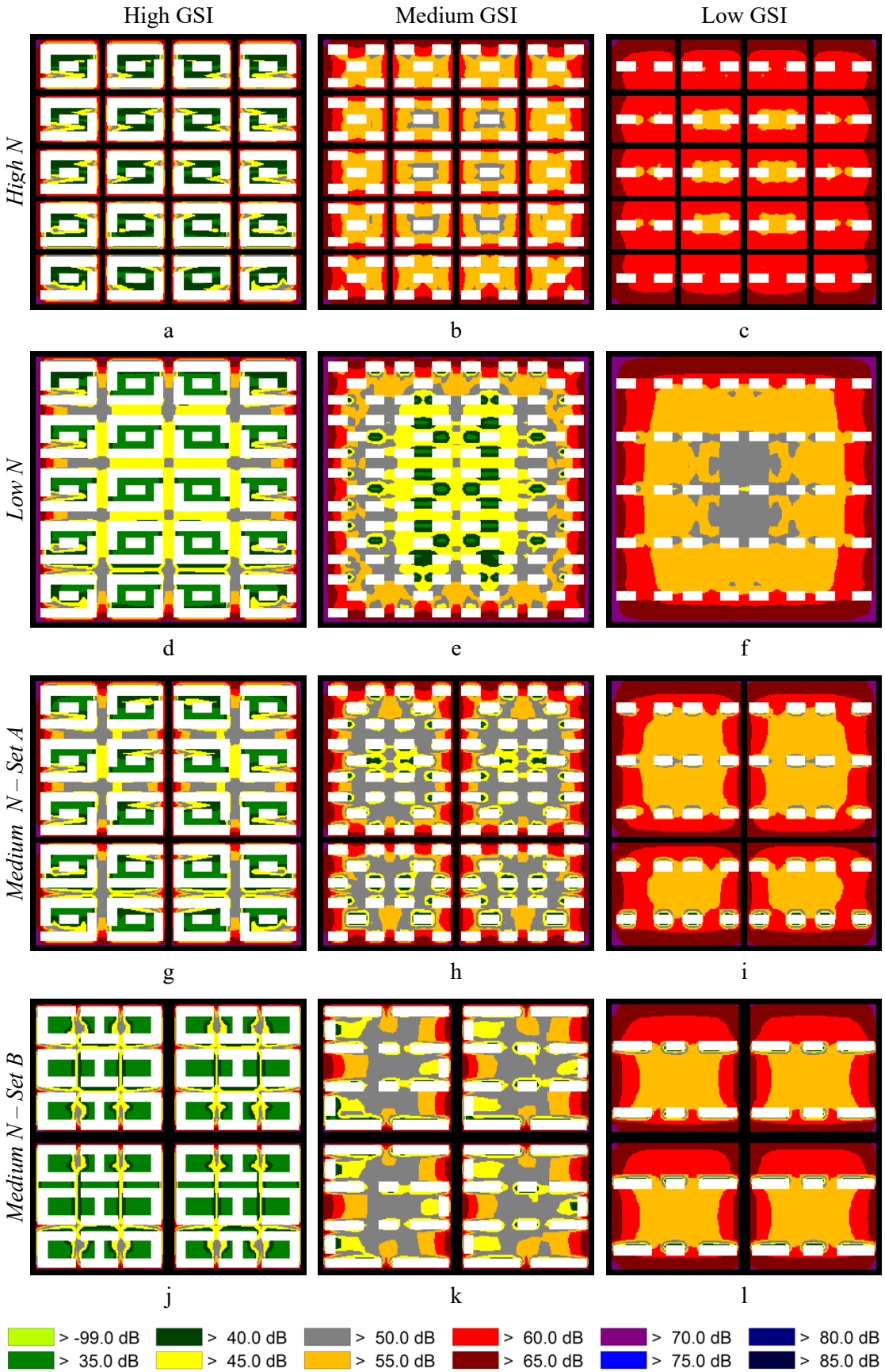

Figure 7.5 Grid noise maps of typical fabrics with relatively high FSI = 2.19

7.3.2 Traffic noise resistance of different urban density

In this section the average and median noise level of all cases grouped by three pre-defined urban morphological indices *N*, FSI and GSI are compared. The indices of L_{50} and L_{avg} of all spatial noise index types as shown in Figure 7.6, Figure 7.7 and Figure 7.8 are compared systematically.

In the meantime, to examine the change in key urban morphological indices on the overall quietness in the idealised cases, the indices of L_{50} that measures the median noise level of all three types are compared among each other and also with the threshold of quietness. The horizontal mark line of 55 dBA in each chart indicates can be seen as a threshold of quietness for urban traffic noise assessment with regard to human perception that are adopted in both EU (EEA, 2010) and China (MEP China, 2008), which is also recommended as a key target level for strategic noise mapping (EPA, 2011). Thus, the L_{50} being lower than 55 dBA can serve as an indicator which denotes whether 50% of the studied space is within the threshold of quietness.

Nonetheless, it is to note that the idealised cases in this research are designed with the most fundamental combination of urban form elements, i.e. roads and building blocks without considering noise abatement factors in real urban environment e.g. foliage, large open spaces like parks and parking lots, etc., and the traffic density which determines the upper limit of the traffic noise is also set to a fixed typical value, the value of 55 dBA only serves as a referential threshold for the purpose of brief assessment. The main acoustic focus of this study is the most typical traffic noise and its distribution.

7.3.2.1 Different road network density

- ***Noise level comparison***

First of all, it can be seen that, in general the road network density *N* does not have clear linear relationship with the general noise levels, although the average value of L_{avg} and L_{50} are generally higher for cases with high network density *N,* on all surfaces including at the ground level and at all attitude of the building façades. As shown in Figure 7.6 that between the cases with high-*N* and low-*N* there are disparities of up to 2.4 dBA, 2.4 dBA

and 1.9 dBA for the GL_{avg}, $GFL_{avg,}$ and TFL_{avg}, respectively. It may mainly be due to the effect of the wider spread of traffic flow caused by the increased amount of branch roads.

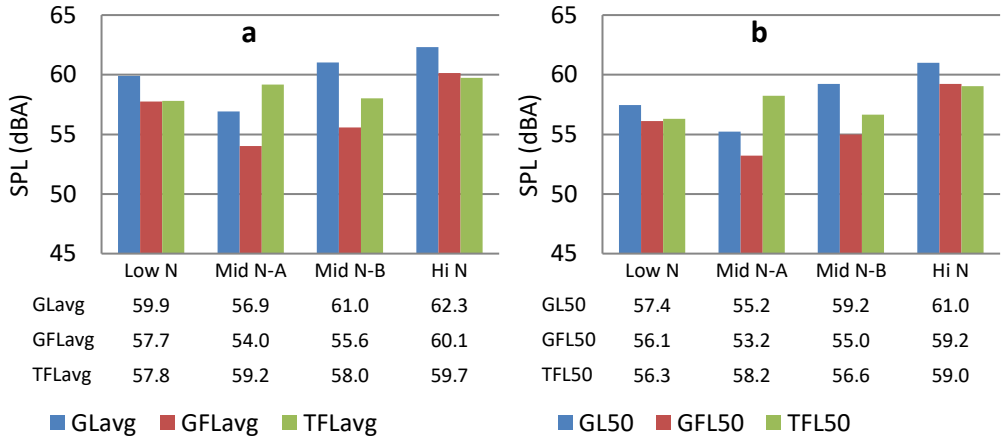

Figure 7.6 Comparison of average L_{50} (a) and L_{avg} (b) of different groups of cases with low, medium and high *N* values

Nevertheless, the two medium-*N* case groups have nearly opposite results as can be seen in Figure 7.6. For the general ground noise levels, comparing with the low-*N* cases, the GL_{avg} and GL_{50} of Set A cases are lower than the low-N cases for 3.0 dBA and 2.2 dBA respectively; while that of the Set B are higher for 1.1 dBA and 1.8 dBA respectively. For ground façade spatial noise indices, the average Set A and Set B are both lower than the low-N cases especially the medium-*N* Set A, the GFL_{avg} and GFL_{50} of which is 3.7 dBA and 2.9 dBA lower than the low-*N* cases. For the total façade noise level, the TFL_{avg} and TFL_{50} of both cases are higher than the low-*N* cases, and are lower than the high-*N* cases, although the TFL_{avg} and TFL_{50} of the Set-B are slightly higher than that of the low-N case for 0.2 dBA and 0.3 dBA respectively.

- ***Threshold of quietness***

Firstly, for the façades noise it is found that the average values of the median noise index L_{50} are generally higher than the threshold of 55 dBA by 1.3–4.0 dBA despite the change of network density, although the relationship between the excessive level and the rising network density is not linear. It denotes in the idealised scenarios in this research, despite the change of network density, less than 50% of the façades can be regarded as quiet in general, and the noisy area increases with *N*.

In the meantime, the exceeded median noise levels above 55 dBA in the high-*N* cases are more distinctive comparing with the other categories of cases: the GL_{50}, GFL_{50} and TFL_{50} of the high-N cases are averagely 6.0 dBA, 4.2 dBA and 4.0 dBA higher than 55 dBA respectively, while that of the low-*N* cases has relatively low excessive level value of 2.4 dBA, 1.1 dBA and 1.3 dBA respectively. This thus indicates that by distributing the traffic flow into a denser road network especially with a large amount of branch roads would clearly reduce the quiet space in the open ground as well as on all altitude of building façades. Furthermore, the large fabric size created by the low network density may be the reason of the lower excessive level on all surfaces.

In the meantime, it is clear to see that for the medium-N cases, the excess level varies from index to index and have some unexpected values that are lower than 55 dBA. The quietest is the medium-N set A cases at which the GL_n is 1.8 dBA lower, and the GL_n is only 0.2 dBA higher than the 55 dBA threshold; while at the same time the excess level of total façade indices TFL_n is 3.2 dBA higher than 55 dBA; which denotes that the averagely 50% space on the ground of the medium-N set cases are relatively quiet, while 50% of the façade surface are above the threshold.

On the contrast, the medium-N set B cases has the excess level of GL_{50}, GFL_{50} and TFL_{50} of are 4.2 dBA, 0 dBA and 1.6 dBA, which indicates that 50% of the open ground noise level are much higher above the 55 dBA threshold comparing with the set A cases, while 50% of the building façades can be regarded as quiet.

- ***Summary***

Considering that the median noise level L_{50} reflects the 50% division of noisier and quieter spaces in the tested areas of the medium-*N* cases, it is interesting to note that the slightly different design of road network with the same network density and traffic distribution pattern can have significant influence on the general distribution of the traffic noise on both open ground and different level of building façades.

Generally, for two medium noise case groups, Set-A cases with narrower branch roads and irregular fabric sizes tend to have higher total façade noise level and lower ground noise levels both on the open ground and close to the façades; the Set-B cases with widened and evenly distributed branch roads have higher overall ground noise levels and

lower façade level on all altitudes. It may be due to the change of network pattern affects the building forms and arrangement significantly as can be seen in Figure 7.2, thus building as the major barrier affects the noise propagation significantly, it is to be further studied following sections. It suggests that, by comparison, the medium-N cases with medium size basic urban fabrics have some potential in mitigating the general impact of traffic noise.

7.3.2.2 Different building floor space ratio

- ***Noise level comparison***

Regarding the FSI that reflects the total construction intensity of the planned area in terms of both building mass and height, the rise of it generally brings a constant decrease in average and median noise level on all ground surface and building façades. As can be seen in Figure 7.7, the average values of L_{avg} and L_{50} of three categories are compared among different case groups with low, medium and high FSI value, the average and medium noise levels do decrease in general. When the FSI increases from the lowest value of 0.36 to the highest value of 2.09, the average values of GL_{50}, GFL_{50} and TFL_{50} decrease for 3.5 dBA, 4.5 dBA, and 4.1 dBA respectively; and the GL_{avg} GFL_{avg} and TFL_{avg} decrease for 1.6 dBA, 4.3 dBA and 4.2 dBA respectively. It denotes that the noise impact to the open space and building façades, in general, is less when the total building density in terms of FSI increases despite other morphological factors.

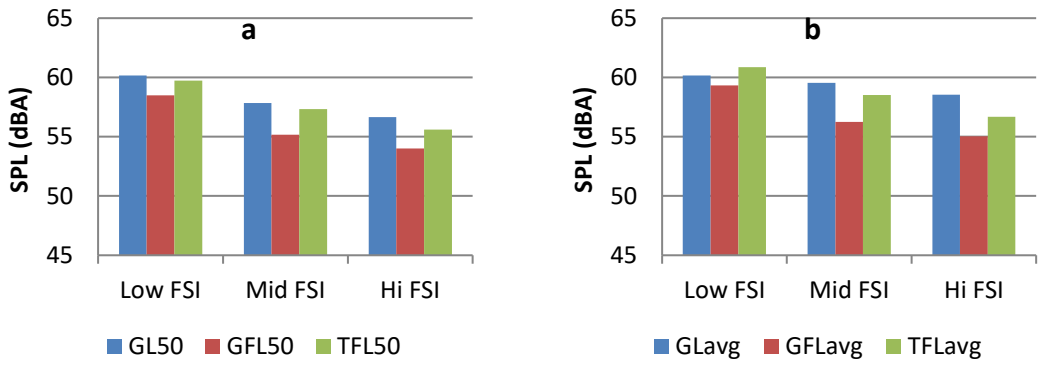

Figure 7.7 Comparison of average L_{50} (a) and L_{avg} (b) of different groups of cases with low, medium and high FSI

- ***Threshold of quietness***

It is found that the average values of the median noise index L_{50} mostly exceeds the threshold noise level of 55 dBA, except the ground façade index GFL_{50} of the high-FSI cases as shown in Figure 7.7a which are averagely 1.0 dBA lower than the threshold.

In the meantime, the excess median noise levels in the low-FSI cases are more evident than the other two categories of cases: the GL_{50}, GFL_{50} and TFL_{50} of the low-FSI cases are averagely 5.2 dBA, 3.5 dBA and 4.7 dBA higher than 55 dBA respectively, while for the medium-FSI and high-FSI cases, the average excess noise levels are all lower than 3 dBA.

- ***Summary***

It can be seen that the average and median spatial noise level of all three types evidently increases when the floor space ratio FSI rises; consequently, the high-FSI cases have the comparatively quietest noise level. It denotes that the increased urban density of buildings in terms of FSI significantly limits the propagation of traffic noise on the ground and on all altitude of the building façades.

7.3.2.3 Different building ground space index

- ***Noise level comparison***

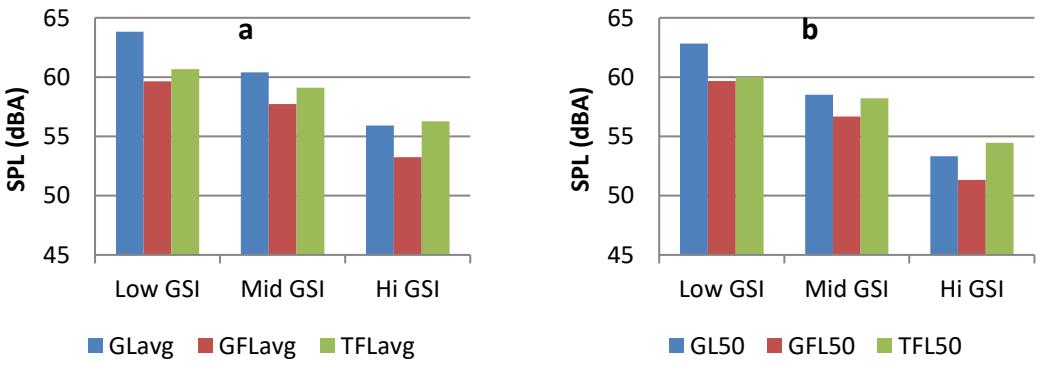

Figure 7.8 Comparison of average L_{50} (a) and L_{avg} (b) of different groups of cases with low, medium and high GSI

Similarly, it is found that when the GSI that reflects the total building ground space coverage, the average and median noise values also generally decrease, and the changes are much higher than that when the FSI value increases. It can be seen in Figure 7.8 that, when the GSI increases from the lowest value of 0.08 to the highest value of 0.36, the

average values of GL_{50} GFL_{50} and TFL_{50} decrease for 7.9 dBA, 6.4 dBA and 4.4 dBA respectively; and the GL_{avg}, GFL_{avg} and TFL_{avg} decreases for 9.5 dBA, 8.3 dBA and 5.5 dBA respectively. It indicates that the increase of building density in terms of ground coverage may also have a positive effect on the abatement of noise impact on ground and building façades in general.

From the results above, it can be concluded that the changes in building density measured by both FSI and GSI in the studied cases have clear impact on general noise level: the higher the building density, the lower the average and median noise levels. Nevertheless, with the rising of road network density in terms of *N*, the average value of L_{avg} and L_{50} increases in general but without a linear relationship, the L_{50} at the ground level even decreases when *N* rise from low to medium. Considering that the change of network density also re-defines the size and pattern of planned fabric with identical FSI and GSI, the change of network density may consequently change the arrangement and form of buildings and therefore the noise distribution pattern is also affected, as can be seen in Figure 7.3–7.5. Therefore, it is important to examine more urban morphological indices that can better explain this phenomenon.

- ***Threshold of quietness***

It is clear to see in Figure 7.8 that, the excess level of all three types of indices declines clearly with the increase of GSI. For low-GSI and medium-GSI L_{50} of all indices are higher than 55 dBA indicating less quiet area in the cases. For the high-GSI cases, the GL_{50}, GFL_{50} and TFL_{50} are all lower than 55 dBA by 1.7 dBA, 3.7 dBA and 0.5 dBA respectively.

- ***Summary***

From the results above, it can be seen that the increase of building density in terms of GSI can clearly reduce the average and median noise level in the open space and on all level of building façades. When the GSI rises to a certain level, i.e. the building coverage becomes large enough; the general impact of traffic noise can be reduced to an acceptable level despite the other urban morphological factors.

7.3.2.4 A primary correlation analysis

Table 7.4 Correlation between three density-related urban morphological indices and the spatial average and median noise levels, the R value of both one-tailed and two-tailed Bivariate correlation with * indicating $p < 0.01$ and ** indicating $p < 0.05$ are shown.

Pearson Correlation		GL_{avg}	GL_{50}	GFL_{avg}	GFL_{50}	TFL_{avg}	TFL_{50}
N	Sig. (2-tailed)	–	–	–	–	–	–
	Sig. (1-tailed)	–	.281*	.314*	.315*	–	–
FSI	Sig. (2-tailed)	–	–	-.375*	-.355*	-.573**	-.477**
	Sig. (1-tailed)	-.301*	–	-.375*	-.355*	-.573**	-.477**
GSI	Sig. (2-tailed)	-.712**	-.730**	-.591**	-.690**	-.616**	-.657**
	Sig. (1-tailed)	-.712**	-.730**	-.591**	-.690**	-.616**	-.657**

The relationship between the average and median noise level and three fundamental urban morphological indices, *N*, GSI and FSI which represents the urban density in terms of road length, building floor space and building ground space coverage, are examined. The effect of the density indices on the general quietness is also analysed. It is found that the three indices can more or less affect the general noise level in the urban environment and its impact to the indoor space.

- ***Building density***

The FSI and GSI are proven to be both negatively correlated with the average and median spatial noise level at the ground, ground façade, and total façade level, while the GSI seem to have stronger and a more global influence. As can be seen in Table 7.4 that the GSI has a strong negative correlation with all indices checked, while the FSI mainly has a negative correlation to a weaker extent with the ground and ground façade indices, the correlation of which with the total façade indices are stronger.

It means that, without considering the increasing of vehicles, when the overall building density is higher, the overall noise level could be reduced evidently, which may partially tribute to the stronger screening effect caused by the buildings. In the meantime, this effect seems to be related more with the ground coverage of the buildings than the plot ratio, it indicates that increasing the number or ground coverage of the buildings has a stronger effect on mitigate the general traffic noise impact than simply raise the number of building storeys.

- ***Road density***

Regarding the network density *N*, it can be seen in Table 7.4 that it is not globally correlated with the average and median noise levels, and the only three 1-tailed significant correlations are found on the ground level, no correlations are found between network density and the façade the total noise level. Considering that the overall vehicle amount is fixed in all the idealised case, it indicates that the increasing of road density in terms of length is not certainly related with stronger impact to the traffic noise impact, especially when all the building façades are considered.

Moreover, as discussed earlier, there are three classes of *N* values examined; the high-N cases generally have higher average and median noise levels than the low-N cases due to greater amount of branch roads and broader traffic distribution. In contrast, the two types of medium-N cases with the same value of network density seems to have complicated relationship with the spatial noise indices. It may mainly be due to the change in the scale of the urban fabric, and the arrangement of the buildings that are changed by altered arrangements of the road networks, which may hence influence the general noise impact to the open ground and the building façades.

The findings have two significant implications in practice. Firstly, the network density in terms of length could not solely be employed to predict the overall traffic noise impact, more indices need to be taken into account. Secondly, it implies a potential of mitigating the general noise level by re-arrange the network grid patterns, especially on the overall building façade level.

7.3.3 Effect of urban-density-related indices on the variation and distribution of spatial noise levels

Further observation of the noise calculation results is made in this section. The value of all six statistical spatial noise indices of three categories are derived from both the grid noise maps and the building façade noise maps of all 36 cases and demonstrated based on three categorisation standards: *N*, FSI, and GSI. The calculation results of the all spatial noise indices are collectively compared in four groups according to the four road network types shown in Figure 7.3–7.5; while the FSI and GSI are grouped according to three hierarchies shown in Figure 7.3.

As demonstrated in Figure 7.13, Figure 7.16 and Figure 7.9 that the maximum, average and minimum values of the indices of each category are highlighted in dark lines. The gap between the maximum value and minimal values can be seen as an indicator of the noise levels variation of the spatial indices. The noise attenuation is also analysed as shown in the stepwise comparison chart in Figure 7.12, Figure 7.15 and Figure 7.18, in which the attenuation from L_{max} to L_{min} is divided into four sections by three statistical indices, the L_{10}, $L_{50,}$ and L_{90}. The length of each section indicates the average amount of attenuation, in the open area, on the ground level, close to the ground façade and at all the building façades respectively.

7.3.3.1 Effect of network density N

- ***Variation of noise level***

It is also notable that for all case groups with different N values and network modality, the higher noise levels are evidently concentrated while the lower noise levels are more varied, both on the open ground and on all building façades. It is clear to see in Figure 7.9 that for all indices the vibration of SPL from L_{max} to L_{50} is much smaller than that of from L_{50} to L_{min}. As also shown in Figure 7.10 that, the SD of the noise index values in the noisier half especially that of L_{max} and L_{10} tend to be much smaller than that of the L_{90} and L_{min} in all cases. The SD of the L_{max} and L_{10} of all types range from 0 to 1.8 dBA, and 0.6 to 3.6 dBA respectively, while that of the L_{min} and L_{90} manifest much larger vibration globally with the SD ranging from 4.8 dBA to 6.8 dBA and from 4.3 dBA to 6.9 dBA respectively.

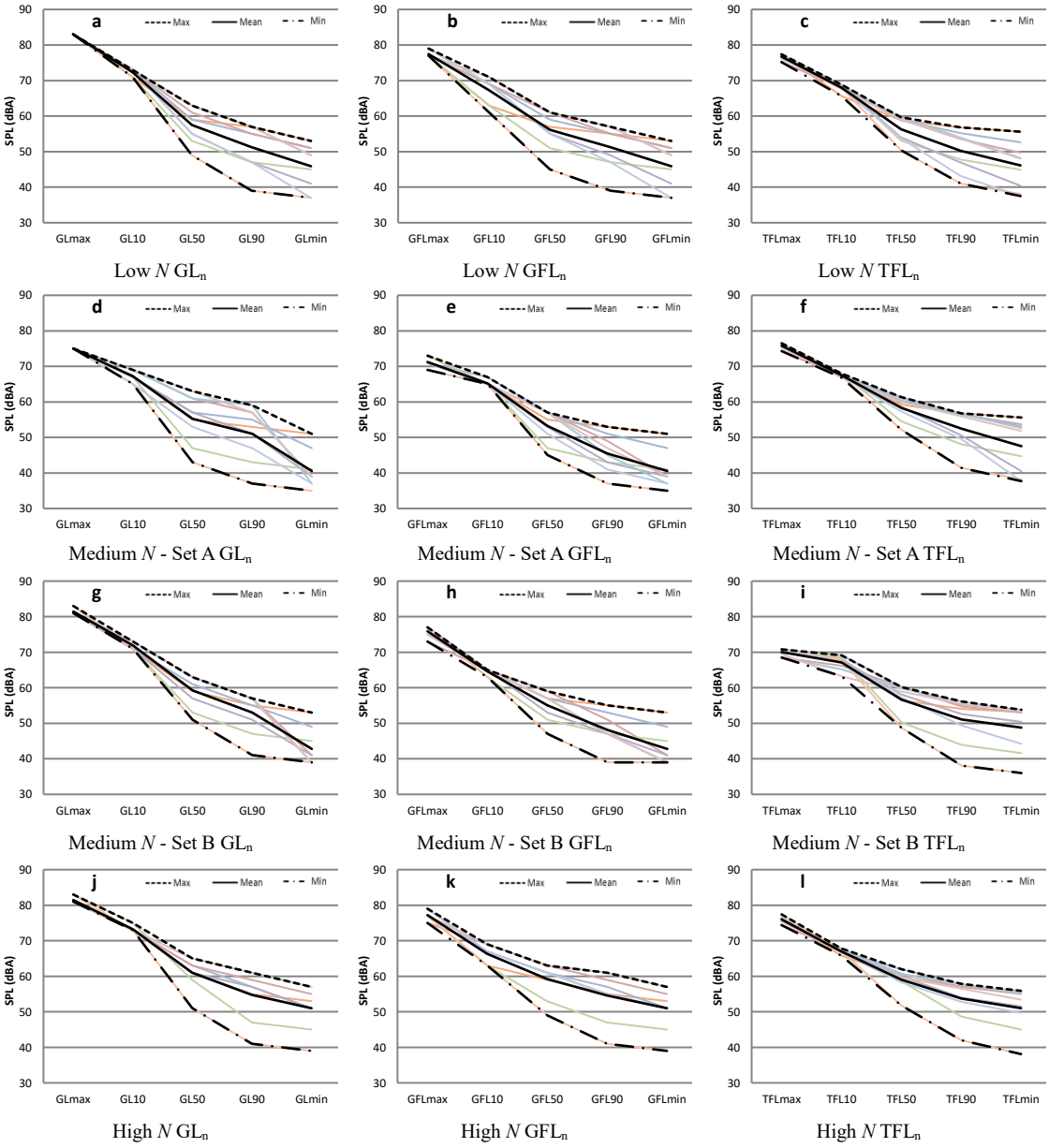

Figure 7.9 The value distribution of spatial noise indices of cases categorised by high, medium and low network density *N*

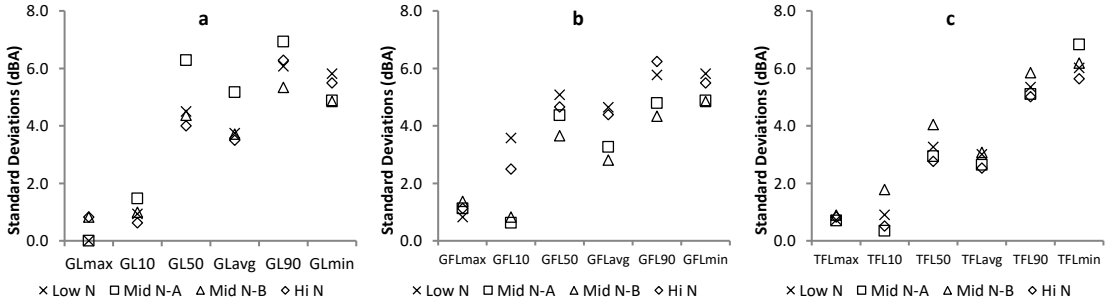

Figure 7.10 The standard deviation of three types of spatial noise indices in three different network density *N* groups: (a) Ground spatial noise indices GL_n; (b) Ground façade spatial noise indices GFL_n; (c) Total façade spatial noise indices TFL_n.

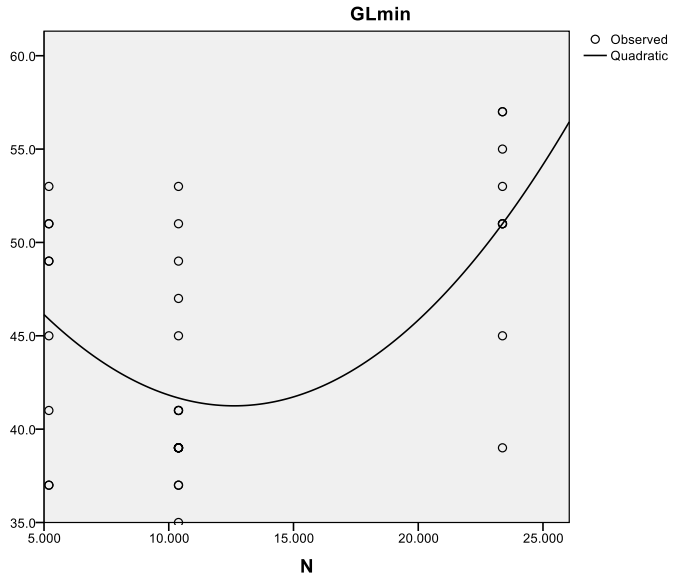

Figure 7.11 A quadratic relationship is found ($R^2 = 0.341$, $p < 0.05$) between network density *N* and the minimum SPL of the spatial ground noise level GL_{min}.

Although with a limit amount of road network density values and total case numbers (*N* = 36), as also shown in Figure 7.11 that, there is a statistically significant correlation found between *N* and GL_{min} ($R^2 = 0.341$, $p < 0.05$). It indicates that with the same given number of vehicles, the change of road length density could have significant effect on the spatial noise levels in the quietest ground space.

- ***Noise attenuation***

It is interesting to note that in at the ground level, the noise attenuation from the noisiest end to the quietest end at both ground level and building façades is profoundly but nonlinearly affected by the change of density index *N* and the network modalities. It can be seen in Figure 7.12 that the increase of network density *N* generally decreases the attenuation from L_{max} to L_{min} of both GL_n and GFL_n except the medium-*N* Set B case, which can be explained by the fact that when network density increases, the basic fabric size defined by the interval of the roads is correspondingly downsized as can be seen in Figure 7.3–Figure 7.5. Hence the maximum attenuation distance from the road sources to the quietest areas which normally locates in the heart of the urban fabrics also decreases.

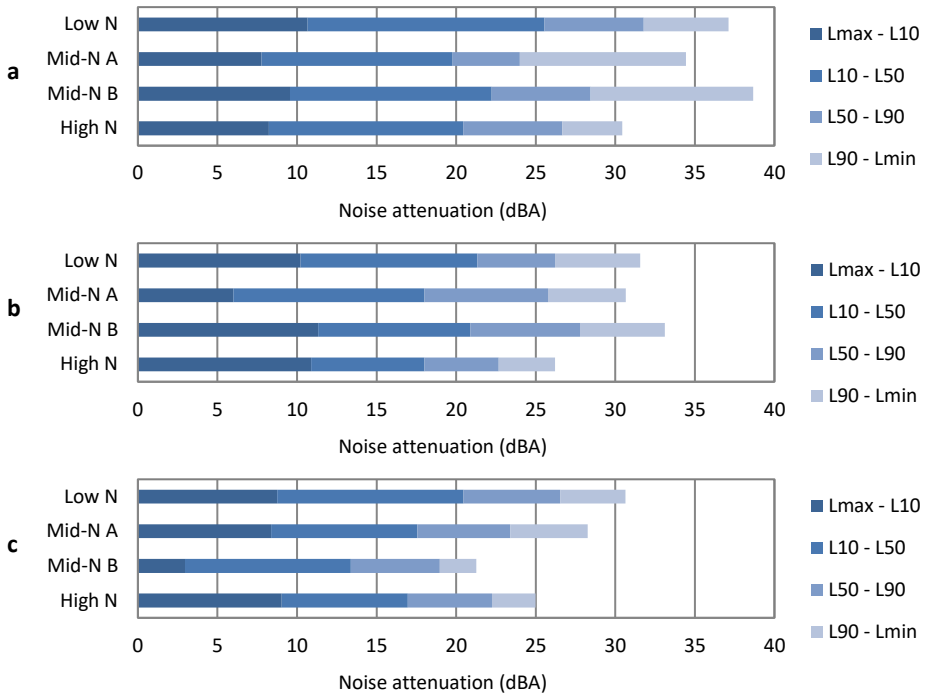

Figure 7.12 The mean attenuation of three types of spatial noise indices in four different *N* case groups demonstrated by sections of attenuation: (a) GL_n; (b) GFL_n; (c) TFL_n.

It is also found that the traffic noise of the two medium-*N* case groups has distinct pattern of attenuations. As can be seen in Figure 7.12 that the cases of medium-*N* Set A follow the general trend found earlier and have less overall attenuation than the low-N cases and higher attenuation than the high-N cases for all three types of spatial noise indices. In contrast, for the cases in medium-*N* Set B, it has the highest attenuation on the ground level for both GL_n and GFL_n comparing with all case groups, and for the total façade noise, the TFL_n of which is the lowest among all cases. Considering the average fabric size of the medium-*N* set B is identical as set A, it indicates that the medium *N* set B cases have other urban morphological features that helped to creates quieter space in the quietest area on the ground level, though it may have causes the overall rise of noise level at the quietest part of all building façades.

Another finding is that the attenuation of traffic noise in the noisy half is generally much higher than that at the quiet half, which can be measured by L_{max}-L_{50} and L_{50}-L_{min} respectively. It could be globally found in the result of all three types of indices and all network density groups shown in Figure 7.12. Statistically if only compare the L_{10}-L_{50} and L_{50}-L_{90} that represents the attenuation in noisier and quieter area reprehensively, the same finding can also be found in all indices and case groups, as can be seen in Figure

7.12. The trend can also be found in Figure 7.9 that the tendency of SPL decline between L_{max} and L_{50} is generally higher than that of from L_{50} to L_{min}, indicating stronger attenuation in the noisier half of measured by all type of indices. The finding may be explained by that the flanking buildings play an import role in reducing the range of noisier area, which may majorly distribute in the street space and the around the buildings close to the road as can be seen in Figure 7.3–7.5.

For the noisiest and quietest part on the ground and close to all building façades, the noise attenuation varies and has no distinctive pattern. As can be seen in Figure 7.12, the change of L_{max}-L_{10} and L_{90}-L_{min} of all case groups with different N varies. It indicates that the sound environment in the noisiest street canyon and the quietest space behind the flanking buildings has relatively more diverse conditions, which may partially because the change of N has changed the average street width and the building arrangement.

7.3.3.2 Effect of FSI

- ***Variation of noise level***

By comparing the results of case groups with three different FSI values, it can be seen that, for the medium and high FSI groups, the noisier half has similar but less concentration comparing with that of when the cases are categorised with different N.

As shown in Figure 7.13 that, the variation of noise levels in the noisier half of all medium and high FSI cases from L_{max} to L_{50} is generally smaller than that of L_{50} to L_{min}, although the variations at L_{max} and L_{10} are larger comparing with that of when the results are grouped by network density. This can also be seen in Figure 7.14 that the SD of L_{max} and L_{10} are all higher than that of the L_{90} and L_{min} measured by all three types of spatial noise indices; while comparing with the results of the different N groups the L_{max} and L_{10} of the different FSI groups are generally higher. It is understandable as within each FSI groups there are four different road network types, each of which has distinct traffic flow pattern as well as varying maximum noise level that directly emitted from the arteries and major roads.

Nevertheless, it can be seen from both Figure 7.13 and Figure 7.14 that, in general the noise level varies more when the FSI is higher especially in the quiet half; the SD are also

generally higher when the FSI is higher, especially the low-FSI group cases which tend to have relatively more evenly distributed variations in most of the spatial noise indices. As can be seen from Figure 7.13 that, for the low-FSI cases the difference between the maximum and minimum values of all indices are more evenly and narrowly distributed comparing with the medium and high FSI cases. It is also demonstrated in Figure 7.14 that the SDs of all six spatial noise indices of GL_n, GFL_n and TFL_n derived from the low-FSI cases range from 1.5-4.7 dBA, 2.0-4.7 dBA, and 0.9-2.7 dBA respectively, which are all lower than the same indices derived from the medium-FSI and high-FSI cases.

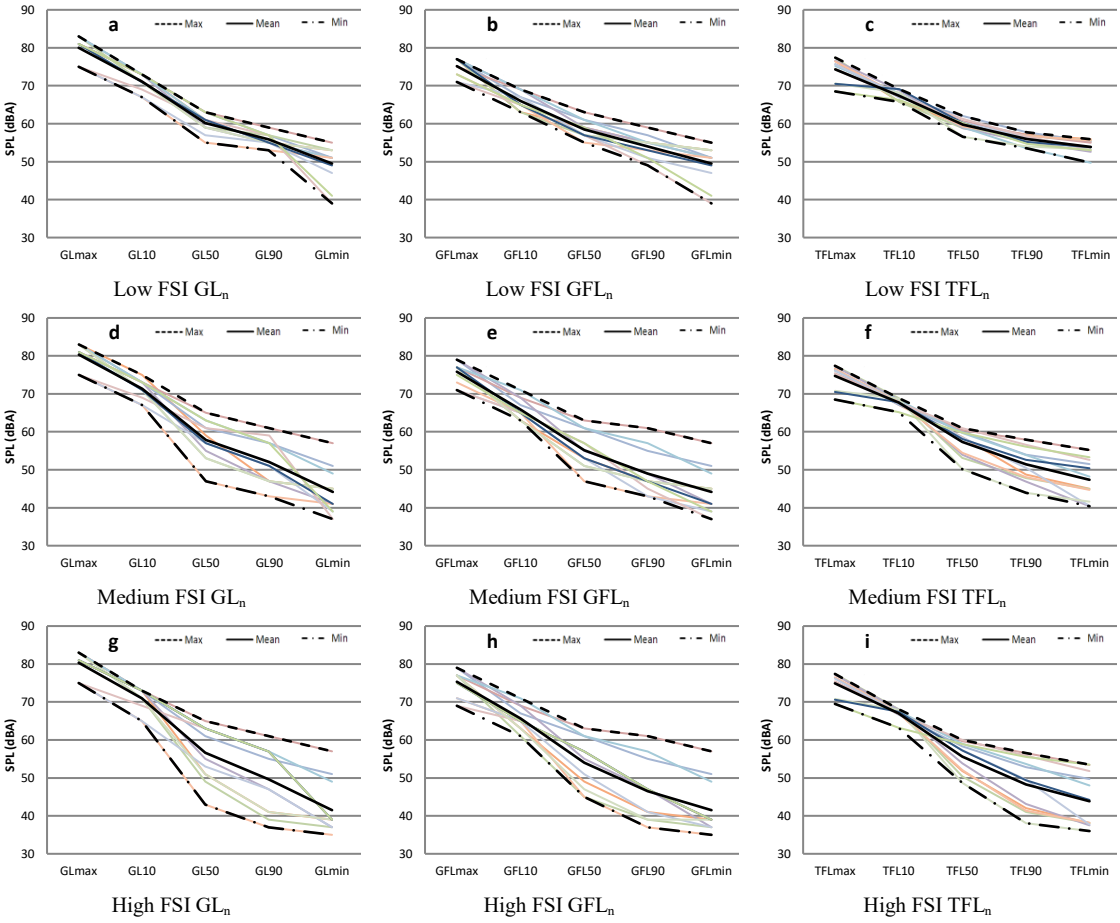

Figure 7.13 The value distribution of spatial noise indices of cases categorised by high, medium and low FSI

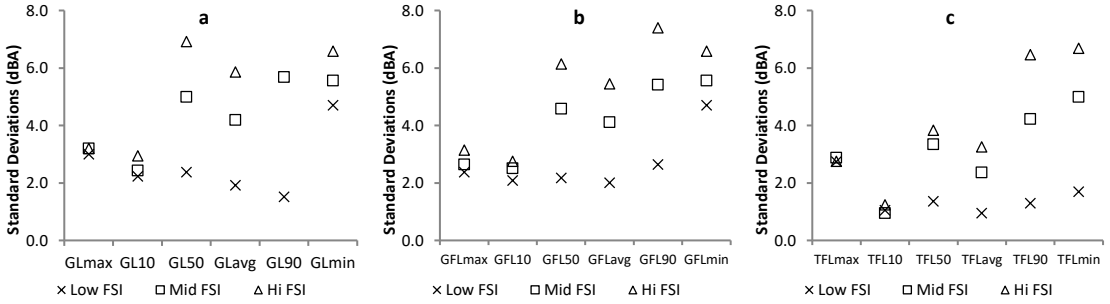

Figure 7.14 The standard deviation of three types of spatial noise indices in three different FSI groups. (a) Ground spatial noise indices GL_n; (b) Ground façade spatial noise indices GFL_n; (c) Total façade spatial noise indices TFL_n

It is potentially due to that comparing with higher FSI cases the lower FSI cases have smaller building mass, which is reflected in relatively smaller building scale and more open space as can be seen in Figure 7.2. Hence it brings less screening effect for rooftop and lateral noise propagation around the buildings, and consequently more evenly distributed noise level on both ground level and on all building façades.

- ***Noise attenuation***

It can be seen that the strongest attenuation of all cases and all types of indices occurs in the noisiest section measured by L_{max}-$L_{10,}$ which also has very similar value despite the change of FSI. As can be seen in Figure 7.15 that, the variation of L_{max}-L_{10} of each type of spatial noise indices among cases with different FSI are very tiny, the SD of which are 0.3 dBA, 0.4 dBA and 0.5 dBA for GL_n, GFL_n and TFL_n respectively. It indicates that the change of FSI does not significantly affect the noise propagation in the street canyons where the most attenuation occurs.

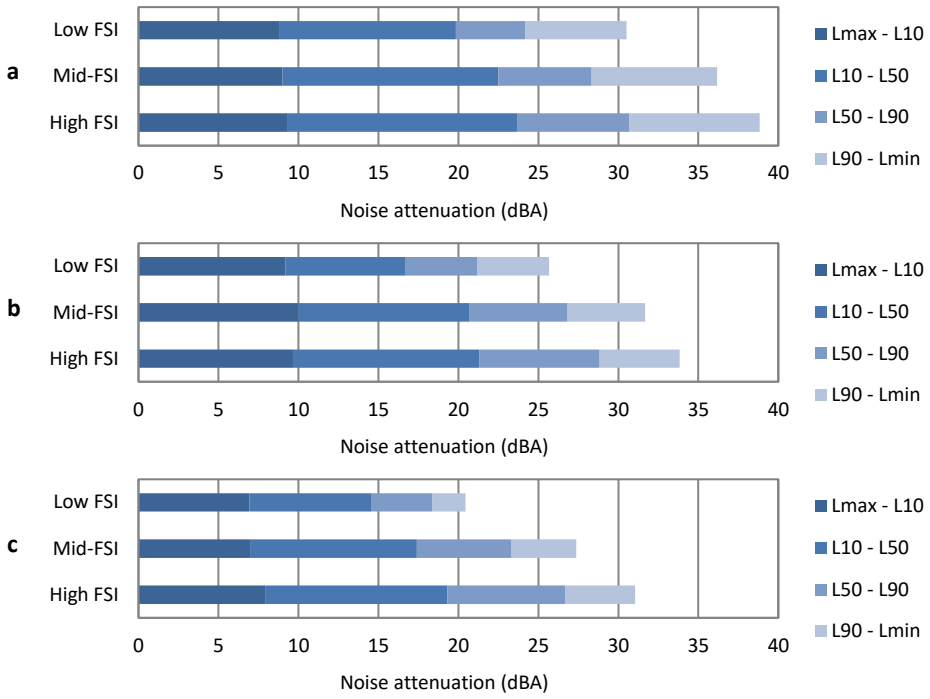

Figure 7.15 The mean attenuation of three types of spatial noise indies in three different FSI case groups demonstrated by sections of attenuation: (a) GL_n; (b) GFL_n; (c) TFL_n

Meanwhile, the noise attenuation at the noisier half measured by L_{max}-L_{50} of all cases are much higher than that of the quieter half measured by L_{50}-L_{min}, similar findings can also be seen in the comparison of case groups with different N in Figure 7.12.

When the FSI rises higher, the overall attenuation from the noisiest to the quietest area measured by all indices also increases. As shown in Figure 7.15 that, the overall attenuation in terms of L_{max}-L_{min} of the GL_n, GFL_n, and TFL_n in the high-FSI cases is averagely 8.3 dBA, 5.0 dBA and 10.6 dBA higher than in the low-FSI cases respectively. Meanwhile the average L_{10}-L_{90} of the high-FSI and low-FSI cases has similar differences of 6.0 dBA, 7.2 dBA and 7.3 dBA for GL_n, GFL_n, and TFL_n respectively.

It can also be seen that the façade spatial noise indices are less sensitive to the change of FSI than the spatial noise indices on the ground level. For instance, as can be seen in Figure 7.15 that the overall attenuation L_{max}-L_{min} on all building façades in terms of TFL_n is 2.8 dBA and 7.8 dBA lower than that of the ground façade noise GFL_n and general ground noise level GL_n respectively, the L_{10}-L_{90} also has similar but smaller gap of 0.4 and 2.6 dBA respectively. A similar trend is also found in the comparison between different N groups in Figure 7.12 in the previous section.

7.3.3.3 *Effect of GSI*

- ***Variation of noise level***

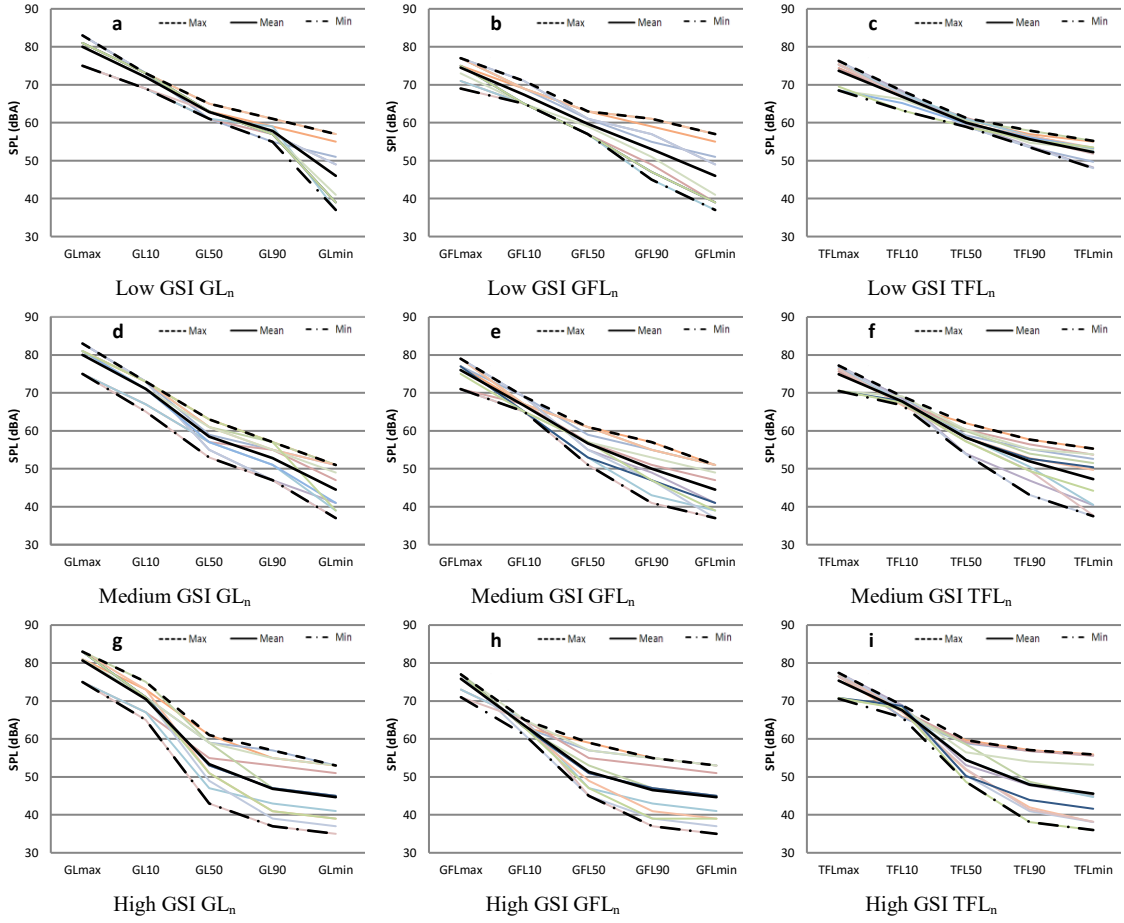

Figure 7.16 The value distribution of spatial noise indices of cases categorised by high, medium and low GSI

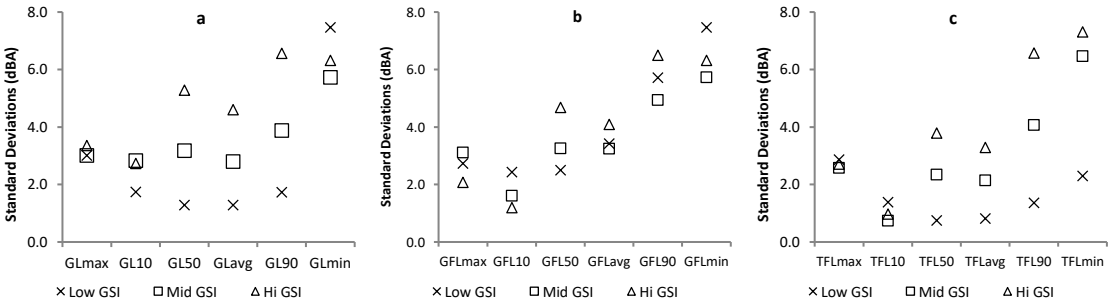

Figure 7.17 The standard deviation of three types of spatial noise indices in three different GSI groups: (a) Ground spatial noise indices GLn; (b) Ground façade spatial noise indices GFL_n; (c) Total façade spatial noise indices TFL_n

Firstly, in most of the cases there the noise level at the noisier half is more concentrated than the quiet half. As can be seen in Figure 7.16 that in the majority of the cases the interval between the maximum and minimum values of all spatial noise indices in the

noisier half from L_{max} to L_{50} tend to be generally smaller, except the Figure 7.16a, Figure 7.16c and Figure 7.16d in which the variation is generally small and even. It indicates that the noise level on the open ground and at all façade level tend to be less diversified when the GSI is low, despite the changes of other urban morphological factors. This is similar to the findings in the comparison among different FSI cases in the previous section as shown in Figure 7.13. Considering the height of the buildings can still be diverse when only the GSI is low, it may be caused by the increase of the scale of intervals between the buildings, especially the roadside buildings, and may also be due to the increase of open space ratio.

It is also notable that the variation of noise level at the quiet half tends to increase with the increase of GSI. From Figure 7.17 it can be seen that the SD from of the medium and low GSI cases are generally lower than that of the high GSI cases, this is especially evident in the Figure 7.17a and Figure 7.17c, indicating more diversified noise levels, both the GL_n and the TFL_n. It indicates that at the open ground level and on all building façades, the noise level at the quiet half is prone to be affected by other urban morphological characteristics.

- ***Noise attenuation***

It is interesting to note that the three types of spatial noise indices, GL_n, GFL_n and TFL_n have distinct patterns when affected by the changes of GSI. As can be seen in Figure 7.15 that, the overall attenuation of TFL_n in terms of L_{max}-L_{min} has clear tendency of increasing when the GSI increases, i.e. when there is higher density in terms of GSI, the noise level at all building façades tends to attenuate more evidently. It is also shown in the comparison of standard deviation in Figure 7.19a where the SD of the TFL_n is more evidently affected by the increase of GSI.

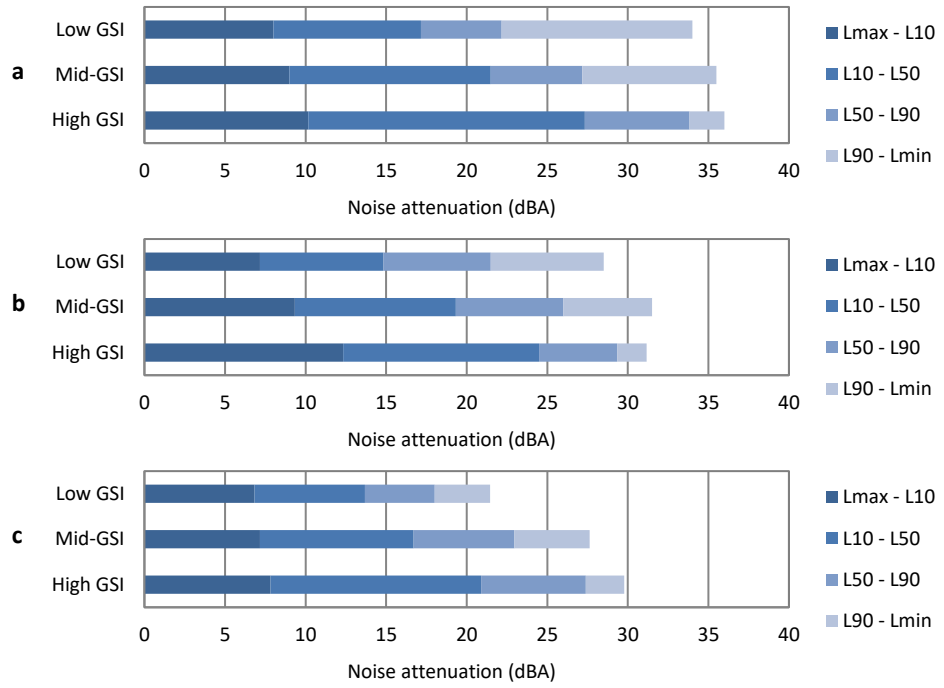

Figure 7.18 The mean attenuation of three types of spatial noise indices in three different GSI case groups demonstrated by sections of attenuation: (a) GL_n; (b) GFL_n; (c) TFL_n.

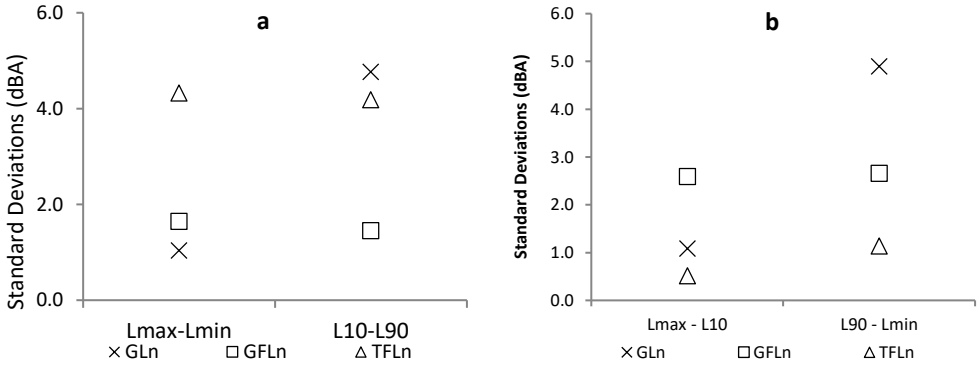

Figure 7.19 The standard deviations of the attenuation of three types of spatial noise indices due to the change of GSI: (a) attenuation in the quietest and noisiest end; (b) overall attenuation, absolute and statistical.

Nonetheless from Figure 7.19a it can also be seen that, when the overall attenuation is calculated in between the spatial intrusive noise and background noise, i.e. L_{10}-L_{90}, the variation of the GL_n and TFL_n is very similar and both are prone to be affected by the change of GSI, while the GFL_n on the ground façade level manifests less tendency of being affected by the change of GSI which is still similar to that of L_{max}-L_{min}. This implies that there are unique patterns of attenuation in the noisiest and quietest area on the ground level.

As shown in Figure 7.19b, the noise attenuation at the noisiest end and the quietest end measured by L_{max}-L_{10} and L_{90}-L_{min} respectively, both façade indices GFL_n and TFL_n have similar SD that indicates similar changes of attenuation; while that of the GL_n on all open ground manifests distinct patterns of attenuation, especially at the quietest end. The SD of the GL_{max}-GL_{10} and GL_{90}-GL_{min} is 1.1 dBA and 4.9 dBA respectively. From Figure 7.15a, it is also clear to see that, the attenuation of the spatial ground noise level in the quietest end is as large as 11.8 dBA and which declines to 2.2 dBA, which suggests that the rise of GSI has significantly reduced the attenuation of spatial ground noise in the areas far from the roadside.

As can be seen in Figure 7.3–7.5 that, the lower GSI cases has less confined building arrangement and more open spaces in the centre of each basic urban fabrics, it allows the direct transmission of the traffic noise keep attenuating along with increasing distance; while in the higher GSI case tend to have denser and more confined building arrangement, which screens the intrusive noise and creates large quiet zones in the centre of each basic urban fabrics, and hence have smaller changes in the quietest end in terms of L_{90}-L_{min}.

Generally speaking, it can also be seen that the ground noise level GL_n are more prone to be affected by the change of GSI, while the ground façade noise level GFL_n and total façade noise level TFL_n are relatively less affected by the change of GSI. From Figure 7.15 it can be seen that the overall attenuation level of the GL_n is generally higher than the other two type of spatial noise indices. It is also found in the comparison among different *N* and FSI groups, which indicates a general phenomenon that at all altitudes the building façades, the noise impact is more evenly distributed and less affected by the change of urban density. It may because the buildings with different heights generally receives the impact from both direct noise transmission and all types of noise reflections and diffractions that magnifies the noise level of the quieter part of the façades.

7.3.4 Summary

The section examines the relationship between three urban density related indices and the variation of spatial noise levels and the pattern of attenuation. It is found that in the noisiest space both on the open ground and all façade level, the noise levels are more

concentrated, which is especially evident among cases with the same type of road network. It reflects that noise level concentration close to the roads.

In general, none of the three indices can explain the complicated variation of noise in the quieter spaces on the ground and all façades. Nonetheless, there is also some general patterns when the cases area compared by different building density in terms of floor space and ground coverage. It denotes that when there the building density in terms of FSI or GSI is relatively low, the variation of the noise level in the quieter space is also smaller in general.

Regarding the noise attenuation, it is found that generally despite the urban morphological type, the noise level attenuates more sharply in the noisier half that locates is closer to the road, and gently in the quiet half. This is found in three all types of spatial noise indices disregard what density index is used to categorise the case groups. It is also notable that, the increase of GSI can significantly reduce the noise attenuation of the quietest end on the ground level that locates far from the road source.

It is also notable that the noise attenuation, in general, is stronger in the open ground and weaker on all altitudes of the building façades. It is also found that case groups with higher FSI and GSI tend to have higher total attenuation, especially when it is measured by L_{10}-L_{90}. Although this is also generally true for low-*N* and high-*N* cases, it is especially interesting to note that, with the same medium-*N* settings, the total attenuation can be much higher due to different building arrangement, which implies that there are more urban morphological indices that can have strong influence on the general noise distribution in the urban space.

7.4 Multilinear correlation analysis on urban morphological and spatial noise indices

The linear correlations between sixteen morphological indices and three types of spatial noise indices in the open ground GL_n, on the ground façade level GFL_n and on all building façades TFL_n and the attenuation indices are systematically analysed, and exhibited in Table 7.5, Table 7.6 and Table 7.7. Considering the nature of the parametric study conducted, only the Pearson correlation coefficient R with Sig. value of $p < 0.01$ are high-

lighted. There are a series of significant correlations found, between a large number of urban morphological indices and spatial noise indices of all three types.

The implications of the significant correlations are interpreted and discussed in detail. The urban morphological indices are divided into three different groups, the urban density related indices, and the urban geography related indices. Six spatial noise indices of the open ground, the ground façade level and on all façade level are tested, it is to note that, merely no significant correlations are found in the analysis on the spatial maximum noise level L_{max} of three types, thus the result of which is not displayed. The noise attenuation indices, L_{10}-L_{90}, L_{50}-L_{min}, L_{90}-L_{min}, L_{max}-L_{10} and L_{max}-L_{50} which represents the spatial noise attenuation of the quietest 10% space, the quiet half space, the noisier half space, and the nosiest 10% area, of each type of spatial noise indices, are also tested and demonstrated respectively.

7.4.1 Controlled urban density related indices

The correlation between the three pre-controlled urban density related indices *N*, FSI, and GSI, as well as one extra index, the road space ratio RSR, and a series of spatial noise indices describing the general level and spatial distribution of traffic noise is systematically analysed. The results are demonstrated in Table 7.5.

7.4.1.1 Road density related indices N and RSR

The road network density *N* is proved again to be positively related to the minimum spatial noise index L_{min} and also proved to be negatively related to the overall noise attenuation measured by L_{10}-L_{90}, for both GL_n and GFL_n derived from the general noise maps at the ground level. It may be explained by the fact that the higher *N* cases generally creates smaller urban fabrics which hence reduces the distance from the noisiest area to the quietest area and increases the minimum spatial noise level.

Table 7.5 Bivariate correlation between controlled urban density related indices and spatial noise indices, the Pearson correlation coefficient R with $p < 0.01$ are listed.

Pearson correlation		L_{avg}	L_{min}	L_{50}	L_{10}	L_{90}	L_{10} -L_{90}	L_{50} -L_{min}	L_{90} -L_{min}	L_{max} -L_{10}	L_{max} -L_{50}
Ground noise indices GL_n											
N	2-tailed	–	–	–	–	–	–	–	–	-.429	–
	1-tailed	–	.413	–	–	–	–	–	–	-.429	–
RSR	2-tailed	–	–	–	–	–	–	–		-.580	–
	1-tailed	–	–	–	–	–	–	–	–	-.580	–
FSI	2-tailed	–	-.483	–	–	–	–	–	–	–	–
	1-tailed	–	-.483	–	–	-.386	.397	–	–	–	–
GSI	2-tailed	-.712	–	–	-.730	-.706	.649	-.559	-.663	.531	.736
	1-tailed	-.712	–	–	-.730	-.706	.649	-.559	-.663	.531	.736
Ground façade spatial noise indices GFL_n											
N	2-tailed	–	–	–	–	–	–	–	–	–	–
	1-tailed	–	.413	–	–	–	-.397	–	–	–	–
RSR	2-tailed	–	–	–	–	–	–	–	–	–	–
	1-tailed	–	–	–	–	–	–	–	–	–	–
FSI	2-tailed	–	-.483	–	–	-.470	.552	–	–	–	–
	1-tailed	–	-.483	–	–	-.470	.552	–	–	–	–
GSI	2-tailed	-.591	–	-.652	-.690	–	–	-.616	-.766	.643	.767
	1-tailed	-.591	–	-.652	-.690	-.419	–	-.616	-.766	.643	.767
Total façade spatial noise indices TFL_n											
N	2-tailed	–	–	–	–	–	–	–	–	–	–
	1-tailed	–	–	–	–	–	–	–	–	–	–
RSR	2-tailed	–	–	–	–	–	–	–	–	–	–
	1-tailed	–	–	–	–	–	–	–	–	–	–
FSI	2-tailed	-.573	-.619	–	-.477	-.559	.485	.574	–	–	–
	1-tailed	-.573	-.619	–	-.477	-.559	.485	.574	.401	–	.411
GSI	2-tailed	-.616	–	–	-.657	-.569	.566	–	–	–	.640
	1-tailed	-.616	-.411	–	-.657	-.569	.566	–	–	–	.640

7.4.1.2 Road density related indices N and RSR

The road network density N is proved again to be positively related to the minimum spatial noise index L_{min} and also proved to be negatively related to the overall noise attenuation measured by L_{10}-L_{90}, for both GL_n and GFL_n derived from the general noise maps at the ground level. It may be explained by the fact that the higher N cases generally creates smaller urban fabrics which hence reduces the distance from the noisiest area to the quietest area and increases the minimum spatial noise level.

- ***Correlations between Road network density N and spatial noise indices***

Meanwhile, no correlation is found between N and any of the TFL_n indices and their attenuation, which is to say that for total façade noise level which reflects the general

impact of traffic noise indoor space of all altitudes is not correlated with the change of road network densities in general.

- ***Correlations between RSR and spatial noise indices***

Similarly, the road space ratio RSR which reflects the road also merely has correlations with the spatial noise indices and their attenuation, except the attenuation close to the road sources measured by L_{max}-$L_{10,}$ which is positively correlated with the RSR.

This further indicates that the indoor noise distribution at relatively higher altitude is not necessarily affected by the variation of network density and road coverage, rather, the distribution and coverage change of the roads without changes in total vehicle amount may not have a significant impact on the variation of noise on higher altitude.

7.4.1.3 Building density related indices

- ***Correlations between FSI and spatial noise indices***

At both the open ground and the ground façade level, the FSI is proved to have a negative correlation with minimum and background noise level L_{min} and L_{90} respectively; and is also found to have a positive while stronger correlation with the overall attenuation measured by L_{10}-L_{90}, as can be seen in Table 7.5. It may be due to that the increase of FSI tends to generally increase the total mass and average height of the buildings in general, as can be seen in Figure 7.2, thus when the FSI is higher, there is more screening effect occurs and the shadowed zones tend to be quieter.

Meanwhile for the total façade noise level measured by TFL_n, more correlations with FSI are found. The L_{avg}, L_{min}, L_{10} and L_{90} all have significant negative correlations with the FSI, which indicates that the increase of FSI can evidently decrease the spatial average, minimum, intrusive and background noise level respectively on all altitudes of the building façades.

- ***Correlations between GSI and spatial noise indices***

The GSI is proved to be the most influential index of all the sixteen morphological indices tested, which is significantly related to spatial average, intrusive and background noise

on the ground level in terms of L_{avg} ($R = -.712$), L_{10} ($R = -.730$) and L_{90} ($R = -.706$) respectively. Similar but slightly weaker correlations are also found between GSI and the spatial ground façade noise (L_{50}, L_{10}, L_{90}) and total façade noise (L_{avg}, L_{min}, L_{10}, L_{90}). It suggests that as an indicator of the two-denominational building density, the increase of GSI can significantly reduce the spatial noise level in the urban environment, and buildings and open space in urban areas with higher building coverage hence has higher chance of having less impact from the impact of traffic noise in general.

Regarding the effect of GSI on noise attenuation, it is notable that, at the ground level, the GSI is negatively correlated with the traffic noise attenuation in the quieter space and positively correlated with the attenuation at the noisier spaces. As can be seen in Table 7.5 that for the GL_n and GFL_n, the GSI has significant negative correlation with L_{50}-L_{min} and L_{90}-L_{min}; and negatively correlated with L_{max}-L_{10}, L_{max}-L_{50}. The strongest correlation if found with L_{max}-L_{50} ($R = -.736\ and\ -.767$ respectively). The GSI is also found to be negatively correlated with the total attenuation measured by L_{10}-L_{90} for both open ground noise and total façade noise. For TFL_n, the GSI is only found to be significantly correlated with L_{max}-L_{50} and L_{max}-L_{50} though with the same tendency as that of GL_n.

It denotes that, despite the change of any other building and road features, in general, the increase of building coverage alone can strongly speed up the traffic noise attenuation in the relatively noisier street and space and around the flanking buildings, on all exposing surfaces including building façades at all altitudes; while it also and sharpens the declining speed of noise level in the relatively quieter shadowed space and façade at the ground level. The effect consequently increases the total attenuation for both ground and indoor noise level.

7.4.2 Building and street geometric indices

There are seven indices chosen to reflect the form and geometry of the buildings and street space. The length related indices *H*, HWR, RWI, BFLI and BRRLI and area related indices the BFASAI and BFR. A series of significant correlations are found between the chosen morphological indices and the spatial noise level and distribution indices as shown in Table 7.6.

7.4.2.1 Length related indices

- ***Correlations between Mean building height H and spatial noise indices***

The mean building height *H* is the sheer average height of all buildings in the planned area, it is found to have merely no correlation with the noise level indices while having a significant correlation with the noise attenuation in the quieter half space and the quietest 10% space at the open ground and ground façade level. As can be seen in Table 7.6 that, for the ground and ground façade noise levels the L_{50}-L_{min} and L_{90}-L_{min} are both found to be positively correlated with the average building height *H*. In the meantime, the GL and GL_{max}-GL_{50} is found to be positively and negatively correlated with *H*, respectively. It denotes that the increasing of average building height is helpful to increase the traffic noise attenuation in the shadowed quieter area and ground level façades, and also increases the ground intrusive noise level through reducing the attenuation in the noisier half; while the finding does not necessarily indicate that the general noise levels and noise levels in the quieter area could consequently be reduced.

For total façade noise level, the *H* has no significant to most of the spatial noise indices nor to the attenuation of them, except the L_{50} where there is negative correlation found indicating the total area of noisier building façades reduces when the buildings are higher in general.

- ***Correlations between Mean building height HWR and spatial noise indices***

In the street space, the average aspect ratio of the street space HWR is found to be only significantly correlated with the attenuation at the quieter half space in terms of L_{50}-L_{min} on the open ground and ground façade level, which may owe to the same effect found in the examination on *H* above considering how the HWR is calculated; and has no correlation at all with total façade noise level and its attenuation. It suggests that this commonly used street space morphological index is not an influential index in the study of the general noise level.

Table 7.6 Bivariate correlation between building and street geometric indices and spatial noise indices, Pearson correlation coefficient R with $p < 0.01$ are listed.

Pearson correlation		L_{avg}	L_{min}	L_{50}	L_{10}	L_{90}	L_{10} -L_{90}	L_{50} -L_{min}	L_{90} -L_{min}	L_{max} -L_{10}	L_{max} -L_{50}
Ground spatial noise indices GL_n											
H	2-tailed	–	–	–	–	–	–	.472	.465	–	–
	1-tailed	–	–	–	.399	–	–	.472	.465	–	-.394
HWR	2-tailed	–	–	–	–	–	–	.425	–	–	–
	1-tailed	–	–	–	–	–	–	.425	–	–	–
RWI	2-tailed	-.671	–	–	-.692	-.654	.557	–	–	.437	.634
	1-tailed	-.671	–	–	-.692	-.654	.557	–	-.420	.437	.634
BFLI	2-tailed	-.793	–	–	-.792	-.752	.634	-.545	-.641	.529	.727
	1-tailed	-.793	–	–	-.792	-.752	.634	-.545	-.641	.529	.727
BPRLI	2-tailed	–	–	–	-.440	–	–	–	–	.683	.556
	1-tailed	–	–	–	-.440	–	–	-.394	–	.683	.556
BFASAI	2-tailed	–	–	–	–	–	–	–	–	–	–
	1-tailed	–	–	–	–	–	–	–	–	–	–
BFR	2-tailed	–	–	–	–	–	–	–	–	–	–
	1-tailed	–	-.393	–	–	–	–	–	–	–	–
Ground façade noise indices GFL_n											
H	2-tailed	–	–	–	–	–	–	.447	.470	–	–
	1-tailed	–	–	–	–	–	–	.447	.470	–	–
HWR	2-tailed	–	–	–	–	–	–	–	–	–	–
	1-tailed	–	–	–	–	–	–	.420	–	–	–
RWI	2-tailed	-.544	–	-.458	-.619	-.477	–	–	-.494	.463	.675
	1-tailed	-.544	–	-.458	-.619	-.477	–	–	-.494	.463	.675
BFLI	2-tailed	-.661	–	-.638	-.761	-.495	–	-.602	-.787	.512	.758
	1-tailed	-.661	–	-.638	-.761	-.495	–	-.602	-.787	.512	.758
BPRLI	2-tailed	–	–	–	–	–	–	–	–	.453	.500
	1-tailed	–	–	–	–	–	–	-.409	–	.453	.500
BFASAI	2-tailed	–	–	–	–	–	–	–	–	–	–
	1-tailed	–	–	–	–	–	–	–	–	–	–
BFR	2-tailed	–	–	–	–	–	–	–	–	–	–
	1-tailed	–	-.393	–	–	–	.420	–	–	–	–
Total façade noise indices TFL_n											
H	2-tailed	–	–	–	–	–	–	–	–	–	–
	1-tailed	–	–	-.392	–	–	–	–	–	–	–
HWR	2-tailed	–	–	–	–	–	–	–	–	–	–
	1-tailed	–	–	–	–	–	–	–	–	–	–
RWI	2-tailed	-.557	-.533	–	-.561	-.569	.585	–	–	–	.599
	1-tailed	-.557	-.533	–	-.561	-.569	.585	–	–	–	.599
BFLI	2-tailed	-.635	-.464	–	-.674	-.587	.584	–	–	–	.663
	1-tailed	-.635	-.464	–	-.674	-.587	.584	–	–	–	.663
BPRLI	2-tailed	–	–	–	-.450	–	–	–	–	–	.494
	1-tailed	–	–	–	-.450	–	–	–	–	–	.494
BFASAI	2-tailed	–	–	–	–	–	–	.463	–	–	–
	1-tailed	–	-.414	-.299	–	-.315	–	.463	.411	–	–
BFR	2-tailed	-.431	-.491	–	–	–	–	.490	–	–	–
	1-tailed	-.431	-.491	–	–	-.413	–	.490	.389	–	–

- ***Correlations between RWI and spatial noise indices***

The RWI, which mainly concerns the fraction of road carriageway width to the street space width, is found be significantly correlated with a series of spatial noise indices and is more influential on spatial noise distribution than the building height related indices. On all exposing surface, the RWI is negatively correlated with the L_{avg}, $L_{10,}$ and L_{90}, and is also negatively correlated with the minimum level on all façade level TFL_{min}. It generally suggests that when the road width comparing with the street space width is higher, the general noise level as well as that of the noisy end and quiet end all tend to be lower.

Nevertheless, regarding the noise attenuation, the RWI is found to be negatively correlated with some of the attenuation indices and is especially found to be positively correlated with the attenuation of in the noisier half in terms of L_{max}-L_{50} on all exposing surfaces.

This explains the relationship between RWI and the spatial noise indices: when the attenuation in the noisier half, i.e. in the street space attenuates more rapidly, the noise level tends to be lower in general. It is due to that, considering the width of road carriageway width, in general, is normally dramatic, higher RWI often means more confined street space, and smaller chances for traffic noise to transmit to quieter areas, as can be seen in the noise maps examples in Figure 7.3 – Figure 7.5.

- ***Correlations between BFLI, BPRLI, and spatial noise indices***

The BFLI and BPRLI examine the ratio of the width of roadside buildings and the total perimeter of building to the road length, respectively. It can be seen that the BPRLI has some significant positive correlations with the ground and total façade background noise level, and the attenuation in the noisier half. In contrast, the BFLI is definitely a more influential index, which is found to be positively correlated with almost all three types spatial noise indices listed, except the GL_{min}, GL_{50}, $GFL_{min,}$ and TFL_{50}. The R values of the correlations at the open ground levels are all over 0.7. The effect of BFLI on noise attenuation is also evident; it is significantly correlated with all five spatial GL_n attenuation indices and four GFL_n indices, suggesting a strong impact on the overall noise distribution in both quieter and noisier spaces; and also a positive correlation with the L_{10}-

L_{90} and L_{max}-L_{50} of the TFL_n. It is found to be especially significantly correlated with the L_{max}-L_{50} of all three types of indices. The findings suggest significant noise abatement effect in general and in the noisier half especially while slowing down the attenuation in the quieter half as the quieter area increases due to the increasing screening effect of the buildings.

7.4.2.2 Area related indices

- ***Correlations between BFR, BFASAI, and spatial noise indices***

The two areas related indices, the building façade area to space area index BFASAI and the building façade to the total planned area ratio BFR are also examined. It can be seen that the influence of BFASAI on the ground and ground façade noise levels and attenuation are negligible, the BFR also has only two negative correlations found with the GL_{min} and GFL_{min} respectively. Nevertheless, on the total façade level, both indices are found to have a significant and negative correlation with the minimal and background level in terms of L_{min} and L_{90}, respectively. The BFR is also found to be negatively correlated with the TFL_{avg}. Both indices are also significantly correlated with the total façade noise attenuation in the quieter half and the 10% quietest area in terms L_{50}-L_{min} and L_{90}-L_{min} respectively. The findings suggest that the only contribution of increasing the BFASAI is to limitedly impact on the reduction of the noise level in the quieter area; while the increase of BFR can significantly contribute to the reduction of both the noise levels in the quieter area and the average total façade noise level.

7.4.3 Urban geography related indices

As can be seen in Table 7.7 that, the effect of five urban geography related indices which concerns majorly about the general geographical form and characteristics of the entire built-up area are tested. The indices are borrowed from a series of the urban environment and urban geography related studies and are presumably to have more or less connection with the propagation and spatial distribution of traffic noise (Adolphe, 2000; Huang et al., 2007).

Table 7.7 Bivariate correlation between urban geography related indices and spatial noise indices of the Greater Manchester cases, Pearson correlation coefficient R with $p < 0.01$ are listed.

Pearson correlation		L_{avg}	L_{min}	L_{50}	L_{10}	L_{90}	L_{10} -L_{90}	L_{50} -L_{min}	L_{90} -L_{min}	L_{max} -L_{10}	L_{max} -L_{50}
Ground spatial noise indices GL_n											
RI	2-tailed	–	-.448	–	–	–	–	–	–	–	–
	1-tailed	–	-.448	–	–	–	–	–	–	–	–
BBAI	2-tailed	-.543	-.490	–	-.532	-.515	–	–	–	–	–
	1-tailed	-.543	-.490	-.408	-.532	-.515	–	–	–	–	–
OSR	2-tailed	.628	–	–	.625	.604	-.546	.577	.665	–	-.574
	1-tailed	.628	–	–	.625	.604	-.546	.577	.665	–	-.574
CAR	2-tailed	–	–	–	–	–	–	–	–	–	–
	1-tailed	–	–	-.393	–	–	–	–	–	–	–
BSAPAR	2-tailed	–	–	–	–	–	–	–	–	–	–
	1-tailed	–	-.414	–	–	–	.404	–	–	–	–
Ground façade spatial noise indices GFL_n											
RI	2-tailed	–	-.448	–	–	-.448	.523	–	–	–	–
	1-tailed	–	-.448	–	–	-.448	.523	–	–	–	–
BBAI	2-tailed	-.561	-.490	-.431	-.566	-.550	.471	–	–	–	.489
	1-tailed	-.561	-.490	-.431	-.566	-.550	.471	–	–	–	.489
OSR	2-tailed	.489	–	.633	.574	–	–	.634	.802	-.580	-.624
	1-tailed	.489	–	.633	.574	–	–	.634	.802	-.580	-.624
CAR	2-tailed	–	–	–	–	–	–	–	–	–	–
	1-tailed	–	–	-.393	–	–	.420	–		–	–
BSAPAR	2-tailed	–	–	–	–	–	.472	–	–	–	–
	1-tailed	–	-.414	–	–	-.416	.472	–	–	–	–
Total façade spatial noise indices TFL_n											
RI	2-tailed	-.547	-.594	–	-.449	-.533	.458	.557	–	–	–
	1-tailed	-.547	-.594	–	-.449	-.533	.458	.557	.390	–	.399
BBAI	2-tailed	-.448	-.474	–	–	-.463	.451	–	–	–	–
	1-tailed	-.448	-.474	–	-.420	-.463	.451	.391	–	–	–
OSR	2-tailed	.485	–	–	.507	.448	-.434	–	–	–	-.552
	1-tailed	.485	–	–	.507	.448	-.434	–	–	–	-.552
CAR	2-tailed	-.431	-.491	–	–	–	–	.490	–	–	–
	1-tailed	-.431	-.491	–	–	-.413	–	.490	.389	–	–
BSAPAR	2-tailed	-.581	-.592	–	-.495	-.552	.473	.515	–	–	.429
	1-tailed	-.581	-.592	–	-.495	-.552	.473	.515	–	–	.429

- ***Correlations between RI and spatial noise indices***

The rugosity index (RI) is found to be more correlated with the total façade spatial noise indices than on the ground level. The RI describes the mean height of the entire urban canopy, different from the average building height H, which is calculated as the mean height of all land objects including the buildings and all open grounds with zero height, and is often used in the atmosphere in the urban area (Edussuriya, Chan, & Ye, 2011). It is found that, the RI is not correlated with the average or median noise level of GL_n and

GFL_n, although it is found to be negatively correlated GL_{min}, GFL_{min} and GFL_{90}, it denotes that with higher RI, the noise level at the quieter end on the ground and ground façades tend to be lower.

Regarding attenuation, the RI is found to be not correlated with any indices in the open ground and is only positively correlated with the L_{10}-L_{90} on the ground façades. For total façade noise levels, the RI is found to be positively correlated with the total noise attenuation L_{10}-L_{90}, the attenuation in the noisier and quietest space L_{50}-L_{min} and L_{90}-L_{min} and also with that of the noisier half measured by L_{max}-L_{50}. The L_{max}-L_{10} in the noisiest façades is not affected significantly.

The findings suggest that with higher rugosity, the indoor noise level at all altitudes in the quieter and noisier area tend to be significantly reduced, it implies that the screening effect of the buildings tends to be increased due to the increase of the mean height of the urban canopy, which also explains the reduction of minimal spatial noise level on the ground and ground façade level. Comparing with the building height index *H*, the RI is more crucial on the prediction of the indoor noise level in general.

- ***Correlations between BBAI and spatial noise indices***

The building block area index (BBAI) can be seen as an indicator that reflects the density of the building settlement aggregation in the planned area, which is found to be directly influencing the spatial noise indices on all exposing surfaces, while not as important when the attenuation is mentioned. As can be seen in Table 7.7, the BBAI is found to be negatively correlated with nearly all spatial noise indices all three types listed, except the TFL_{50}. Nonetheless, it is found to be not correlated with any attenuation indices in the open ground level, and it is only found to be positively correlated with the L_{10}-L_{90} of the ground façade and total façade noise levels, and the L_{50}-L_{min} of the latter.

The findings suggest that the increase of BBAI which mostly related to the increasing of the occupation of built-up areas, as well as the shrinking of street space in general, can significantly reduce the impact of traffic noise on all exposing surfaces. Although the causation between both in the open ground is not related to potential increasing of noise attenuations, it does have some connection with the increasing of noise attenuation on all the building façades, especially in the quieter half of the total façades noise levels.

- ***Correlations between OSR and spatial noise indices***

The open space ratio (OSR) or the porosity index is an indicator of the coverage of accessible spaces beside the road space and buildings ground space in the urban area, which is found to be one of the most influential indexes of all indices tested and is significantly correlated with the increasing of noise level in general. It can be seen that, the OSR is significantly correlated with the average spatial noise level L_{avg} and the intrusive noise level L_{10} of all three types of indices, and is also found to be positively correlated with the background level L_{90} of both the ground noise level and the total façade noise level; meanwhile it is also found to be correlated with the L_{50} of the ground façade level.

The OSR is also found to be highly influential on the noise attenuations especially on the ground level. For the ground noise levels, it is negatively correlated with the total attenuation in terms of L_{10}-L_{90} and L_{max}-L_{50}, meanwhile, it is positively correlated with L_{50}-L_{min} and L_{90}-L_{min}. It denotes that the increasing of OSR can significantly reduce the attenuation in the relatively noisier area and increase the speed of attenuation in the quieter half, although overall the total attenuation still declines with the increase of OSR.

Similar effect is also found for the ground façade noise, it is correlated with four of five indices tested except the total attenuation in terms of L_{10}-L_{90}, it is to note that, the R value of the correlation between OSR and the attenuation in the quietest 10% in terms of L_{90}-L_{min} is exceptionally high ($R^2 = .802$).

For the total façade noise levels, the OSR is found to be less influential while still significantly and negatively correlated with the total attenuation L_{10}-L_{90} and the attenuation in the noisier half measured by L_{50}-L_{min}.

It is notable that, for all three types of spatial noise indices, the increase of OSR significantly reduce the attenuation in the noisier half in terms of L_{max}-L_{50}, this explains why the OSR correlates with the spatial intrusive noise level L_{10} of all three types and consequently the spatial average level L_{avg} of all three types. This is due to that the OSR and GSI are highly correlated ($R^2 = 0.878$, $p < 0.01$) as can be seen in Figure 7.20, when the OSR increases, the GSI tend to decreases hence more interval space are be created, and it forms higher transmission rate through the built-up area around and behind the

roadside flanking buildings, which consequently allows less affected free transmission in the noisier half on all surfaces.

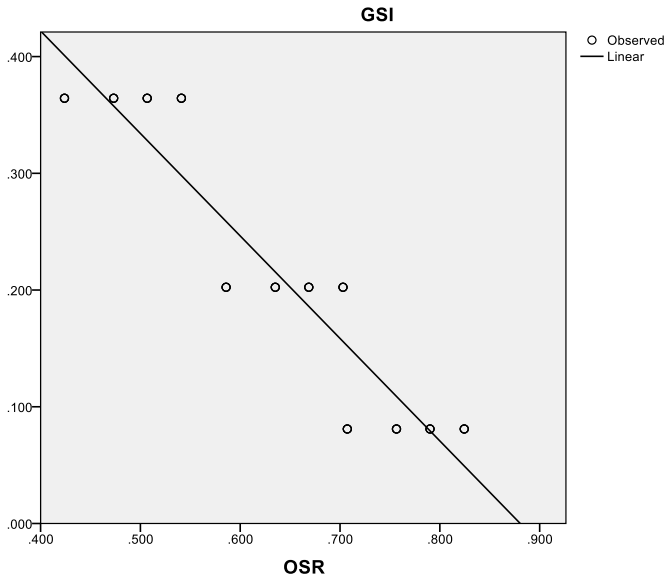

Figure 7.20 Linear correlation between OSR and GSI ($R^2 = .878$, $p < 0.01$)

The negative correlations between the OSR and attenuations indices in the quieter space thus could also be explained, as when the OSR increases, the GSI also increases and creates more penetrable street interface and porous inter-building space, therefore the attenuation in the quieter end are less affected by the screening and reflection of the buildings and tend to decay more quickly, and vice versa when the OSR decreases, the higher GSI creates more confined street interface which screens most of the noise in the street space and the traffic may quickly decay to the background noise level before reaching the quietest area behind the flanking buildings, and attenuation appears becomes slower.

- ***Correlations between CAR and spatial noise indices***

The complete aspect ratio (CAR) is to have limited effect on spatial noise distribution, especially on the ground and ground façade level. The CAR indicates the ratio of all roughness elements to the horizontal area of the study region, while in this study the roughness elements refer to the area of all building façades, open ground area and the open ground space (Burian, Brown, & Linger, 2002).

For the ground and ground façade noise levels, the CAR has a very limited impact and is only found to be negatively correlated with the median noise level L_{50} and the total noise attenuation of the ground façade noise levels. For the total façade noise level, the CAR is found to have comparable broader and stronger impact, which is found to be positively correlated with the L_{avg}, L_{min} and L_{90}. Meanwhile, it is also found to be significantly correlated with the attenuation of total façade noise level in the quieter space in terms of L_{50}-L_{min} and L_{90}-L_{min}.

The findings denote that the increase of CAR can significantly reduce the noisy space at the ground level and mitigate the average traffic noise impact and to the indoor environment at all altitudes through speeding its attenuation in the quieter area.

Considering that the increase of CAR reflects in a given region implies higher roughness elements, which is mainly brought by the rising of the total façade area of buildings as can be seen in Equation 7.1:

$$\mathrm{CAR} = \frac{\sum(A_{fa} + A_{rf}) + A_G}{A_T} = \frac{\sum A_{fa} + A_T}{A_T} \tag{7.1}$$

where the A_G represents the total exposing area except the buildings and considering the upright form and flat roof of all buildings, the A_{rf} is equivalent of building ground space area A_g. Thus, the CAR can be calculated as the ratio of the sum of total planned area A_T building façade area $\sum(A_{fa})$ to the total planned area A_T. The rise of CAR thus indirectly reflects the increase of total façade area of the buildings and hence higher amount of frontal façades facing the road sources and larger scale of shadowed façades, which could bring broader screening and absorption effect and consequently reduces the average and minimum noise levels.

- ***Correlations between BSAPAR and spatial noise indices***

Comparing to CAR, the BSAPAR directly calculates the ratio of the total building surface area to the planned area, it is found to have similar but stronger effect on the spatial noise distribution, especially for the total façade spatial noise indices. Unlike the building

façade ratio (BFR), the BSAPAR concerns the ratio of all exposing surface of the buildings including the roof to the planned area.

For the general noise level in the open ground and at the ground façade level, the BSAPAR is not correlated with the mean or median noise it is significantly correlated with the L_{min} of both types of indices and the L_{90} at the ground façade level. It may be explained by the fact that the BSAPAR is positively correlated with the total attenuation from the intrusive to background level L_{10}-L_{90} of both types.

The BSAPAR has stronger and broader impact on the total façade noise level TFL_n. For the total façade noise level, the BSAPAR is found to be significantly correlated with the total attenuation in terms of L_{10}-L_{90} and the attenuation in both quieter and a noisier half in terms of L_{50}-L_{min} and L_{max}-L_{50}.

The increasing of BSAPAR indicates significant rise of total surface area including the building façade area and roof area, thus as discussed in the study on the complete aspect ratio, the rise of BSAPAR may also indicate higher screening and absorption on the façades, hence it leads to the speed-up of noise decay on all altitude of façades and less impact on the indoor environment in general.

7.5 Noise evaluation models based on multiple linear regression

From the analysis on the correlation between a series of urban morphological indices and spatial noise distribution indices, it can be seen that there is strong indication that the change of certain urban morphological characteristics can significant affect the general level and distribution of traffic noise impact in the open ground and to the indoor environment.

To further test the effectiveness of the variables and providing a practical tool for urban noise estimation and abatement in the earliest stage of the urban planning process, a series of prediction models are produced through a hierarchical linear regression analysis. The independent variables (IV) or the predictors of the models are the urban morphological with Pearson correlation significance value of $p < 0.01$, and the dependent variables (DV) are the L_{avg}, L_{10}-L_{90} of three types of spatial noise indices. The independent variables (IV)

that have less or no contribution to the model are removed step by step based on its theoretical importance and statistical significance and contribution to the prediction power of the overall model. A collinearity diagnostic method with Variance Inflation Factor (VIF) higher than 5 are adopted, with both statistical and substantial considerations (Heiberger & Holland, 2004).

A series of prediction models are produced, the models with less than 50% explanation power ($R^2 < 0.50$) are regarded as invalid and not listed, especially those for the quieter half noise levels and attenuation indices, i.e. L_{90}, L_{min}, L_{90}-L_{min} and L_{50}-L_{min}. The low predictability of this indices indicates that the attenuations in the quieter zones have higher variations, comparing with that in the noisier space as shown in Figure 7.12, Figure 7.15 and Figure 7.18.

Nevertheless, it is to note that although some of the independent variables have strong collinearity; which also has stronger explanatory power but is put into different models, it does not indicate that any of which is less significant in the prediction of the spatial noise indices. For instance, the GSI and BFLI are significantly inter-correlated ($R^2 = 0.904$, $p < 0.01$) and both indices have significant linear correlations with a series of spatial noise indices and their attenuation, as the two indices measure entirely different aspect of the characteristics and are calculated from the perspective of land-use coverage and street interface intensity respectively.

7.5.1 Prediction models for the general ground noise distribution

The models for the prediction of general ground noise levels L_{avg}, L_{50}; and the attenuation indices L_{10}-L_{90} and L_{max}-L_{50} are demonstrated in Table 7.8. It can be seen that the selected spatial noise indices explains 73.1% and 69.3% of the variance of the spatial average noise level $\underline{L_{avg}}$ (R^2 =.731, F (3, 32) = 29.03, $p < 0.01$) and median noise level L_{50} (R^2 = .693, F(3, 32) = 37.18, $p < 0.01$) in the open ground level in general.

Table 7.8 Prediction models for the general ground noise distribution based on multiple linear regression analysis on idealised cases (N=36)

	B	Standardised β	*t*	Sig.	Tolerance	VIF
a. Ground noise $\underline{L_{avg}}$						
(Constant)	75.004		43.402	.000		
BFLI	-19.681	-.671	-6.661	.000	.828	1.208
BBAI	-5.145	-.248	-2.469	.019	.829	1.206
FSI	-1.296	-.213	-2.314	.027	.988	1.013
R^2 =.731 (p<.01) | SE=2.500 |0% F(3,32)=29.03						
b. Ground noise L_{50}						
(Constant)	68.987		34.838	.000		
N	.201	.254	2.633	.013	.999	1.001
BFLI	-26.905	-.784	-8.117	.000	.999	1.001
R^2 =.693 (p<.01) | SE=3.080 | F(2,33)=37.18						
c. Ground noise L_{10}-L_{90}						
(Constant)	14.807		12.773	.000		
H	-.242	-.933	-6.999	.000	.579	1.727
FSI	8.028	1.002	7.517	.000	.579	1.727
R^2 =.661 (p<.01) | SE=3.650 | F(2,33)=32.14						
d. Attenuation of ground noise level L_{max}-L_{50}						
(Constant)	20.753		8.832	.000		
RSR	-43.500	-.333	-3.242	.003	1.000	1.000
GSI	35.888	.736	7.179	.000	1.000	1.000
R^2 =.653 (p<.01) | SE=3.481 | F(2,33)=31.03						

By comparing the Standardised Beta which reflects the actual contribution of each IV, it is notable that the BFLI which represents the street interface density in terms of building width to the road length ratio is found to contribute the greatest among all predictors in both models (β = -19.681 and -26.905). Nonetheless, the BBAI (β = -5.145) and FSI (β = -1.296) which represents the building density in terms of floor space and the settlement block coverage respectively also contributed significantly and negatively to the model. As discussed earlier, the decrease of BFLI implies increasing noise emission through the enlarged building intervals, and on the ground level this changes can be seen has the most profound impact on the general noise level.

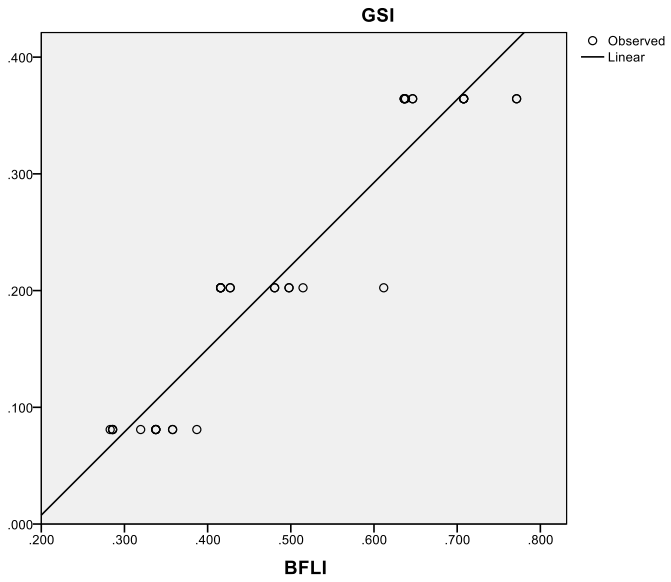

Figure 7.21 Linear correlation between BFLI and GSI (R^2 = .904, p<0.01)

Regarding the models for the noise attenuation, the model consists of the H (β = -.242) and FSI (β = 8.028) explains 66.1% (R^2 = .661, F(2, 33) = 32.14, p < 0.01) of the variation of total noise attenuation between intrusive and background noise levels in terms of L_{10}-L_{90}. It can be seen that the general noise attenuation is significantly influenced by both the total building floor area density in terms of FSI and the average building height H, and both predictors are approximately equally important but with a totally reversed gradient. Nonetheless, in the relatively noisier half, the L_{max}-L_{50} can be 65.3% explained by the model that consists of two independent variables, the RSR (β = -.43.5) and the GSI (β = 35.888). The negative contribution of the RSR can be understood as that, when road surfaces as well as amount decreases, the interval space in the basic urban fabrics increases, thus the attenuation in the noisier half increases due to the longer transmission distance. Where for the GSI, the fact is that the GSI is significantly correlated with the BFLI (R^2 = .904, p < 0.01) as shown in Figure 7.21, and both indices more or less reflect the openness of the street canyon interface, i.e. the extent of noise emission from the street space to the shadowed space behind the flanking buildings.

7.5.2 Prediction models for the ground façade noise distribution

Table 7.9 Prediction models for the ground façade noise distribution based on multiple linear regression analysis on idealised cases (N=36)

	B	Standardised β	*t*	Sig.	Tolerance	VIF
a. Ground façade noise L_{avg}						
(Constant)	70.953		35.202	.000		
FSI	-1.779	-.297	-2.724	.010	.988	1.013
BFLI	-14.371	-.497	-4.17	.000	.828	1.208
BBAI	-6.744	-.330	-2.774	.009	.829	1.206
R^2 =.624 (p<.01) | SE=2.915 | F(3,32) = 17.73						
b. Ground façade noise L_{50}						
(Constant)	72.520		38.145	.000		
FSI	-1.790	-.269	-2.906	.007	.988	1.013
BFLI	-19.810	-.617	-6.094	.000	.828	1.208
BBAI	-6.543	-.289	-2.854	.008	.829	1.206
R^2 =.729 (p<.01) | SE=2.750 | F(3,32) = 28.64						
c. Attenuation of ground façade noise level L_{10}-L_{90}						
(Constant)	9.283		3.039	.005		
RWI	15.239	.287	2.382	.023	.976	1.025
N	-.305	-.398	-3.299	.002	.972	1.029
RI	1.048	.542	4.538	.000	.991	1.009
R^2 =.547 (p<.01) | SE=3.670 | F(3,32) = 12.87						
d. Attenuation of ground façade noise L_{max}-L_{50}						
(Constant)	8.987		6.172	.000		
BSAPAR	3.343	.316	3.228	.003	.992	1.009
GSI	32.707	.738	7.545	.000	.992	1.009
R^2 =.687 (p<.01) | SE=3.006 | F(2,33) = 36.227						

Table 7.9 shows four prediction models for the ground façade indices. For the ground façades level, the first two models explains 62.4% and 72.9% of the variations of average noise level L_{avg} (R^2 = .624, F(3, 32) = 17.73 p < 0.01) and L_{50} (R^2 = .729, F(3, 32) = 28.64, p < 0.01) respectively. The BFLI (β = -14.371 and -19.810) is again proved to be the most influential predictor of all, although the FSI (β = -1.779 and -1.790) and BBAI (β= -6.744 and -6.543) also contribute significantly in both model, suggesting that the street interface density in terms of BFSI can also be utilised to estimate the general façade noise at the ground level.

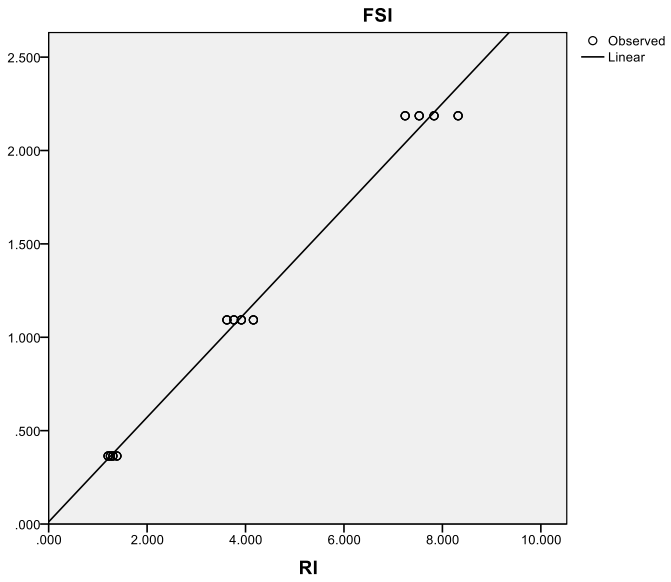

Figure 7.22 Linear correlation between RI and FSI (R^2 = .090, p < 0.01)

For the L_{10}-L_{90}, the model explains 54.7% of the variation (R^2 =.547, F(3, 32) = 12.87, p < 0.01), in which the RI (β = 1.048) is found to be the most important predictor. It denotes that the general noise attenuation on the ground façade level is significantly affected by the mean height of the urban canopy. It is to note that in this model if the RI is substituted by the FSI, the decrease of R-squared in the new model is negligible and the Adjusted R-squared remains the same. Considering that the FSI and RI have significant positive inter-correlation (R^2 =.0.990 p < 0.01) as can be seen in Figure 7.22, the RI thus can be considered as an important backup index when the acquisition of FSI is not feasible. It suggests that the rugosity index which is commonly used in urban air-dynamic studies (Edussuriya, Chan, & Ye, 2011) is also helpful in the estimation of general noise attenuation on the building façades when analysing the strategic noise maps.

The model for the attenuation of ground façade noise at the noisier half in terms of L_{max}-L_{50} explains 68.7% of the variations (R^2 = .687, F(2,33) = 36.23, p < 0.01), in which the GSI is found to have a greater impact. The BSAPAR is also seen to have significant and positive impact, proving again that the geographical indices can also contribute to the prediction of noise levels. The model suggests that with higher building coverage ratio at the ground level and higher building façade surfaces, the traffic noise attenuation in the noisier half close to the road source tends to rise too. It may be due to that the increase of GSI can raise the BFLI as discussed earlier and hence reduce the emission at the ground

level from the road sources; the increase of BSAPAR raises the amount of receiving façades in general, conveniently the façade attenuation close to the road source at the ground level increases.

7.5.3 Prediction models for the façade noise distribution

Table 7.10 Prediction models for the total façade noise distribution based on multiple linear regression analysis on idealised cases (N=36)

	B	Standardised β	*t*	Sig.	Tolerance	VIF
a. Total façade noise level L_{avg}						
(Constant)	64.774		87.873	.000		
GSI	-15.577	-.616	-6.531	.000	1.000	1.000
FSI	-2.246	-.573	-6.074	.000	1.000	1.000
R^2 =.707 (p<.01) | SE=1.661 | F(2,33) = 39.78						
b. Total façade noise level L_{50}						
(Constant)	65.684			.000		
N	.135	.260	.260	.014	.999	1.001
BFLI	-13.606	-.606	-.606	.000	.978	1.023
BSAPAR	-2.944	-.411	-.411	.000	.979	1.022
R^2 =.684 (p<.01) | SE=2.073 | F(3,32) = 23.10						
c. Total façade noise level L_{90}						
(Constant)	68.281		28.390	.000		
BFLI	-15.700	-.442	-3.818	.001	.828	1.208
BBAI	-5.945	-.237	-2.050	.049	.829	1.206
FSI	-3.639	-.495	-4.669	.000	.988	1.013
R^2 =.645 (p<.01) | SE=3.479 | F(3,32) = 19.41						
d. Attenuation of total façade noise level L_{10}-L_{90}						
(Constant)	4.533		2.458	.019		
GSI	29.128	.566	4.881	.000	1.000	1.000
FSI	3.866	.485	4.178	.000	1.000	1.000
R^2 =.556 (p<.01) | SE=4.156 | F(2,33) = 20.64						
e. Attenuation of total façade noise level L_{max}-L_{50}						
(Constant)	5.605		3.104	.004		
FSI	2.492	.404	3.613	.001	.945	1.058
BPRLI	.615	.298	2.261	.031	.680	1.470
BFLI	13.814	.464	3.530	.001	.685	1.459
R^2 =.621(p<.01) | SE=3.012, F(3,32) = 17.49						

Table 7.10 shows three prediction models for the total façade spatial noise indices which can be seen as indicators of the general indoor noise level of all floors. For the average and median indoor noise level, the first two models explains 70.7% and 68.4% of

variations of L_{avg} (R^2 = .707, F(2,33) = 39.78, p < 0.01) and L_{50} (R^2 = .684, F(3,32) = 23.10, p < 0.01) respectively. The back ground level L_{90} of the indoor noise is found to have 64.5% (R^2 = .645, F(3,32) = 19.41, (p < 0.01) explainable by the combined distribution of three indices.

Again the most significant predictors in the models are the inter-correlated GSI and BFLI, both indices dominate the prediction power of the three models. The FSI and the BSAPAR also have a certain extent of effect for the L_{avg} and L_{50} respectively. The model of the L_{90} is relatively more complicated, for the L_{90} reflects the 10% quietest building façades which normally locate in the shadowed spaces. The FSI contributes negatively to the L_{90}, denoting that with increasing BFLI, the increase in floor space, in general, reduces the background noise level. Meanwhile, the increase of BBAI potentially reduces the road-kerb-to-façade distance and enlarges the area of the shadowed area. Thus, with the combined effect of the three indices, the background noise level of the indoor space can be reduced significantly.

Regarding the decay of noise level on all building façades, i.e. the indoor noise level, it is interesting to note that, for the total attenuation from the intrusive to the background noise level in terms of L_{10}-$L_{90,}$ the model contains only two of the basic urban density related indices, the FSI (β = 3.866) and GSI (β = 29.128), explains 55.6% (R^2 =.556, F(2,33) = 20.64, p < 0.01) of the variations, and the GSI is again proved to be the dominant predictor of the two, although the prediction power is relatively smaller than that of the ground and ground façade noise prediction models.

For the decay of noise impact to the indoor environment in the noisier half in terms of L_{max}-L_{50}, the model exhibited explains 62.1% of the variance. The BFLI (β = 13.814) is proved to be the most influential predictor of all three, the FSI (β =2.492) and the BPRLI (β =0.615) also contributes significantly. The BFRIL is not inter-correlated with any other predictors, and the increase of BFRLI in a certain urban area denotes the increase of total building perimeter. Thus, the increase of both BFRLI and BFLI will consequently lead to more buildings in the shadowed area; which may correspondingly lead to the increase of total floor area. Thus, as exhibited in the model, when the three indices increase following the model, the interval spaces between the roadside buildings on all altitudes tend to be

reduced significantly, so does the noise attenuation in the noisier half close to the road source.

It can be seen that, with the combined prediction power of urban morphological indices of all types including the most basic indices used in urban planning practice and study, and the two-dimensional and three-dimensional indices concerns the building form and street geometry as well as geographical characteristics of the urban settlement, the spatial distribution and impact of traffic noise to the indoor space is possible to be predicted quantitatively.

7.5.4 Discussion on the predictors and the models

7.5.4.1 Predictors with dominative prediction power

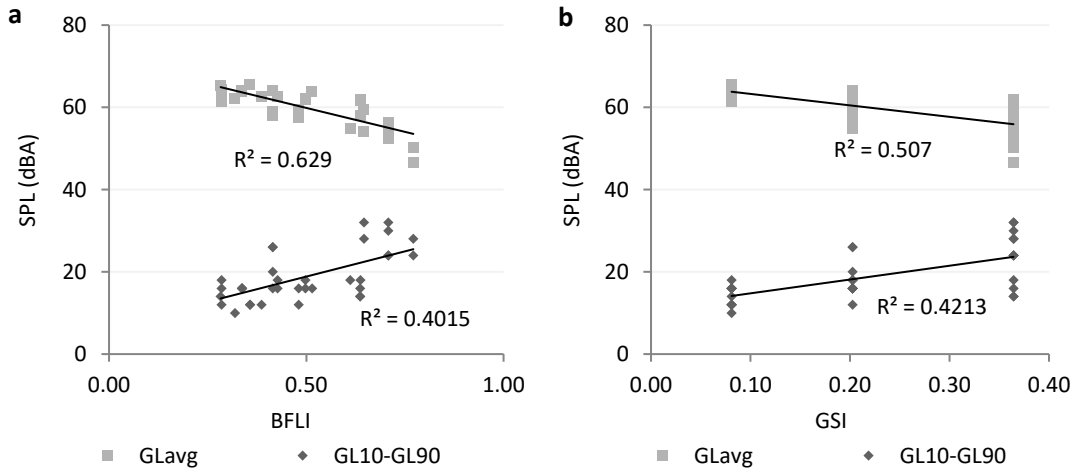

Figure 7.23 Relationship between BFLI (a) and GSI (b), and the L_{avg}, L_{10}-L_{90} of general ground noise level ($p<0.01$)

It can be seen from the prediction models that, for every different spatial noise index, there are different urban morphological indices contribute to the prediction power of the models. Nonetheless, the BFLI and GSI that indicate the one-dimensional density of the street interface and the two-dimensional density of the buildings ground space, both plays relatively the most important role in most of the models; and both indices are significantly correlated with the GL_{avg}, and GL_{10}-GL_{90}, as can be seen in Figure 7.23. Both indices are also significantly and positively inter-correlated as shown in Figure 7.21. It not only denotes that the change of ground coverage can significantly influence the street interface

density but also can contribute to the prediction of general traffic noise distribution on both ground and façade level.

7.5.4.2 Less influential predictors

A series of less influential indices are found to also have a significant impact on the prediction power of the models, which depicts the urban morphological features from different perspectives. Among which three of the significantly inter-correlated indices, the FSI, RI, BSAPAR as shown in Figure 7.22 and Figure 7.24 (R^2 = 0.990, 0.944 and 0.956), is found in most of the models. It denotes that the density of the built-up area measured from the perspectives of the total floor area, the mean rugosity, and the total surface area also effectively contribute to the distribution of traffic noise.

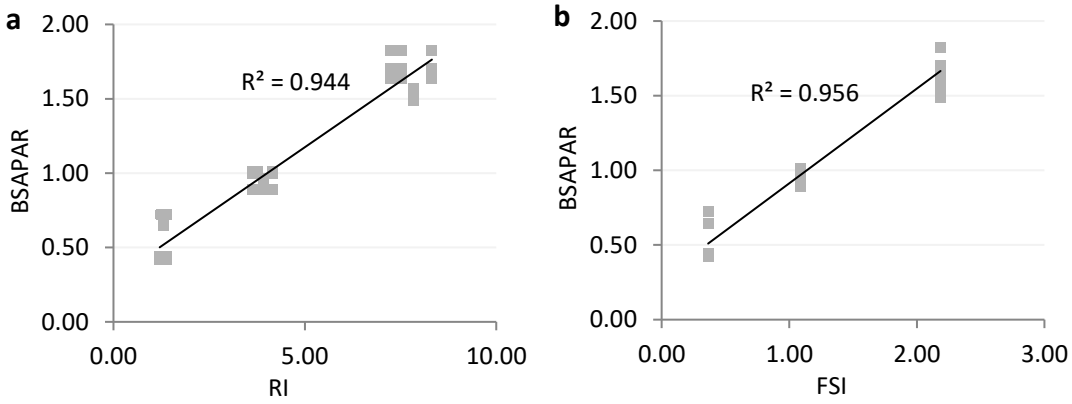

Figure 7.24 Linear correlations between (a) RI and BSAPAR; (b) FSI and BSAPAR ($p<0.01$)

The three indicators reflect the mass of the urban agglomeration a unit planned area from three distinct perspectives, while positively and significantly inter-correlated with each other, denoting there is a fundamental connection between the spatial noise level and the urban development intensity.

7.5.4.3 Supplementary predictors

It is also seen that, in the prediction models, there are also a number of predictors that have relatively less prediction power. In the meantime, a series of indices which are not included in the models, are widely correlated with the ones in the model. It in one hand provides huge potential for the improvement of the current noise prediction models,

considering the limitation of the idealised case raised in this study. Nevertheless, in the other hand, it proves that the selected urban morphological indices have the strongest prediction power, although they are not the only ones that reflect the same type of features of a built-up urban area. This means that the urban planners and policy makers can rely on the limited amount of key indices mentioned in this study and their advisable substitutes, and utilise the refined models to predict or estimate the urban traffic noise impact to current or prospective urbanised area.

7.6 Summary and discussion of the findings

Through the explicit data analysis and prediction model construction, it can be seen that there are significant correlations between a series of urban morphological indices that characterise the urban morphology from varied perspectives and the spatial noise indices that reflect the traffic noise resistance on all exposing surfaces.

7.6.1 Effect of urban density indices on traffic noise resistance

The pre-defined density-related urban morphological indices are found to have a significant impact on the variation of spatial noise level on all exposing surfaces.

- For the building density, the increase of FSI can significantly reduce the general noise level, while the GSI is found to be more widely correlated with most of the spatial noise indices tested, proving that the urban areas with high building ground space coverage tend to have more chance to live in acceptable outdoor and indoor sound environment, despite the change of other urban features.
- It is also found that, the pattern and arrangement of the road network pattern, i.e. the size of the grid and basic urban fabric, can significantly affect the intuitive impression about the linear relationship between roads and traffic noise: more roads not necessary leads to higher noise levels.
- The medium-scale road network with an interval of around 200 meters (187.5m in this study) is found to be the most effective in the abatement of traffic noise impact and creating quiet zones than the case groups with lower or higher network density.

- It suggests that with deliberate planning of the network density pattern and building arrangement without changing the network density *N*, the general noise level can be significantly reduced, and the noise attenuation and the size of the quiet zone can be evidently increased.

7.6.2 Effect of urban density related indices on the variation of spatial noise level and attenuation

The variation of noise levels is also analysed in detail. It is found that there is significant difference in the variation of noise level distribution among each case groups categorised by the three pre-defined density indices. It is to note that the mid-N cases are categorised into two groups based on different road arrangement.

- It is firstly found that in general on all exposing surfaces, the noise level in the noisier space are more concentrated and with much less variation than in the quieter spaces, this effect is stronger when cases area grouped based on network density, as the road patterns of each case group are identical.
- The more vibrant noise level distribution in the quieter-half spaces is not found to have a clear connection with the simple change of the three pre-defined parameters. Nonetheless, it is also found that the noise level variation is more prone to be affected by the change of building density, in terms of both FSI and GSI: in the lower building density cases, there is less variation of the noise level in the quieter space.
- The attenuation of noise level is also tested and compared across case groups. It is found that, in general, the traffic noise attenuates more quickly in the noisier half especially in the noisiest 10% space close to the road source. In the quieter end, the GSI is found to have a clear impact on the decay of noise level than other indices.
- Regarding the difference of noise attenuation on the ground level and the decay of noise level on the ground façade level and that of all building façades which represents the indoor noise level, it is found that the attenuation on the ground levels are much weaker in general.
- The medium-N case groups are again found to have distinct attenuation pattern and it is also found that between the two mid-N case groups there are evident

different in the attenuation patterns simply due to a different arrangement of road pattern and buildings. The medium-*N* case group B with evenly distributed branch roads and 187.5 m road intervals is found to have to highest total noise attenuation from the noisiest area to the quietest area on the ground level, comparing with any other case groups, it confirms again that appropriate planning of the basic urban fabric can have significant effect for the mitigation of general noise level.

7.6.3 Multilinear correlation analysis on urban morphological indices and spatial noise indices

The urban morphological from the perspectives of urban density, building and street geometry, and urban geography are systematically analysed using the bivariate correlation analysis, where only correlations with $p < 0.01$ are discussed. It is found that there are significant correlations between a series of urban morphological indices and the spatial noise indices.

- In general, the density-related indices have a general impact for both the spatial noise indices and the attenuation indices; while the building and street geometric indices tend to have more significant correlations with the noise attenuations; the urban geography related indices, on the contrary, have more correlations with the general noise level than with the noise attenuation.
- The L_{max} on all exposing surfaces is found to have no correlation with any morphological indices as it is mainly related to the variation of traffic flow which is very small in the idealised cases. The CAR is found to have relatively the smallest impact on noise level on the ground level and ground façade level, while having strong correlation with a series of total façade spatial noise indices. The *N*, *H* and the RSR are also found to have limited impact on only some of the indices.
- The most influential indices with regard to the R value and amount of significant correlations ($p < .01$) found includes the FSI, BFLI, and GSI, RWI and BBAI. The OSR, RI and the BSAPAR are also found to have a wide range of impact on the spatial noise distribution on all exposing surfaces.

7.6.4 *Prediction models based on multiple linear regression analysis*

In the prediction models based on multilinear regression, it is found that over 60% percent of the variation can be explained by the combination of 2-3 urban morphological indices. It is also found that generally the noise level and their attenuation in the quieter half space are more difficult to be predicted. Some of the predictors are found to have a much stronger impact than other indices. For indices with strong inter-correlations, only those with strong impact remain in the models.

- The BFLI and GSI are found to be the most influential predictors which exhibits dominate prediction power in terms of adjusted beta in a majority of the prediction models, the FSI, RI and BSAPAR are also found to have strong prediction power in a number of models.
- It also notable that although some of the urban morphological indices are not included in the final models due to strong collinearity with the chosen indices. Nonetheless, they also have relatively significant prediction power to the variation and distribution of spatial noise levels.
- This means that the urban planners and policy makers can rely on the limited amount of key indices mentioned in this study and their advisable substitutes, and utilise the refined models to predict or estimate the urban traffic noise impact to current or prospective urbanised area.

7.7 Conclusions

A series of empirical studies have been conducted to explore the correlation between urban morphological features and the noise distribution, either through empirical comparisons (Guedes, Bertoli, & Zannin, 2011; Tang & Wang, 2007), or geographical research methods (Ariza-Villaverde, Jiménez-Hornero, & Gutiérrez De Ravé, 2014) A in-depth parametric study is conducted in this chapter with applying a quantitative analysis on the effect of urban morphology on the traffic noise distribution is thoroughly examined using 36 idealised urban area cases. It is generally found that, given fixed amount of traffic in a certain urban area, the traffic noise tends to have a lower impact on all exposing surfaces and indoor space when the urban density is higher, especially the building density

in terms of ground space coverage (GSI). Nonetheless, it is also noticed that, the road length density which decides the distribution of the traffic flow, has a more complicated relationship with the general noise impact. The cases group with medium network density (*N*), in which the branch roads evenly distributed with an interval of around 200 m (187.5 m in the idealised cases) is found to have the lowest general noise level, comparing with both the unevenly distributed cases and the case groups with higher or lower network density.

The distribution and the pattern of noise distribution are also examined, it is found that in general the noise level tends to attenuate faster in the noisier space near the road source, and have a more scattered pattern of attenuation among different cases in the quieter area. If only considers building density, the cases with higher building density forms higher total attenuation and hence more tranquil space. The medium-*N* cases with evenly distributed roads again is again found to have the highest total attenuation on the ground and ground façade level, comparing with all other network patterns, it may mainly due to the unique scale of the basic urban fabric size and indicates huge potential of control the traffic noise impact in the early stage of the urban planning process.

A further multilinear correlation study is conducted between 16 urban indices describing the urban morphology from the perspective of general urban density, building and street geometry and the urban geography. A number of indices are found to have significant correlations to the traffic noise distribution: the building density is again found to be highly influential on the noise distribution on all exposing surfaces; the building and street interface related indices is found to mainly significantly affect the attenuation of the noise level.

A multiple regression is conducted for the sake of finding effective models for the prediction of traffic noise impact and distribution. A series of urban morphological indices are found to be capable of utilised for the prediction of traffic noise impact and distribution. The GSI and BFLI are found to have dominated prediction power; the FSI, RI and BSAPAR are also found to be helpful in the prediction models. A series of morphological indices which are significantly inter-correlated with the stronger predictors may also be utilised as alternative predictors in the practice of urban noise prediction.

Chapter 8 Conclusions and future works

8.1 Conclusions and discussion

The study explored the relationship between the urban morphology features and the traffic noise distribution in the urban area, and some major findings and contributions are concluded in this section. The hypothesis of the study is that certain features of the urban forms can have a significant effect on the general level and distribution of noise in the urban area.

A comparison between urban morphology samples with distinct density and form is conducted to test the hypothesis in the real urban situation. A series of urban areas in two cities with distinctive features: Wuhan in China and Greater Manchester in the UK, are selected and tested.

Prior to the comparison study, a systematic applicability test is conducted for the sake of validating the applicability and effectiveness of the traffic simulation tool, i.e. the noise-mapping methods and packages in typical Chinese urban environment. Through the test, a series of optimisation of the recommended calculation configurations are then abstracted. Meanwhile, a series of typical urban scenarios where systematic calculation errors may occur are also tested, suggestions and solutions are proposed for the sake of eliminating potential errors and improving the calculation accuracy.

Beyond the comparison of the general noise levels and noise distribution in the selected sample areas in both Wuhan, and Greater Manchester, a parametric study from a more general perspective on the urban morphology is conducted. A series of idealised urban forms with identical traffic amount and building floor area quantity and distinct urban morphological features are tested. The correlation between a series of urban morphological indices and spatial noise indices are studied. For some key spatial noise indices, a series of prediction models are proposed based on multilinear correlation analysis.

The key findings and potential contribution of the studies conducted are listed in Section 8.2, the limitation of the research method and potential work to be carried out in the future are discussed in Section 8.3. Contribution of the thesis

8.1.1 The optimisation of EU noise mapping calculation method in typical Chinese urban environment

Chapter 4 answers the following research questions: whether the calculation algorithm and the recommended calculation configurations are applicable and optimisable in typical Chinese urban environment, and what are the pattern and reason.

- ***Main findings***

The primary finding is that, the appropriate configuration can ensure the general calculation accuracy in open space. By simply setting the ground absorption coefficient according to the ground surface condition, the maximum reflection order to 3, and disabling the opposite façade reflection correction set in the selected package, the mean absolute error (MAE) is within 2 dBA for the receiver points locating at varying heights and slant distances from the road source. Between 500 Hz and 4000 Hz the accuracy is generally acceptable. Nonetheless, at the energy-concentrated lower frequencies from 31.5 Hz to 250 Hz, the calculated noise levels are generally underestimated. Meanwhile, at 8000 Hz the calculated noise levels are also globally underestimated.

For the reflection settings, the commonly used method of correction for the opposite façade reflection is more effective for receiver points closer to the road source, say within 40 m in the study area. Regarding the calculation of the ground effect, it is found in a parametric test that the ground effect that is only calculated within a certain range of distance and height according to the mainstream methods, and the reflected wave from the ground surface is largely ignored at higher altitude by up to 3 dBA. Alternations of most of other settings of the default configuration of the state-of-the-art EU noise-mapping package in this simple urban scenario have no observable influence on the general accuracy.

It is also notable that the calculation errors increase along with the slant distance. The MAE of the receiver points locating within 60 m from the source are 0.7 dBA smaller

than of the receiver points ranging from 120 m to 150 m. Similar phenomena were also found in the brief correlation analysis, where a significant and positive correlation is found between the slant distance and the SPL at 8000 Hz. The higher errors at the remote locations my mainly occur close to the surrounding building or ground objects, where there are more complicated reflections from surrounding structures and surfaces.

The effect of the high-rise main buildings on the calculation accuracy is evident for all receiver points locating close to it, where there are more complicated reflections from surrounding structures and surfaces. For the four façades receiver points with different height, a brief hypothetical test shows that the influence of the main building and the podium is not sufficiently considered in the calculation. The receiver points locating in the shadowed area on the rear side of the main building shows the highest error of up to -11.8 dBA due to the potential inaccuracy in the calculation of the screening effect and lateral refraction caused by the main building.

- ***General practical suggestions***

By summarising the findings in the pilot test conducted in this chapter, a set of configuration settings based on the typical settings of the tested EU noise-mapping method and package, for the sake of achieving acceptable accuracy in noise mapping practice in urban areas in China.

First of all, it is advised that the maximum reflection order shall be set to at least 1 in most of the urban scenarios with relatively open space; while there is any multi-story buildings or barriers exist, the maximum reflection may be set to at least 3 for the sake of counting in the multiple orders of façade reflections without evidently increasing the calculation time. The 1.5 dB correction for the opposite façade reflection should mainly be taken into account for large scale noise mapping practices and should be switched off in the scenarios with complicated urban spatial features. For the acoustic environment modelling settings, the ground absorption shall be set according to the ground surface conditions; the actual ground reflections shall be calculated with given modelling measures, e.g. 3D reflectors, when the receiver points are located close to the road edge and the ground surface are reflective. The façade absorption/reflection coefficient shall be set in accord with the actual surface conditions, especially when the noise levels close

to the building façades are to be evaluated. It is also to be noted that, in general the current methods may not be able to accurately calculated the atmosphere divergence due to distance increasing of the noise level of frequencies higher than 4 kHZ, measures of compensation or algorithm improvement may be necessary.

8.1.2 Systematically tests on the applicability of the EU simulation methods in typical Chinese urban environment

Chapter 5 answered the following research question: How is the performance of typical EU strategic noise-mapping software in a typical urban environment with heavily constructed road infrastructures and dense buildings in major cities of China, and what are the feasible measures to optimise the applicability.

A series of representative Chinese urban morphological and building features commonly found in Chinese major cities are further tested in the selected study areas in Chapter 5. It is found that increasing maximum reflection orders or change the default way of modelling can be helpful to reduce the calculation error at some hard-to-reach locations. For some sensitive locations that are affected by unique urban form and building features, some systematic calculation inaccuracy cannot be simply eliminated by tuning the configuration or modelling method.

- ***Urban village***

The calculated attenuation at the locations without direct exposing to the road source in the low-rise and high density urban village are highly underestimated in the calculation comparing with that in the normal modern multi-storey residential area. The omitted multi-order reflections and complicated lateral and top-side refractions may be the cause. The unique pedestrian-dominated alleys may also bring a difficulty to the noise measurement and simulation.

- ***High-rise street canyon case***

The high-rise buildings in the typical high-rise street canyon play a significant role in screening the noise propagation inside the canyon, and the potential inaccuracy occurs in the calculation of reflection and refractions causes relatively high errors in general, say,

the MAE of 6.3 dBA for the receiver points shielded by the high-rise building and 4.1 dBA inside the street canyon when maximum reflection order raising to 4. Higher reflection orders can evidently reduce the calculation errors for the receiver points in the shadowed area, especially for those locating closer to the flanking buildings. Nevertheless, inside the street canyon, keep increasing the reflection order is not as helpful for the error reduction when the maximum reflection order is set to higher than 1. It is also notable that peculiar shape of the high-rise building can cause high calculation errors in some partially screened space close to the building façade; special attention is required in the modelling process and the calculation of diffractions.

- ***Comparison between two cases with street canyon and elevated road***

Generally, the accuracy level in the relatively open street canyon is better than that of the narrow one, the increasing of maximum reflection order is also more helpful for enhancing the calculation accuracy in the latter, say, higher than 4 is preferred. Nonetheless, due to the relatively complicated propagation path shaped by the elevated road, some specific receiver points especially those beneath the elevated roads, and those in the peculiar space partially shielded by the building parts manifest systematic calculation inaccuracy.

For the full spectrum SPL, in the wide space canyon with an open elevated road, the receiver points locating higher than the elevated road, at all central frequencies the calculation accuracy is generally within acceptable range except 8000 Hz where the SPL at all points is underestimated. Nonetheless, in the relatively narrow street canyon with the barrier-enclosed elevated road, it is firstly found that the screening effect of the noise barrier installed on the elevated road is overall well simulated with errors lower than 3 dBA, except SPL of frequencies higher than 4000 Hz. By introducing improvement measures on the default modelling methods for the thick base slab and the barriers of the elevated road, the calculation accuracy of the screening effect and the specular reflection beneath the elevated road is greatly enhanced.

- ***General practical suggestions***

Through the tests, a series of improvement measures regarding the calculation accuracy are introduced based on the typical building and urban form characteristics that have been

tested in the four cases in Wuhan, China. The suggestions are given based on the optimised calculation configurations

For the noise calculation of locations amid high density and low-rise building aggregations, e.g. typical urban village in Chinese large cities, it is recommended that the maximum reflection order shall be increased to value higher than 3. Adjusting the transparent ratio settings when modelling the buildings may also help to gain improvement in calculation accuracy.

In urban areas with high-rise street canyons that are very common urban space in many high-density cities, firstly, increasing the maximum reflection from 3 to 4 is helpful in general, for receivers located inside the street canyon and shielded by the flanking buildings, but improvement is more obvious for the latter. Secondly when the form flanking building is complicated, increasing reflection order is not sufficient to reduce the large errors that may occur in the slots shaded by the intruding façades of the flanking building or the podium buildings. Simplification of the building form may help, though it may also suggest that improvement in the calculation algorithms or configuration of the top side and lateral refraction is necessary.

Lastly, the studies of two main roads with elevated parts suggests that, in the complicated space formed by the road slabs and flanking buildings, the improvement of calculation accuracy is limited by simply increasing the maximum reflection order; alternative modelling measures that better reflects the reflective and screening acoustic features of the elevated road slabs and the noise barriers is proven to be helpful to enhance the calculation accuracy but only to a limited extend.

In general, the suggestions are based on the application of current traffic noise simulation methods and configurations, it can be seen that further improvement is still needed to fundamentally ensure the calculation accuracy in relatively complicated spaces in typical high density urban areas in China.

8.1.3 A comparison study between UK and China on the effect of urban morphology using novel research method

Chapter 6 answered the following research questions: whether the general noise level and distribution in high-density Chinese urban environment distinct from that of similar EU cities; what urban morphological features have caused the difference in the traffic noise level and distribution pattern.

- ***Novel and original research method***

A series of statistical spatial noise indices are derived from the noise map maps using a novel Matlab programme developed by the author, with which some two-dimensional urban morphological indices can also be obtained. This method can be and have since been used in other studies that involve distribution of traffic noise (Hao, Kang, Krijnders, et al., 2015; Margaritis & Kang, 2016).

The Strong effect of urban morphology on the noise distribution is revealed through the comparison of different urban areas with identical size, similar land-use category, as well as distinct urban morphological characteristics in two representative cities, Greater Manchester and Wuhan China with essential differences in urban density and morphological features. As the GSI in the Wuhan cases are evidently higher for averagely 10.2% than that of the Greater Manchester, while the road space coverage in terms of RSR in Wuhan is averagely 3.4% lower. In the meantime, the GSI as a key factor of the building density is proved to have significant correlations with both RSR and OSR in the Wuhan cases, while in Greater Manchester cases it is found to only positively correlate with the OSR.

- ***Distinct pattern of traffic noise impact due to morphological differences***

It is firstly found by simple comparison that, generally for ground and façade noise level, the spatial average and minimum SPL in most of the Greater Manchester cases is higher than that in Wuhan. Nonetheless, in the meantime, the maximum noise level in Greater Manchester is much lower than that of Wuhan due to the more concentrated traffic and less number of roads in the latter. It suggests that although the source noise level near the main roads in Wuhan is generally higher than that of Greater Manchester, the overall

impact of the traffic noise to the urban environment and the buildings are milder in the former, which also makes the quiet spaces more tranquil. Moreover, it indicates that certain urban morphological characteristics as shown in the Wuhan cases can contribute to the mitigation of the general traffic noise impact.

Further correlation analysis suggests that the increase of building coverage density occupies more open spaces and leaves fewer propagation pathways for the traffic noise in both cities. The higher GSI in Wuhan as found in the study cases consequently lower down the road coverage by providing less small roads and a higher concentration of traffic on the massive main roads. Street canyons full of vehicles and severe traffic noise conditions are thus formed.

The effects can be seen evidently in the comparison of two extreme case categories. In the comparison of public square cases, the median noise level caused by traffic in the Wuhan case is 16 dBA lower than that of the Greater Manchester case due to much narrower interval space between the buildings and more concentrated roads distribution. The comparison of the street canyon with commercial block cases shows that, although the RSR in Wuhan case is 12.5% lower than that of the Greater Manchester case due to the exceptionally high concentration of road distribution, the tremendous amount of traffic is only concentrated on the large-scale street canyon formed by the main road and high-rise flanking buildings. It consequently creates much noisier road source and a large area of tranquil spaces in the shadowed areas and causing 9.4–14 dBA lower for average and median noise level and 8–16 dBA lower in the quietest space.

- ***Preliminary study on the effect of socio-economic factor***

An additional comparison is conducted in Wuhan to test potential correlations between socio-economic factors in terms of average income and the traffic noise level. It is found that although the maximum noise level in the low-income area is 4 dBA higher, the average and median noise level in the low-income area are both evidently lower than that of the high-income area. It may be primarily due to the lack of vehicle-accessible small roads. Moreover, the buildings in the low income area consist of low-rise residential buildings or multi-storey apartments which can cause higher attenuation, while the high-

rise building consists of tower-shape residential towers and creates more open space for direct noise transmission.

8.1.4 Parametric study on the correlation between urban morphology and traffic noise

Chapter 7 answered the following research question: How certain urban morphological feature and relevant morphological index affects the noise distribution pattern, and if it is predictable.

- ***A thoroughgoing parametric study method***

The parametric study further explores the relationship between urban morphological features and the traffic noise distribution. 36 idealised cases with varied combinations of urban morphological characteristics, in terms of FSI, GSI and network density *N* are calculated. Sixteen novel urban morphological indices are introduced or raised in this study for the sake of better interpreting the urban morphology from the perspectives of density, building and street geometrics, urban geography respectively. Some previous studies have already made effort in this field, while may not have cover as many spatial noise indices as current research (Ariza-Villaverde et al., 2014; Salomons & Pont, 2012). The relationship between the urban morphological indices and three types of spatial noise indices and the attenuation indices describing the traffic noise impact to all exposing façade, including the indoor space of all altitudes, are systematically analysed.

- ***Effect of urban density indices on traffic noise resistance***

It is found that the case groups with higher urban density in terms of FSI or GSI, can both have a quieter urban environment in general, while the GSI tend to have a stronger effect. For the case groups hierarchically categorised with different *N*, it is found that the exact pattern of the network and the corresponding building arrangement can have significant potential of reducing this effect, although there is still a certain correlation between *N* and the spatial noise indices.

The road interval of around 200 m, or to be exact, medium-*N* of 187.5 m in the studied cases, is found to have the most desirable is found to have the least noise impact of all

case groups in terms of general noise level and quiet zone. It indicates the strong potential of reducing the traffic noise impact by improving the fundamental urban planning scheme.

- ***Effect of urban density related indices on the variation of spatial noise level and attenuation***

The effect of the urban morphological indices on the noise distribution is also analysed. It is found that on all exposing surfaces and all cases, the noise distribution is more concentrated and decays more quickly in the noisier space, especially in the 10% percent space close to the road source. In the quieter space, due to the scattering and screening of the buildings, the variation of the noise levels is higher and decays slower, especially in urban areas with higher building density, especially when which is measured with GSI. The general attenuation on the ground level from noisier space to the quieter space is also found to be slower than on the building façades. The two mid-*N* case groups again are found to have distinct patterns of noise attenuation due to the distinguishing road network pattern and corresponding building arrangement.

- ***Multilinear correlation analysis with more urban morphological indices***

It is found that the density related indices have broad and significant influence on both noise level and attenuations; the building and geometric indices and the urban geography indices tend to mainly have more impact on attenuation and noise level respectively. The FSI, BFLI, GSI, RWI and BBAI was found to have the strongest impact on the noise distribution, the OSR, RI and BSAPAR are also found to have a relatively wider impact. The implication of the significant correlations is listed and briefly analysed.

- ***Models based on multiple linear regressions***

The study also focuses on how the research findings can be applied in the assessment and prediction of traffic noise, thus a series of prediction models for a series of spatial noise indices are proposed based on a systematic multiple regression. A hierarchical cleaning process of the prediction variables, i.e. the urban morphological indices that has significant ($p < .01$) was implemented to keep the most crucial factors.

It is found that the BFLI and GSI have the most widely existed prediction power in a majority of the prediction models, the FSI, RI and BSAPAR are also found to have

relatively strong prediction power. It is to note that, due to the nature of the urban environment, the urban morphological indices proposed describes the physical features of the urban built-up area from a series of different perspectives, thus there are strong collinearities between a number of indices. Thus, it does not mean that the other indices which do not remain in the models cannot be adopted in the prediction of spatial noise distribution in practice.

8.2 Future works

8.2.1 Further applicability test

As revealed in Chapter 4 and Chapter 5 that, the more complicated urban sound environment in China can cause systematic errors in the calculation results. Therefore, the applicability test may need to be conducted in more diverse urban environment scenarios, and localisation research may be necessary for the improvement of the default calculation process. There are several more topics may need to be considered in further applicability studies.

8.2.1.1 The improvement of the modelling method

The main influential factors to the calculation accuracy in Chapter 4 and Chapter 5 is the unique building or road structures, which is challenging for strategical noise mapping methods that are primarily based on ray tracing calculation method, especially when complicated path of reflection, refraction and screening effect is involved.

Based on the improvement of modelling measures discussed and calculation method in this research, further improvement of the default modelling and corresponding calculation method in more urban scenarios can be a prospective topic in future studies. Potential improvement may lie in the modelling and calculation method of:

- Building complex that is constituted of large podium and high-rise buildings are erected on it, where the calculation of diffraction and screening effect may be distorted;

- Penetrable opening or suspensions in the ground floor of buildings, where the default modelling method cannot properly accomplish;
- Better method of modelling the elevated road with thick base slabs, better methods for the screening and edge diffraction are both need to be considered;
- The modelling and calculation method for the foliage, which is not involved in this study but can potentially cause extra attenuation and scattering of the traffic noise (Yang, 2013) but are largely neglected or over-simplified in most of the current methods.

8.2.1.2 Default calculation configuration and algorithm in the current method

Based on the findings in the applicability study, a series of aspects for potential improvement of the current calculation may need to be considered including:

- The calculation of reflective wave from the ground surface, which is found to be neglected for up to 3dBA with the default settings;
- Improvement for the default calculation method of diffractions, especially the lateral diffractions in high density urban environment;
- Improved method for the simulation of vibrant event noise, e.g. the noise from community activities, or the noise of a pedestrian street;
- A series of wave-based methods which are normally used in indoor or small-scale urban scenarios, are proposed for the sake of enhancing the calculation accuracy, can provide more accurate results, while the calculation may be lower than the state-of-the-art noise simulation methods (Kang & Huang, 2005; Alves et al., 2016). It would be thus interesting to combine the advantage of both in complicated urban sound environment, e.g. the study cases in China mentioned in this research;

8.2.1.3 Further comparative case Study

In Chapter 6, a series of comparison between the urban sound environment are conducted between the UK and China, the focus of which was to reveal how urban noise level and its distribution differs due to distinct urban morphological features. It can be seen that the effect of urban morphology on the urban noise impact is evident. Some potential

expansion and application of the research methodology can be achieved through a series of prospective directions:

- ***Comparison between more cities***

It would be interesting to carry on the comparison among cities with distinct background or distinct urban spatial structure, e.g. to compare cities in developed and undeveloped countries with similar urban morphological features. Large-scale comparison can also be conducted between cities with officially published noise maps, the urban morphological indices can be obtained with the help of geometric information system (GIS), some further analysis may also be conducted in the integrated database using GSI (CSTB, 2007). Some more findings could be abstracted for potential policymaking or computer-aided urban sound environment planning.

- ***Expanded sampling of study sites***

For similar studies as conducted in Chapter 6, stratified sampling method can be applied in larger scale, for the sake of further examination of the effects of urban morphological features on the traffic noise impact and distribution.

For large-scale comparison between cities or urban areas of different context, total random case selection of multiple sampling areas in a relatively homogenous urban area can be adopted with the help of GIS.

8.2.2 Further correlation analysis and parametric study

Further study of correlations between urban morphological or socio-economic indices and the spatial noise indices can be developed beyond the parametric study in Chapter 7.

8.2.2.1 Further parametric study

The parametric study method in Chapter 7 has some pro and cons due to the limitaion of resources, and it is potentially upgradable in future research given sufficient resources and time. More urban morphological types and urban morphology modalities can be explored in the future study.

In the real urban planning practice, the density of buildings and road pattern are sometimes prefixed due to the specific land-use type and development needs. The planning authority mainly controls the urban development density in the master planning scale and mainly controls the height, shape and arrangement of the buildings in the zone planning and urban design guidelines (Wu & Li, 2011; American Planning Association, 2006). Thus, in future research, it is helpful to focus on the urban morphological indices apart from the urban density or focusing on specific types of land-use and building types, e.g. residential buildings. The parametric study can then focus on the arrangement of buildings and road network.

8.2.2.2 Verification of the noise prediction models

The noise prediction models derived from multilinear correlation analysis provides effective tools for the assessment and prediction of urban noise levels, especially in the urban planning practices when large-scale noise mapping is not feasible. Potential expansion of the correlation study could bring better understanding and may also help to bring the potential of future upgrades in the prediction models. The prediction models can be improved for better prediction power with the help of integrating more urban morphological indices. It is also significant to apply and verify the model's prediction power in real-world scenarios and provide potentially feasible tools for the urban noise planning practitioners.

8.2.3 Application in more fields and in urban planning policy making and practice

It is found that the method provided in this study has the potential of being implemented in more fields and in the practice of urban noise planning.

8.2.3.1 Socioeconomics related research

In future research, more socio-economics related indices and factors could be introduced in the correlation analysis. In Chapter 4 there are two cases with distinct income level in Wuhan, China being studied, and with the in-situ survey data, it is proved that in the two studied cases, there is certain correlation between the average house income and the impact of traffic noise. What is not reported in the study is that there are more than the

income data surveyed in the questionnaire, including social status, sound preference and sleep qualitative survey of sleep quality, etc. Moreover, the exact locations of the in-situ surveys were also recorded and can be related to the exact noise levels on the noise map. There is thus a huge potential for further studies on the correlation between more socio-economics related indices and the noise distribution based on in-situ surveys.

Beyond the data collected in situ, there are also a large amount of socio-economic data available in a variety of official and third-party database. The noise-mapping technique is essentially developed for strategic assessment and planning purpose. Therefore, there is also potential in the analysing the available statistical socio-economic data and the noise distribution, e.g. education, health care and impact assessment, etc.

8.2.3.2 Strategical application and action plan for urban noise planning

It is noted in Chapter 7 that, the noise attenuation in a different urban environment is evidently affected by basic urban-density-related indices that are also widely used in the urban planning and management practice. Therefore, is suggests that there is huge potential for the research method and the outcome of the parametric study to be applied in actual urban planning and policy making practice, especially in the application of zone planning and urban design guidelines making. There are several specific fields that may be interested:

It is found in Chapter 4 that, with similar road network density, the spatial noise distribution especially the total attenuation of noise level is distinct. It denotes that with similar urban density, which is hard to control in many cases, by solely changing the network density, i.e. the basic fabric size and shape, as well as the corresponding building arrangement, there is a huge potential of mitigating the traffic noise impact.

As discussed in the literature review in Chapter 2 that, there are large numbers of road grid network types available in the real-world urban environment, the cases studied in Chapter 4, 5 and 6 in China and EU manifests distinct patterns of both road network and building arrangement, the noise distribution pattern are also distinct. Thus, it is possible to reveal more patterns that can mitigate the general noise impact and develop certain noise mitigation guidelines from the urban zone planning and urban design perspective. This is especially essential for rapidly urbanising countries like China.

PUBLICATIONS

List of academic publications produced during the PhD studies.

Kang, J., Chourmouziadou K., Sakantamis, K, Wang, B., Hao, Y. (ed.) (2013) Soundscape of European cities and landscapes. EU COST, Oxford.

Wang, B. & Kang, J. (2011). Effects of Urban Morphology on the Traffic Noise Distribution through Noise Mapping: A Comparative Study between UK and China. *Applied Acoustics*, 72(8), 556–568. Retrieved June 22, 2011, from http://linkinghub.elsevier.com/retrieve/pii/S0003682X11000247

Barclay, M., Kang, J., Sharples, S., Wang, B. & Du, H. (2010a). Estimating Urban Natural Ventilation Potential by Noise Mapping and Building Energy Simulation. *Proceedings of 20th International Congress on Acoustics. Sydney, Australia*, (August), 1–7.

Barclay, M., Kang, J., Sharples, S., Wang, B. & Du, H. (2010b). The Challenge of Balancing the Demands for a Comfortable Thermal and Acoustic Built Environment in a Sustainable Future, in: *International Symposium on Sustainability in Acoustics (ISSA).* Auckland, New Zealand.

Wang, B., Kang, J. & Zhou, J. (2008). Comparison of Traffic Noise Distribution between High and Low Density Cities, in: *37th international Congress and Exposition on Noise Control Engineering*.

Wang, B., Kang, J. & Zhou, J. (2007). Effects of Urban Morphological Characteristics on the Noise Distribution: A Comparison between the UK and China, in: *Proceedings of the 19th international congress of acoustics*. Madrid: Sociedad Espanola de Acustica. Retrieved from http://www.sea-acustica.es/WEB_ICA_07/fchrs/papers/env-08-005.pdf

REFERENCES

A.J. Lane. (1993). Urban Morphology and Urban Design: A Review. *University of Manchester Department of Planning and Landscape Occasional Paper*, No. 35.

AASHTO. (2001). *A Policy on Geometric Design of Highways and Streets*. Washinton, US: American Association of State Highway and Transportation Officials.

Abbott, P. & Nelson, P. (2002). *Converting the UK Traffic Noise Index LA10, 18h to EU Noise Indices for Noise Mapping*. Retrieved November 18, 2013, from http://collection.europarchive.org/tna/20061009092805/http://defra.gov.uk/environment/noise/research/crtn/pdf/noise_crtn.pdf

Adolphe, L. (2000). A Simplified Model of Urban Morphology Application to an Analysis of the Environmental Performance of Cities. *Environment and Planning B: Planning and Design*, 28(2), 183–200. Retrieved from http://epb.sagepub.com/content/28/2/183.abstract

AEAT NL. (2004). *IMAGINE – State of the Art. Deliverable 2 of the IMAGINE Project*. Deliverable 4 of the IMAGINE project Project: Improved Methods for the Assessment of the Generic Impact of Noise in the Environment. Document identity: IMA10TR-040423-AEATNL32.

AGMA. (2006). *Transport Statistics Manchester*. Manchester, UK: Association of Greater Manchester Authorities, UK.

Akinwande, M. O., Dikko, H. G. & Samson, A. (2015). Variance Inflation Factor: As a Condition for the Inclusion of Suppressor Variable(s) in Regression Analysis. *Open Journal of Statistics*, 5(7), 754–767. Retrieved from http://www.scirp.org/journal/doi.aspx?DOI=10.4236/ojs.2015.57075

Alves, S., Altreuther, B., Scheuren, J., Kropp, W. & Forssén, J. (2016). *Urban Sound Planning – the SONORUS Project*.

American Planning Association. (2006). *Planning and Urban Design Standards* (E. Sendich, Ed.). New York: John Wiley & Sons.

Andrusz, G. D., Harloe, M. & Szelenyi, I. (Eds.). (1996). *Cities After Socialism: Urban and Regional Change and Conflict in Post-Socialist Societies*. Wiley-Blackwell.

Arana, M., Martín, R. S., Nagore, I. & Pérez, D. (2011). What Precision in the Digital Terrain Model Is Required for Noise Mapping? *Applied Acoustics*, 72(8), 522–526. Retrieved November 4, 2013, from http://linkinghub.elsevier.com/retrieve/pii/S0003682X10001507

Ariza-Villaverde, A. B., Jiménez-Hornero, F. J. & Gutiérrez De Ravé, E. (2014). Influence of Urban Morphology on Total Noise Pollution: Multifractal Description. *The Science of the total environment*, 472, 1–8. Retrieved April 13, 2014, from http://www.sciencedirect.com/science/article/pii/S0048969713012357

ARPAT. (2007). *IMAGINE – WP1 Final Report: Guidelines and Good Practice on Strategic Noise Mapping*. Deliverable 8 of the IMAGINE project: Improved Methods for the Assessment of the Generic Impact of Noise in the Environment. Document identity: IMA01-TR22112006-ARPAT12.

B. Berglund; T. Lindvall. (1995). Community Noise, in: *Archives of the Center for Sensory Research*. Stockholm, Sweden: Jannes Snabbtryck.

Badiu Inc. (2011). Baidu Digital Map Service. Retrieved January 1, 2011, from http://map.baidu.com/

Barboza, D. (2011). China's Cities Piling Up Debt To Fuel Boom. *The New York Times*, A1. Retrieved from http://www.nytimes.com/2011/07/07/business/global/building-binge-by-chinas-cities-threatens-countrys-economic-boom.html?pagewanted=all&_r=0

Barclay, M., Kang, J. & Sharples, S. (2012). Combining Noise Mapping and Ventilation Performance for Non-Domestic Buildings in an Urban Area. *Building and Environment*, 52, 68–76. Retrieved from

http://dx.doi.org/10.1016/j.buildenv.2011.12.015

Beijing Review. (2013). Should Square Dancing Be Stopped in Public? *Beijing Review*. Retrieved from http://www.bjreview.com.cn/print/txt/2013-12/09/content_583072.htm

Bennett, G., King, E. & Curn, J. (2010). Environmental Noise Mapping Using Measurements in Transit. *... Conference on Noise ...*, 1795–1810. Retrieved April 10, 2014, from https://www.isma-isaac.be/past/conf/isma2010/proceedings/papers/isma2010_0682.pdf

Berg, M. van den & Gerretsen, E. (1996). Comparison of Road Traffic Noise Calculation Models. *Journal of Building Acoustics*, 3(1), 13–22.

Bolt, R. H., Lukasik, S. J., Nolle, A. W. & Frost, A. D. (Eds.). (1952). Handbook of Acoustic Noise Control. Vol. I, Physical Acoustics, in: *WADC Technical Report 52-204*, (p. 390). Wright-Patterson Air Force Base, Ohio: Wright Air Development Center.

Bowker, G. E., Baldauf, R., Isakov, V., Khlystov, A. & Petersen, W. (2007). The Effects of Roadside Structures on the Transport and Dispersion of Ultrafine Particles from Highways. *Atmospheric Environment*, 41(37), 8128–8139. Retrieved November 6, 2013, from http://linkinghub.elsevier.com/retrieve/pii/S1352231007005985

Bray, D. (2005). *Social Space and Governance in Urban China: The Danwei System from Origins to Reform*. Stanford: Stanford University Press.

Burian, S. J., Brown, M. J. & Linger, S. P. (2002). Morphological Analyses Using 3D Building Databases. *La-Ur-02-0781*, (October 2002).

Burton, E., Jenks, M. & Williams, K. (2004). *The Compact City: A Sustainable Urban Form?* Taylor & Francis.

Cai, W. (2009). China's First Noise Map Is Surveyed in Beijing - the Impact of Noise Is Visible Now. *Beijing Daily*. Retrieved from http://scitech.people.com.cn/GB/10089929.html

Calderón, C. & Servén, L. (2004). *The Effects of Infrastructure Development on Growth and Income Distribution*.

Calthorpe Associates. (2012). *Design Manual for Low Carbon Development*.

Can, A., Leclercq, L., Lelong, J. & Botteldooren, D. (2010). Traffic Noise Spectrum Analysis: Dynamic Modeling vs. Experimental Observations. *Applied Acoustics*, 71(8), 764–770. Retrieved November 17, 2013, from http://linkinghub.elsevier.com/retrieve/pii/S0003682X10000836

Cheng, V., Steemers, K., Montavon, M. & Compagnon, R. (2006). Urban Form , Density and Solar Potential. *Solar Energy*, (September), 6–8.

CIESIN. (2013). Urban-Rural Population and Land Area Estimates, Version 2. *Center for International Earth Science Information Network (CIESIN), Columbia University*. Retrieved from http://sedac.ciesin.columbia.edu/data/set/lecz-urban-rural-population-land-area-estimates-v2

De Coensel, B., De Muer, T., Yperman, I. & Botteldooren, D. (2005). The Influence of Traffic Flow Dynamics on Urban Soundscapes. *Applied Acoustics*, 66(2), 175–194.

Cohen, J., Cohen, P., West, S. G. & Aiken, L. S. (2003). *Applied Multiple Regression/Correlation Analysis for the Behavioral Sciences*. London: Routledge. Retrieved from http://books.google.com/books?hl=de&lr=&id=fuq94a8C0ioC&pgis=1

Conzen, M. R. G. (1960). *Alnwick, Northumberland: A Study in Town-Plan Analysis - Institute of British Geographers Publication 27*. London: George Philip.

Crow, G. (2009). Urban Village. *International Encyclopedia of Human Geography*, 101–105.

CSTB. (2000). *MITHRA Environmental Noise Prediction Software Overview*.

CSTB. (2007). *IMAGINE – WP1 Specifications for GIS-NOISE Databases*. Deliverable 4 of the IMAGINE project Project: Improved Methods for the Assessment of the

Generic Impact of Noise in the Environment. Document identity: IMA10-TR250506-CSTB05.

DAL. (1987). *Joint Nordic Method: Environmental Noise from Industrial Plants– General Prediction Method*. Danish Acoustical Laboratory.

DataKustik. (2007). Cadna/A Road Noise Calculation Using CRTN.

DataKustik. (2012a). Cadna/A Reference Manual Release 4.3.

DataKustik. (2012b). Introduction to CadnaA V4.3.

Defrance, J. (2009). *Benchmark/Testing of Noise Assessment Methods HARMONOISE/NMPB – A Comparison of Formulations Used for Ground and Diffraction Effects*. Brussels. Retrieved from https://circabc.europa.eu/webdav/CircaBC/env/noisedir/Library/Public/cnossos-eu/roadpropa_17-18nov2009/defrance_formulations/Report on comparison of formulations used for ground and diffraction effects.pdf

EC. (1996). The Green Paper on Future Noise Policy (COM(96) 540).

EC. (2002). Directive 2002/49/EC of the European Parliament and the Council of 25 June 2002 Relating to the Assessment and Management of Environmental Noise. *Official Journal of the European Communities*, 189, 12–25.

ECAC. (1997). *Report on Standard Method of Computing Noise Contours around Civil Airports*. European Civil Aviation Conference,.

EDINA Digimap. (2008). Ordnance Survey Collection. Retrieved January 1, 2008, from http://digimap.edina.ac.uk/

Edmonds, R. L. (1994). *Patterns of China's Lost Harmony: A Survey of the Country's Environmental Degradation and Protection*. London; New York: Routledge.

Edussuriya, P., Chan, A. & Ye, A. (2011). Urban Morphology and Air Quality in Dense Residential Environments in Hong Kong. Part I: District-Level Analysis.

Atmospheric Environment, 45(27), 4789–4803. Retrieved July 16, 2014, from http://www.sciencedirect.com/science/article/pii/S135223100900661X

EEA. (2010). *Good Practice Guide on Noise Exposure and Potential Health Effects*. Copenhagen: EEA. Retrieved from https://www.google.co.uk/url?sa=t&rct=j&q=&esrc=s&source=web&cd=1&ved=0ahUKEwjFssGn4IfOAhVHB8AKHRNTCTMQFggeMAA&url=http%3A%2F%2Fwww.eea.europa.eu%2Fpublications%2Fgood-practice-guide-on-noise%2Fdownload&usg=AFQjCNH71S1crMyyRkeGhC1vPZC8PiUbJA&sig2=_OviNgnI

EEA. (2014). *Noise in Europe 2014*. European Environmental Agency. Retrieved from https://www.eea.europa.eu/publications/noise-in-europe-2014/file

EPA. (2011). *Guidance Note for Strategic Noise Mapping for the Environmental Noise Regulations 2006*. Wexford: Environmental Protection Agency, Ireland.

ETC/TE EEA. (2005). *State of the Art of Noise Mapping in Europe*. European Topic Centre Terrestrial Environment (ETC/TE), Europe Environment Agency (EEA).

Fang, C. & Yu, D. (2016). *China's New Urbanization: Developmental Paths, Blueprints and Patterns*.

FHWA. (2004). *TNM VERSION 2.5 ADDENDUM to Validation of FHWA's Traffic Noise Model (TNM): Phase 1*. Cambridge, MA. Retrieved from http://www.fhwa.dot.gov/environment/noise/traffic_noise_model/tnm_v25/

Field, A. (2005). *Discovering Statistics Using SPSS*. Retrieved from http://www.amazon.com/Discovering-Statistics-Introducing-Statistical-Methods/dp/0761944524

Forshaw, J. H. & Abercrombie, P. (1943). *County of London Plan*. London: MacMillan and Co. Ltd.

Friedmann, J. (1967). The Institutional Context, in: B. M. Gross (Ed.), *Action Under Planning. The Guidance of Economic Development*. New York.: McGraw Hill.

Garg, N. & Maji, S. (2014). A Critical Review of Principal Traffic Noise Models: Strategies and Implications. *Environmental Impact Assessment Review*, 46, 68–81. Retrieved July 20, 2014, from http://linkinghub.elsevier.com/retrieve/pii/S0195925514000195

Gaubatz, P. (1999). China's Urban Transformation: Patterns and Processes of Morphological Change in Beijing, Shanghai and Guangzhou. *Urban Studies*, 36(9), 1495–1521.

Gaubatz, P. (2008). New Public Space in Urban China. *China Perspectives*, (4), 72–83.

Gaubatz, P. (2014). Understanding Contexts Chinese Urban Form : For Interpreting and Change Continuity. , 24(4), 251–270.

Ge, J. (2002). Shanghai: Froma Common County Seat to an International Megalopolis, in: Minoru, S. (Ed.), *Urban Morphology and the History of Civilization in East Asia*. International Research Center for Japanese Studies.

Germany FMoT. (1990). *RLS-90: Guidelines for Noise Protection at Roads*. Bonn, Germany, Germany: Department of Road Construction, Federal Ministry of Transportation. Retrieved from http://www.staedtebauliche-laermfibel.de/?p=100&p2=3.1.2.4

Google Inc. Google Maps Service. Retrieved January 1, 2008, from http://www.google.co.uk/maps

Gu, K. (2001). Urban Morphology of China in the Post-Socialist Age: Towards a Framework for Analysis. *Urban Design International*, 6(3/4), 125–142. Retrieved from http://www.palgrave-journals.com/doifinder/10.1057/palgrave/udi/9000051

Guedes, I. C. M., Bertoli, S. R. & Zannin, P. H. T. (2011). Influence of Urban Shapes on Environmental Noise: A Case Study in Aracaju-Brazil. *The Science of the total environment*, 412–413, 66–76. Retrieved November 4, 2013, from http://www.ncbi.nlm.nih.gov/pubmed/22078329

H.G. Jonasson; S. Storeheier. (2001). *Nord 2000: New Nordic Prediction Method for*

Road Traffic Noise.

Hachem, C., Athienitis, A. & Fazio, P. (2011). Parametric Investigation of Geometric Form Effects on Solar Potential of Housing Units. *Solar Energy*, 85(9), 1864–1877. Retrieved August 30, 2011, from http://linkinghub.elsevier.com/retrieve/pii/S0038092X11001472

Hao, Y. & Kang, J. (2014). Influence of Mesoscale Urban Morphology on the Spatial Noise Attenuation of Flyover Aircrafts. *Applied Acoustics*, 84, 73–82. Retrieved July 24, 2014, from http://linkinghub.elsevier.com/retrieve/pii/S0003682X1300282X

Hao, Y., Kang, J., Krijnders, D. & Wörtche, H. (2015). On the Relationship between Traffic Noise Resistance and Urban Morphology in Low-Density Residential Areas. *Acta Acustica united with Acustica*, 101(3), 510–519.

Hao, Y., Kang, J. & Krijnders, J. D. (2015). Integrated Effects of Urban Morphology on Birdsong Loudness and Visibility of Green Areas. *Landscape and Urban Planning*, 137(May), 149–162.

Haupt, P., Pont, M. B. & Moudon, A. V. (2005). *Spacemate; the Spatial Logic of Urban Density*. Delft: Delft University Press.

Heiberger, R. M. & Holland, B. (2004). Statistical Analysis and Data Display: An Intermediate Course with Examples in S-Plus, R, and SAS. , 730. Retrieved from http://www.springer.com/us/book/9781441923202

Hendy, D. (2013). *Noise: A Human History of Sound and Listening*. London: Profile Books.

Hepworth, P. (2006). Accuracy Implication of Computerized Noise Predictions for Environmental Noise Mapping, in: *Proceedings of the 35th International Congress on Noise Control Engineering*. Hawaii: nstitute of Noise Control Engineering of the USA.

Hepworth, P., Trow, J. & Hii, V. (2006). User Controlled Settings in Noise Mapping

Software - The Effects on Calculation Speed and Accuracy, in: *Euronoise 2006*. Tempere.

Heutschi, K. (2004). Son Road: New Swiss Road Traffic Noise Model. *Acta Acust United Acust*, 90, 548–554.

Huang, J., Lu, X. X. & Sellers, J. M. (2007). A Global Comparative Analysis of Urban Form: Applying Spatial Metrics and Remote Sensing. *Landscape and Urban Planning*, 82(4), 184–197.

Huang, Y. (2006). Urban Development in Contemporary China, in: *China's Geography: Globalization and the Dynamics of Political, Economic and Social Change*, (pp. 233–262). Lanham: Rowman & Littlefield Publishers.

IBM Corp. (2011). *IBM SPSS Statistics 22 Brief Guide*. Chicago: IBM Corp. Retrieved from http://www-01.ibm.com/support/docview.wss?uid=swg27038407#en

Ireland MTE. (2006). *Environmental Noise Regulation 2006*. Ireland. Retrieved from http://www.housing.gov.ie/sites/default/files/migrated-files/en/Legislation/Environment/Miscellaneous/FileDownLoad,1318,en.pdf

ISO. (1996). ISO 9613-2 Acoustics — Attenuation of Sound during Propagation Outdoors — Part 2 : General Method of Calculation.

Isukapalli, S. S. & Georgopoulos, P. G. (2001). *Computational Methods for Sensitivity and Uncertainty Analysis for Environmental and Biological Models*. Piscataway. Retrieved July 12, 2014, from http://www.ccl.rutgers.edu/ccl-files/reports/EPA/edmas_v3_epa.pdf

J. D. McCallum. (1976). Comparative Study in Planning: Explanations of the 'Political Culture' of Planning inBritain and the United States. *Department of Town and Regional Planning*.

J. Kang. (2006). *Urban Sound Environment*. London: Taylor & Francis incorporating Spon.

Jenkins, E. (2012). *To Scale: One Hundred Urban Plans*. Routledge.

Jesshim, K. (2003). Multicollinearity in Regression Models. *Multicollinearity Doc*, 1–8.

Jin, W. (1993). The Historical Development of Chinese Urban Morphology. *Planning Perspectives*, 8(1), 20–52. Retrieved January 5, 2012, from http://www.tandfonline.com/doi/abs/10.1080/02665439308725762

Jun, W. (2013). *Ancient Chinese Encyclopedia of Technology–Translation and Annotation of the Kaogong Ji (the Artificers' Record)*. Oxon: Routledge.

Kang, J. (2000). Sound Propagation in Street Canyons: Comparison between Diffusely and Geometrically Reflecting Boundaries. *The Journal of the Acoustical Society of America*, 107(3), 1394–404. Retrieved from http://www.ncbi.nlm.nih.gov/pubmed/10738794

Kang, J. (2001). Sound Propagation in Interconnected Urban Streets: A Parametric Study. *Environment and Planning B: Planning and Design*, 28(2), 281–294. Retrieved June 22, 2011, from http://www.envplan.com/abstract.cgi?id=b2680

Kang, J. (2002). Numerical Modelling of the Sound Fields in Urban Streets With Diffusely Reflecting Boundaries. *Journal of Sound and Vibration*, 258(5), 793–813. Retrieved from http://linkinghub.elsevier.com/retrieve/pii/S0022460X02951503

Kang, J. (2005). Numerical Modeling of the Sound Fields in Urban Squares. *The Journal of the Acoustical Society of America*, 117(6), 3695. Retrieved January 5, 2012, from http://link.aip.org/link/JASMAN/v117/i6/p3695/s1&Agg=doi

Kang, J. (2006). *Urban Sound Environment*. Oxon: Taylor & Francis.

Kang, J. & Huang, J. (2005). Noise-Mapping : Accuracy and Strategic Application, in: *Internoise 2005 - Environmental Noise Contriol*. Rio de Janeiro.

Kenworthy, J. & Hu, G. (2002). Transport and Urban Form in Chinese Cities. *disP - The Planning Review*, 38(February 2015), 4–14.

Kephalopoulos, S., Paviotti, M. & Anfosso-Lédée, F. (2012). *Common Noise Assessment Methods in Europe (CNOSSOS-EU)*. Luxembourg: Publications Office of the European Union. Retrieved November 24, 2013, from http://scholar.google.com/scholar?hl=en&btnG=Search&q=intitle:Common+noise+assessment+methods+in+Europe+(CNOSSOS-EU)+EUR+25379+EN#0

Kephalopoulos, S., Paviotti, M., Anfosso-Lédée, F., Van Maercke, D., Shilton, S. & Jones, N. (2014). Advances in the Development of Common Noise Assessment Methods in Europe: The CNOSSOS-EU Framework for Strategic Environmental Noise Mapping. *The Science of the total environment*, 482–483, 400–10. Retrieved July 12, 2014, from http://www.ncbi.nlm.nih.gov/pubmed/24582156

Kephalopoulos, S., Paviotti, M. & Gergely, B. (2008). Differences among European Noise Mapping Methods. *Journal of the Acoustical …*, 765–770. Retrieved June 24, 2014, from http://www.conforg.fr/acoustics2008/cdrom/data/articles/003190.pdf

Khakee, A. (1996). *Urban Planning in China and Sweden in a Comparative Perspective*. Oxford: Pergamon Press. Retrieved from http://linkinghub.elsevier.com/retrieve/pii/0305900696000049

Kihlman, T. & Berillon, J. (1999). Soundscape in Cities, Limits to the Noise Limits? *The Journal of the Acoustical Society of America*, 105(2), 1070.

Kihlman, T. & Kropp, W. (2001). City Traffic Noise - A Local or Global Problem? *Noise Control Engineering*, 49(4), 165–169.

Kim, B. (2016). Hierarchical Linear Regression. *Research Data Services + Sciences*. Retrieved September 11, 2017, from http://data.library.virginia.edu/hierarchical-linear-regression/

King, E. A., Murphy, E. & Rice, H. J. (2011). Implementation of the EU Environmental Noise Directive: Lessons from the First Phase of Strategic Noise Mapping and Action Planning in Ireland. *Journal of environmental management*, 92(3), 756–64. Retrieved November 4, 2013, from

http://www.ncbi.nlm.nih.gov/pubmed/21084147

King, E. a. & Rice, H. J. (2009). The Development of a Practical Framework for Strategic Noise Mapping. *Applied Acoustics*, 70(8), 1116–1127. Retrieved June 8, 2014, from http://linkinghub.elsevier.com/retrieve/pii/S0003682X09000206

Konvitz, J. W. (1985). *The Urban Millennium : The City-Building Process from the Early Middle Ages to the Present*. Carbondale: Southern Illinois University Press.

Kostof, S. & Tobias, R. (2004). *The City Shaped: Urban Patterns and Meanings Through History*. Boston: Bullfinch Press.

Kragh, J., Jonasson, H., Plovsing, B. & Sarinen, A. (2006). *User ' S Guide Nord2000 Road*. Hørsholm.

Lam, K.-C. & Ma, W.-C. (2012). Road Traffic Noise Exposure in Residential Complexes Built at Different Times between 1950 and 2000 in Hong Kong. *Applied Acoustics*, 73(11), 1112–1120. Retrieved November 6, 2013, from http://linkinghub.elsevier.com/retrieve/pii/S0003682X12001053

Leder, S., Pereira, F., Claro, A. & Ramos, M. (2006). Impact of Urban Design on Daylight Availability. *The 23rd conference on …*. Retrieved January 22, 2014, from http://www.unige.ch/cuepe/html/plea2006/Vol1/PLEA2006_PAPER209.pdf

Letzel, M. O., Krane, M. & Raasch, S. (2008). High Resolution Urban Large-Eddy Simulation Studies from Street Canyon to Neighbourhood Scale. *Atmospheric Environment*, 42(38), 8770–8784. Retrieved September 1, 2011, from http://linkinghub.elsevier.com/retrieve/pii/S1352231008007036

Leventhall, G. (2003). *A Review of Published Research on Low Frequency Noise and Its Effects*.

Li, D. (2001). *Principles of Urban Planning (3rd Ed.)*. Beijing: China Architecture and Building Press.

Li, H. (2013). The Implications of the Planning of Beijing ' S Imperial City for

Sustainable Community Development The Implications of the Planning of Beijing ' S Imperial City for Sustainable Community Development The Implications of the Planning of Beijing ' S Imperia.

Li, H., Yu, W., Lu, J., Zeng, L., Li, N. & Zhao, Y. (2008). Investigation of Road Traffic Noise and Annoyance in Beijing : A Cross-Sectional Study of 4 Th Ring Road.

Li, L. H., Lin, J., Li, X. & Wu, F. (2014). Redevelopment of Urban Village in China – A Step towards an Effective Urban Policy? A Case Study of Liede Village in Guangzhou. *Habitat International*, 43, 299–308. Retrieved from http://www.sciencedirect.com/science/article/pii/S0197397514000447

Li, X. & Yeh, A. G.-O. a. G.-O. (2004). Analyzing Spatial Restructuring of Land Use Patterns in a Fast Growing Region Using Remote Sensing and GIS. *Landscape and Urban Planning*, 69(4), 335–354.

Licitra, G. (2013). *Noise Mappin in the EU - Models and Procedures* (G. Licitra, Ed.). Boca Raton: CRC Press, Taylor & Francis Group.

Licitra, G. & Memoli, G. (2008). Limits and Advantages of Good Practice Guide to Noise Mapping. *Acoustics 08 Paris*, 771–776. Retrieved from http://webistem.com/acoustics2008/acoustics2008/cd1/data/articles/002677.pdf

M. Paviotti & Kephalopoulos, S. (2008). *Assessment of the Equivalency of the National Noise Mapping Methods against the Interim Methods*. Joint Research Centre of the European Commission (JRC).

M. Zhou. (2007). Traffic Noise Mapping of Guangzhou Inner Ring Road. *Journal of South China University of Technology (Nature Science Edition)*, Vol. 35 Su.

Mank, J. (2000). *Vergelijking Van Drie Rekenprogramma's Voor Wegverkeerslawaai*.

Manvell, D. & Hartog van Banda, E. (2011). Good Practice in the Use of Noise Mapping Software. *Applied Acoustics*, 72(8), 527–533. Retrieved November 4, 2013, from http://linkinghub.elsevier.com/retrieve/pii/S0003682X10002173

Margaritis, E. & Kang, J. (2016). Relationship between Urban Green Spaces and Other Features of Urban Morphology with Traffic Noise Distribution. *Urban Forestry & Urban Greening*, 15, 174–185. Retrieved from http://dx.doi.org/10.1016/j.ufug.2015.12.009

Marquez, L. O. & Smith, N. C. (1999). A Framework for Linking Urban Form and Air Quality. *Environmental Modelling & Software*, 14(6), 541–548. Retrieved January 29, 2018, from https://www.sciencedirect.com/science/article/pii/S1364815299000183

Marry, S. & Baulac, M. (2010). Sound Perception Parameters in Urban Public Spaces, in: *Internoise 2010 - Noise and Sustainability*. Lisbon: Internoise 2010 - Noise and Sustainability.

Marshall, S. (2005). *Streets and Patterns*. Abingdon: Spon Press.

MEP China. (2008). *GB 3096-2008 Environmental Quality Standards for Noise*. Beijing, China.

MEP China. (2009). *HJ 2.4-2009 Technical Guidelines for Noise Impact Assessment*. China Ministry of Environment Protection.

MEP China. (2011). *China Environmental Noise Prevention and Control Annual Report 2011*. Beijing.

MEP China. (2015). *China Environmental Noise Prevention and Control Annual Report 2015*. Beijing: Ministry of Environmental Protection of the People's Republic of China.

MEP China. (2016). *China Environmental Noise Prevention and Control Annual Report 2016*. Ministry of Environmental Protection of the People's Republic of China.

Moudon, A. V. (1997). Urban Morphology as an Emerging Interdisciplinary Field. *Urban Morphology*, 3–10.

Mozas, J. & Per, A. F. (2006). *Density - New Collective Housing (in Spanish)*. Vitoria-

Gasteiz: a+t ediciones.

Murphy, E. A. & King, E. (2010). Strategic Environmental Noise Mapping: Methodological Issues Concerning the Implementation of the EU Environmental Noise Directive and Their Policy Implications. *Environment international*, 36(3), 290–8. Retrieved November 4, 2013, from http://www.sciencedirect.com/science/article/pii/S0160412009002360

Murphy, E. & King, E. A. (2014). *Environmental Noise Pollution: Noise Mapping, Public Health, and Policy*. Burlington: Elsevier. Retrieved August 1, 2014, from http://books.google.com/books?hl=en&lr=&id=_bPrAgAAQBAJ&oi=fnd&pg=PP1&dq=Environmental+Noise+Pollution_+Noise+Mapping,+Public+Health,+and+Policy&ots=0sP3l3cpSz&sig=akBnGJjGxxal6pe27xccSPlY8_o

Myers, R. H. (2000). *Classical and Modern Regression with Applications*. Duxbury: Pacific Grove.

NBS China. (2001). *Urban Statistical Yearbook of China 2001*. Beijing: China Statistics Press. Retrieved from https://wenku.baidu.com/view/f9458588d5bbfd0a795673cb.html?pn=51

NBS China. (2006). *China Statistical Year Book 2006*. Beijing: China Statistics Press. Retrieved from http://www.stats.gov.cn/tjsj/ndsj/2006/indexch.htm

Newton, P. W. (1997). Re-Shaping Cities for a More Sustainable Future : Exploring the Link between Urban Form, Air Quality, Energy and Greenhouse Gas Emissions.

Nijland, H. a. & Van Wee, G. P. (2005). Traffic Noise in Europe: A Comparison of Calculation Methods, Noise Indices and Noise Standards for Road and Railroad Traffic in Europe. *Transport Reviews*, 25(5), 591–612. Retrieved June 29, 2014, from http://www.tandfonline.com/doi/abs/10.1080/01441640500115850

O'Malley, V., King, E., Kenny, L. & Dilworth, C. (2009). Assessing Methodologies for Calculating Road Traffic Noise Levels in Ireland – Converting CRTN Indicators to the EU Indicators (Lden, Lnight). *Applied Acoustics*, 70(2), 284–296. Retrieved

November 24, 2013, from http://linkinghub.elsevier.com/retrieve/pii/S0003682X08000807

Oliveira, V. (2016). *Urban Morphology: An Introduction to the Study of the Physical Form of Cities*. AG Switzerland: Springer Nature.

Oliver-Solà, J., Josa, A., Arena, A. P., Gabarrell, X. & Rieradevall, J. (2011). The GWP-Chart: An Environmental Tool for Guiding Urban Planning Processes. Application to Concrete Sidewalks. *Cities*, 28(3), 245–250.

ONS UK. (2001). 2001 Census: Aggregate Data (England and Wales) [Computer File]. Retrieved from http://casweb.ukdataservice.ac.uk

Petersen, R. (2004). Sustainable Transport: A Sourcebook for Policy-Makers in Developing Cities Module 2a: Land Use Planning and Urban Transport, in: Für, D. G. (Ed.), *Sustainable Transport: A Sourcebook for Policy-Makers in Developing Cities*, (p. 41). Roßdorf, Germany: TZ Verlagsgesellschaft mbH. Retrieved from http://www.sutp.org/files/contents/documents/resources/A_Sourcebook/SB2_Land-Use-Planning-and-Demand-Management/GIZ_SUTP_SB2a-Land-use-Planning-and-Urban-Transport_EN.pdf

Pointer, G. (2005). The UK's Major Urban Areas, in: *Focus on People and Migration: 2005*, (pp. 45–60). London: UK Data Service Census Support, Office for National Statistics UK. Retrieved from https://link.springer.com/chapter/10.1007/978-1-349-75096-2_3

Pont, M. B. & Haupt, P. (2005). The Spacemate: Density and the Typomorphology of the Urban Fabric. *Urbanism Laboratory for Cities and Regions Progress of Research Issues in Urbanism 2007*, 4(4), 55–68. Retrieved from http://www.arkitekturforskning.net/tidsskrift/2005/2005_4/Berghauser_haupt.pdf

Pont, M. B. & Haupt, P. (2009). *Space, Density and Urban Form*. Delft: Delft University of Technology. Retrieved from http://repository.tudelft.nl/view/ir/uuid:0e8cdd4d-80d0-4c4c-97dc-dbb9e5eee7c2/

Probst, W. (1998). Calculation of Noise Levels in an Environment with Highly Reflecting Objects and Surfaces, in: *European Conference on Noise Control Engineering (Euronoise 1998)*, (pp. 1–7). Munich.

Probst, W. (2010a). About the Calculation of Road Noise – a Comparison of European Methods, in: *DAGA 2010*.

Probst, W. (2010b). Accuracy and Precision in Traffic Noise Prediction, in: *Internoise 2010 - Noise and Sustainability*, (pp. 1–6). Lisbon. Retrieved November 24, 2013, from http://www.datakustik.com/fileadmin/user_upload/PDF/Papers/EAA_Euroregio_2010_TrafficNoisePrediction.pdf

Probst, W. (2014). Calculation of Sound Propagation with Highly Reflective Environments. *INternoise 2014 - Improving the World through Noise Control*. Retrieved April 25, 2015, from http://www.acoustics.asn.au/conference_proceedings/INTERNOISE2014/papers/p543.pdf

Rode, P., Floater, G., Thomopoulos, N., Docherty, J., Schwinger, P., Mahendra, A., Fang, W., Cities, L. S. E., Friedel, B., Gomes, A., Heeckt, C. & Slavcheva, R. (2014). *Accessibility in Cities: Transport and Urban Form*. Retrieved from http://files.lsecities.net/files/2014/11/LSE-Cities-2014-Transport-and-Urban-Form-NCE-Cities-Paper-03.pdf

Rodríguez-Álvarez, J. (2016). Urban Energy Index for Buildings (UEIB): A New Method to Evaluate the Effect of Urban Form on Buildings' Energy Demand. *Landscape and Urban Planning*, 148, 170–187. Retrieved from http://dx.doi.org/10.1016/j.landurbplan.2016.01.001

Salomons, E. M. & Pont, M. B. (2012). Urban Traffic Noise and the Relation to Urban Density, Form, and Traffic Elasticity. *Landscape and Urban Planning*, 108(1), 2–16. Retrieved November 4, 2013, from http://linkinghub.elsevier.com/retrieve/pii/S0169204612002228

Salomons, E., Van Maercke, D., Defrance, J. & De Roo, F. (2011). The Harmonoise Sound Propagation Model. *Acta Acustica united with Acustica*, 97(1), 62–74.

Sarralde, J. J., Quinn, D. J., Wiesmann, D. & Steemers, K. (2014). Solar Energy and Urban Morphology: Scenarios for Increasing the Renewable Energy Potential of Neighbourhoods in London. *Renewable Energy*. Retrieved August 19, 2014, from http://www.sciencedirect.com/science/article/pii/S0960148114003681

Schoenauer, N. (1981). *6000 Years of Housing*. New York: WW Norton and Company.

Schulte, N., Tan, S. & Venkatram, A. (2015). The Ratio of Effective Building Height to Street Width Governs Dispersion of Local Vehicle Emissions. *Atmospheric Environment*. Retrieved April 17, 2015, from http://www.sciencedirect.com/science/article/pii/S135223101500285X

Schwarz, N. (2010). Urban Form Revisited-Selecting Indicators for Characterising European Cities. *Landscape and Urban Planning*, 96(1), 29–47. Retrieved from http://dx.doi.org/10.1016/j.landurbplan.2010.01.007

Sétra. (2009). Road Noise Prediction - Part 2: Noise Propagation Computation Method Including Meteorological Effects (NMPB 2008). *Public Works*, (june), 1–136.

Shelton, B. (1999). *Learning from the Japanese City, West Meets East in Urban Design*.

Silva, L. T., Oliveira, M. & Silva, J. F. (2014). Urban Form Indicators as Proxy on the Noise Exposure of Buildings. *Applied Acoustics*, 76, 366–376. Retrieved November 4, 2013, from http://linkinghub.elsevier.com/retrieve/pii/S0003682X13001990

Song, Y. & Zenou, Y. (2012). Urban Villages and Housing Values in China. *Regional Science and Urban Economics*, 42(3), 495–505. Retrieved from http://dx.doi.org/10.1016/j.regsciurbeco.2011.06.003

Souza, L. C. L. De & Giunta, M. B. (2011). Urban Indices as Environmental Noise Indicators. *Computers, Environment and Urban Systems*, 35(5), 421–430. Retrieved November 4, 2013, from

http://linkinghub.elsevier.com/retrieve/pii/S0198971511000603

State Council of China. (2006). *China National Environmental Protection Plan in the Eleventh Five-Years (2006-2010）*.

State Council of China. (2011). *China National Environmental Protection Plan in the Twelfth Five-Years（2011-2015）*. Beijing.

Steele, C. (2001). A Critical Review of Some Traffic Noise Prediction Models. *Applied Acoustics*, 62(3), 271–287.

Steinhardt, N. S. (1990). *Chinese Imperial City Planning*. Hawaii: University of Hawai'i Press.

Svensson, A. (2004). Arterial Streets towards Sustainability. *Proceedings of the European Transport Conference (Etc) 2004 Held 4-6 October 2004, Strasbourg, France*, (January), 14p.

Tang, K. (2010). Urban Planning System in China - Basic Facts and Reform Progress, in: *The International Conference on China's Planning System Reform*. Retrieved from http://www.sciencedirect.com/science/article/pii/B9780080970868740530

Tang, U. W. & Wang, Z. S. (2007). Influences of Urban Forms on Traffic-Induced Noise and Air Pollution: Results from a Modelling System. *Environmental Modelling & Software*, 22(12), 1750–1764. Retrieved November 4, 2013, from http://linkinghub.elsevier.com/retrieve/pii/S136481520700028X

Tang, W.-S. (2000). Chinese Urban Planning at Fifty: An Assessment of the Planning Theory Literature. *Journal of Planning Literature*, 14(347). Retrieved from http://jpl.sagepub.com/cgi/content/abstract/14/3/347

Tencent Inc. (2011). Tencent Digital Map Sercice. Retrieved January 1, 2011, from http://map.qq.com/

The MathWorks, I. (2009). Matlab7 Getting Started Guide. Natick; 2009.

Thorsson, P. & Ogren, M. (2005). Macroscopic Modeling of Urban Traffic Noise – Influence of Absorption and Vehicle Flow Distribution. *Applied Acoustics*, 66(2), 195–209. Retrieved January 5, 2012, from http://linkinghub.elsevier.com/retrieve/pii/S0003682X04001203

Tobergte, D. R. & Curtis, S. (2013). Decoding the Urban Grid: Or Why Cities Are Neither Trees nor Perfect Grids Lucas. *Journal of Chemical Information and Modeling*, 53(9), 1689–1699.

UCD Denver. (2016). Hierarchical Multiple Regression in SPSS.

UK Defra. (1999). *Noise Cimate Assessment: Review of National and European Practices*. Lodon: UK Department for Environment, Food and Rural Affairs, (Defra).

UK Defra. (2005). *Research Project NANR 93: WG-AEN's Good Practice Guide and the Implications for Acoustic Accuracy - Final Report: Data Accuracy Guidelines for CRTN*. The Department for Environment, Food and Rural Affairs (DEFRA).

UK DfT. (1988). *Calculation of Road Traffic Noise (CRTN)*. UK: Department of Transport Welsh Office, HMSO.

UK DfT. (1995). Calculation of Rail Noise (CRN). (U. K. D. for Transport, Ed.).

UN. (2013). *2012 UN Demographic Yearbook*. New York. Retrieved from http://unstats.un.org/UNSD/Demographic/products/dyb/dybsets/2012.pdf

UN. (2015). United Nations Population Division's World Urbanization Prospects, the 2015 Revision. Retrieved from https://esa.un.org/unpd/wup/

United Nations. (2010). *2008 Demographic Yearbook*. New York. Retrieved from http://unstats.un.org/UNSD/Demographic/products/dyb/dybsets/2008 DYB.pdf

Wang, B. & Kang, J. (2011). Effects of Urban Morphology on the Traffic Noise Distribution through Noise Mapping: A Comparative Study between UK and China. *Applied Acoustics*, 72(8), 556–568. Retrieved June 22, 2011, from

http://linkinghub.elsevier.com/retrieve/pii/S0003682X11000247

Wang, B., Kang, J. & Zhou, J. (2007). Effects of Urban Morphological Characteristics on the Noise Distribution: A Comparison between the UK and China, in: *Proceedings of the 19th international congress of acoustics*. Madrid: Sociedad Espanola de Acustica. Retrieved from http://www.sea-acustica.es/WEB_ICA_07/fchrs/papers/env-08-005.pdf

Wang, B., Kang, J. & Zhou, J. (2008). Comparison of Traffic Noise Distribution between High and Low Density Cities, in: *37th international Congress and Exposition on Noise Control Engineering*.

Wang, J. (2010). *The Framework of National Environmental Protection Plan in 12th Five Years*. Chinese Academy for Environmental Planning. Retrieved from http://wenku.baidu.com/view/94b94e3143323968011c9255.html#%23%23

Wang, R. W. (2010). Social Mix in Central Post-Reform Shanghai. , (November).

Wang, Y., Teter, J. & Sperling, D. (2011). China's Soaring Vehicle Population: Even Greater than Forecasted? *Energy Policy*, 39(6), 3296–3306.

WCTPDI. (2006). *Wuhan Transportation Development Report 2006*. Wuhan: Wuhan Institute of Integrated Transportation Planning and Design.

WCTPDI. (2011). *Small Sample Traffic Flow Investigation of Wuhan 2011*. Wuhan: Wuhan Institute of Integrated Transportation Planning and Design.

Wen, G. (1991). *The Urban Traffic and Road System Planning*. Beijing: Tsinghua University Press.

WG-AEN. (2006). *Position Paper Final Draft – Good Practice Guide for Strategic Noise Mapping and the Production of Associated Data on Noise Exposure – Version 2*. Brussels. Retrieved from http://sicaweb.cedex.es/docs/documentacion/Good-Practice-Guide-for-Strategic-Noise-Mapping.pdf

WG-AEN. (2007). *Position Paper – Good Practice Guide for Strategic Noise Mapping and the Production of Associated Data on Noise Exposure – Version 2*. European Commission Working Group Assessment of Exposure to Noise (WG-AEN). Retrieved from https://www.lfu.bayern.de/laerm/eg_umgebungslaermrichtlinie/doc/good_practice_guide_2007.pdf

WHO. (2009). *Night Noise Guidelines for Europe*. Copenhagen: WHO Regional Office for Europe. Retrieved November 24, 2013, from http://books.google.com/books?hl=en&lr=&id=aHKhgXwJdXYC&oi=fnd&pg=PR7&dq=Night+Nosie+Guildlines+for+Europe&ots=hTlIx9RY6g&sig=MssU1JVE3n94rUEtZPjQdaVIf6Y

Willmott, C. J. & Matsuura, K. (2006). On the Use of Dimensioned Measures of Error to Evaluate the Performance of Spatial Interpolators. *International Journal of Geographical Information Science*, 20(1), 89–102. Retrieved from http://www.tandfonline.com/doi/abs/10.1080/13658810500286976

Wolde, T. (2002). The EU Noise Policy and Its Research Needs. *Revista de Acustica*, 33, 15–20.

Woltman, H., Feldstain, A., Mackay, J. C. & Rocchi, M. (2012). An Introduction to Hierarchical Linear Modeling. *Tutorials in Quantitative Methods for Psychology*, 8(1), 52–69.

World Bank. (1996). *Sustainable Transport: Priorities for Reform*. Washington, DC: World Bank.

World Bank. (2017). World Development Indicators. *Data bank*. Retrieved June 15, 2017, from http://databank.worldbank.org/data/reports.aspx?source=world-development-indicators

Wu, Z. & Li, D. (2011). *Principles of Urban Planning (4th Ed.)*. Beijing: China Architecture and Building Press.

Wuhan Environmental Protection Bureau. (2011). *Wuhan Evironmental Codition Annual Report*. Wuhan. Retrieved from http://www.whemc.cn/news/2013219/n44061452.html

Wuhan Statistics Bureau. (2005). *Wuhan Statistical Yearbook 2005* (S. Jianping, Ed.). Beijing: China Statistics Press.

Wuhan Statistics Bureau. (2006). *Wuhan Statistical Yearbook 2006* (S. Jianping, Ed.). Beijing: China Statistics Press.

Wuhan Statistics Bureau. (2011). *Wuhan Statistical Yearbook 2011* (Y. Chen, Ed.). Beijing: China Statistics Press. Retrieved from http://www.whtj.gov.cn/tjnj/tjnj2011.pdf

Wuhan Statistics Bureau. (2014). *Wuhan Statistical Yearbook 2014* (Y. Chen, Ed.). Beijing: China Statistics Press. Retrieved from http://www.whtj.gov.cn/Attachment/201412/201412291427132395.pdf

Xie, H. & Kang, J. (2009). Relationships between Environmental Noise and Social-Economic Factors: Case Studies Based on NHS Hospitals in Greater London. *Renewable Energy*, 34(9), 2044–2053. Retrieved from http://dx.doi.org/10.1016/j.renene.2009.02.012

Xie, H. & Kang, J. (2010). On the Relationships between Environmental Noise and Socio-Economic Factors in Greater London. *Acta Acustica united with Acustica*, 96(3), 472–481.

Xie, H., Li, H. & Kang, J. (2014). The Characteristics and Control Strategies of Aircraft Noise in China. *Applied Acoustics*, 84, 47–57.

Xunchu, X. & Huang, J. (2007). *Urban Roads and Transporation Planning Part II*. Beijing: China Architecture and Building Press.

Yamamoto, K. (2010). Road Traffic Noise Prediction Model 'ASJ RTN-Model 2008': Report of the Research Committee on Road Traffic Noise. *Acoustical Science and Technology*, 31(1), 2–55.

Yang, H. S. (2013). Outdoor Noise Control by Natural / Sustainable Materials in Urban Areas. , (September).

Yuan, C., Ng, E. & Norford, L. K. (2014). Improving Air Quality in High-Density Cities by Understanding the Relationship between Air Pollutant Dispersion and Urban Morphologies. *Building and Environment*, 71(2), 245–258. Retrieved April 9, 2014, from http://linkinghub.elsevier.com/retrieve/pii/S0360132313002990

Zhang, C. & Wang, L. (2014). Research on the Correlation of Transportation and Economic Development in Wuhan. *Applied Mechanics and Materials*, 745–749.

Zhang, M., Kang, J. & Jiao, F. (2012). A Social Survey on the Noise Impact in Open-Plan Working Environments in China. *Science of the Total Environment*, 438, 517–526. Retrieved from http://dx.doi.org/10.1016/j.scitotenv.2012.08.082

Zhao, Y. J. (2002). From Plan to Market: Transformation in the Microscale Roads and Land Use Pattern. *City Planning Review (in Chinese)*, 26, 24–30.

Zhou, M. (2007). Traffic Noise Mapping of Guangzhou Inner Ring Road. *Journal of South China University of Technology (Natural Science Edition)*, 35. Retrieved January 5, 2012, from http://en.cnki.com.cn/Article_en/CJFDTOTAL-HNLG2007S1042.htm

Zhou, Z., Kang, J., Zou, Z. & Wang, H. (2016). Analysis of Traffic Noise Distribution and Influence Factors in Chinese Urban Residential Blocks. *Environment and Planning B: Planning and Design*. Retrieved from http://epb.sagepub.com/lookup/doi/10.1177/0265813516647733